MICROCOPY RESOLUTION TEST CHART

NATIONAL BUREAU OF STANDARDS-1963-A

AD-A149 986

(12)

MATERIAL PROPERTIES OF NEVADA TEST SITE TUFF RELATING TO THE DIABLO HAWK STRUCTURES EXPERIMENTS AND CONTAINMENT EVALUATION

Terra Tek, Incorporated
420 Wakara Way
Salt Lake City, Utah 84108

1 November 1978

Final Report for Period 1 September 1977—31 August 1978

DTIC FILE COPY

DTIC
ELECTE
FEB 4 1985

B

Prepared for
Director
DEFENSE NUCLEAR AGENCY
Washington, DC 20305

84 11 19 103

REPORT DOCUMENTATION PAGE		READ INSTRUCTIONS BEFORE COMPLETING FORM
1. REPORT NUMBER DNA 4864F	2. GOVT ACCESSION NO. AD-A149986	3. RECIPIENT'S CATALOG NUMBER
4. TITLE *(and Subtitle)* MATERIAL PROPERTIES OF NEVADA TEST SITE TUFF RELATING TO THE DIABLO HAWK STRUCTURES EXPERIMENTS AND CONTAINMENT EVALUATION		5. TYPE OF REPORT & PERIOD COVERED Final Report for Period 1 Sep 77—31 Aug 78
		6. PERFORMING ORG. REPORT NUMBER TR 78-78
7. AUTHOR(s) D.S. Gardiner A.H. Jones S.W. Butters		8. CONTRACT OR GRANT NUMBER(s) DNA 001-77-C-0322
9. PERFORMING ORGANIZATION NAME AND ADDRESS Terra Tek, Incorporated 420 Wakara Way Salt Lake City, Utah 84108		10. PROGRAM ELEMENT, PROJECT, TASK AREA & WORK UNIT NUMBERS Task J45GAXYX-97309
11. CONTROLLING OFFICE NAME AND ADDRESS Director Defense Nuclear Agency Washington, DC 20305		12. REPORT DATE 1 November 1978
		13. NUMBER OF PAGES 226
14. MONITORING AGENCY NAME & ADDRESS*(if different from Controlling Office)* Field Command Defense Nuclear Agency Kirtland AFB, NM 87117		15. SECURITY CLASS *(of this report)* UNCLASSIFIED
		15a. DECLASSIFICATION/DOWNGRADING SCHEDULE N/A since UNCLASSIFIED

16. DISTRIBUTION STATEMENT *(of this Report)*

Approved for public release; distribution unlimited.

17. DISTRIBUTION STATEMENT *(of the abstract entered in Block 20, if different from Report)*

18. SUPPLEMENTARY NOTES

This work was sponsored by the Defense Nuclear Agency under RDT&E RMSS Code K400077462 J45GAXYX97309 H2590D.

19. KEY WORDS *(Continue on reverse side if necessary and identify by block number)*

Nuclear Test	Tuff
Hydrostatic	Grout
Uniaxial Strain	Pressure
Triaxial Compression	Load

20. ABSTRACT *(Continue on reverse side if necessary and identify by block number)*

Material properties testing has been conducted for the Defense Nuclear Agency Field Command. The testing was in support of the Nevada Test Site nuclear test program and covered the period 1 October 1977 through 31 August 1978. The contract number was DNA 001-77-C-0322 and Mr. J.W. LaComb was the Contracting Officer Representative.

The primary task during this report period was material evaluation for the Diablo Hawk Structures experiments and the on-going containment

DD FORM 1473 EDITION OF 1 NOV 65 IS OBSOLETE

20. ABSTRACT (Continued)

evaluation study. Tuff, grout, saturated sand and "reconstituted" tuff were tested. The material evaluations are used for initial nuclear test site selection, detailed site evaluation, shock effect evaluation and support of related experiments. The majority of the tests were uniaxial strain tests with accompanying physical property and ultrasonic velocity measurements. Additionally, hydrostatic and triaxial compression, bursts, permeability and scanning electron microscope tests were conducted.

PREFACE

The authors would like to express their thanks for the guidance of Mr. J. W. LaComb (DNA, Mercury, Nevada). They would also like to thank Mr. W. Tay and Mr. F. Prater for assistance in conducting the laboratory tests and Ms. J. Grant, Ms. C. Nabrotzky and Ms. L. Twitchell for the transcript preparation.

Accession For

NTIS GRA&I

DTIC TAB

Unannounced

Justification

By

Distribution

Availability Codes

Dist   Avail and/or Special

A-1

DTIC COPY INSPECTED

1

TABLE OF CONTENTS

INTRODUCTION

Material properties of the containment media (tuff) and related con-
struction materials associated with individual nuclear events at the
Nevada Test Site (NTS) are a vital part of the Defense Nuclear Agency (DNA)
nuclear test program. Material properties are primarily needed in the
evaluation of stemming and containment designs of the nuclear tests and
in material models designed to predict ground motion and wave propagation.

This report summarizes the materials testing program conducted by
Terra Tek from September 1977 through August 1978 for the Test Directorate,
Field Command, DNA. The purpose of the test program was material character-
ization for the DIABLO HAWK Structures experiments and the on-going con-
tainment evaluation studies. Tuffs and grouts from various locations at
NTS were tested for specific mechanical and physical properties. During
the contract period, reports were published upon completion of testing
and distributed to designated agencies. This final report includes those
reports plus some additional test data not yet distributed. A synopsis of
the testing and analytical procedures is as follows:

Diablo Hawk Structures

The Diablo Hawk event has several ground shock-structures interaction
experiments. These experiments are located in an area 150 to 700 feet
to the south of the working point. In conjunction with these experiments,
tuffs, grouts and sands were evaluated for their material properties.

Reports describing the above work are:

>Some Material Properties of Diablo Hawk Tuff Associated with
>the TRW Experiment, TR 77-95

High Pressure Mechanical Properties of Lapis Lustre Sand, TR
77-70

Some Material Properties of Diablo Hawk Tuff Associated with
the AA (Agbabian Associates) Water Filled Tunnel

Shear Moduli of Select U12n.10A DNFF Tuff

Material Properties of the Diablo Hawk Camera/Borescope Drill
Hole Tuffs

Material Properties of Select Interface Tuffs

Containment Evaluation

In a continuing effort to understand containment phenomena and plan
for new events, material properties were measured to assist with evaluating
the media's potential for hydraulic fracturing. Interest was in materials
from previous events or, in particular, the Hybla Gold event from which
cavity gases were allowed to penetrate outside of the "residual stress"
field.

The test results are, at this time, inconclusive. However, the data
is supportive of larger cavity experiments.

Exploratory Drill Holes in U12n.11 Tunnel

Site exploration is an essential part of proper resource utilization
at NTS. The continuing requirement for new test locations dictates con-
tinual exploration. Exploratory drill holes provide a means of determining
site usability for a nuclear test prior to extending tunnels into an area.

An evaluation of a site may be determined by examining the material
properties of exploratory drill hole cores and comparing results with data
from previously tested sites. This report examines both the physical and
mechanical properties of the proposed U12n.11 area as the future Miner's
Iron test site.

4

Residual Stress in Thick-Walled Cylinders of Ash-Fall Tuffs Subjected to Internal Pressurization

Field measurements and calculations indicate that postshot residual stresses may exist around a cavity. To investigate this possibility, internal pressurization tests on thick-walled tuff cylinders were conducted to determine whether residual stresses can exist. Work investigating the possibilities of forming residual stresses began during the last contract year on both tuffs and tuff matching grouts. The report presents further data on selected tuff samples.

Properties of Reconstituted Tuff

In support of siting future nuclear events in the proximity of previous events and hence the "chimney" from the event (i.e. the volume of material above the cavity from which material has collapsed into the cavity), laboratory tests were conducted. Material property tests were conducted on tuff material that was crushed and recompacted to simulate the densities of *in situ* "chimney materials". The test program includes evaluation of sample size effects, particle size effects and finally tuff type effects. This year's report presents the physical and mechanical properties of reconstituted Paintbrush tuff of varying sample sizes.

Ultrasonic Velocities as a Function of Fracturing

The objective of this study was to determine the effects of fracture on the acoustic velocities in ash-fall tuff to explain the reduction in seismic velocities with time noted in the pillars at underground locations. The measured reduction in velocity has been as much as 30 percent below the original values. The objective of this test program was to gain a better

understanding of the mechanism that causes the velocity change. The initial phase of the program was to determine if comparable velocity reductions could be produced (under simulated field conditions) in the laboratory.

Specific Retention Tests

Because of the requirement to know the gas-filled void content of tuff material to a high degree of accuracy, tests were conducted to evaluate the possibility of fluid invasion during drilling. Apparent "wet" tuff samples were placed in a high humidity environment to determine if the samples would gain moisture.

Additionally, "dry" tuff samples were also placed in the high humidity environment to determine if they would return to their original *in situ* moisture content. Previous work has shown that dry samples placed in a near 100 percent relative humidity environment gain weight (moisture) to the suspected *in situ* condition.

Stanford Research Institute (SRI) Grout

In support of the DAN containment program, SRI conducts experiments of the hydrofracture properties of tuff matching grout. Mechanical and physical properties of these grouts were determined by Terra Tek to provide data required for calculations of the SRI experiments. Tests conducted by TTI during this contract year are described in:

Material Properties of Stanford Research Institute Superlean Grout

DIABLO HAWK STRUCTURES

SOME MATERIAL PROPERTIES OF DIABLO HAWK TUFF

ASSOCIATED WITH THE TRW EXPERIMENT

by

D. S. Gardiner
S. W. Butters

SUMMARY

Mechanical property tests were conducted on core samples from two long (230 foot) and five short (21 foot) drill holes relating to the Diablo Hawk event at the Nevada Test Site. The drill holes were designated TRCX#1 and 2 and TRCX#4, 7, 12, 17, and 21 for the long and short holes respectively. These particular cores are from the vicinity of the TRW experiment and were tested to provide material properties for calculating ground motion response. A plan view showing the relative locations of the drill holes is shown below in Figure 1.

Mechanical testing consisted of unconfined compression tests and uniaxial strain tests to 4 kbars confining pressure. Table 1 lists the unconfined compressive strength, and stress difference and permanent
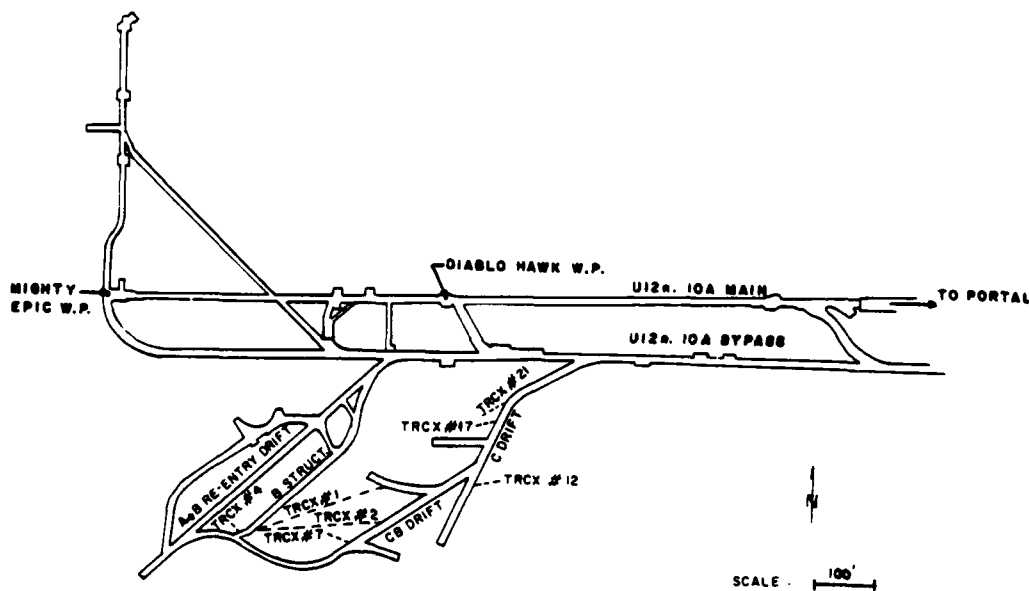
Figure 1. Plan view of Diablo Hawk structures drifts showing the relative locations of the TRCX drill holes.

8

TABLE 1

TRW Experiment Mechanical Test Data -- U12n.10A Cable Holes

Drill Hole/Footage		Unconfined Compressive Strength (kb)	Uniaxial Strain	
			Measured Permanent Compaction ( )	Stress Difference a₁₃ = 4 kb (kb)
TRCX#1	10	--	1.3	0.30
	20	0.14		
	30	0.07		
	39	0.24		
	48	0.17		
	51	0.11		
	61	--	2.7	0.58
	72	0.48		
	80	0.52,0.57*		
	89	0.37		
	99	0.19		
	103	0.17		
	111	--	0.5	0.42
	120	0.17		
	131	0.40		
	141	0.33		
	149	0.11		
	152	0.13		
	160	--	1.0	0.36
	172	0.57,0.85*		
	181	0.37		
	191	0.15		
	199	0.29		
	203	0.43		
	212	--	1.2	1.20
	222	0.82,0.80*		
	229	0.33		
TRCX#2	10	--	1.8	0.43
	25	0.13		
	33	0.12		
	38	0.11		
	49	0.13		
	51	--	4.4	0.43
	61	0.12		
	71	0.11		
	80	0.12		
	91	0.16		
	101	--	3.0	1.75
	124	0.09		
	154	--	0.2	1.70
	164	0.18		
	172	0.09		
	179	0.16		
	190	0.30		
	204	--	1.2	0.75
	214	0.08		
	222	--	1.0	0.23
	231	0.11		
TRCX#4	4	0.29		
	8	0.29		
	13	0.35		
	17	--	1.5	0.60
	20	--	1.2	0.41
TRCX#7	5	0.36		
	8	--	1.2	0.55
	13	0.59		
	17	--	1.0	1.27
	20	0.18		
TRCX#12	6	0.38		
	11	--	2.6	0.59
	13	0.10		
	16	--	1.7	1.47
	19	0.25		
TRCX#17	1	0.23		
	8	--	4.3	0.85
	14	0.15		
	21	--	2.0	0.55
	29	0.16		
TRCX#21	1	0.50		
	11	--	5.8	0.44

* Duplicate tests were conducted to verify apparent high strength.

volume compaction observed during the uniaxial strain tests *for each*
drill hole. Figures 3 and 4 show the unconfined compressive strengths
as a function of the drill hole footage for drill holes TRCX#1 and #2
respectively. Appendix A shows the unconfined compression test curves
and Appendix B shows the uniaxial strain test curves.

Although drill holes TRCX#1 and #2 were collared from the same
point (see Figure 2), the samples have quite different strength proper-
ties. TRCX#2 samples exhibited very consistent unconfined compressive
strengths averaging 0.13 kbars with a standard deviation of 0.05 kbars.
These results are consistent with previous test data (i.e. U12n.10 UG#4
$\bar{x}$ = 0.18 kbars and ISS#5 $\bar{x}$ = 0.19 kbars) obtained for the nearby Mighty
Epic event.* TRCX#1 samples on the other hand exhibited quite different
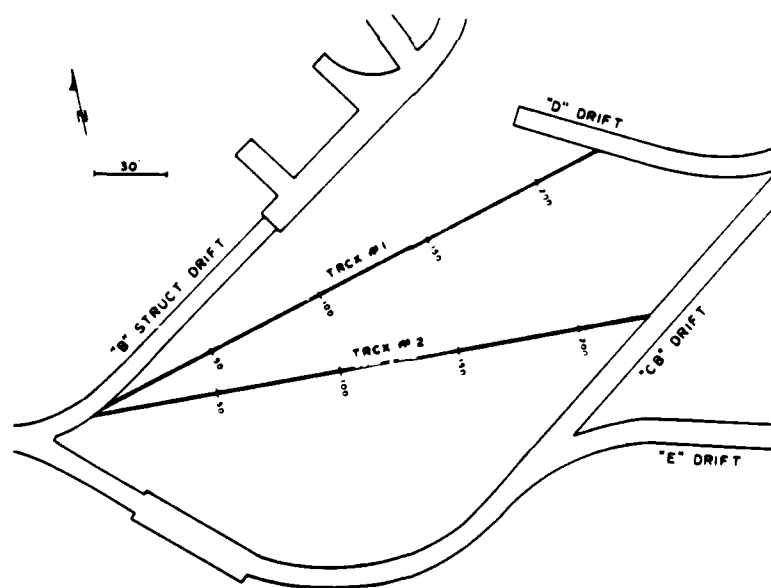
Figure 2. Map showing locations of TRCX#1 and #2 core samples.

---

* Butters, S. W., Dropek, R. K., and Jones., A. H., "Material Properties
of Nevada Test Site Tuff and Grout with Emphasis on the Mighty Epic
Event," Terra Tek Report TR 76-63, November 1976.
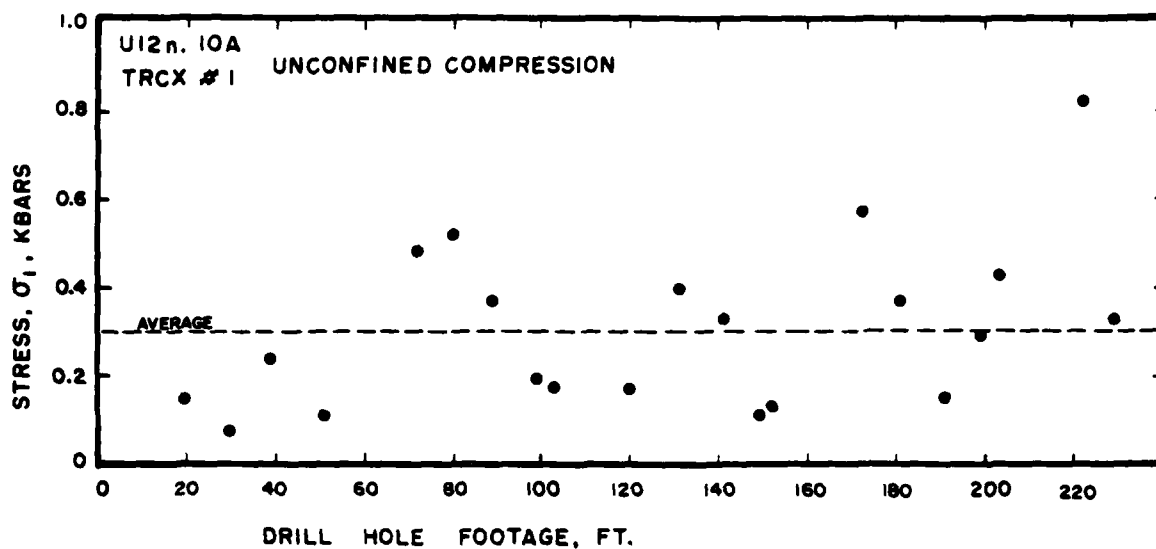
Figure 3. Unconfined compressive strength versus drill hole footage
for U12n.10A TRCX#1 tuffs.
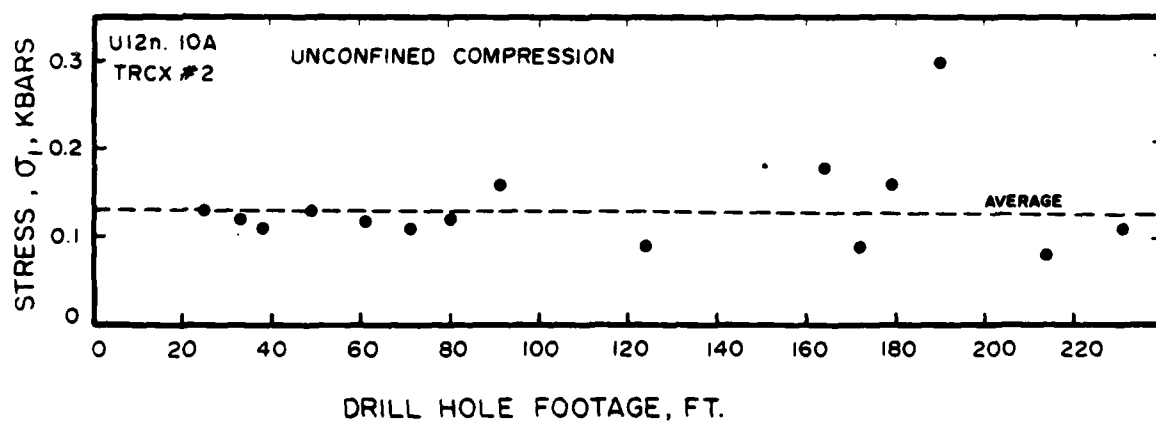
Figure 4. Unconfined compressive strength versus drill hole footage
for U12n.10A TRCX#2 tuffs.

11

behavior. The average unconfined compressive strength was 0.30 kbars
with a standard deviation of 0.19 kbars. A possible explanation for
the apparent difference in material properties between the two holes is
found in the fact that the TRCX#1 drill hole crosses through two differ-
ent lithologic subunits while the TRCX#2 drill hole lies entirely within
the same subunit.* Densities computed from the test sample dimensions
and weights verify the apparent material differences. Variation in the
sample bulk density of the TRCX#1 test specimens was considerable, rang-
ing from 1.73 to 2.15 gm/cc while the density variation for the TRCX#2
samples ranged from 1.81 to 2.04 gm/cc. Figure 5 shows this variation
and its effect on unconfined compressive strength.

Only a limited number of uniaxial strain tests were conducted on
the TRCX drill hole samples. Tests were conducted on samples from
approximately 8 foot intervals for the short drill holes and 50 foot
intervals for the long drill holes. The same material variations shown
in the unconfined compressive tests are evidenced in the uniaxial strain
tests by the variation in the stress difference of from 0.23 to 1.75 kbars
(at 4.0 kbars). The permanent volume compaction is generally less than 2
percent by volume with a couple of samples in the 3 to 4 percent range
and one sample at 6 percent.

---

* Conversation with Dean Townsend, U.S. Geological Survey, April 17, 1978.
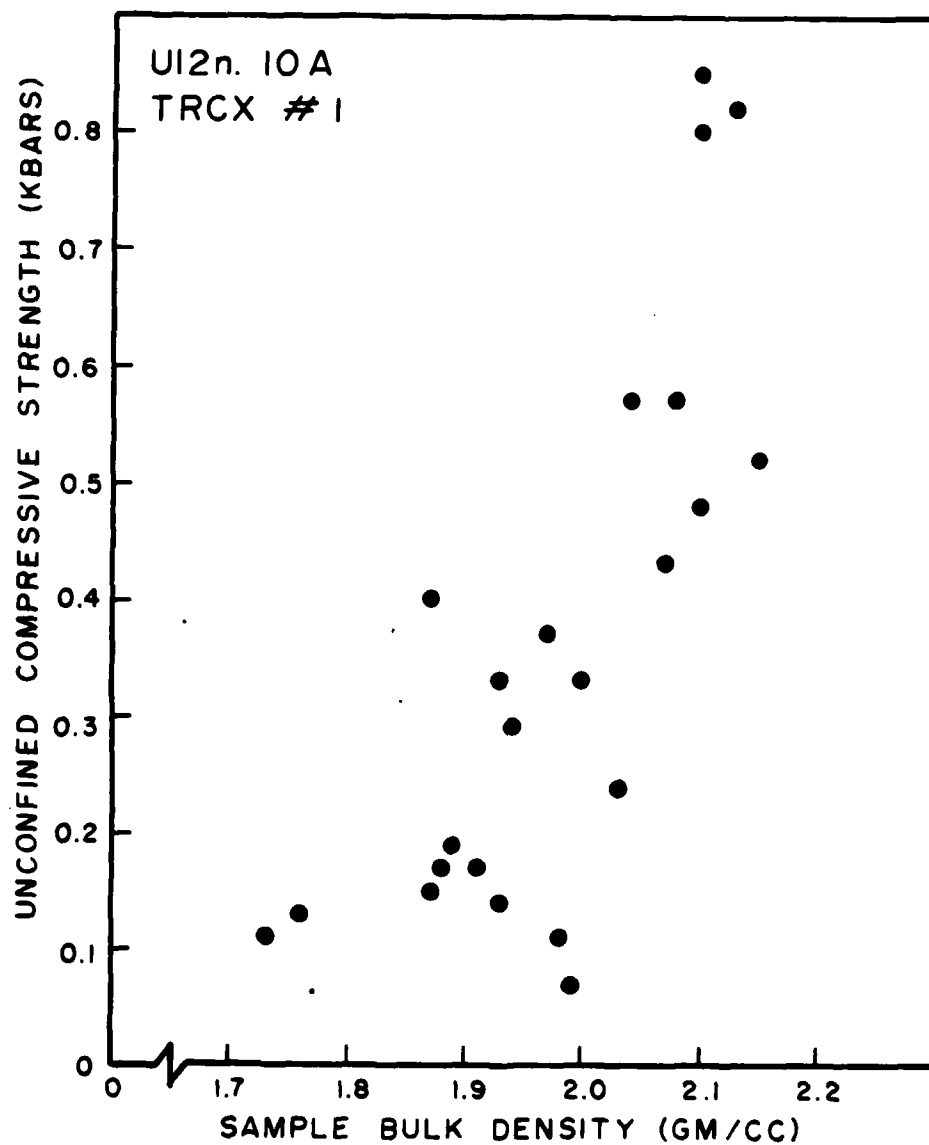
Figure 5. Unconfined compressive strength versus sample bulk density for TRCX#1 drill hole tuff.

14

Unconfined Compression Test Curves on U12n.10A TRCX Tuffs
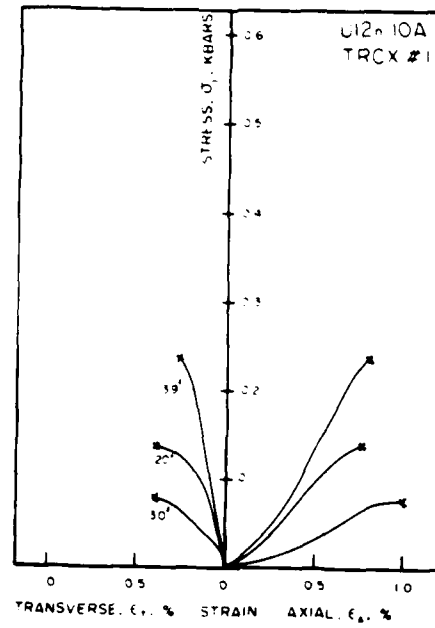
Figure 6.   Unconfined compression test on U12n.10A TRCX#1 tuff --
stress versus axial and transverse strains.
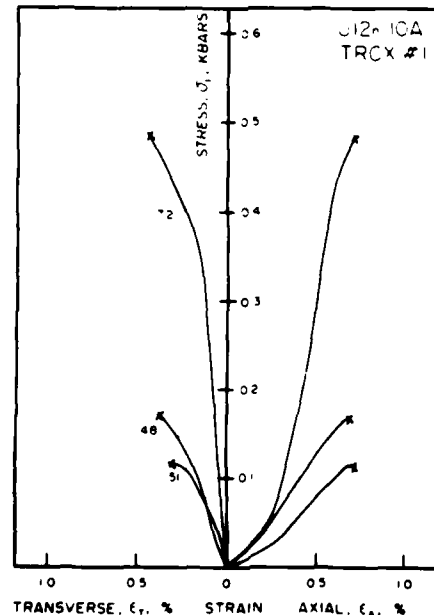
Figure 7.   Unconfined compression test on U12n.10A TRCX#1 tuff --
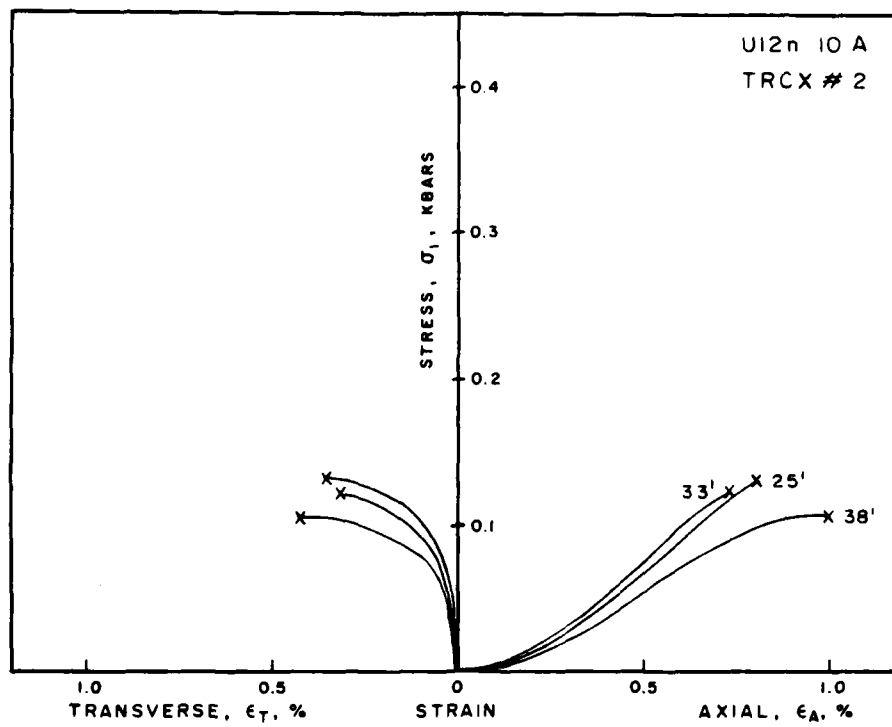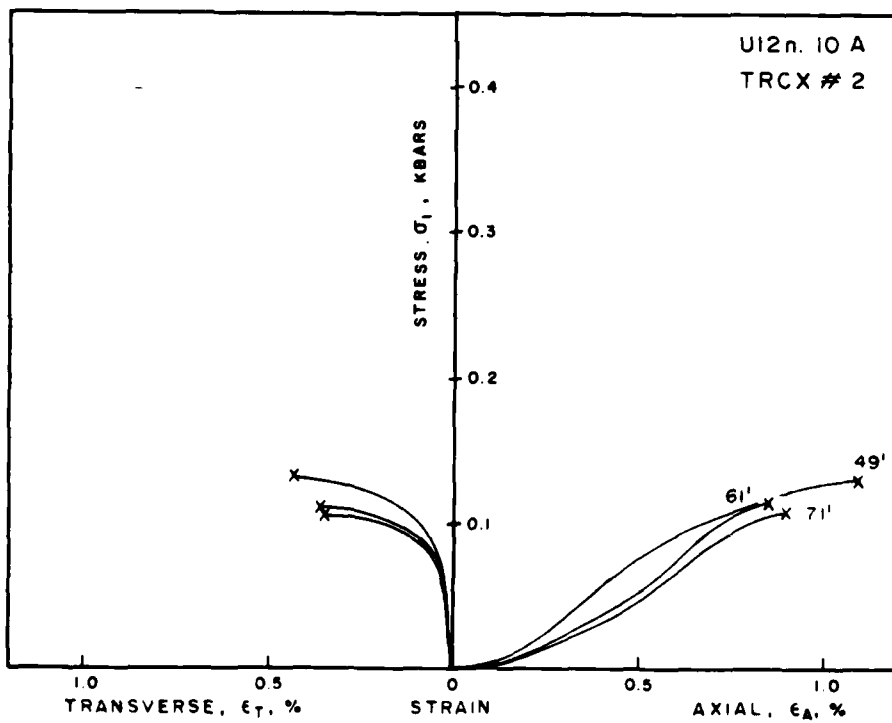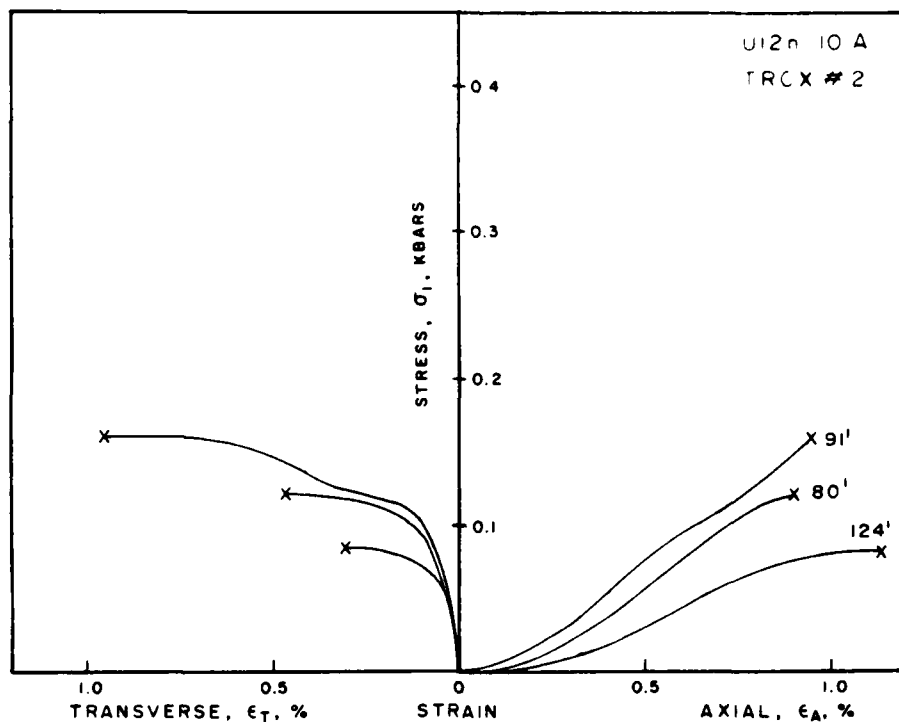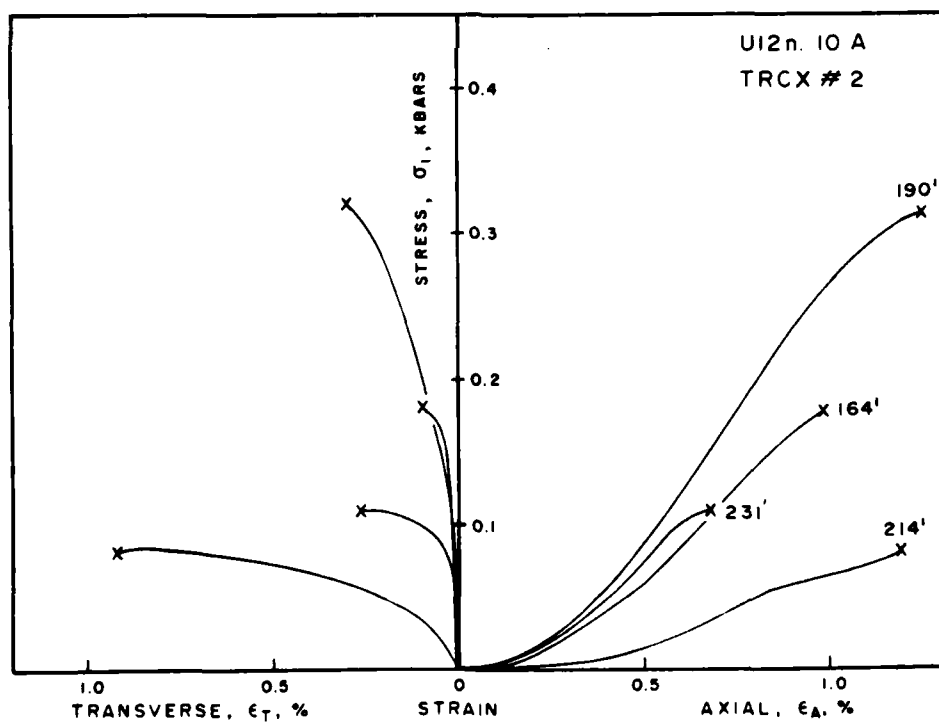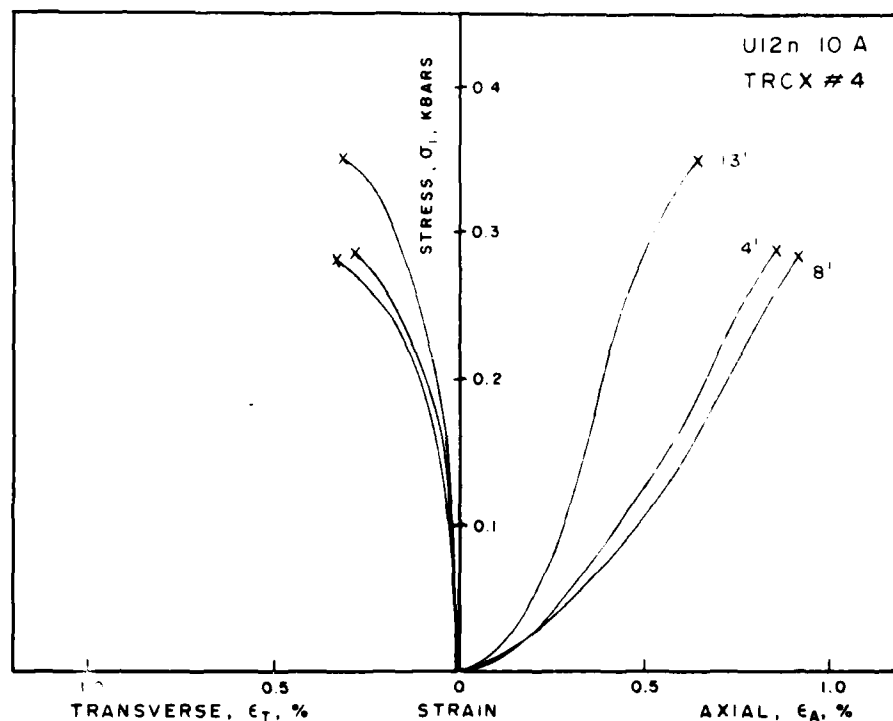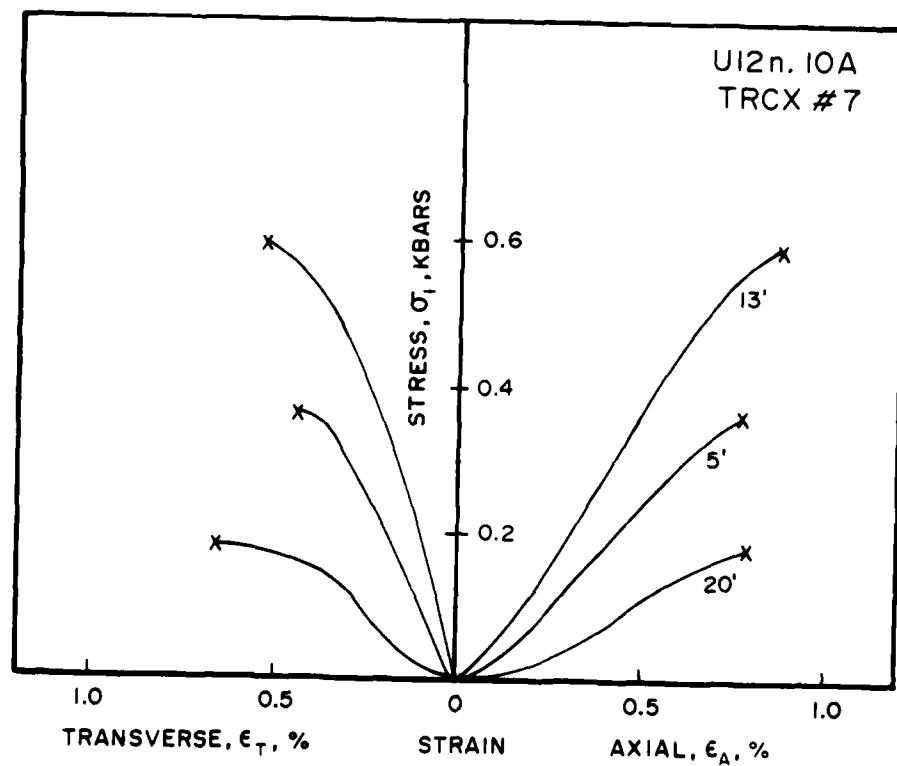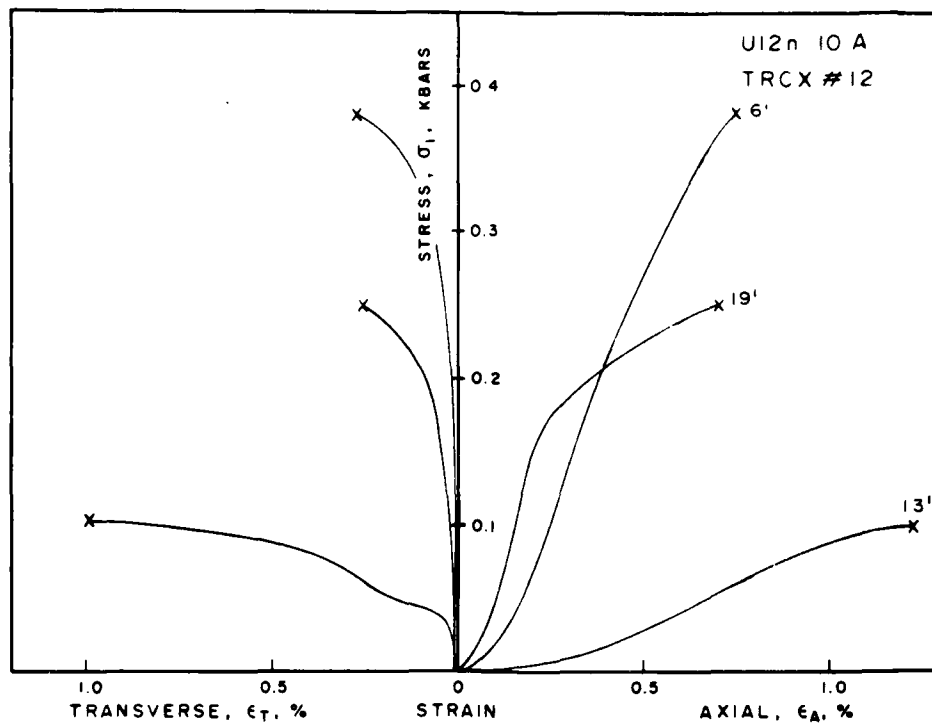stress versus axial and transverse strains.
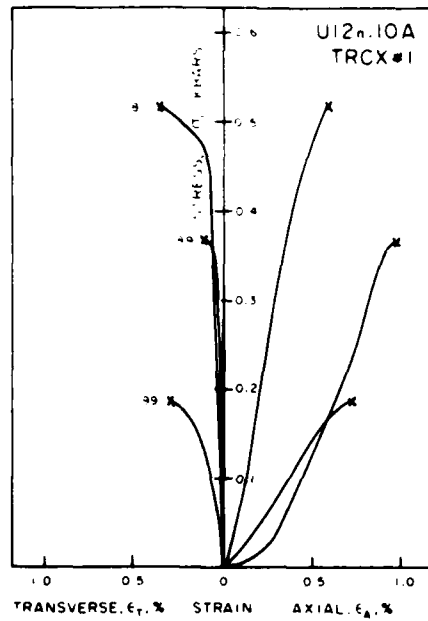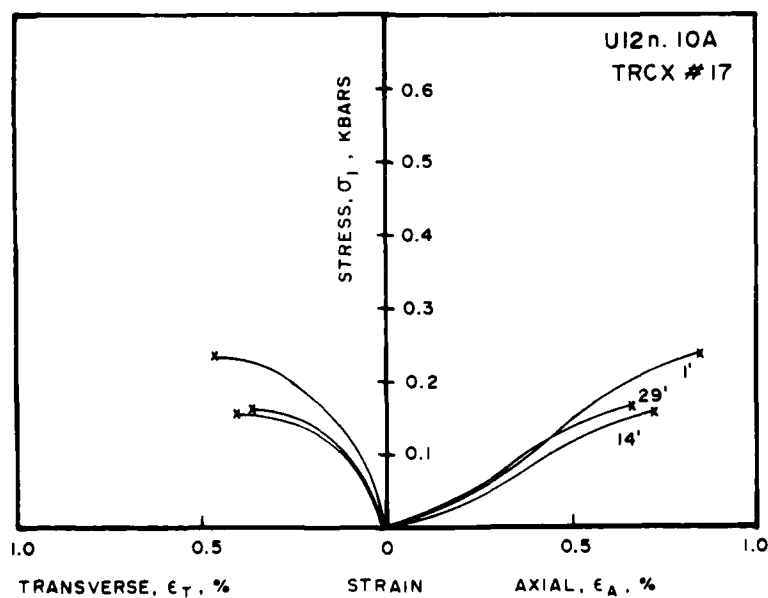
Figure 8. Unconfined compression test on U12n.10A TRCX#1 tuff --
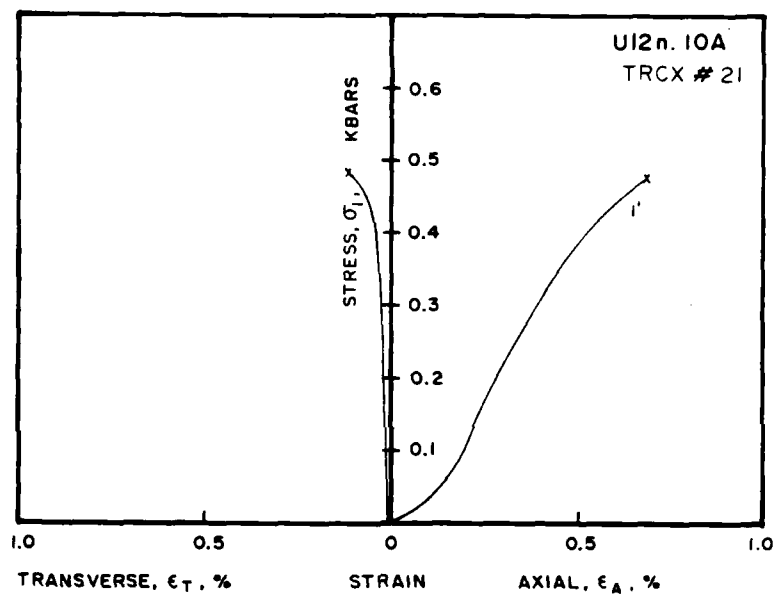stress versus axial and transverse strains.
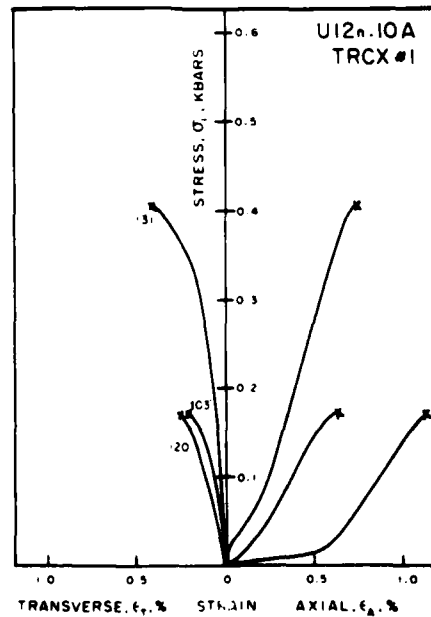
Figure 9. Unconfined compression test on U12n.10A TRCX#1 tuff --
stress versus axial and transverse strains.
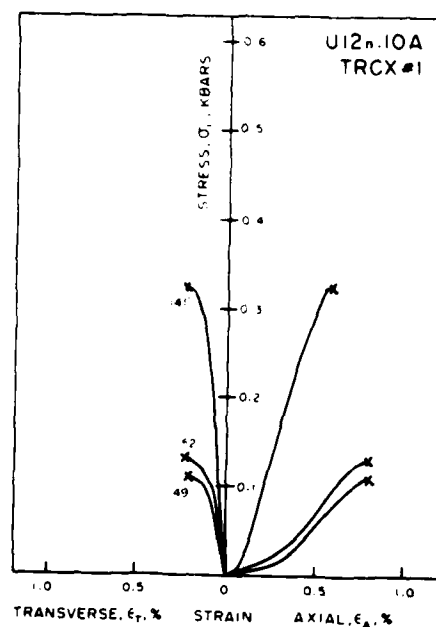
Figure 10. Unconfined compression test on U12n.10A TRCX#1 tuff --
stress versus axial and transverse strains.

Figure 11. Unconfined compression test on U12n.10A TRCX#1 tuff --
stress versus axial and transverse strains.

17
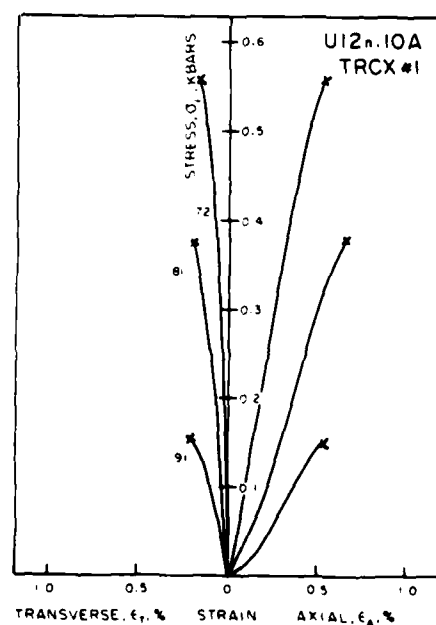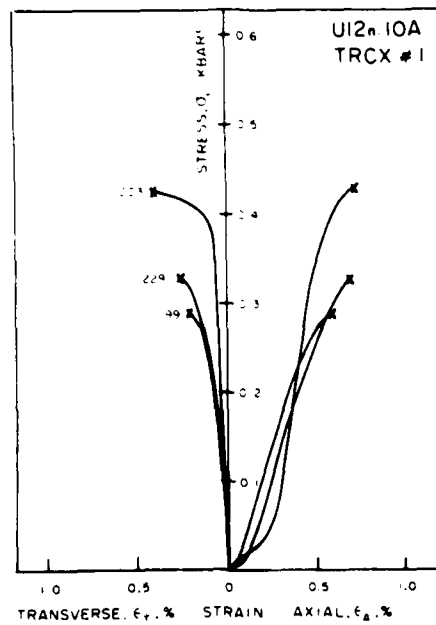
Figure 12.   Unconfined compression test on U12n.10A TRCX#1 tuff --
stress versus axial and transverse strains.

Figure 13.   Unconfined compression test on U12n.10A TRCX#1 tuff --
stress versus axial and transverse strains.

18
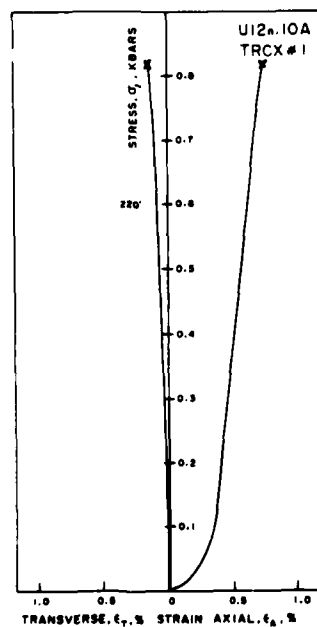
Figure 14. Unconfined compression test on U12n.10A TRCX#2 tuff --
stress versus axial and transverse strains.

Figure 15. Unconfined compression test on U12n.10A TRCX#2 tuff --
stress versus axial and transverse strains.

Figure 16.   Unconfined compression test on U12n.10A TRCX#2 tuff --
             stress versus axial and transverse strains.

Figure 17.   Unconfined compression test on U12n.10A TRCX#2 tuff --
             stress versus axial and transverse strains.

20

Figure 18. Unconfined compression test on U12n.10A TRCX#4 tuff -- stress versus axial and transverse strains.

Figure 19. Unconfined compression test on U12n.10A TRCX#7 tuff -- stress versus axial and transverse strains.

21

Figure 20. Unconfined compression test on U12n.10A TRCX#12 tuff --
stress versus axial and transverse strains.

Figure 21. Unconfined compression test on U12n.10A TRCX#17 tuff --
stress versus axial and transverse strains.

22

Figure 22. Unconfined compression test on U12n.10A TRCX#21 tuff --
stress versus axial and transverse strains.

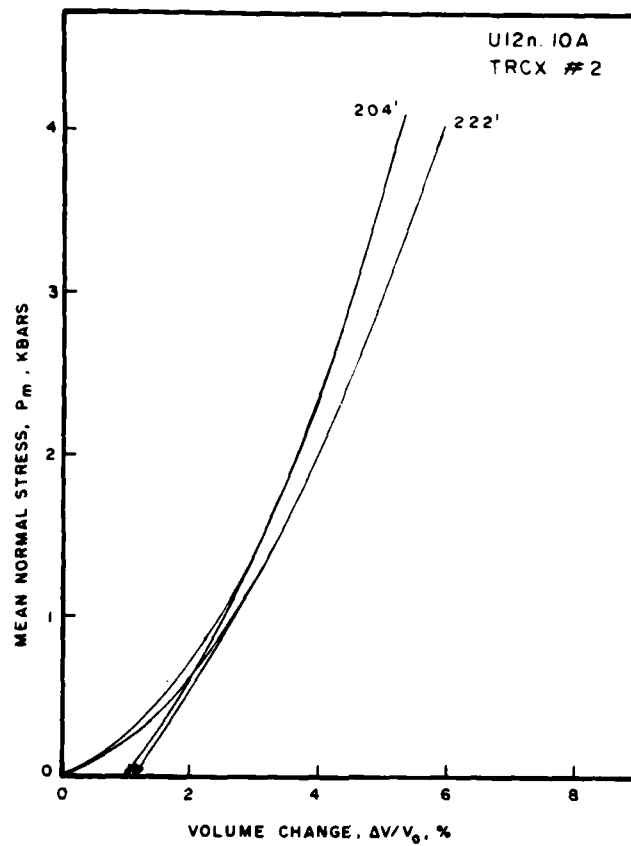Uniaxial Strain Test Curves on U12n.10A TRCX Tuffs
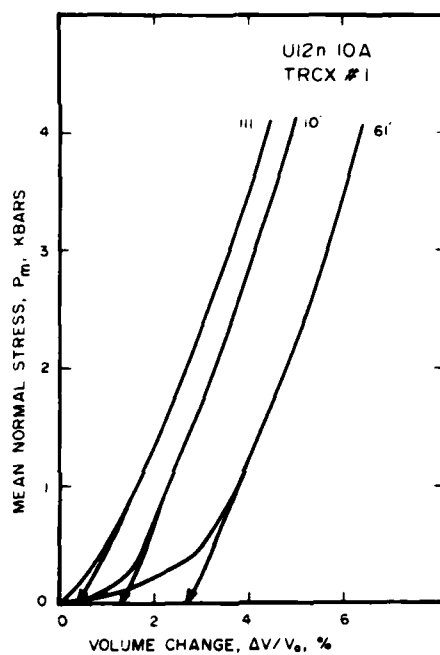
Figure 23. Uniaxial strain test to 4 kbars on U12n.10A TRCX#1 tuff --
mean normal stress versus volume change.

Figure 24. Uniaxial strain test to 4 kbars on U12n.10A TRCX#1 tuff --
stress difference versus confining pressure.

25
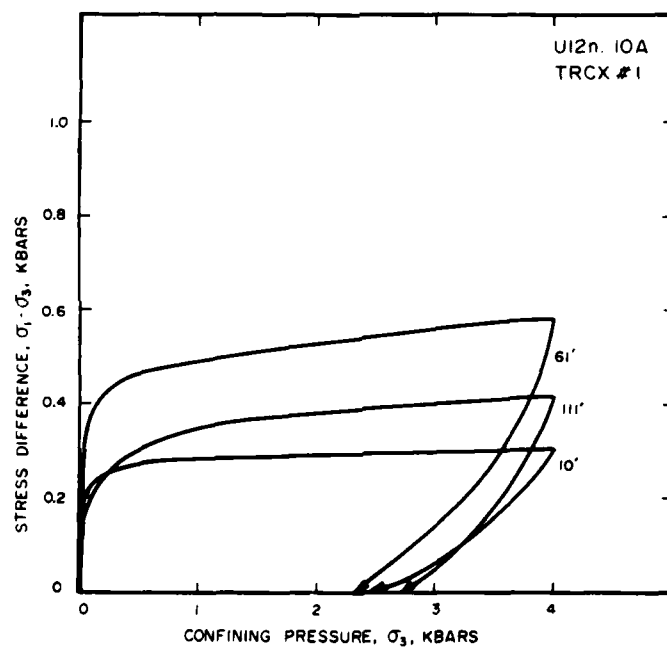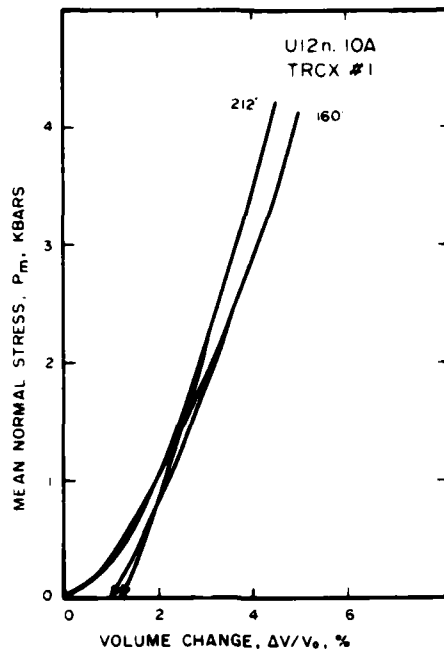
Figure 25. Uniaxial strain test to 4 kbars on U12n.10A TRCX#1 tuff --
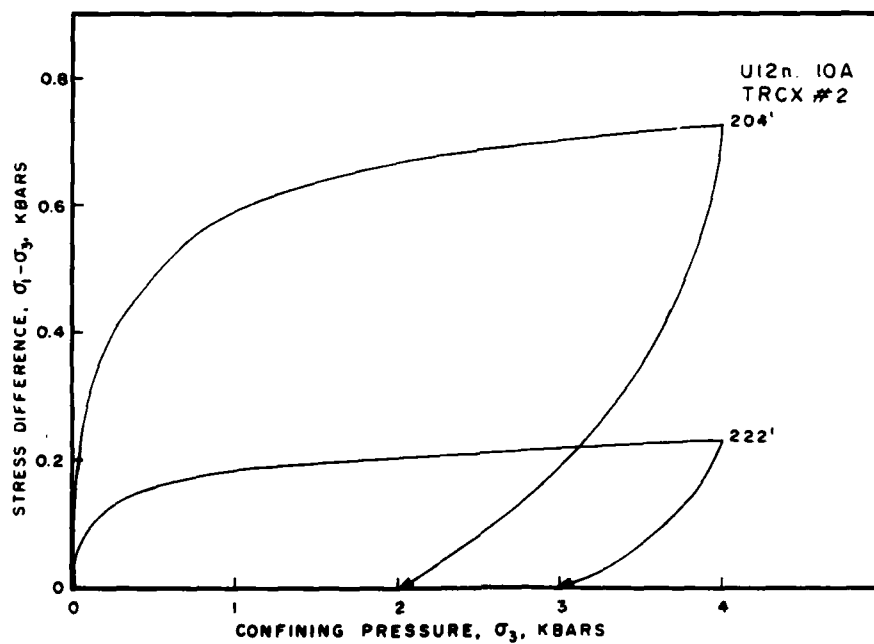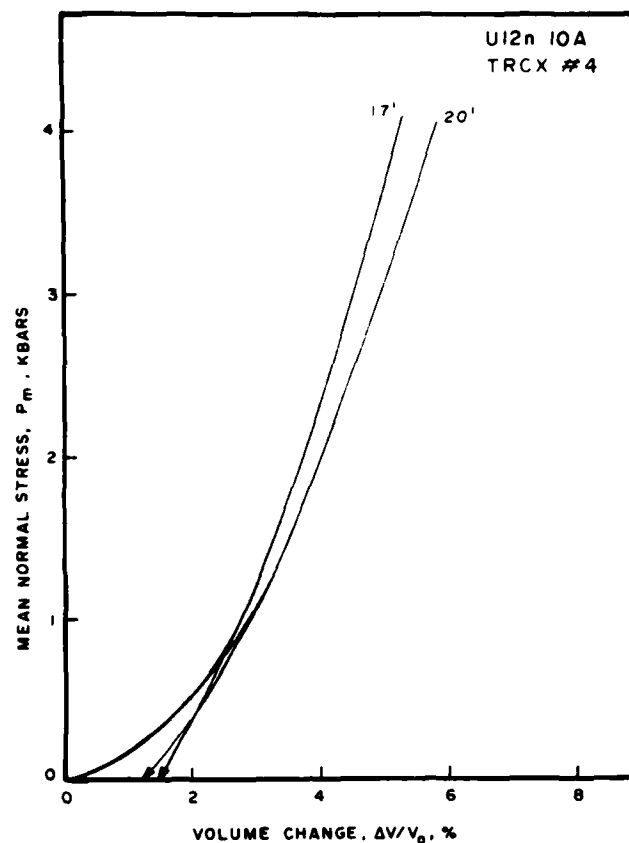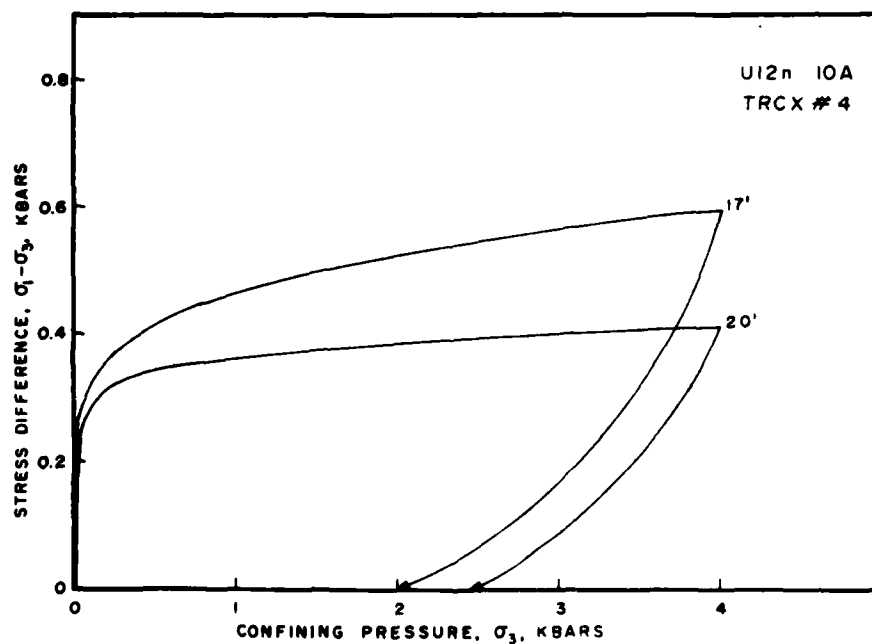mean normal stress versus volume change.
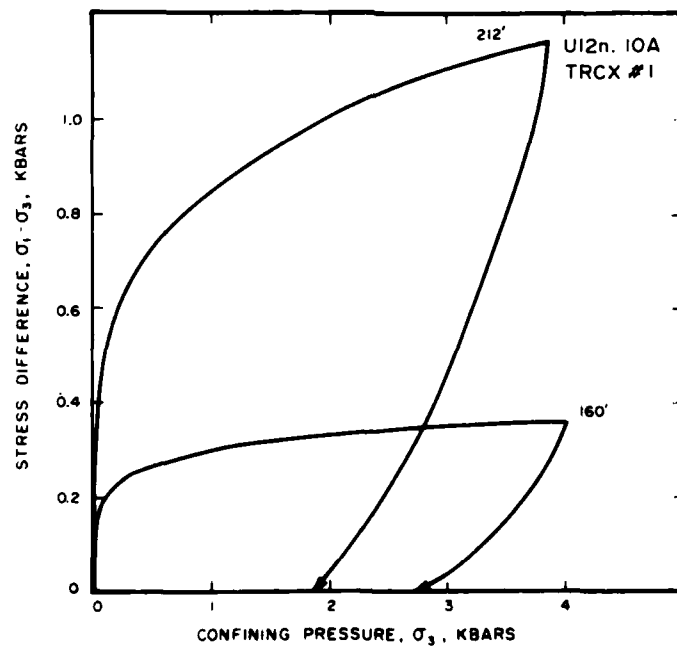
Figure 26. Uniaxial strain test to 4 kbars on U12n.10A TRCX#1 tuff --
stress difference versus confining pressure.
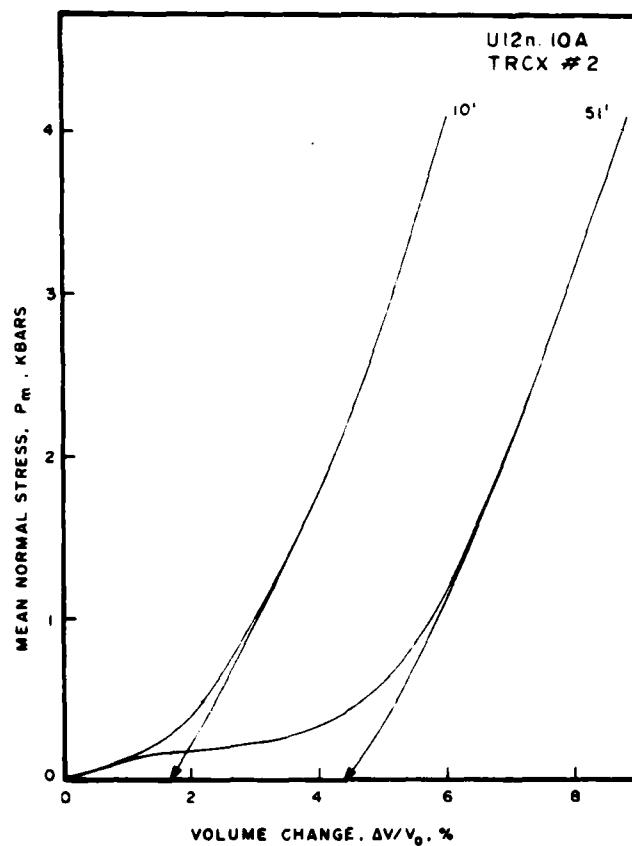
Figure 27. Uniaxial strain test to 4 kbars on U12n.10A TRCX#2 tuff --
mean normal stress versus volume change.

Figure 28. Uniaxial strain test to 4 kbars on U12n.10A TRCX#2 tuff --
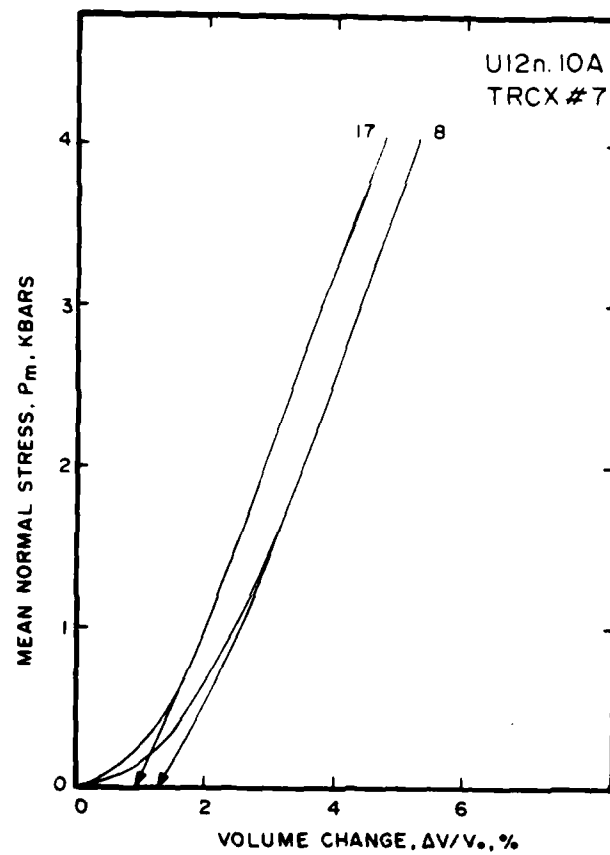stress difference versus confining pressure.

27
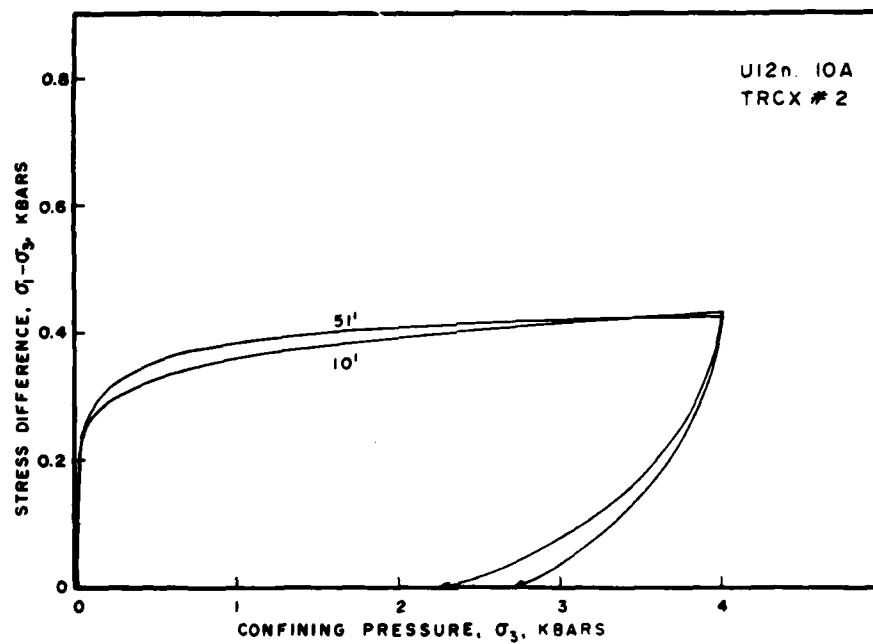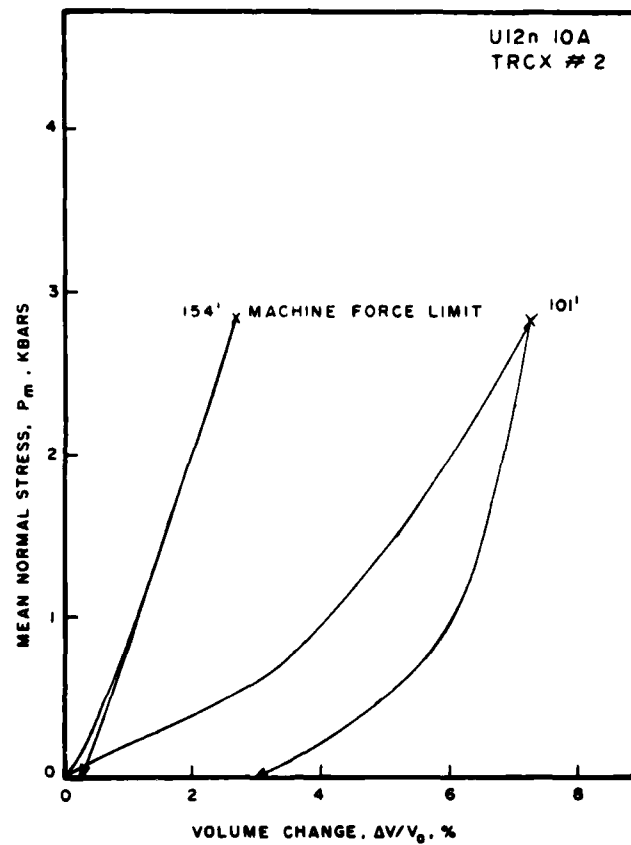
Figure 29. Uniaxial strain test to 4 kbars on U12n.10A TRCX#2 tuff -- mean normal stress versus volume change.
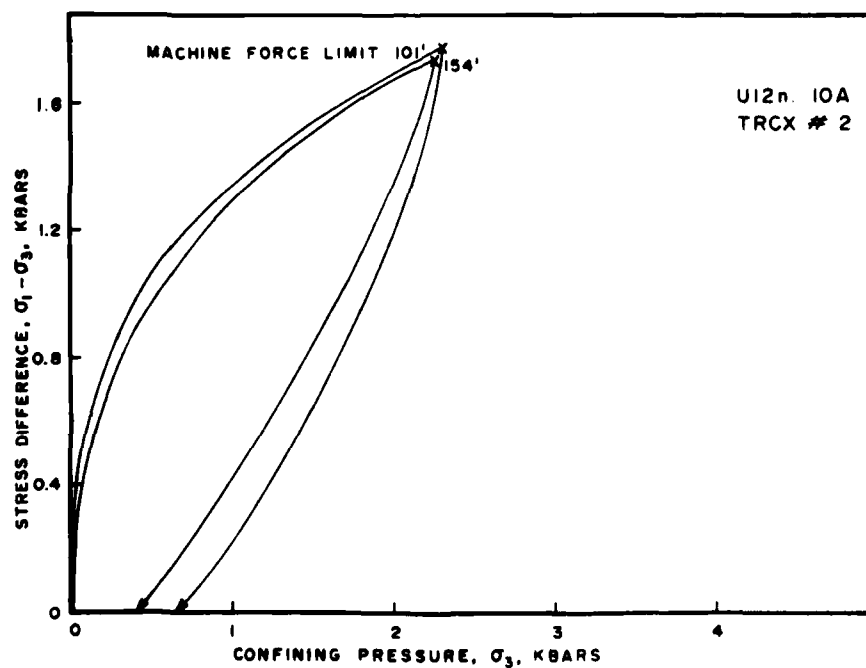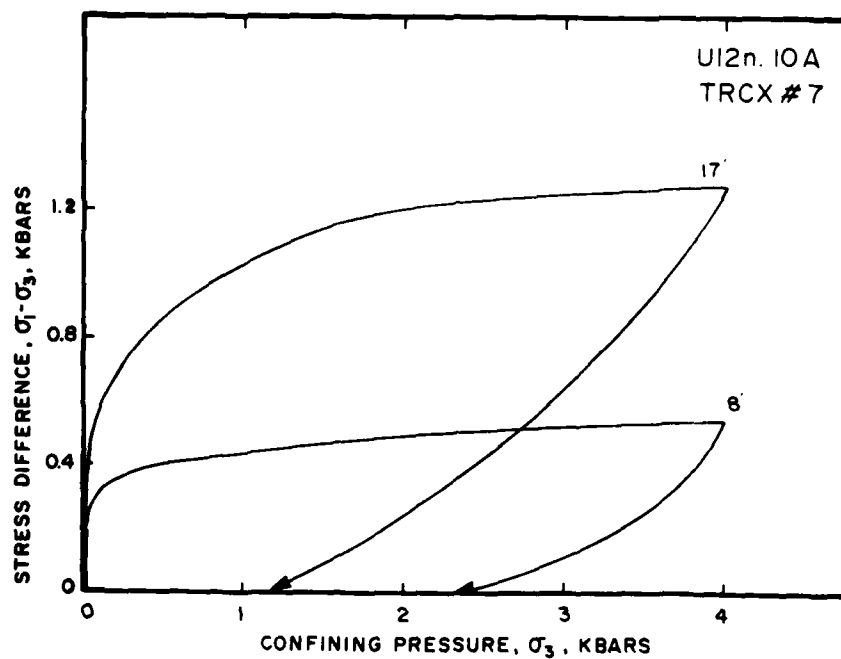

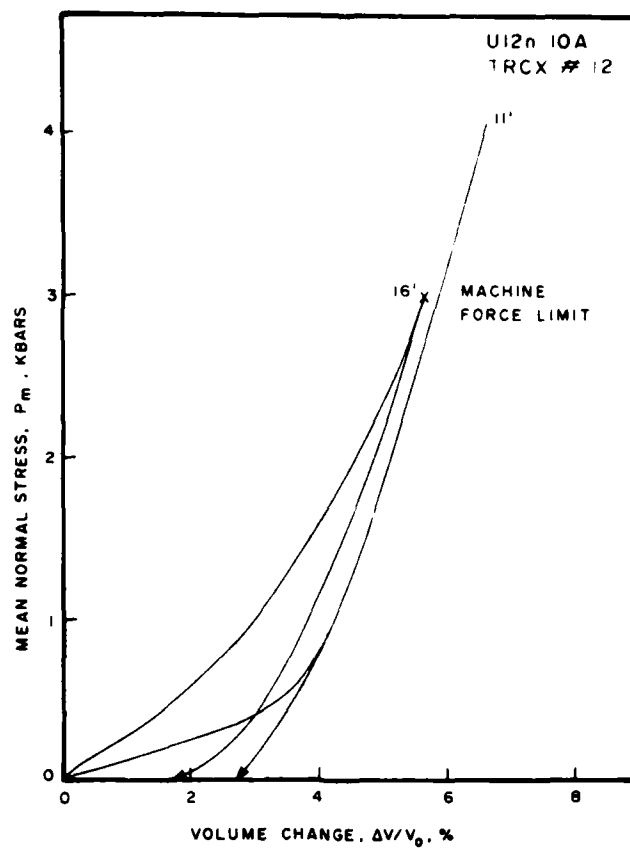Figure 30. Uniaxial strain test to 4 kbars on U12n.10A TRCX#2 tuff -- stress difference versus confining pressure.

Figure 31. Uniaxial strain test to 4 kbars on U12n.10A TRCX#2 tuff -- mean normal stress versus volume change.
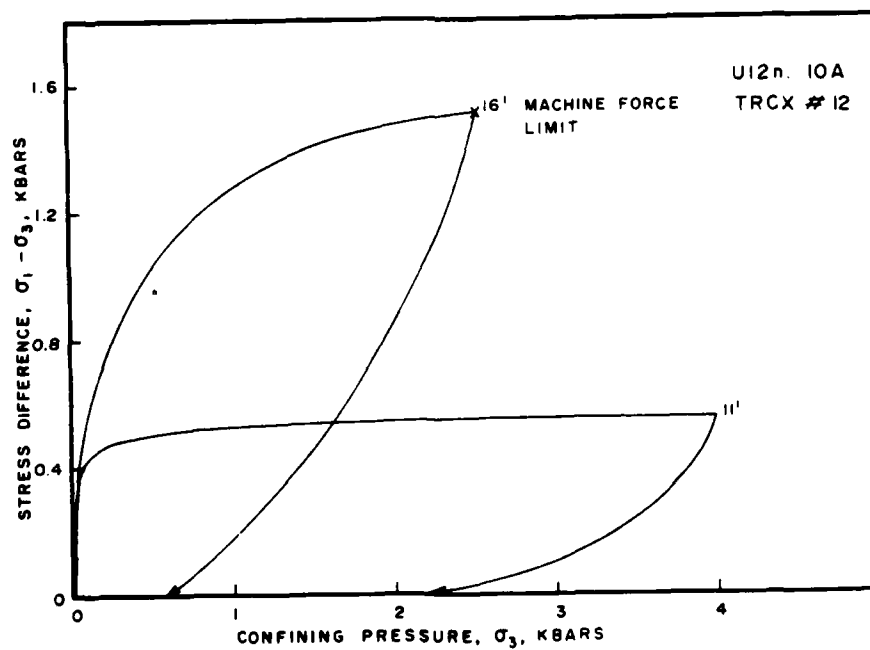

Figure 32. Uniaxial strain test to 4 kbars on U12n.10A TRCX#2 tuff -- stress difference versus confining pressure.

29

Figure 33. Uniaxial strain test to 4 kbars on U12n.10A TRCX#4 tuff --
mean normal stress versus volume change.

Figure 34. Uniaxial strain test to 4 kbars on U12n.10A TRCX#4 tuff --
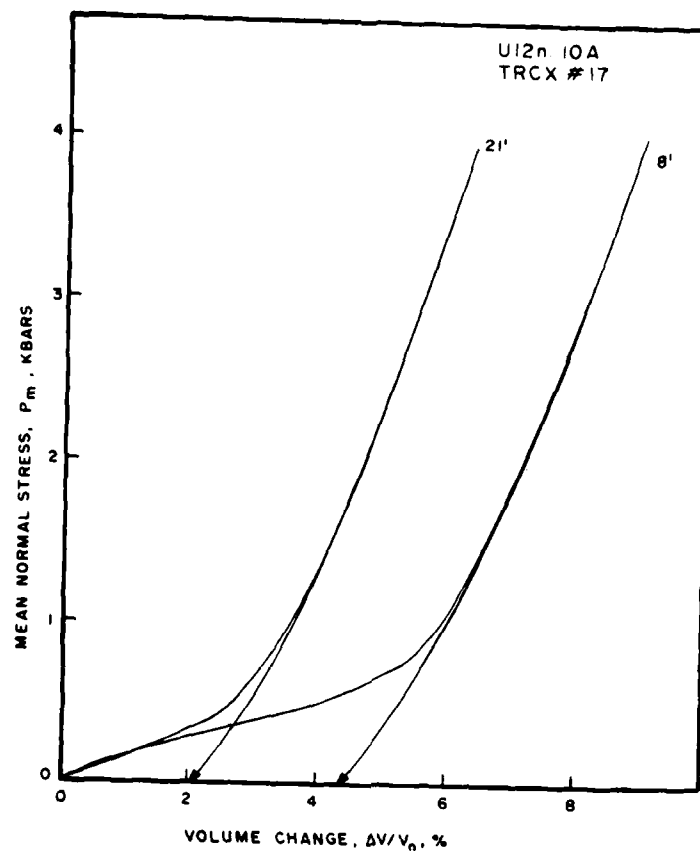stress difference versus confining pressure.

30

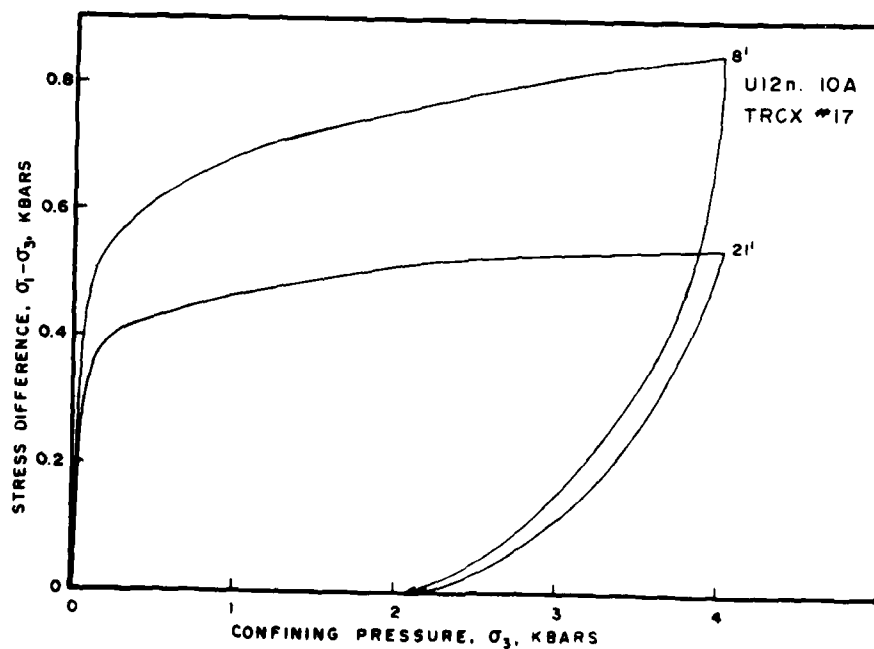Figure 35. Uniaxial strain test to 4 kbars on U12n.10A TRCX#7 tuff -- mean normal stress versus volume change.

Figure 36. Uniaxial strain test to 4 kbars on U12n.10A TRCX#7 tuff -- stress difference versus confining pressure.

Figure 37. Uniaxial strain test to 4 kbars on U12n.10A TRCX#12 tuff --
mean normal stress versus volume change.

Figure 38. Uniaxial strain test to 4 kbars on U12n.10A TRCX#12 tuff --
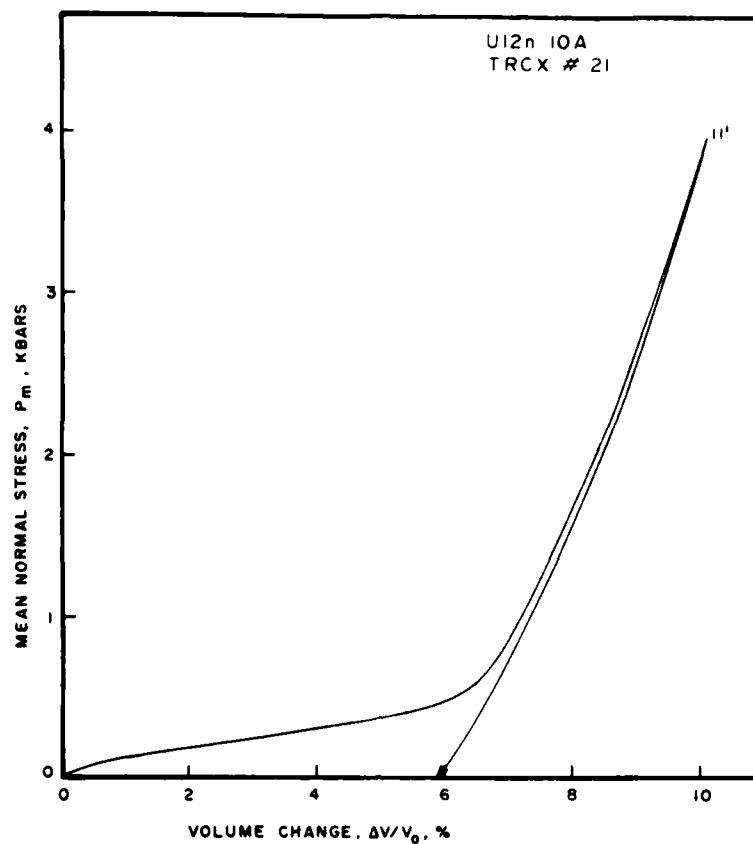stress difference versus confining pressure.

Figure 39. Uniaxial strain test to 4 kbars on U12n.10A TRCX#17 tuff --
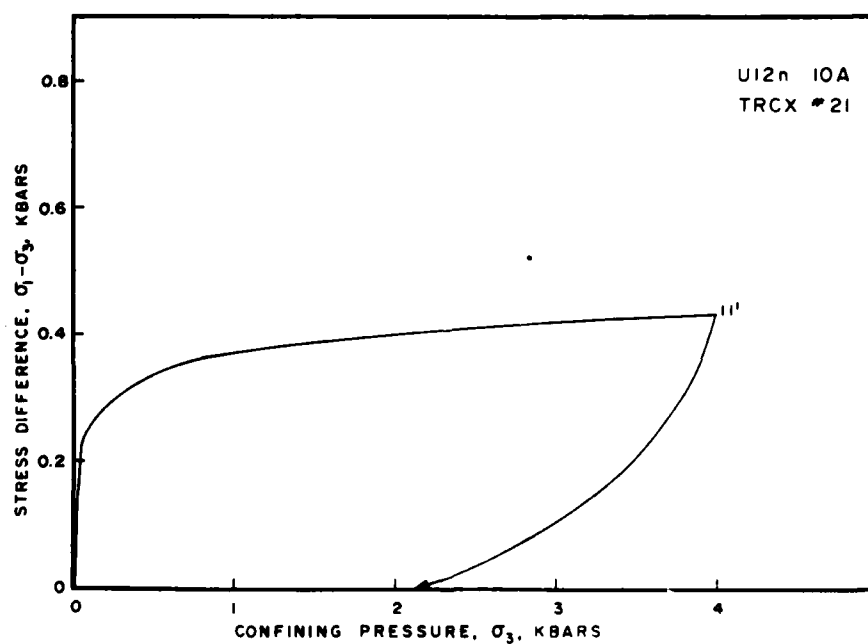mean normal stress versus volume change.

Figure 40. Uniaxial strain test to 4 kbars on U12n.10A TRCX#17 tuff --
stress difference versus confining pressure.

Figure 41.   Uniaxial strain test to 4 kbars on U12n.10A TRCX#21 tuff --
mean normal stress versus volume change.

Figure 42.   Uniaxial strain test to 4 kbars on U12n.10A TRCX#21 tuff --
stress difference versus confining pressure:

34

HIGH PRESSURE MECHANICAL PROPERTIES OF LAPIS LUSTRE SAND

by

D. S. Gardiner
S. W. Butters

35

ABSTRACT

Saturated Lapis Lustre sand will be used in a horizontal sand column to be located near the Diablo Hawk event at the Nevada Test Site. High pressure mechanical properties were determined to provide data for pre-test ground motion calculations. Sand samples at 37 and 40 percent porosities were tested in static hydrostatic compression, triaxial compression and uniaxial strain to 4 kbars confining pressure. Principal stresses and strains as well as pore pressures were measured in both drained and undrained configurations.

Test results indicate that saturated sand observes the "effective stress law". Drained samples (high effective stress) exhibited very high shear strength while undrained samples (low effective stress) exhibited relatively low shear strengths. Increased porosity also results in a reduction in shear strength in undrained sand.

36

TABLE OF CONTENTS

LIST OF ILLUSTRATIONS

LIST OF ILLUSTRATIONS (Continued)

LIST OF ILLUSTRATIONS (Continued)

LIST OF ILLUSTRATIONS (Continued)

INTRODUCTION

An experiment designed to evaluate the response of saturated sand to shock loading is being fielded by the Boeing Company[*]. It involves the placement of a saturated sand in a tunnel extending horizontally from near ground zero in the future Diablo Hawk nuclear test at the Nevada Test Site. Pre-test ground motion calculations will be performed to assist with calibration of instrumentation in and around the sand column and to evaluate shock loading prediction capabilities. These calculations require a material model for the saturated sand. For this reason, laboratory testing was performed on both drained and undrained Lapis Lustre sand.

The possibility existed that the exact conditions of the sand-water mixture might not be measurable or that there would be variations in the conditions as a function of location in the tunnel. Laboratory tests were therefore required to investigate the influence of initial porosities and saturations over the range of values expected in the tunnel. It was also necessary, in evaluating the laboratory's measured properties, to address the effect of sample preparation techniques, aspect ratios and sand gradation.

The actual tunnel sand is expected to range between 37 and 40 percent porosity. Therefore, 37 percent (referred to as Grade A sand in this report) and 40 percent (Grade B) porosities were chosen as initial test

---

* Boeing Company, Seattle, Washington.

porosities. The majority of the tests were conducted on saturated (i.e. 99-100 percent) Grade A sand -- both undrained and drained configurations -- over the confining pressure range of 50 bars to 4 kbars. The Terra Tek test program is shown in Table 1.

TABLE 1

Test Matrix by Figure Number

Initial Test Conditions			Triaxial Compression				Uniaxial Strain	Gradation Analysis
Saturation(%)	Drainage	Porosity(%)	50 Bar	100 Bar	1 KB	4 KB	4 KB	
99-100	Drained	37	Fig. 1,5	Fig. 2,5	Fig. 3,5	Fig. 4,5	Fig. 6	Fig. 13,14
99-100	Undrained	37	Fig. 7,11	Fig. 8,11	Fig. 9,11	Fig. 10,11	Fig. 12	Fig. 15,16
99-100	Undrained	40	--	Fig. 17,19	--	Fig. 18,19	--	--

43

SAMPLE PREPARATION

Sand Composition

Approximately 800 pounds of Lapis Lustre sand was received from DNA Field Command, Nevada Test Site. Five random gradation analyses were performed. Results are listed below in Table 2, along with the gradation analysis of field test sand.

TABLE 2

Gradation Analysis - Lapis Lustre Sand

	Expected Range*	1 %	2 %	3 %	4 %	5 %
Past #16	100	100	100	100	100	100
Past #20	35-45	48	52	52	58	57
Past #30	6-8	9	9	12	14	12
Past #35	--	2	3	4	5	4
Past #40	<1	--	--	--	--	--

* Field test results furnished by Mr. J. W. LaComb, Mercury, Nevada.

Obviously, the test sand contains higher percentages of fine grains than does the field sand. It was therefore decided (by mutual agreement between DNA Field Command and Terra Tek) to sieve the test sand and remix it to a gradation closer to that of the field sand. The resulting test sand gradation was

Past #16	100%
Past #20	40%
Past #30	7%
Past #40	< 1%

Over 99 percent of the sand consisted of clear to milky quartz grains with the remainder being made up of grains containing minor amounts of ferro magnesium minerals. Mean grain density of the sand was found to be 2.625 gm/cc with a standard deviation of 0.009 gm/cc. For determining porosities, the grain density used was 2.625 gm/cc.

A 20.5 inch long, 3.26 inch diameter cylinder was used to form a sand column for determining maximum and minimum obtainable dry densities. Densities obtained ranged from 1.73 gm/cc (34 percent porosity) to 1.52 gm/cc (42 percent porosity). When water was added to the sand column, the high porosities became more difficult to obtain as settlement would readily occur with any slight movement.

Preparation Technique

Method 1 - Samples were prepared by wrapping and sealing a 18 mil thick polyurethane jacket to two 2-inch diameter steel endcaps spaced 2.5 inches apart. The upper endcap had a hole through which the sand was poured while the lower endcap housed the pore pressure transducer. Knowing the sample volume, a predetermined amount of sand was funnelled in through the upper endcap. A computed amount of water, based on the desired saturation, was then added and a plug was placed in the top hole. After emplacement of axial and transverse strain cantilevers, the sample was inserted into the pressure vessel and tested. All test samples were prepared via this method unless specifically stated otherwise.

It should be noted that this sample preparation method resulted in some sand settlement during placement of the water and during handling prior to testing. That is, the sand matrix settled to slightly below

the upper endcap (to approximately 34 percent porosity), leaving a small layer of water on top. As discussed later in this report, this water layer had no significant effects on the mechanical properties and the samples prepared are representative of the 37 and 40 percent porosities (based on the ratios of water to sand).

Method 2 - This method of sample preparation was used to investigate the effects of the above mentioned top water layer. It is basically the same as Method 1, except to a 4-inch length. Also, cantilevers were mounted and the sample assembly was placed in the pressure vessel before the water was added. These modifications minimized sample movement and sand settlement was controlled so contact was maintained between the upper endcap and the sand matrix. Porosities of 37 and 40 percent with no top water layer were obtainable via this method.

Method 3 - A third method used a back pressure saturation technique to investigate the effects of different saturation methods. Rather than adding a computed amount of water as in Methods 1 and 2, water was added to the point where incremental increases in confining pressure ($\Delta\sigma_3$) caused equivalent incremental increases in pore pressure ($\Delta\sigma_p$). When the ratio of these incremental changes (B factor) was equal to or greater than 0.96, the sample was said to be fully saturated[1]. That is:

$$B = \frac{\Delta\sigma_p}{\Delta\sigma_3} > 0.96 = \text{fully saturated state.}$$

A 5 psi effective mean normal stress was maintained during this saturation process to inhibit grain settlement. It was found that samples

reached saturation at approximately 20 ps   ng pressure. After

saturation was obtained, no water movement   mitted, and hydrostatic

compression was started. The volume strair   y this saturation process

was negligible and the upper endcap remained in contact with the sand.

Drained Tests (Grade A)

Hydrostatic Compression - Pressure-volume response for the drained Grade A sand during hydrostatic compression is shown in Figures 1 through 4 for 0.05, 0.1, 1.0 and 4.0 kbars confining pressures, respectively. Larger individual plots are shown in the Appendix. Volume strain ranged from approximately 3 percent at 0.05 kbars to 27 percent at 4.0 kbars confining pressure. Volume strains shown are determined from the axial and transverse strains (i.e. $\Delta V/V_0 = \varepsilon_A + 2\varepsilon_T$). The large volume strains observed during hydrostatic compression are attributed to pore water migration from the sample. Actual grain breakdown (see Figure 13) also contributes to the volume decrease as higher confining pressures are applied.

Triaxial Compression - Shear response during triaxial compression for Grade A sand is also shown in Figures 1 through 4 for 0.05, 0.1, 1.0 and 4.0 kbars confining pressures. Volumetric strain during shear is attached to the top of the hydrostatic compression curves. Again, more detailed individual graphs are shown in the Appendix.

Failure points at these confining pressures are shown in Figure 5 as stress difference values taken at 15 percent axial strain during the triaxial compression. The failure curve is plotted using both engineering stress (based on initial cross-sectional area) and true stress (based on cross-sectional area taken at 15 percent axial strain).

Test data shows increased shear strength and matrix stiffness with increased confining pressure. The pore pressure for these tests is zero,

Figure 1. Hydrostatic and triaxial compression test curves for drained Grade A Lapis Lustre sand.
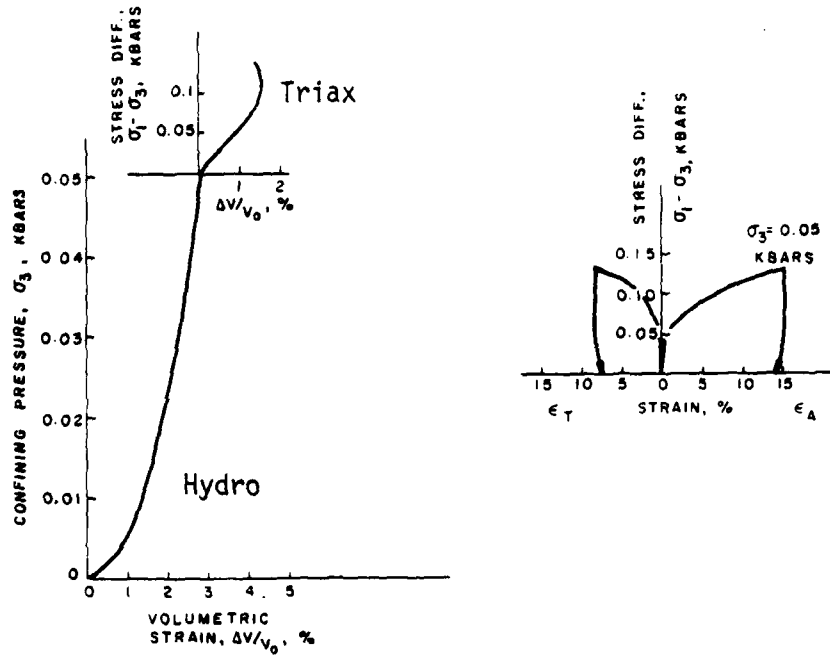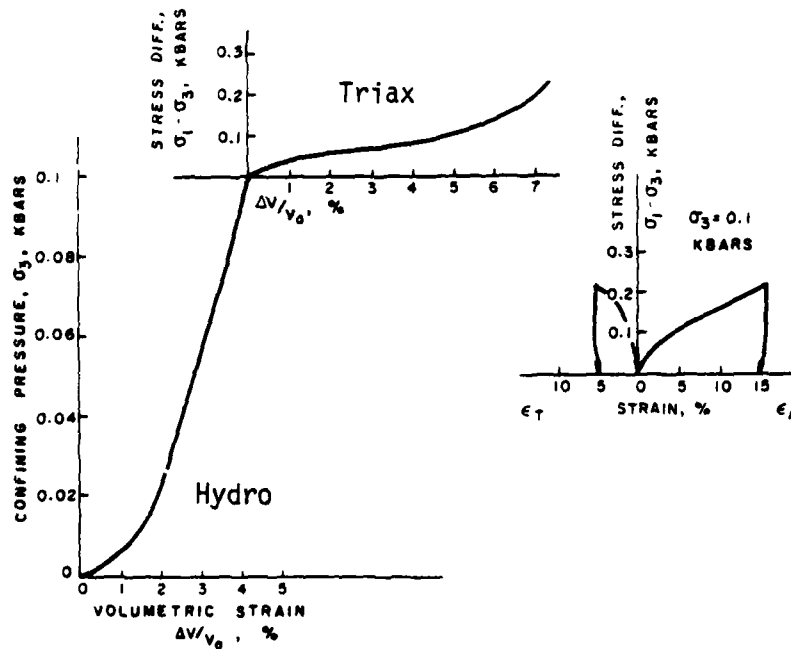

Figure 2. Hydrostatic and triaxial compression test curves for drained Grade A Lapis Lustre sand.
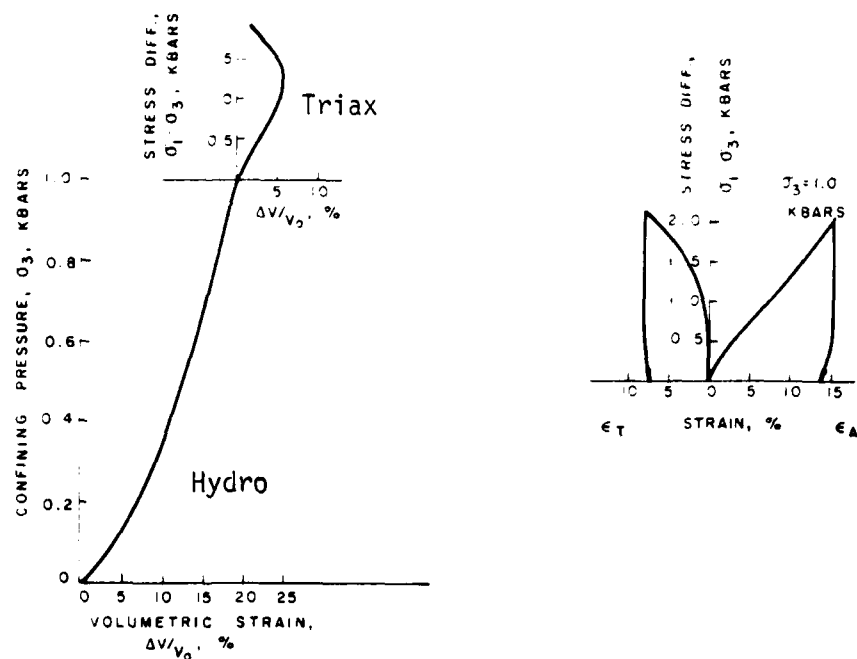
Figure 3.   Hydrostatic and triaxial compression test curves for
            drained Grade A Lapis Lustre sand.
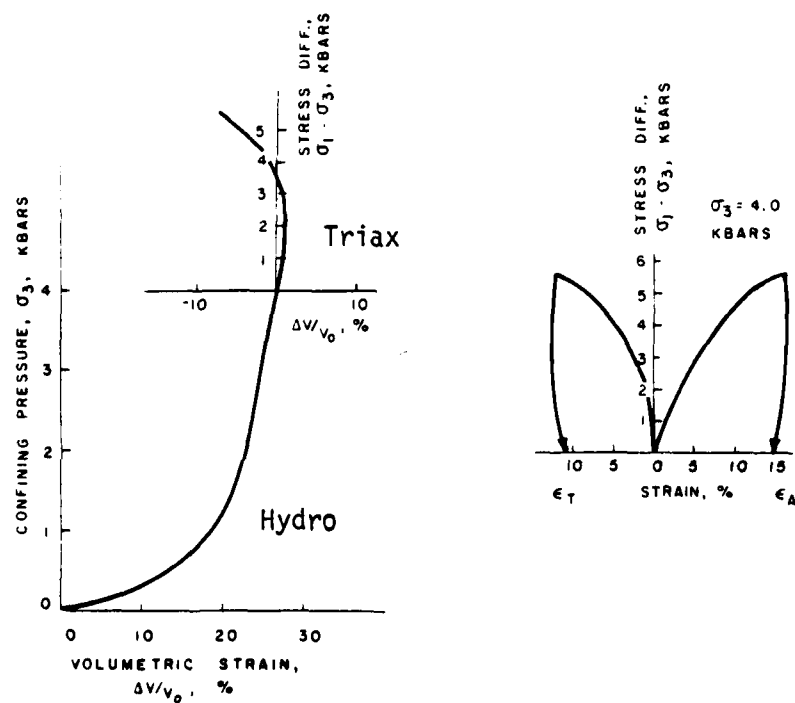

Figure 4.   Hydrostatic and triaxial compression test curves for
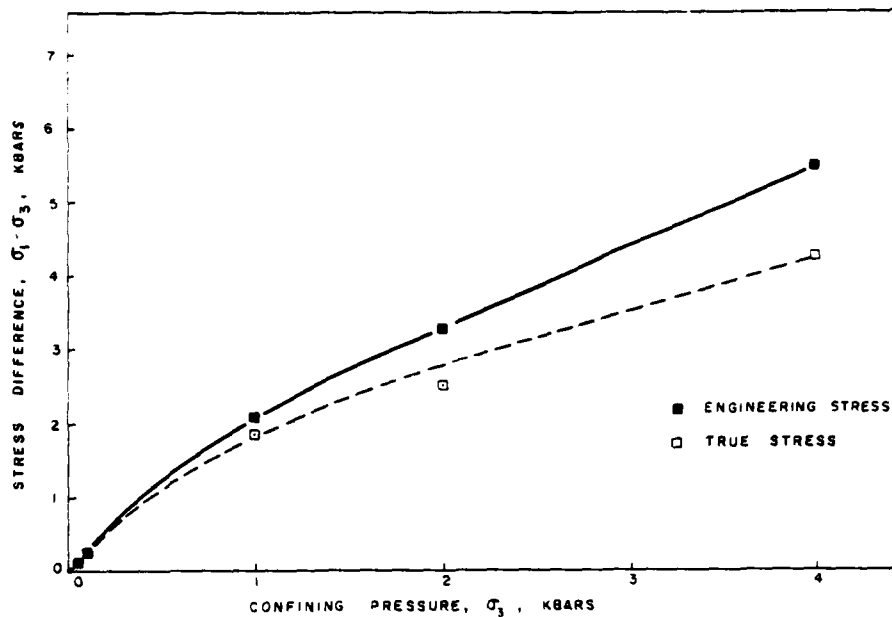   drained Grade A Lapis Lustre sand.

Figure 5. Triaxial compression stress difference values at 15 percent axial strain for drained Grade A sand.

therefore, the effective stress and confining pressure are equal at all times. The shear strength is a function of effective stress and hence the expected strength increase with increasing confining pressure.

Volume change during shear showed some initial compaction followed by dilatancy (volume increase). Exact magnitudes of compaction and dilation, however, are questionable because the large axial and transverse strains resulted in slight barreling which led to erroneous volume strains. The trend toward dilatancy however is clear and substantiates work done by other investigators[2]. It should be noted, however, that even with dilation, the sample volume does not surpass that of the initial pre-hydrostatic volume.

Uniaxial Strain - The uniaxial strain test for drained Grade A sand is shown in Figures 6a and 6b as mean normal stress versus volumetric strain

51

and stress difference versus confining pressure. Test results show shear strength increasing with confining pressure. Volume strains are large (over 20 percent at 3 kbars mean normal stress) and measured permanent compaction is high. High volume strains result from water drainage, compaction, as well as grain breakdown (see Figure 14) at the higher stress states.
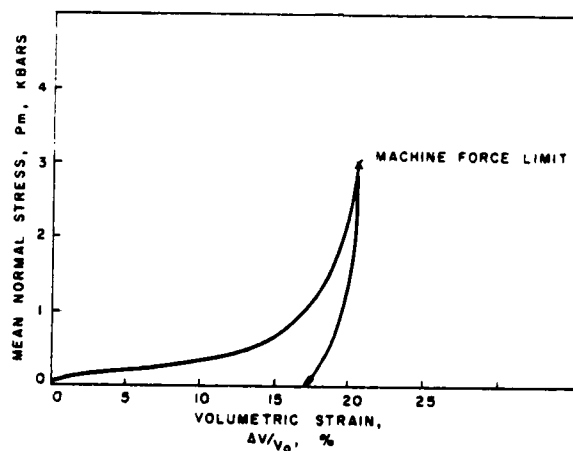

Figure 6a.   Uniaxial strain test on drained Grade A Lapis Lustre sand -- mean normal stress versus volumetric strain.
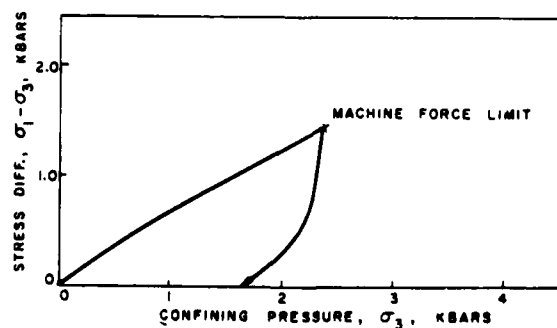

Figure 6b.   Uniaxial strain test on drained Grade A Lapis Lustre sand -- stress difference versus confining pressure.

Undrained Tests (Grade A)

Hydrostatic Compression - Hydrostatic pressure-volume response for
the undrained Grade A sand is shown in Figures 7 through 10 for confining
pressures to 0.05, 0.1, 1.0 and 4.0 kbars (more detailed test curves are
shown in the Appendix). Volume strains range from approximately 0.2 per-
cent at 0.05 kbars to 3.5 percent at 4.0 kbars.

Undrained saturated sand is an inelastic two-phase medium composed
of pore water and a solid skeleton of sand grains. Volumetric strain
during hydrostatic compression therefore is primarily a measure of the
water compressibility (individual grain compressibility is negligibly
small)[3]. The volume strain is significantly less than that of drained
sand since the pore water supports the bulk of the hydrostatic stress.
This is substantiated by the fact that the pore pressure equaled the con-
fining pressure during the hydrostatic compression.

Triaxial Compression - Triaxial compression test results at 0.05,
0.1, 1.0 and 4.0 kbars confining pressures for Grade A sand samples are
also shown in Figures 7 through 10. The state of zero strain for these
curves is the top of the hydrostatic compression. Both axial and trans-
verse strains were measured. Samples exhibited immediate barreling re-
quiring that volume change be computed using the pore pressure measure-
ment. An explanation of this method of volumetric strain determination
is given later. Figures 7 through 10 also show the pore pressure measure-
ments and the computed volumetric strains for each triaxial compression
test. The negative pore pressure changes shown on the plots represent
a decrease in the pore pressure during the shearing portion of the test
(i.e. while confining pressure is constant). Figure 11 shows the maximum
stress at each confining pressure in both engineering and true stress.
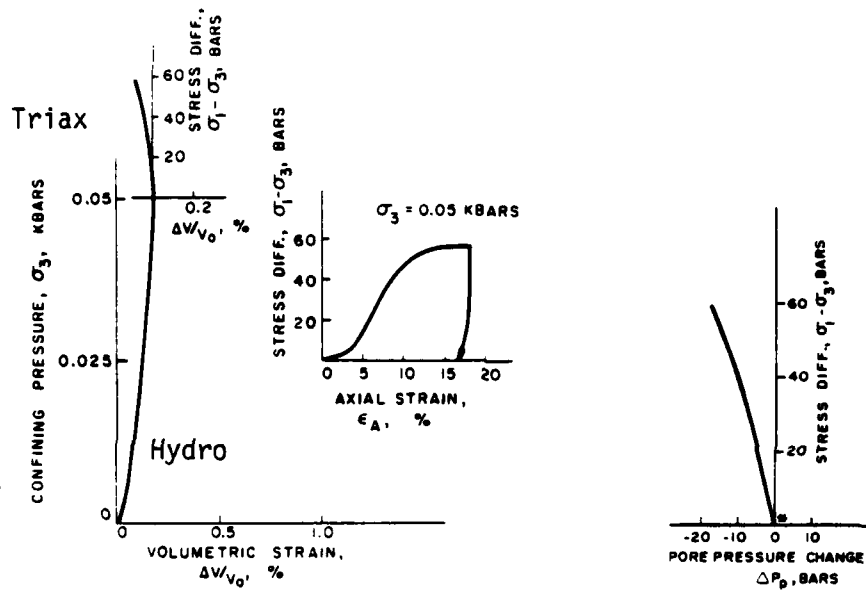
53

Figure 7. Hydrostatic and triaxial compression test curves for undrained Grade A Lapis Lustre sand. *See explanation on page 12.
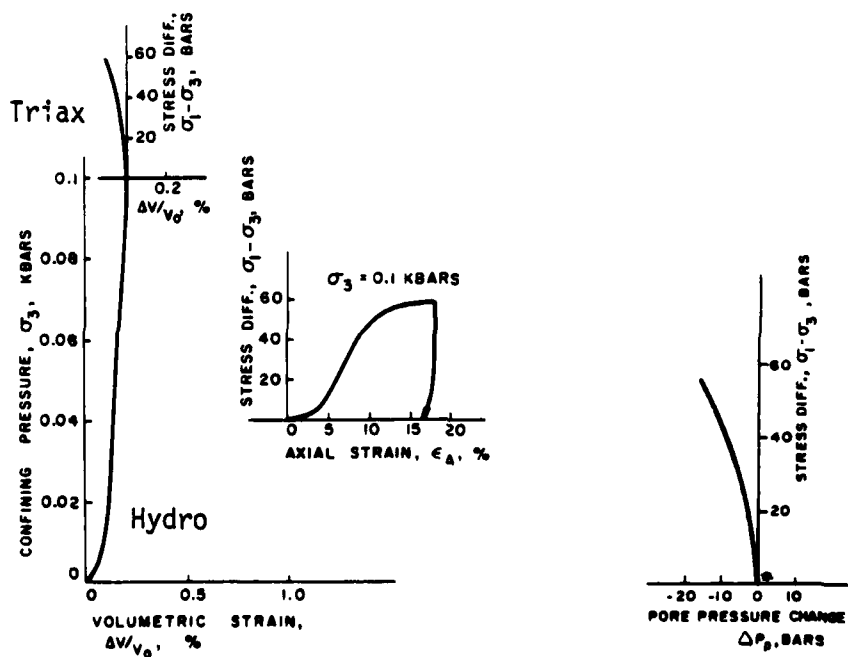

Figure 8. Hydrostatic and triaxial compression test curves for undrained Grade A Lapis Lustre sand. *See explanation on page 12.
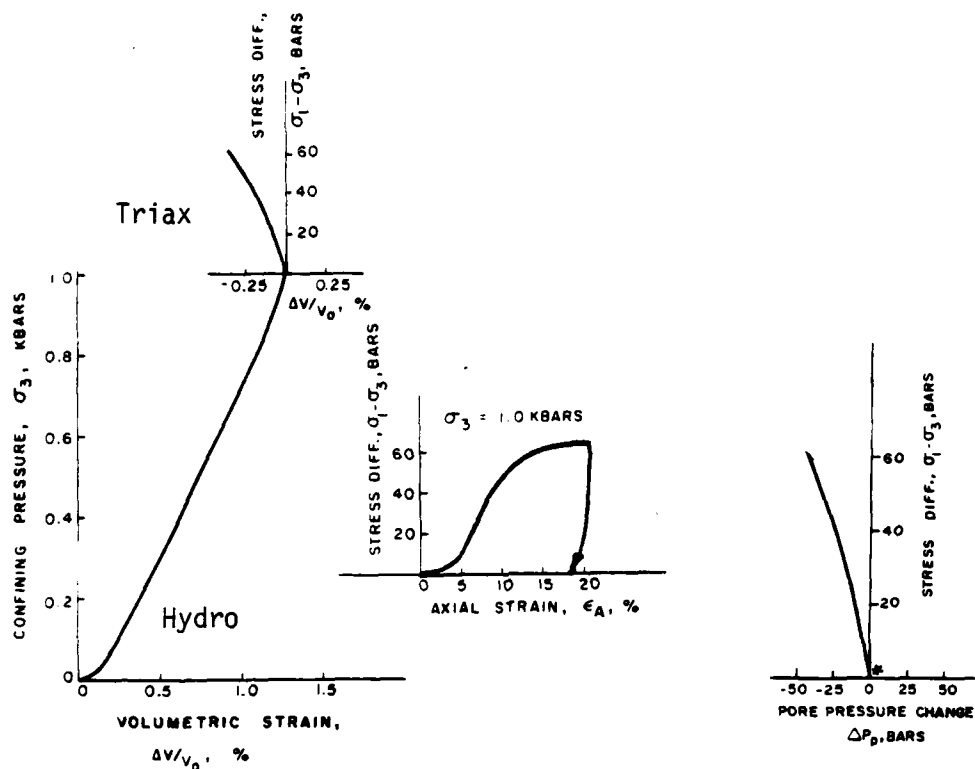
Figure 9. Hydrostatic and triaxial compression test curves for undrained Grade A Lapis Lustre sand. *See explanation on page 12.
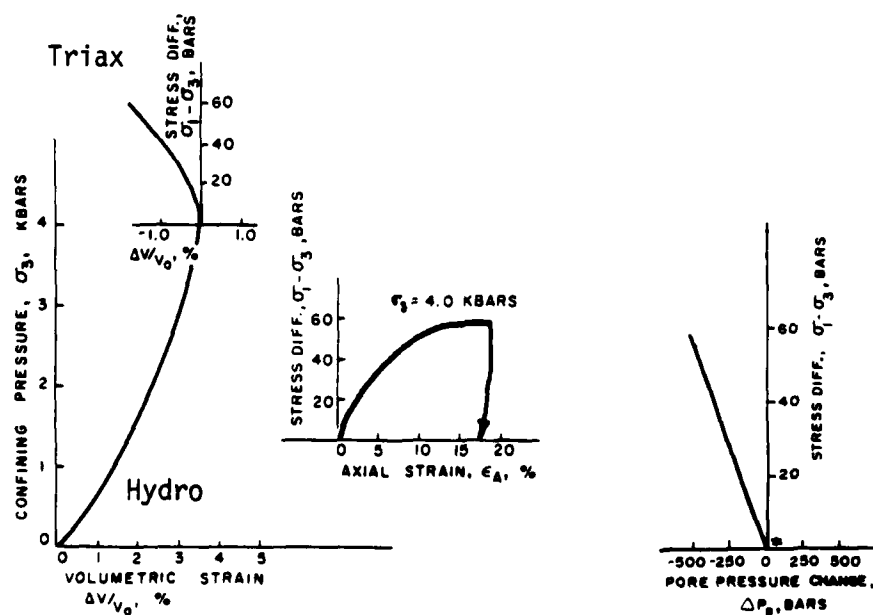

Figure 10. Hydrostatic and triaxial compression test curves for undrained Grade A Lapis Lustre sand. *See explanation on page 12.
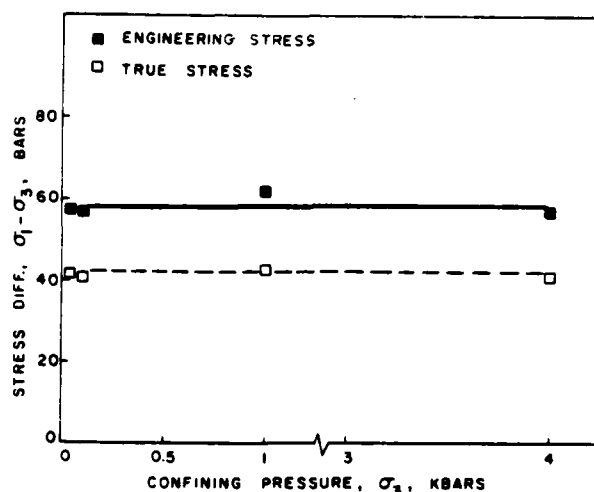
Figure 11. Triaxial compression failure (maximum stress difference) for undrained Grade A Lapis Lustre sand.

As deviatoric stress is applied to the sand skeleton, dilation with an accompanying decrease in pore pressure occurs. The volume increase associated with dilation allows grain movement toward less dense grain configurations (higher porosities) thus tending to reduce shear strength. At the same time, reduced pore pressure increases the effective stress on the sand matrix tending to increase shear strength. Apparently these two effects are off setting, however, as evidenced by the "flat" failure surface shown in Figure 11.

As mentioned earlier, dilation occurred with the application of deviatoric stress. Exact magnitude of the dilation could not be measured directly due to sample barreling. Volumetric strain was therefore determined indirectly from the pore pressure measurement. It was reasoned that since a triaxial compression test was constant confining pressure (i.e. constant compressibility), any pore pressure change must represent a pore volume change. This change would be a function of the compressibility of the pore water. This relationship is linear (insofar as the compressibility term is constant) as seen by the equation

56

$$\frac{\Delta V}{V_o} = \beta \; \Delta P.$$

ΔV = Volume Change

V_o = Initial Volume

β = Pore Fluid Compressibility

ΔP = Pressure change

All volumetric strain data for undrained samples was computed using this relationship.

Uniaxial Strain - Uniaxial strain test results on undrained Grade A sand are shown in Figures 12a and 12b. Results are shown as mean normal stress versus volumetric strain and stress difference versus confining pressure. Test results indicate that maximum stress difference is very low, on the order of 5-10 bars. The stress difference does increase somewhat at around 2 kbars confining pressure (see Figure 12b). Although not completely understood, it is thought that at this point the sand grains begin supporting a portion of the confining stress resulting in added shear strength capacity. Only after the sand grains have reached maximum density, however, would a significant increase in stress difference be expected.

Volume strains during uniaxial strain are small (4-6 percent range) when compared to the drained uniaxial tests, again showing the restraining role of pore water.

Post-Test Gradation Analysis

Post-test gradation analysis tests were conducted to determine the effect of different stress states on sand grain response. Drained test sand showed significant grain breakdown through 4 kbars confining pressures (Figures 13 and 14) while undrained test sand showed no measurable grain breakdown (Figures 15 and 16). The dashed lines indicate the pre-test sample gradation.
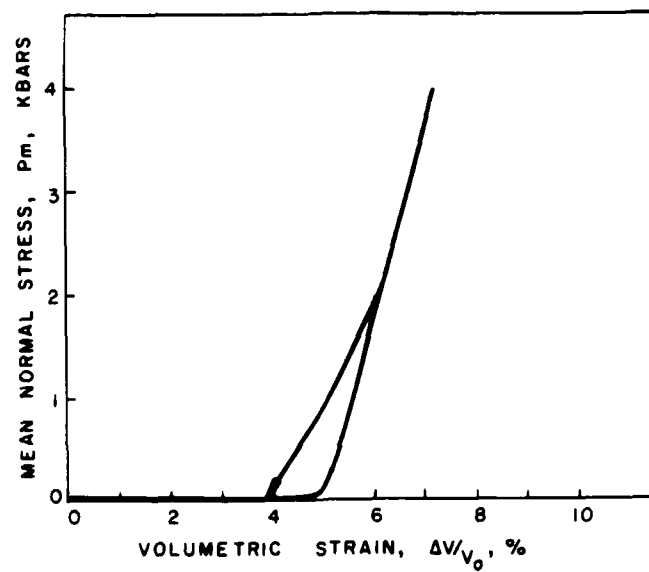
Figure 12a. Uniaxial strain test to 4.0 kbars confining pressure on
undrained Grade A Lapis Lustre sand -- mean normal stress
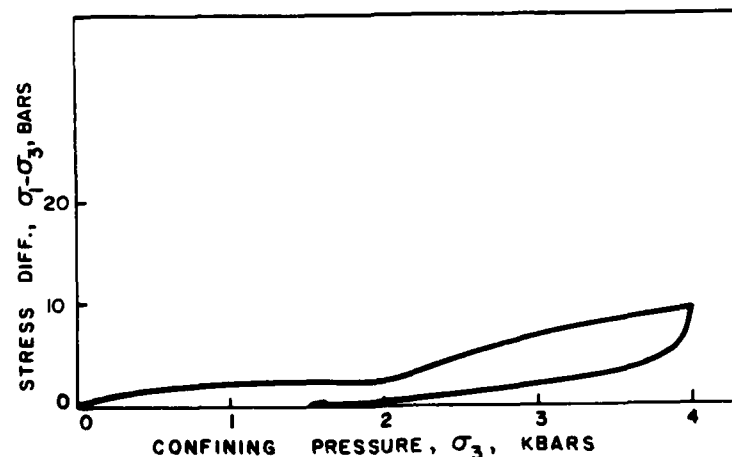versus volumetric strain.

Figure 12b. Uniaxial strain test to 4.0 kbars confining pressure on
undrained Grade A Lapis Lustre sand -- stress difference
versus confining pressure.

58

Figure 13. Gradation analysis of Grade A Lapis Lustre sand after drained 4.0 kbar hydrostatic compression test.
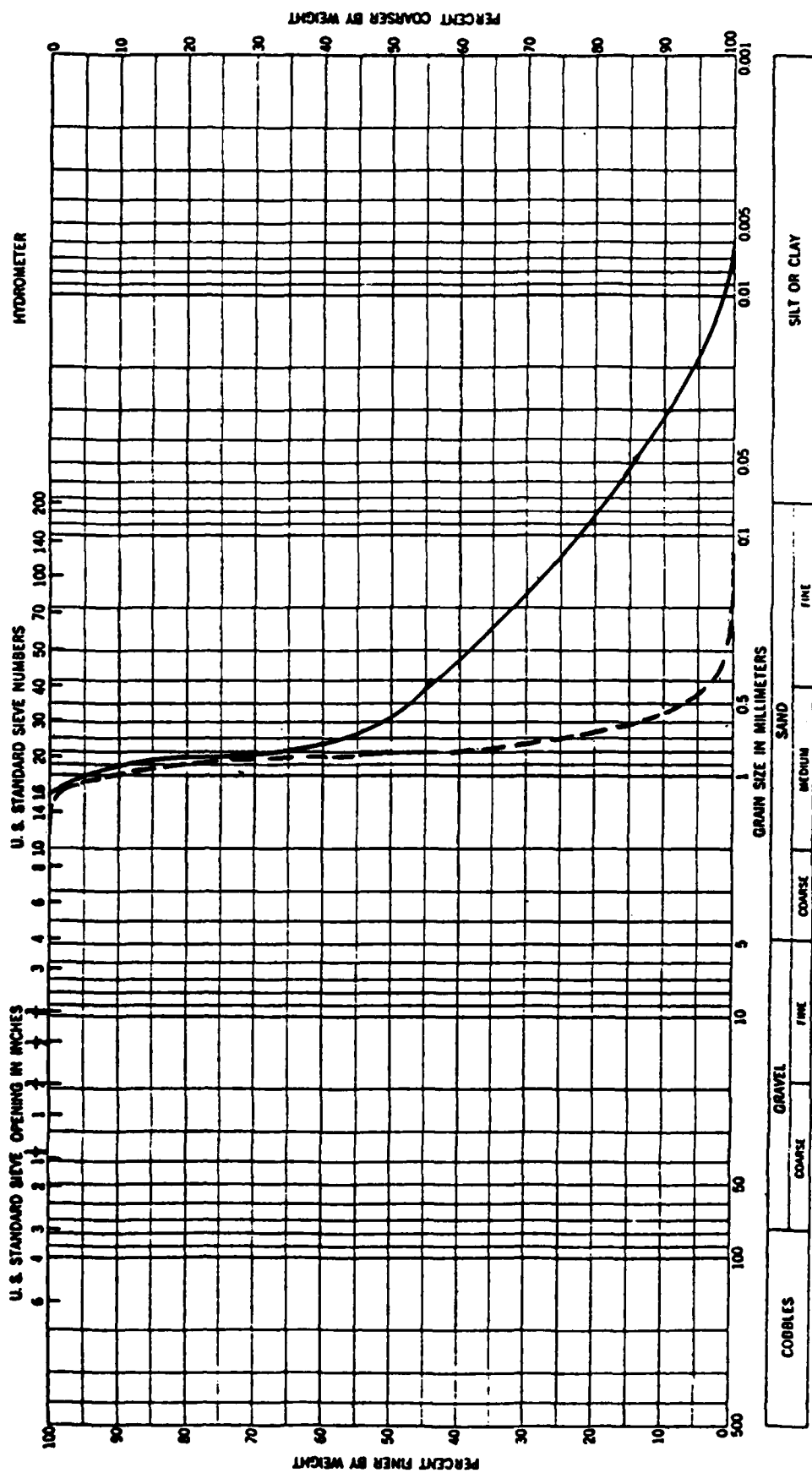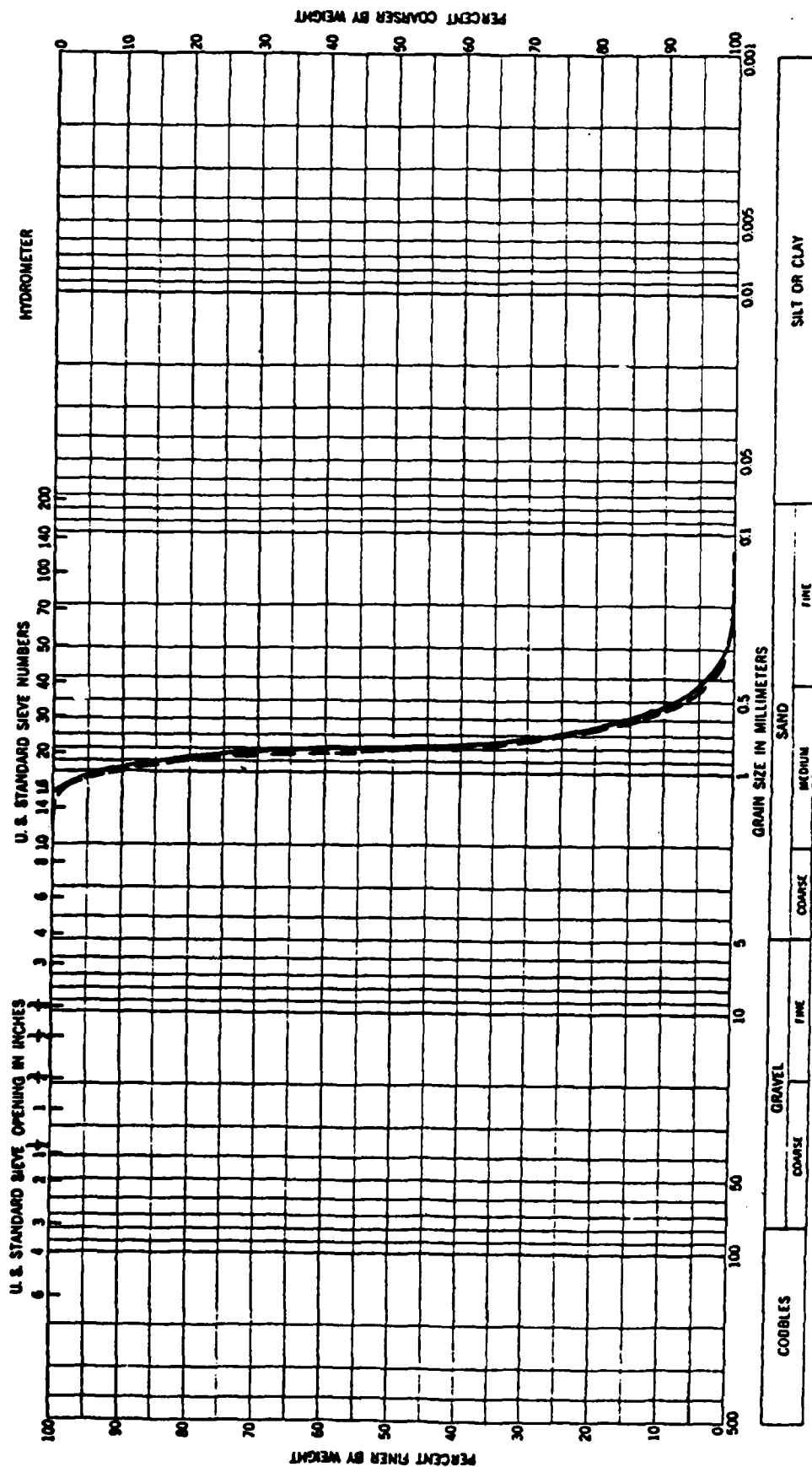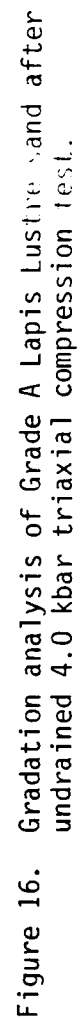
59

Figure 14. Gradation analysis of Grade A Lapis Lustre sand after drained 4.0 kbar uniaxial strain test.

Figure 15. Gradation analysis of Grade A Lapis Lustre sand after undrained 0.1 kbar triaxial compression test.

Figure 16. Gradation analysis of Grade A Lapis Lustre sand before and after undrained 4.0 kbar triaxial compression test.

Undrained Tests (Grade B)

Grade B sand (40 percent porosity) was tested at 0.1 and 4.0 kbars confining pressures in triaxial compression to observe the effects of higher porosity. Stress-strain curves for these tests are shown in Figures 17 and 18. Figure 19 shows the triaxial compression failure points for comparison with Grade A sand.

The general form of the curves appear to be similar to those of Grade A sand however the maximum stress difference is some 20 percent lower. This reduction in shear strength is not unexpected.
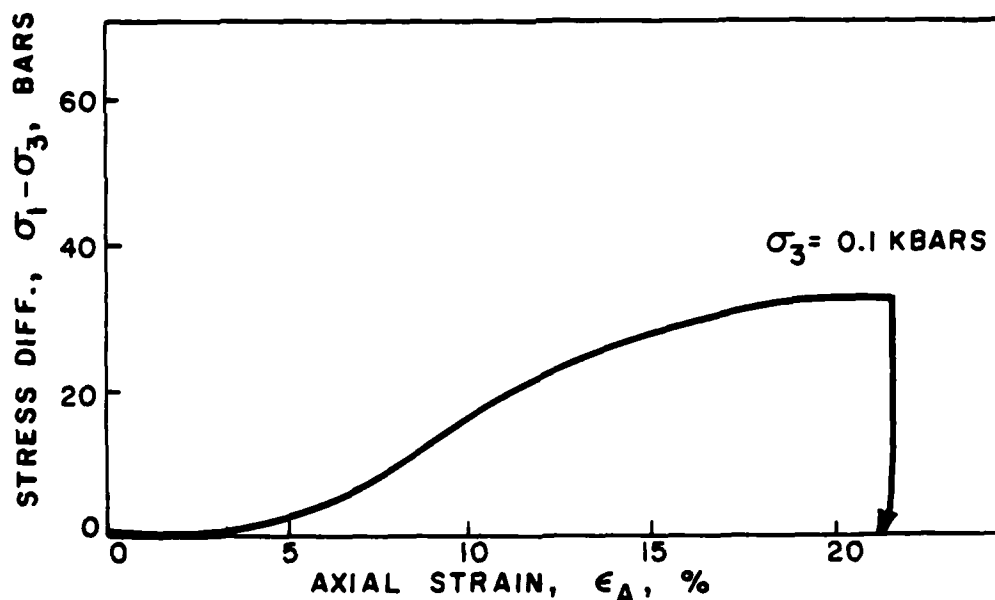

Figure 17. Triaxial compression test on undrained Grade B Lapis Lustre sand. Sample preparation Method II.
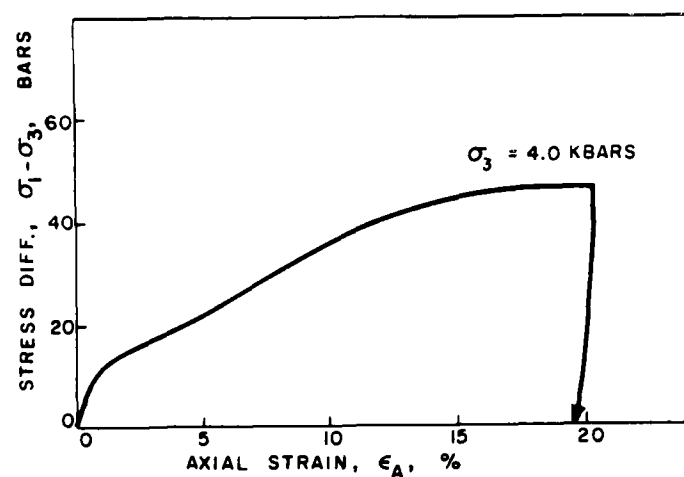
Figure 18. Triaxial compression test on undrained Grade B Lapis Lustre sand. Sample preparation Method II.
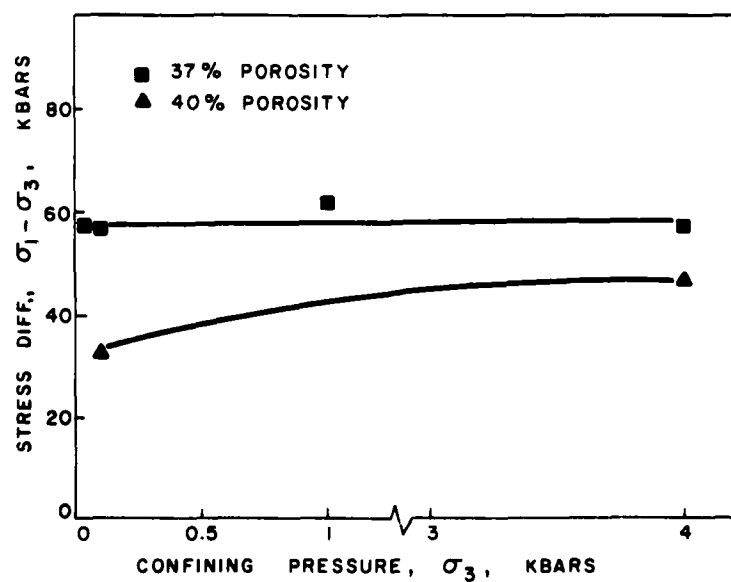

Figure 19. Comparison of triaxial compression failure envelopes for undrained Grade A and B Lapis Lustre sand.

64

Tests Investigating the Effects of Different Initial Conditions

Sand Settlement - Two samples, one prepared via Method I (excess water layer on top) and the other prepared via Method II (no excess water) were tested in hydrostatic and triaxial compression at the same confining pressures to evaluate the effects of sand settlement. Test results are shown in Figure 20. Results show that the curves are virtually the same (within experimental scatter) with no significant difference in volumetric strain or stress-strain response.

Aspect Ratio - Sample preparation Method I used an aspect ratio of 1.25 (i.e. diameter to length ratio). Tests conducted at a ratio of 2 indicated no difference between the two sample mechanical properties.

Back Pressure Saturation - Samples saturated using the back pressure method (Method III) were tested at 0.1 and 4.0 kbars for comparison with previous (Method I) tests. Results are shown in Figures 21 and 22 for both hydrostatic and triaxial compression. Again, no significant differences are apparent.
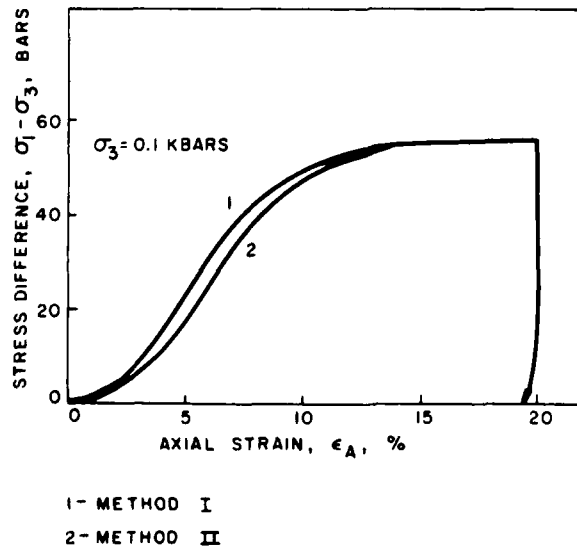

1- METHOD I
2- METHOD II

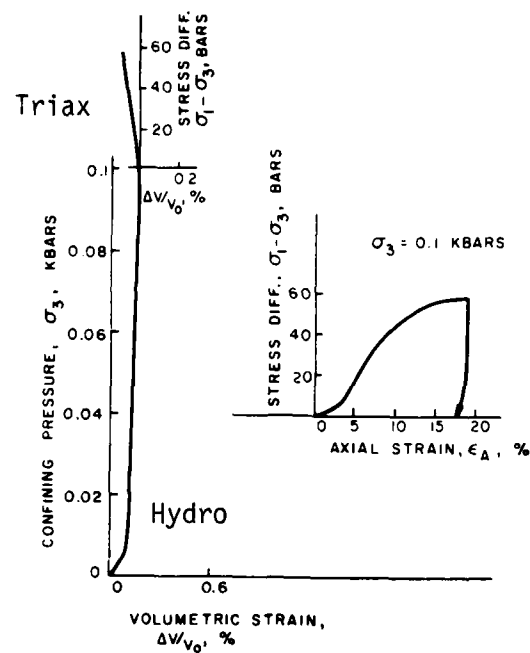Figure 20. Comparison of sand settlement effects on undrained sand response.

65

Figure 21. Hydrostatic and triaxial compression test curves for back pressure saturated sample (Method III).
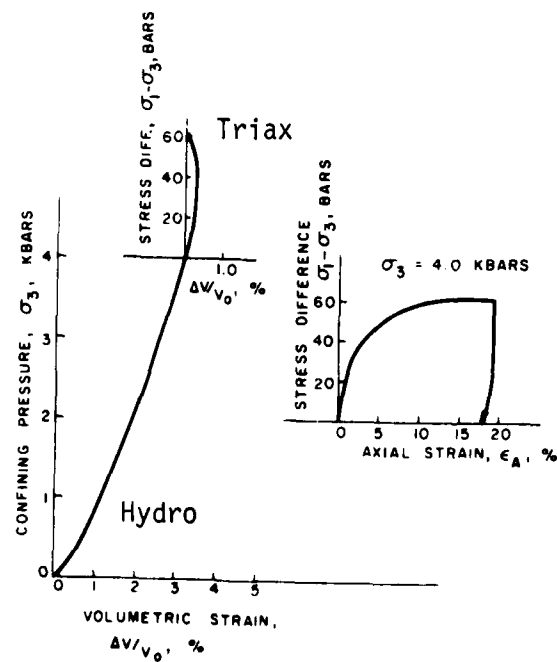

Figure 22. Hydrostatic and triaxial compression test curves for back pressure saturated sample (Method III).

CONCLUSIONS

The intent of the test program has been to determine the mechanical properties of saturated sand. Within the content of this study, the following conclusions can be made.

Test Conditions:

- For drained sand, shear strength increases with increased confining pressure.

- For undrained sand, shear strength remains independent of confining pressure (i.e. the failure curve is "flat").

Porosity:

- The higher porosity samples (i.e. 40 percent) showed a lower shear strength than the 37 percent porosity samples over the complete confining pressure range.

Dilation:

- Volume dilation resulting from the application of deviatoric stress is less than the volume compaction observed during hydrostatic compression over the range tested.

Sample Preparation:

- The various sample preparation techniques did not change pressure-volume or shear response.

REFERENCES

1. Block, D. K., and Lee, K. N., "Saturating Laboratory Samples by Back Pressure," Journal of the Soil Mechanics and Foundations Division ASCE, No. SMI, pp. 76-93, January 1973.

2. Sadasivan, S. K., and Raju, V. S., "Shear Strength of Sand at Constant Volume," Journal of Testing and Evaluation, JTEVA, Vol. 5, No. 3, pp. 224-230, May 1977.

3. Bazant, Z. P., and Krizek, R. J., "Saturated Sand as an Inelastic Two-Phase Medium," Journal of the Engineering Mechanics Division, Proceedings of the American Society of Civil Engineers, Vol. 101, No. EM4, pp. 317-332, August 1975.
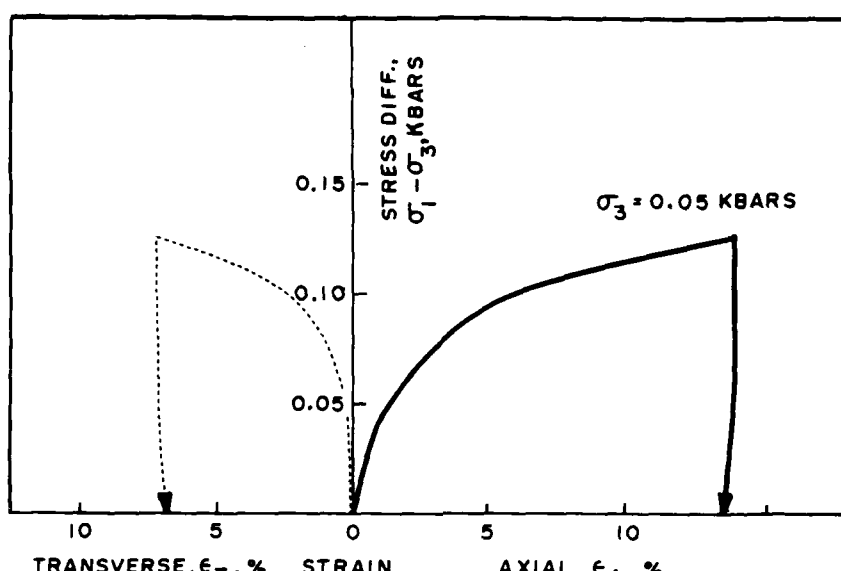
Figure A1. Triaxial compression stress-strain curve for drained
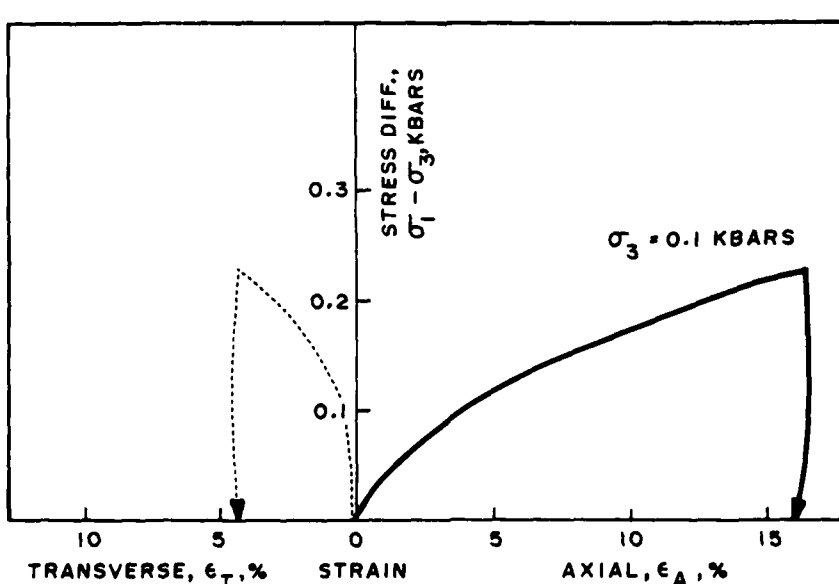Grade A Lapis Lustre sand at 0.05 kbars confining
pressure.

Figure A2. Triaxial compression stress-strain curve for drained
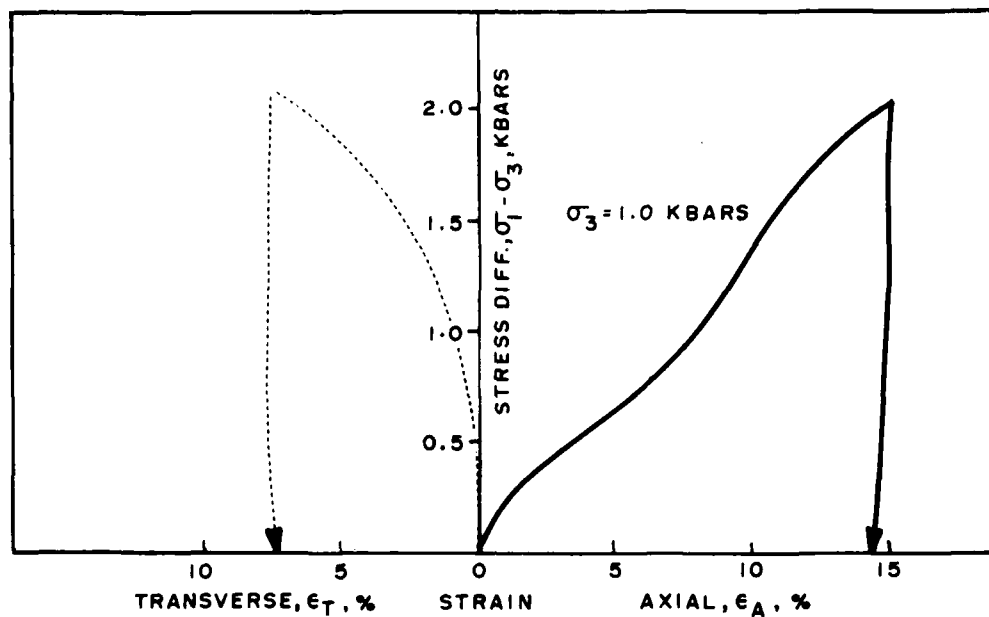Grade A Lapis Lustre sand at 0.1 kbars confining pres-
sure.

Figure A3.   Triaxial compression stress-strain curve for drained
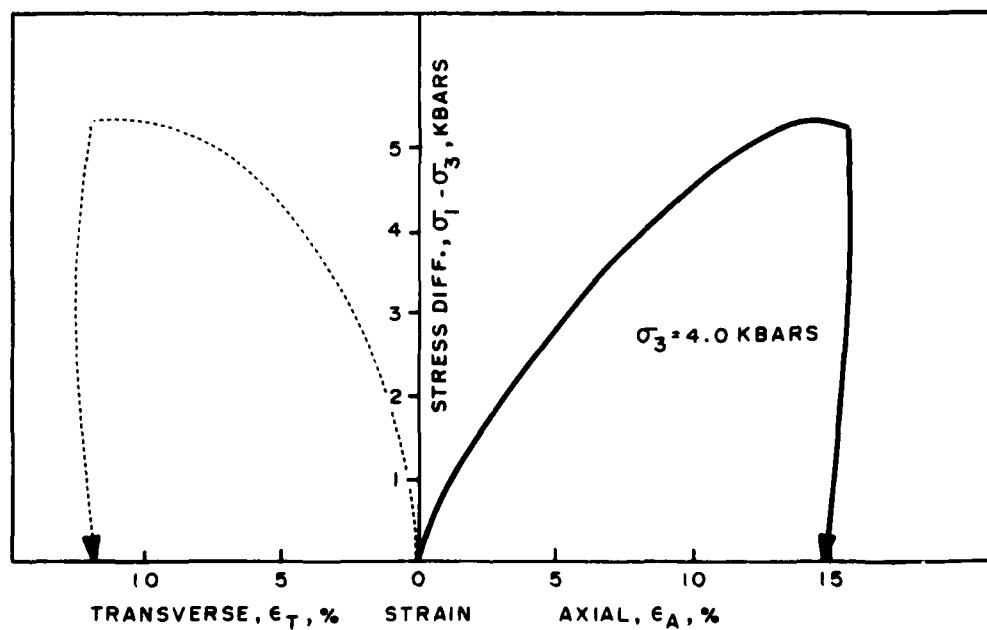   Grade A Lapis Lustre sand at 1.0 kbars confining pres-
            sure.

Figure A4.   Triaxial compression stress-strain curve for drained
            Grade A Lapis Lustre sand at 4.0 kbars confining pres-
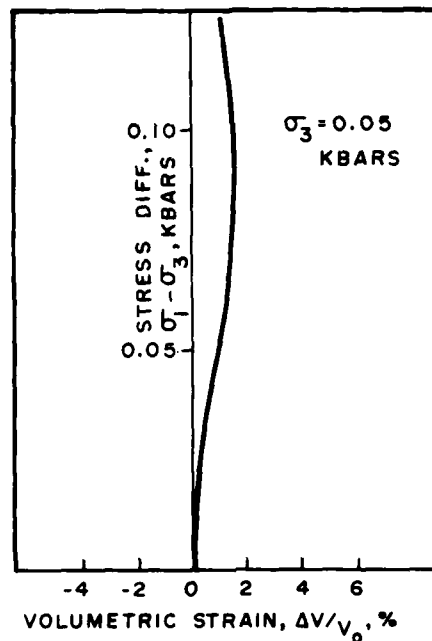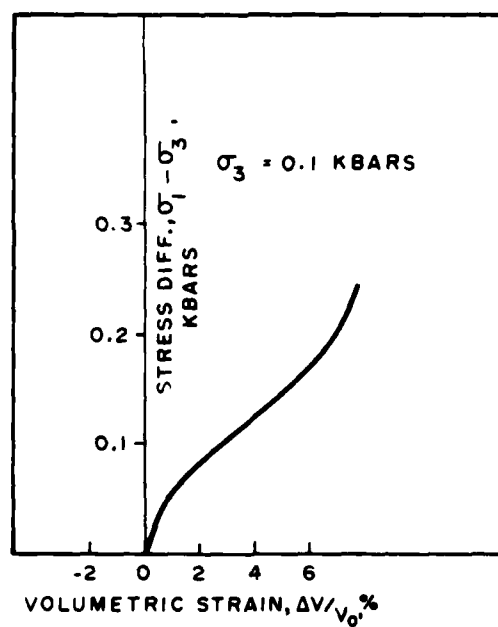   sure.

70

Figure A5. Volumetric strain during triaxial compression for drained Grade A Lapis Lustre sand at 0.05 kbars confining pressure.

Figure A6. Volumetric strain during triaxial compression for drained Grade A Lapis Lustre sand at 0.1 kbars confining pressure.
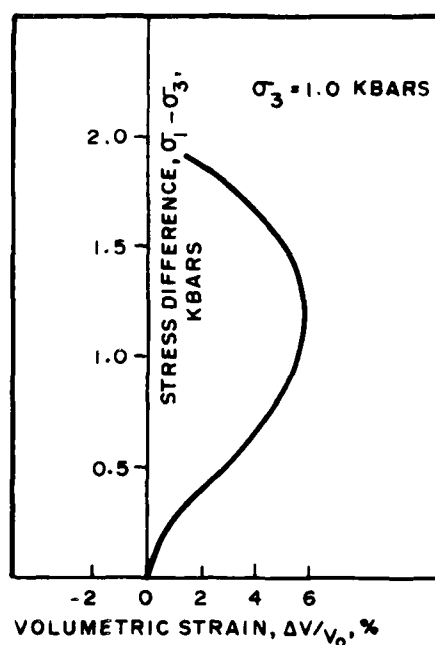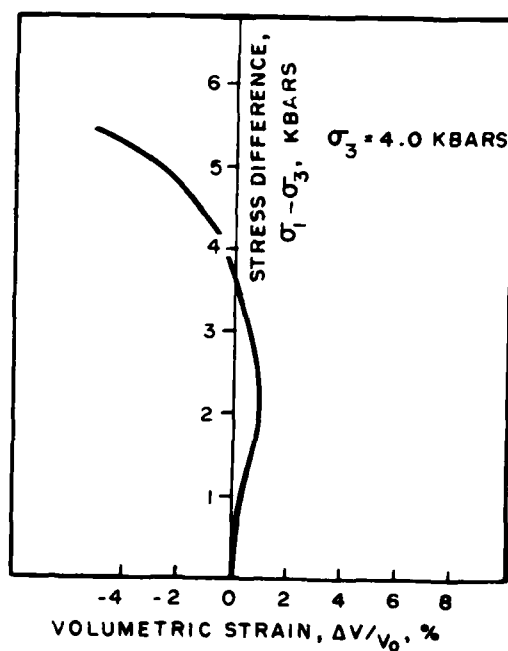
71

Figure A7. Volumetric strain during triaxial compression for
drained Grade A Lapis Lustre sand at 1.0 kbars
confining pressure.

Figure A8. Volumetric strain during triaxial compression for
drained Grade A Lapis Lustre sand at 4.0 kbars
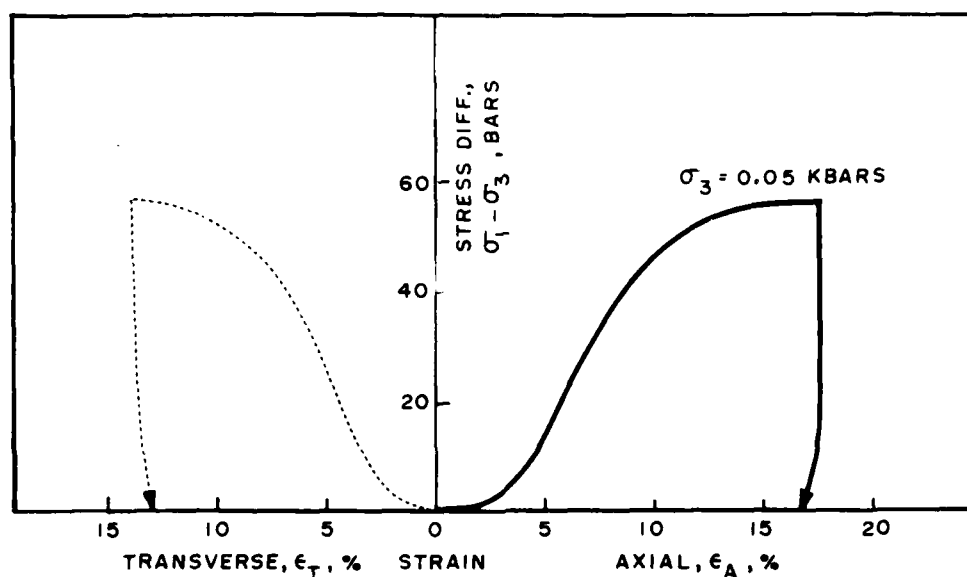confining pressure.

Figure A9. Triaxial compression stress-strain curve for undrained Grade A Lapis Lustre sand at 0.05 kbars confining pressure.
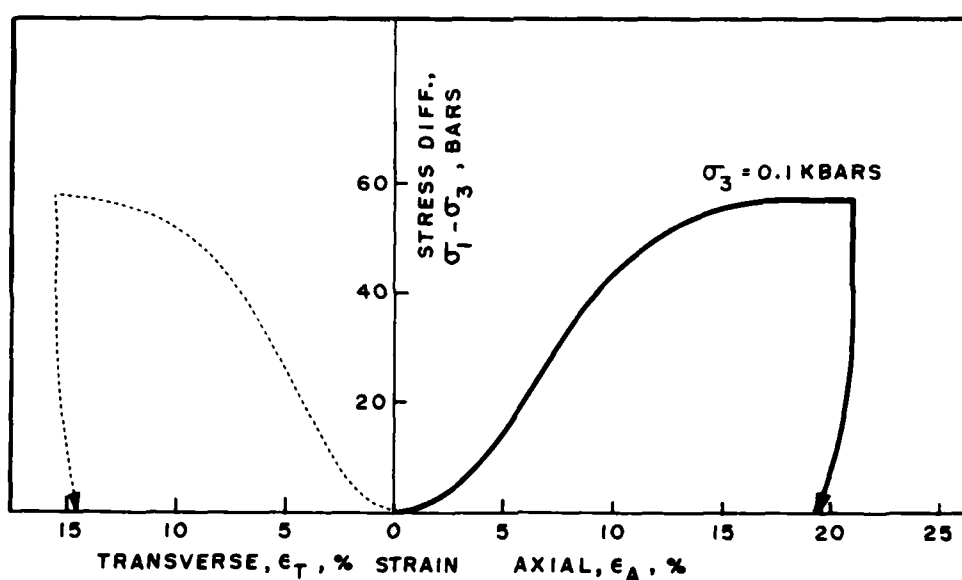

Figure A10. Triaxial compression stress-strain curve for undrained Grade A Lapis Lustre sand at 0.1 kbars confining pressure.
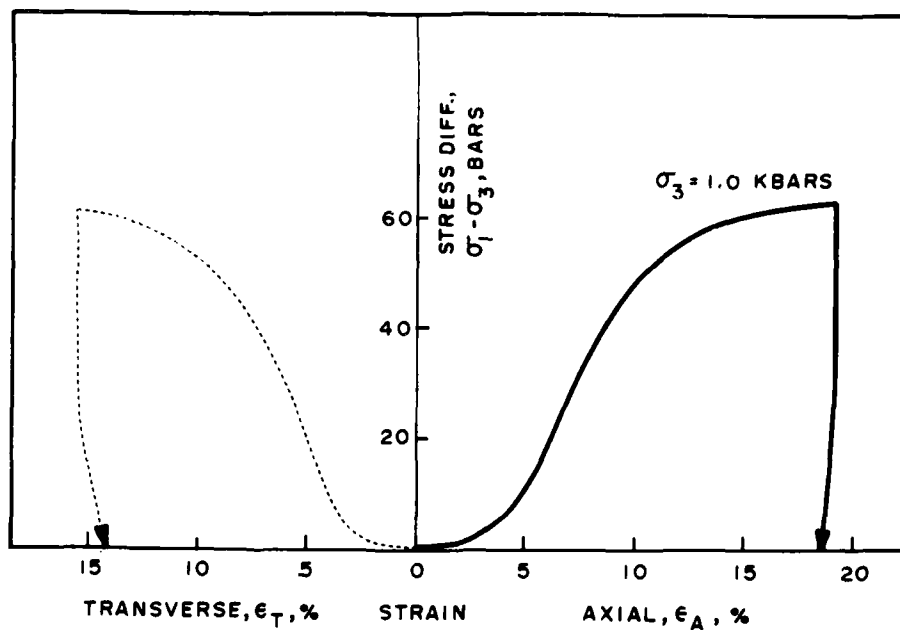
73

Figure A11. Triaxial compression stress-strain curve for undrained
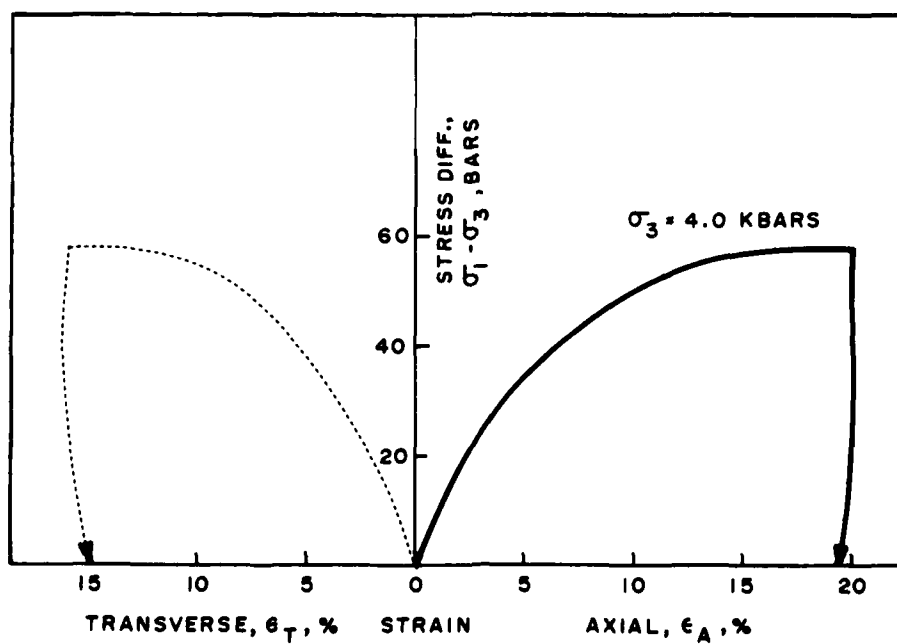Grade A Lapis Lustre sand at 1.0 kbars confining pressure.

Figure A12. Triaxial compression stress-strain curve for undrained
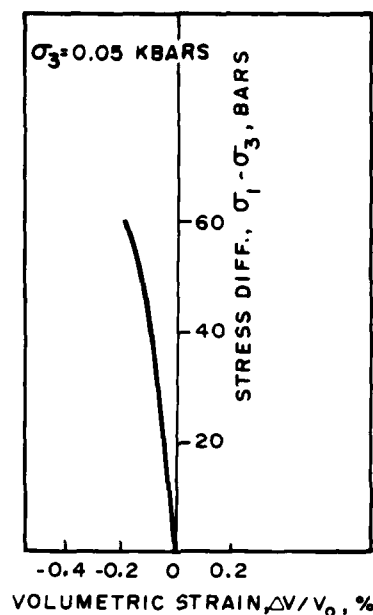Grade A Lapis Lustre sand at 4.0 kbars confining pressure.

Figure A13. Volumetric strain (computed from pore pressure) during triaxial compression for undrained Grade A Lapis Lustre sand at 0.05 kbars confining pressure.

Figure A14. Volumetric strain (computed from pore pressure) during triaxial compression for undrained Grade A Lapis Lustre sand at 0.1 kbars confining pressure.

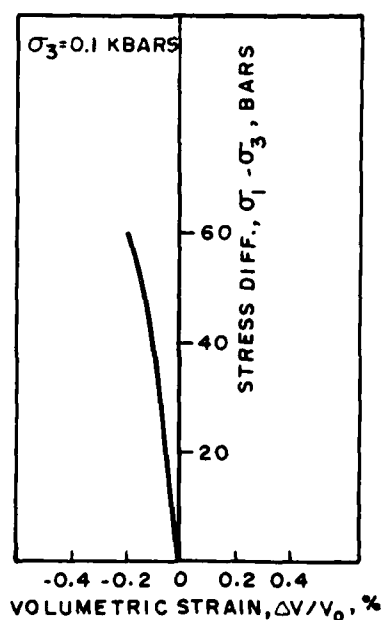Figure A15. Volumetric strain (computed from pore pressure) during triaxial compression for undrained Grade A Lapis Lustre sand at 1.0 kbars confining pressure.
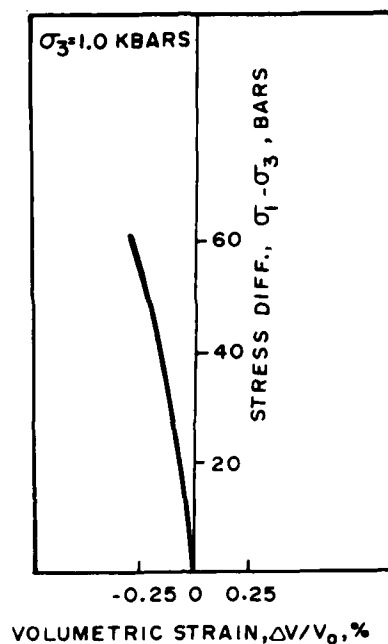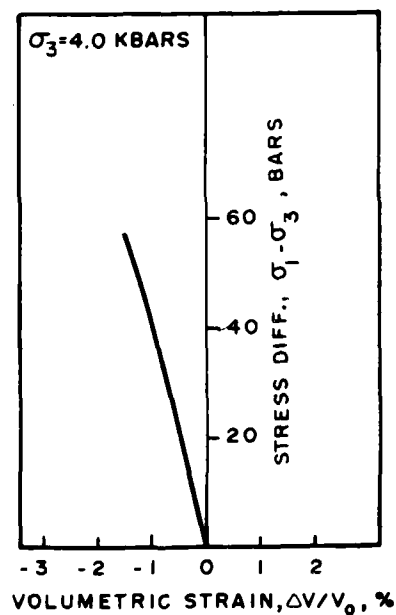

Figure A16. Volumetric strain (computed from pore pressure) during triaxial compression for undrained Grade A Lapis Lustre sand at 4.0 kbars confining pressure.
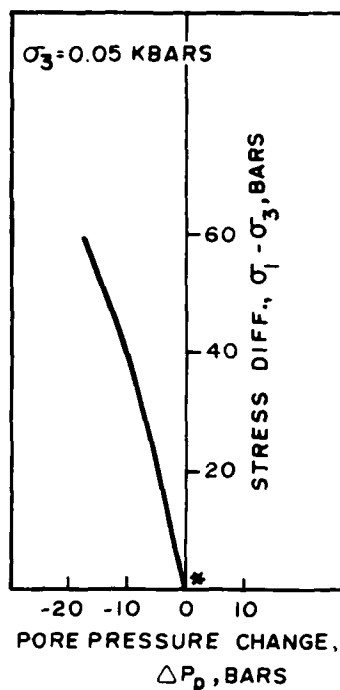
Figure A17. Pore pressure during triaxial compression for undrained Grade A Lapis Lustre sand at 0.05 kbars confining pressure. *See explanation on page 12.

Figure A18. Pore pressure during triaxial compression for undrained Grade A Lapis Lustre sand at 0.1 kbars confining pressure. *See explanation on page 12.

Figure A19.   Pore pressure during triaxial compression for undrained
Grade A Lapis Lustre sand at 1.0 kbars confining pres-
sure.   *See explanation on page 12.

Figure A20.   Pore pressure during triaxial compression for undrained
Grade A Lapis Lustre sand at 4.0 kbars confining pres-
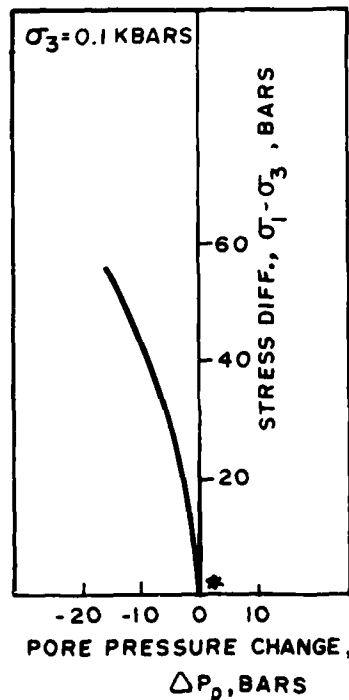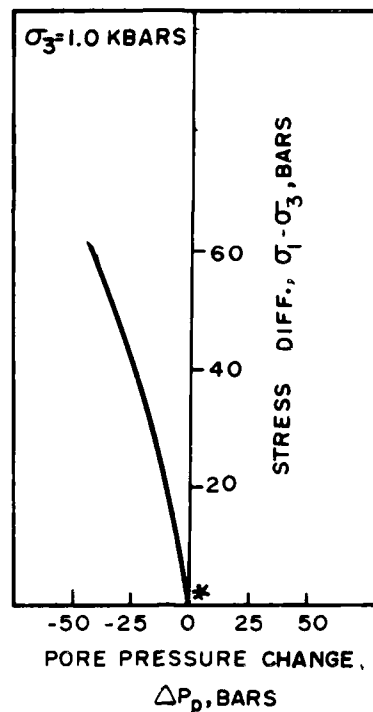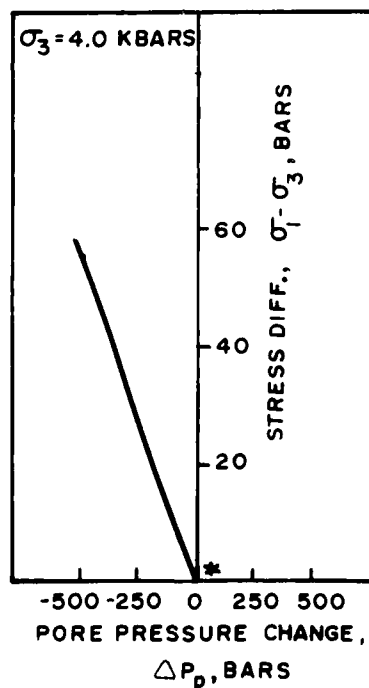sure.   *See explanation on page 12.

78

SOME MATERIAL PROPERTIES OF DIABLO HAWK TUFF
ASSOCIATED WITH THE AA (AGBABIAN ASSOCIATES)
WATER FILLED TUNNEL

SUMMARY

The AA water filled tunnel experiment is located in D drift of the Diablo Hawk structures area, approximately 180 feet to the south of the working point. Cores from four drill holes, DNFF#7, 8, 9 and 10, were tested for physical and mechanical properties. Each hole ranged in depth from 17 to 24 feet.

Results of the physical property measurements are listed in Table 1. Table 2 lists the respective unconfined compressive strengths and the measured stress difference at 4.0 kbars confining pressure during the uniaxial strain test. Stress-strain and stress-stress curves for the individual tests are shown in Figures 1 through 11.

Test data indicate a nearly saturated tuff with a few areas of undersaturation. Unconfined compressive strengths were consistent at about 0.2 kbars. Stress difference observed at 4.0 kbars confining pressure during uniaxial strain, however, varied from 0.31 to 1.5 kbars.

TABLE 1

Physical Properties, Uniaxial Strain Permanent Volume Compaction and Ultrasonic Wave Velocities of AA Water Filled Tunnel

DRILL HOLE FOOTAGE	DENSITY (gm/cc)			WATER BY WET WEIGHT (%)	POROSITY (%)	SATURATION (%)	CALC. AIR VOIDS (%)	MEAS. PERMANENT COMP. (%)	VELOCITY (km/sec)	
	AS-RECEIVED	DRY	GRAIN						LONG	SHEAR
DNFF#7										
1	1.79	1.43	2.40	20.0	40.3	88.7	4.5	7.5	2.60	1.21
20	1.85	1.49	2.36	19.3	36.6	97.5	0.9	2.6	3.38	1.70
DNFF#8										
1	1.83	1.45	2.39	20.7	39.3	96.6	1.3	3.5	2.56	1.22
5	1.88	1.51	2.45	19.6	38.4	96.7	1.3	1.1	3.50	1.96
16	1.91	1.59	2.37	16.8	33.0	97.6	0.8	0.9	3.47	1.89
23	1.97	1.67	2.48	15.0	32.5	91.0	2.9	2.1	2.94	1.48
DNFF#9										
1	1.86	1.54	2.43	18.4	36.7	94.6	2.0	2.5	2.71	1.32
24	1.83	1.52	2.46	16.5	38.0	80.0	7.7	4.0	3.24	1.81
DNFF#10										
1	1.89	1.55	2.40	18.2	35.6	96.7	1.2	1.8	2.95	1.57
17	1.85	1.46	2.46	20.8	40.6	94.6	2.2	2.4	2.45	1.16

TABLE 2

U12n.10A Tuff Mechanical Test Results

Drill Hole/Footage		Unconfined Compressive Strength (kb)	Uniaxial Strain Test [Stress Difference @ $\sigma_3 = 4$ kb (kb)]
DNFF#7	1	0.14	0.45
	20	0.24	0.80
DNFF#8	1	0.19	0.35
	5	--	0.31
	16	--	1.24
	23	0.20	0.81
DNFF#9	1	0.24	0.50
	24	--	1.50*
DNFF#10	1	--	0.66
	17	--	0.30

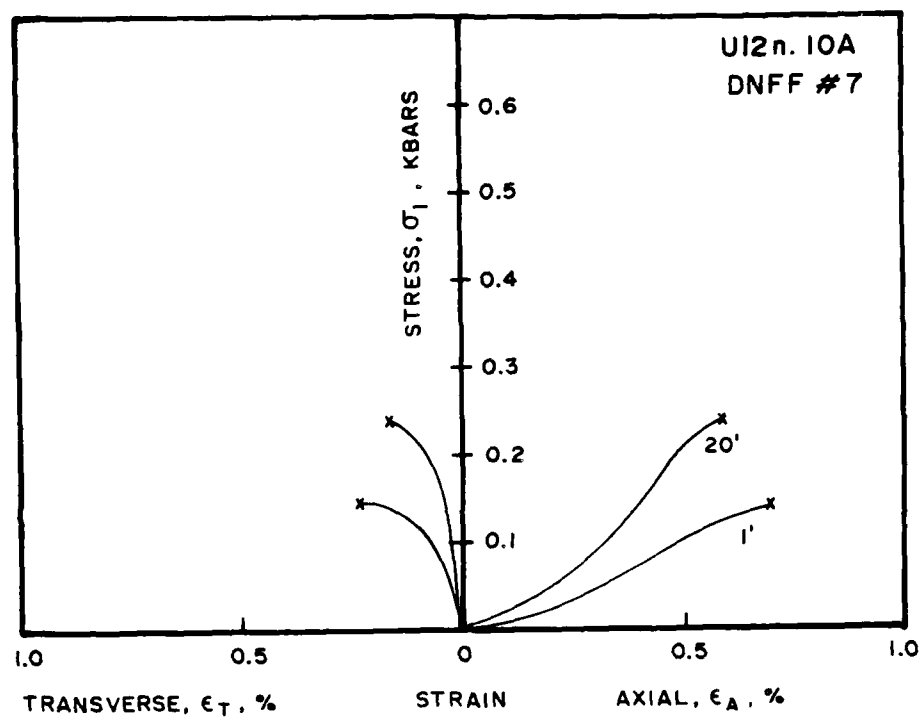* Machine force limit reached at ~2.5 kbars confining pressure.

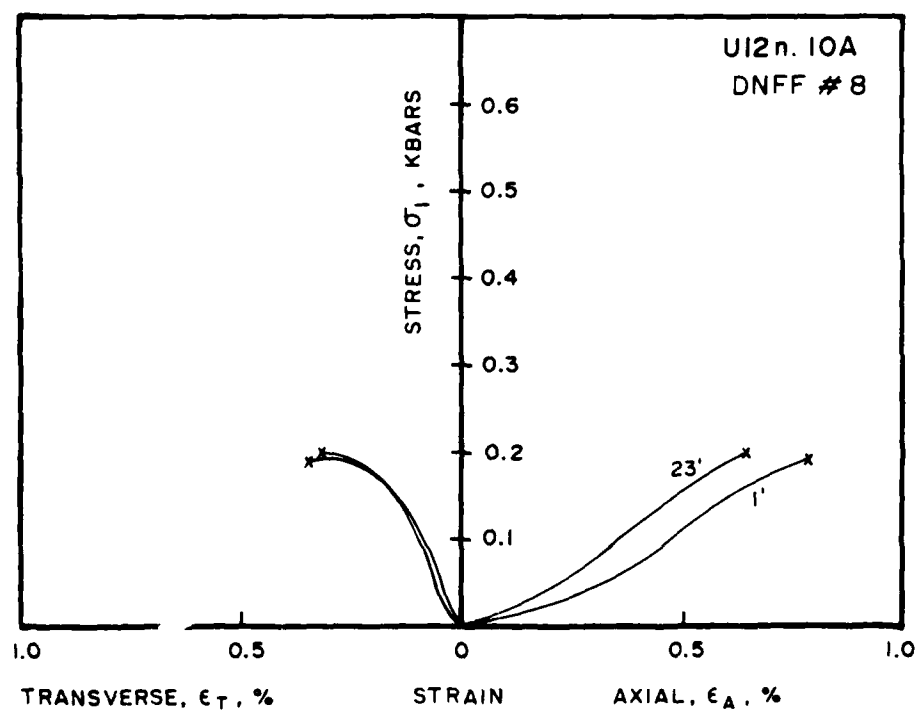Figure 1.   Unconfined compression tests.

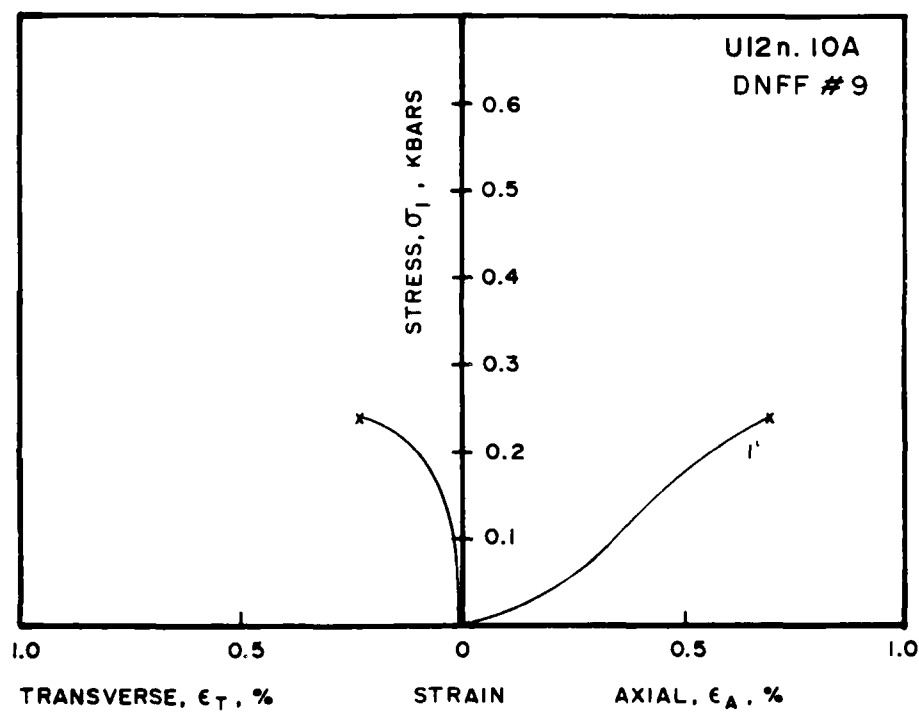Figure 2.   Unconfined compression tests.

81

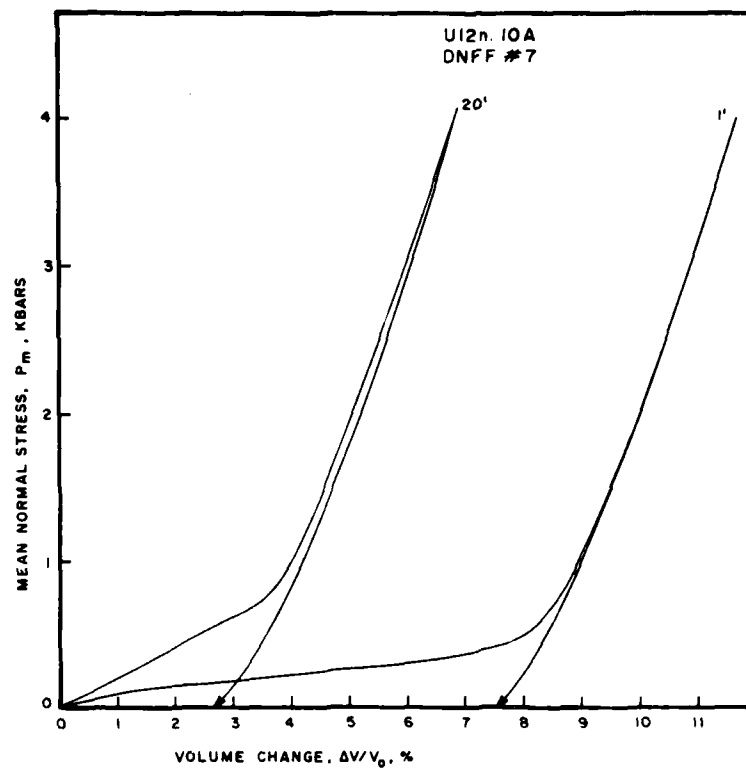Figure 3.   Unconfined compression tests.

82

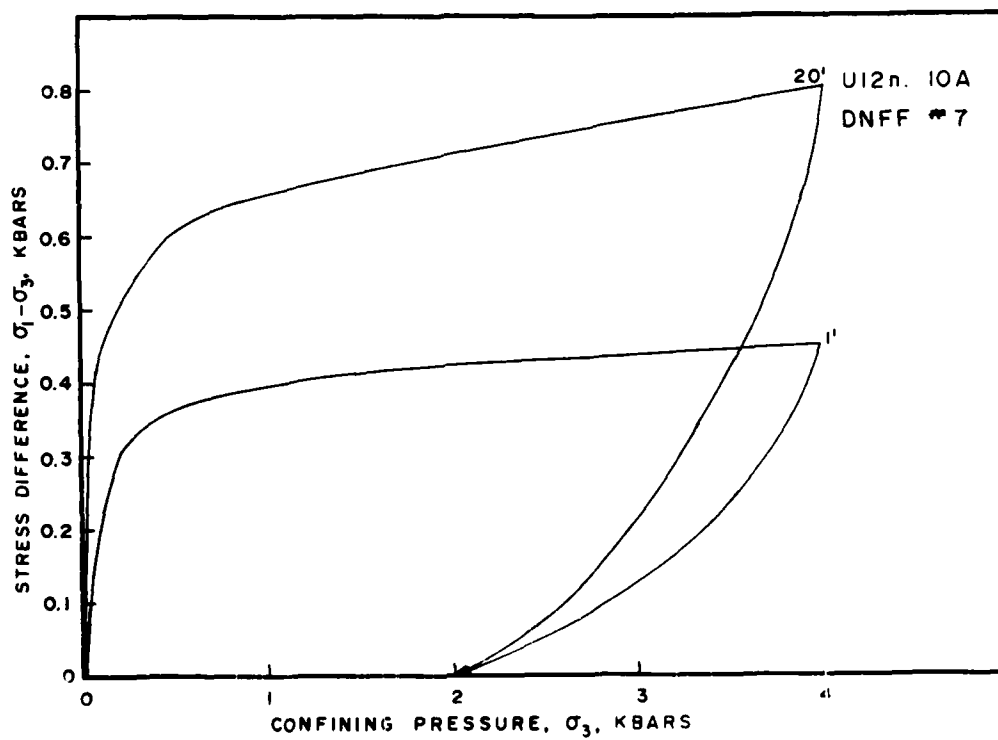Figure 4.   Uniaxial strain tests, stress-strain response.

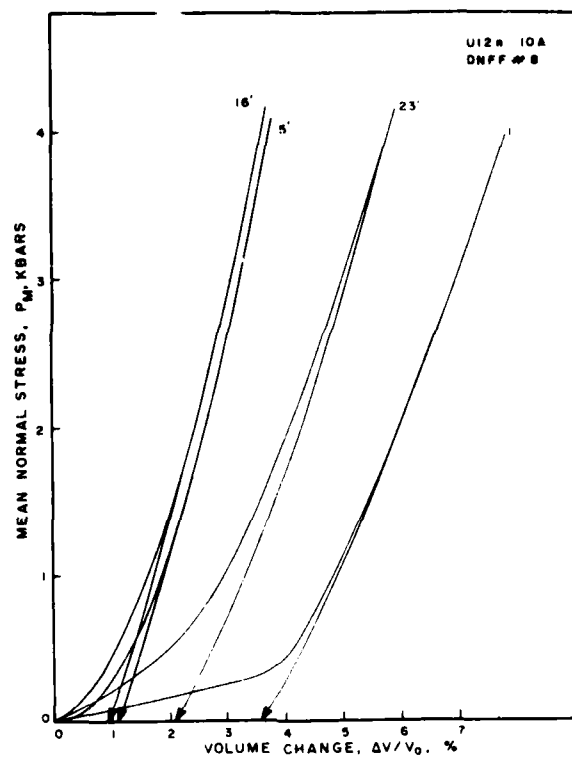Figure 5.   Uniaxial strain tests, stress-stress response.

83

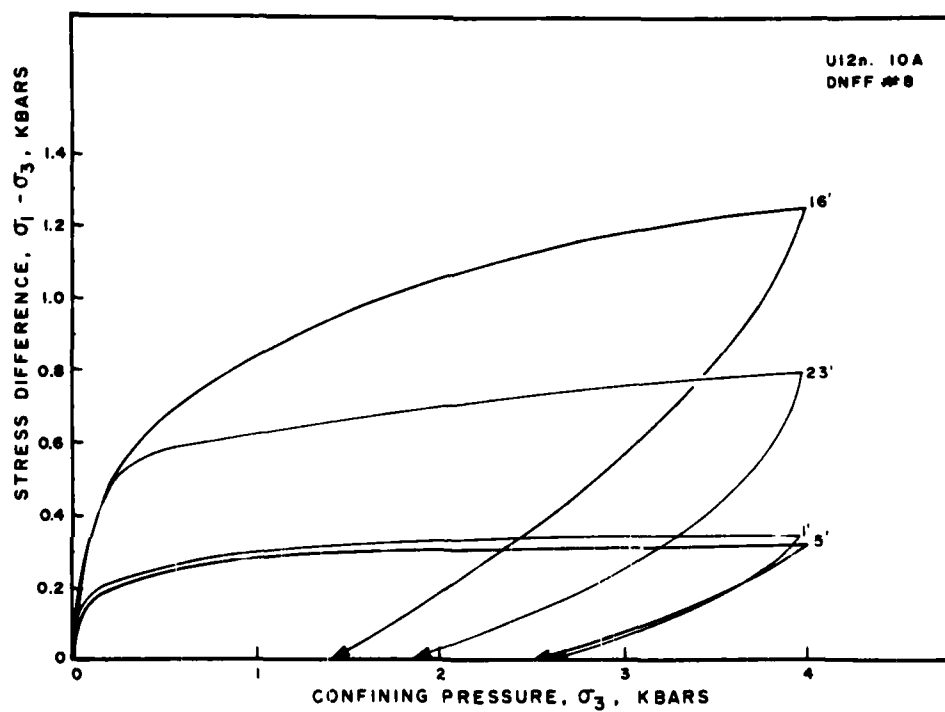Figure 6. Uniaxial strain tests, stress-strain response.

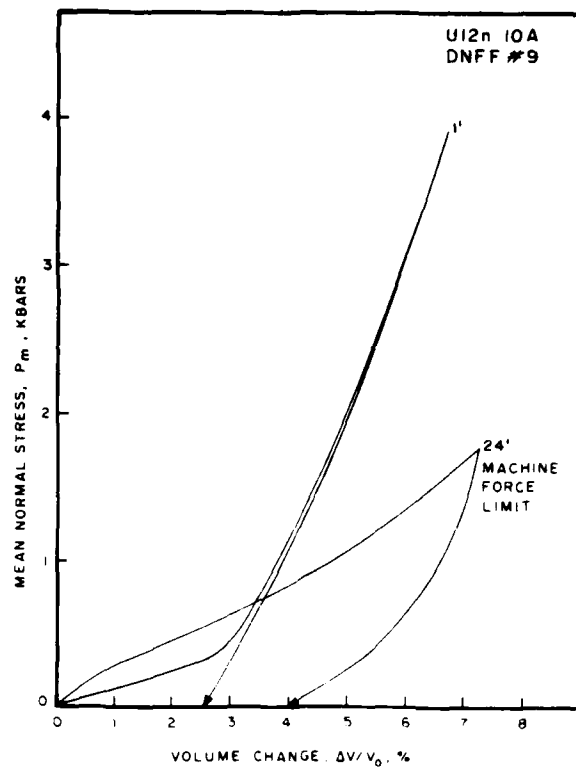Figure 7. Uniaxial strain tests, stress-stress response.

84

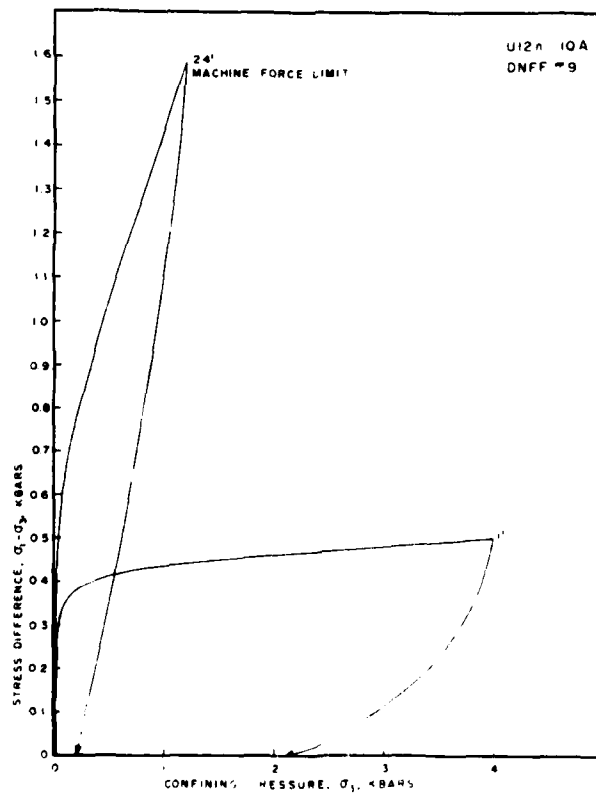Figure 8. Uniaxial strain tests, stress-strain response.

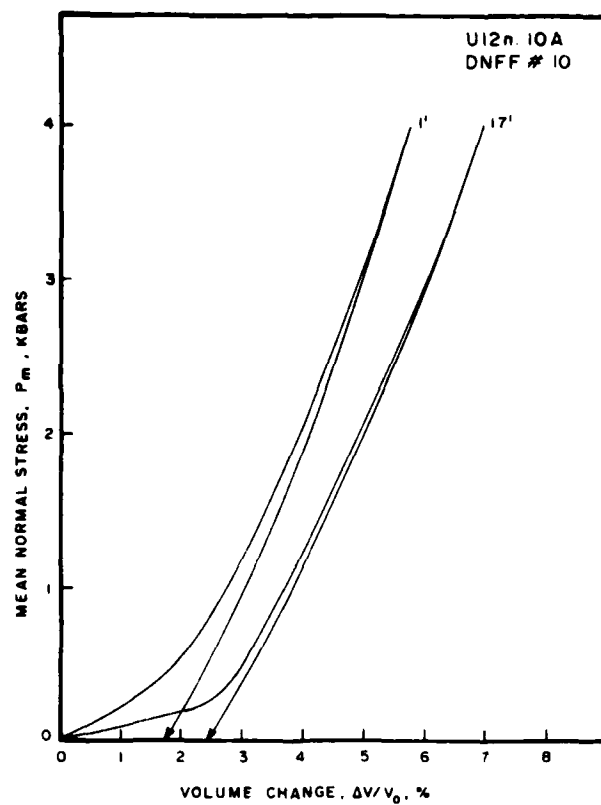Figure 9. Uniaxial strain tests, stress-stress response.

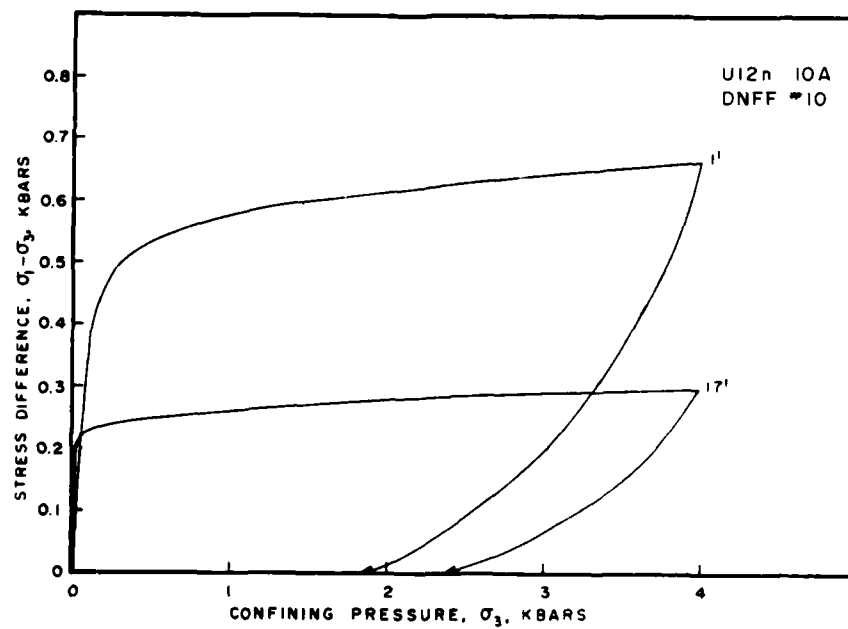Figure 10. Uniaxial strain tests, stress-strain response.

Figure 11. Uniaxial strain tests, stress-stress response.

86

SHEAR MODULI OF SELECT U12n.10A DNFF TUFF

SUMMARY

Cycled triaxial compressiᵥ tests were conducted on U12n.10A DNFF
tuff samples to evaluate the effect of confining pressure on apparent
shear modulus. Samples were axially loaded while at 0, 34.5 and 69.0
bars confining pressure. Axial and transverse strains were measured.
At C and 34.5 bars confining pressure, the samples were loaded only
far enough to scale slopes from the "elastic" portion of the stress-
strain curves (i.e. typically above 0.02 kbars). At 69.0 bars confining
pressure, samples were loaded to failure. The respective shear moduli
are shown below.

Sample Identification	Shear Modulus (Kbars)		
	$\sigma_3 = 0$ Bars	$\sigma_3 = 34.5$ Bars	$\sigma_3 = 69.0$ Bars
DNFF#8 15'	10	17	18
DNFF#8 19'	25	30	30
DNFF#9 16'	13	18	21
DNFF#10 15'	17	26	30

As expected, the shear modulus increases with increased confining
pressure. Also, these moduli appear to be in the same range as your
field measurements.

To date, six triaxial compression tests at 69.0 bars confining pres-
sure have been conducted on DNFF drill hole tuffs. The average strength
is 0.37 kbars with a standard deviation of 0.12 kbars. These values are
within the range of earlier test results on samples from nearby drill
holes ("Material Properties on Samples from Mighty Epic Drill Holes
U12n.10 UG#4, U12n.10 UG#6a and U12n.10 UG#7," Terra Tek Report TR 75-50).
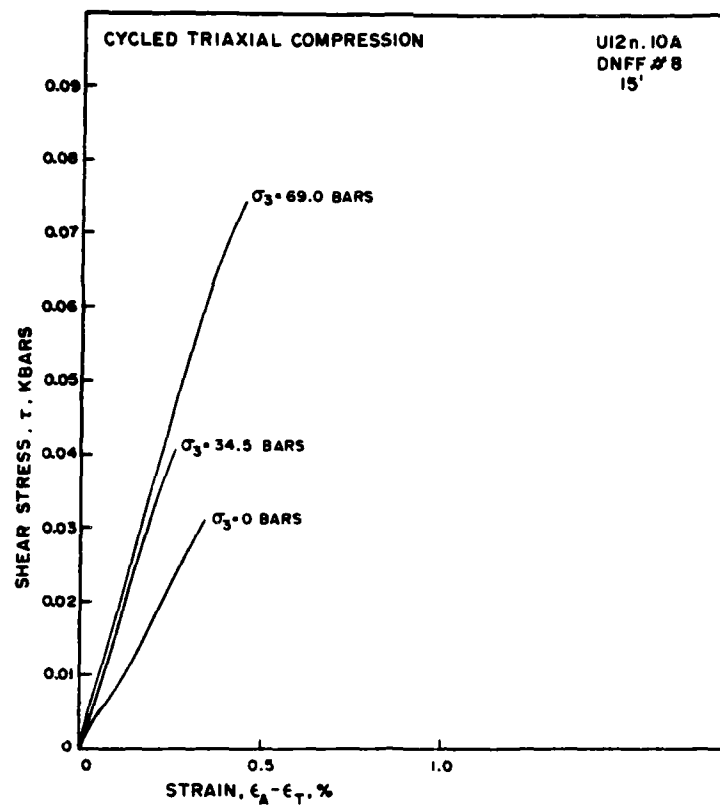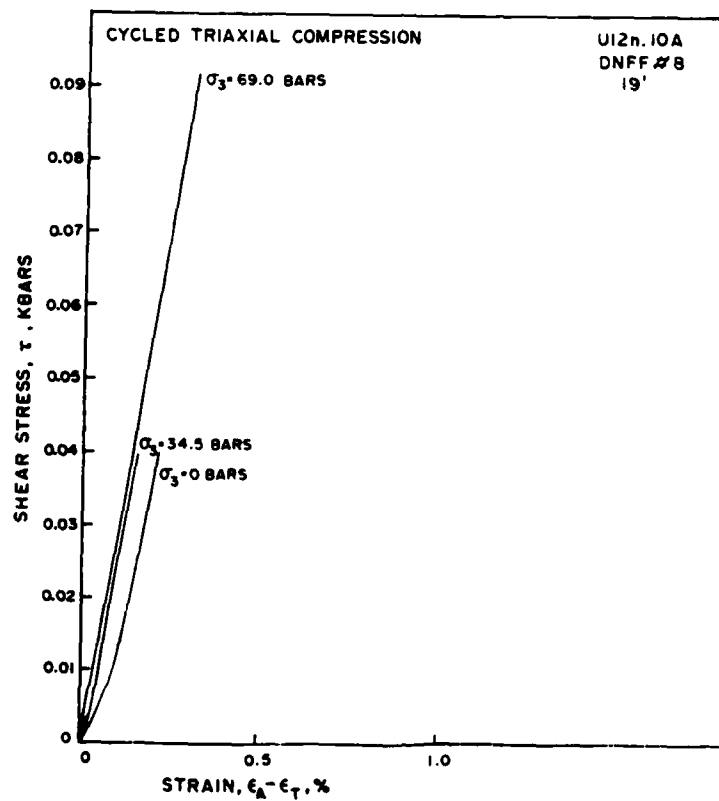
Figure 1. Triaxial compression tests.
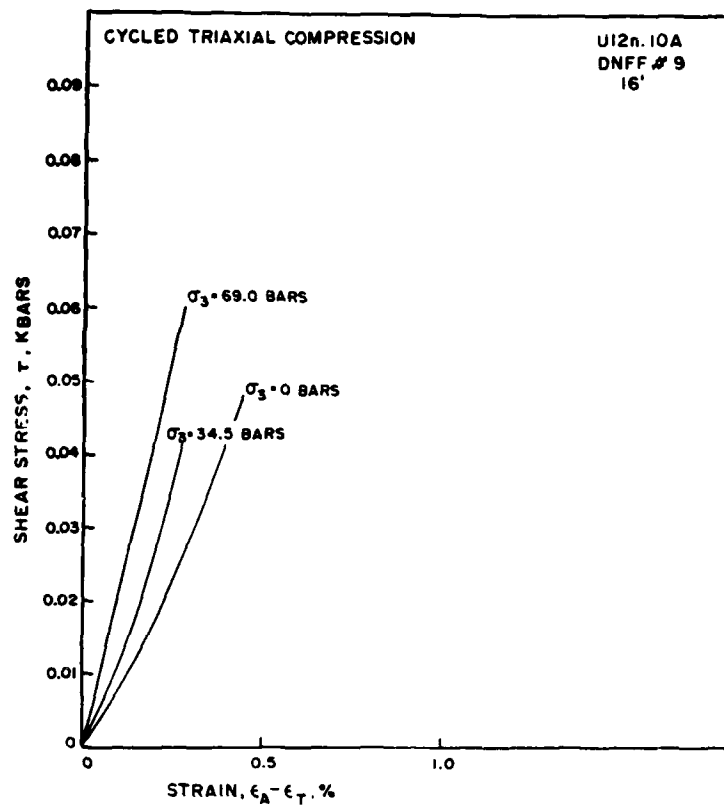

Figure 2. Triaxial compression tests.
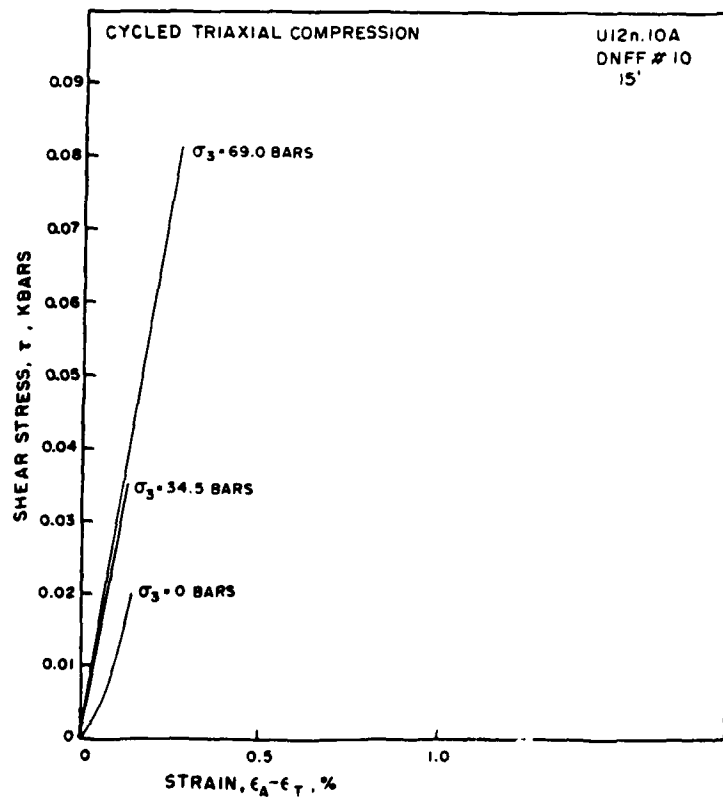
88

Figure 3. Triaxial compression tests.

Figure 4. Triaxial compression tests.

89

MATERIAL PROPERTIES OF THE DIABLO HAWK
CAMERA/BORESCOPE DRILL HOLE TUFFS

SUMMARY

The camera/borescope drill holes are located near F and G drifts in the Diablo Hawk (U12n.10A) structures area. Cores from 19 drill holes were tested for both physical and mechanical properties. Physical property testing included density, porosity, moisture content, and ultrasonic velocity measurements. Mechanical testing included unconfined compressive and uniaxial strain tests.

Physical property and ultrasonic velocity data are listed in Table 1. Physical property tests indicate that the tuffs have an average bulk density and porosity of 1.85 gm/cc and 37.4 percent, respectively. A number of samples had gas filled voids greater than 2 percent, as evidenced by the physical properties and the volume response of the uniaxial strain tests. This is not unusual for the subject areas, however, as similar anomalies were seen during characterization of the Mighty Epic site*, at which time they were found to be single samples and did not suggest larger volumes of undersaturated tuff.

Figure 1 shows the unconfined compressive strength and stress difference at 4.0 kbars confining pressure during uniaxial strain as a function of drill hole and footage. Both unconfined compression and uniaxial strain tests exhibited random strength variations. Unconfined compressive strengths ranged from 0.04 to 0.52 kbars and stress difference at 4.0 kbars confining pressure during uniaxial strain ranged from 0.22 to over 1.60 kbars.

---

* Butters, S. W., A. H. Jones and S. J. Green, "Material Properties on Samples from Mighty Epic Drill Holes U12n.10 UG#4, U12n.10 UG#6a, and U12n.10 UG#7," Terra Tek Report TR 75-50, September 1975.

TABLE 1

PHYSICAL PROPERTIES, UNIAXIAL STRAIN PERMANENT VOLUME COMPACTION AND ULTRASONIC WAVE VELOCITIES OF U12n.10A CATV TUFFS

| DRILL HOLE FOOTAGE	DENSITY (gm/cc)			WATER BY WET WEIGHT (%)	POROSITY (%)	SATURATION (%)	CALC. AIR VOIDS (%)	MEAS. PERMANENT COMP. (%)	VELOCITY (km/sec)	
	AS-RECEIVED	DRY	GRAIN						LONG	SHEAR
CATV Drill Hole										
#5 0'	1.77	1.44	2.40	18.5	39.8	82.0	7.2	6.0	2.42	1.20
#5 12'	1.99	1.68	2.44	15.6	31.1	99.8	0.1	0.8	3.02	1.55
#6 3'	2.01	1.75	2.45	13.2	28.8	91.7	2.4	1.3	3.32	1.84
#6 13'	1.89	1.56	2.44	17.4	36.1	91.3	3.1	1.3	2.84	1.38
#7 3'	1.81	1.50	2.42	16.9	38.0	80.3	7.5	6.3	2.75	1.26
#7 11'	1.85	1.47	2.41	20.6	39.1	97.0	1.2	2.8	2.88	1.44
#8 0'	1.86	1.50	2.39	19.7	37.6	97.5	0.9	4.5	3.02	1.48
#8 12'	1.81	1.38	2.41	23.5	42.5	100.0	0.2	2.8	2.64	1.22
#9 1'	1.88	1.54	2.35	18.2	34.4	99.3	0.2	2.1	2.96	1.53
#9 17'	1.80	1.49	2.40	17.4	38.1	82.5	6.7	5.2	3.20	1.72
#11 0'	1.84	1.56	2.40	15.5	35.3	80.6	6.9	4.7	2.28	1.21
#11 18'	1.80	1.54	2.38	14.7	35.3	75.4	8.7	1.9	3.07	1.51
#13 3'	1.75	1.32	2.45	24.1	45.9	91.7	3.8	5.5	2.57	1.12
#13 15'	1.77	1.40	2.36	21.1	40.9	91.3	3.5	4.0	2.39	1.26
#14 6'	1.87	1.54	2.42	17.6	36.4	90.3	3.5	0.8	3.18	1.66
#14 15'	1.82	1.49	2.42	18.3	38.5	86.5	5.2	4.4	3.68	1.83
#15 0'	1.70	1.27	2.36	25.4	46.4	93.3	3.1	2.7	2.59	1.08
#15 13'	1.70	1.23	2.41	27.7	49.0	96.1	1.9	2.1	2.71	1.27
#16 5'	1.99	1.73	2.45	12.9	29.3	87.3	3.7	0.8	3.03	1.30
#16 13'	1.86	1.48	2.41	20.6	38.7	99.0	0.4	2.0	2.35	1.36
#17 2'	1.90	1.54	2.41	18.6	36.0	98.0	0.7	2.2	2.70	1.21
#17 19'	1.95	1.68	2.40	13.9	30.0	91.0	2.8	4.2	3.19	1.53
#18 3'	1.81	1.42	2.39	21.6	40.4	96.9	1.3	1.5	3.01	1.54
#18 21'	1.89	1.51	2.45	20.2	38.4	99.3	0.3	2.6	2.97	1.54
#19 5'	1.91	1.57	2.44	17.9	35.6	96.5	1.3	2.6	3.13	1.52
#19 19'	1.96	1.71	2.38	12.9	28.1	89.9	2.8	1.2	3.03	1.70
#20 0'	1.88	1.68	2.35	10.5	28.4	69.4	8.7	4.0	2.54	1.09
#20 20'	1.87	1.47	2.45	21.2	40.0	98.3	0.5	2.9	3.26	1.66
#21 0'	1.90	1.54	2.45	19.4	37.3	99.1	0.3	1.4	2.74	1.26
#21 35'	1.86	1.51	2.38	19.2	36.6	97.4	0.9	2.8	3.26	1.75
#22 12'	1.80	1.41	2.44	21.6	42.2	92.0	3.4	3.0	2.96	1.24
#22 28'	1.86	1.54	2.43	17.0	36.5	86.9	4.8	4.3	2.70	1.05
#23 6'	1.90	1.56	2.38	18.0	34.5	98.9	0.4	1.3	3.13	1.64
#23 28'	1.84	1.49	2.36	18.3	36.3	93.3	2.3	2.9	2.92	1.48
#24 3'	1.79	1.39	2.43	22.6	42.9	94.3	2.4	3.6	2.51	1.17
#24 28'	1.83	1.44	2.44	21.6	41.0	96.6	1.4	3.3	2.80	1.24
#W13 2'	1.94	1.61	2.44	17.2	34.1	97.9	0.7	2.4	2.84	1.42
#W13 14'	1.76	1.41	2.37	19.8	40.5	96.0	5.7	5.5	2.90	1.54
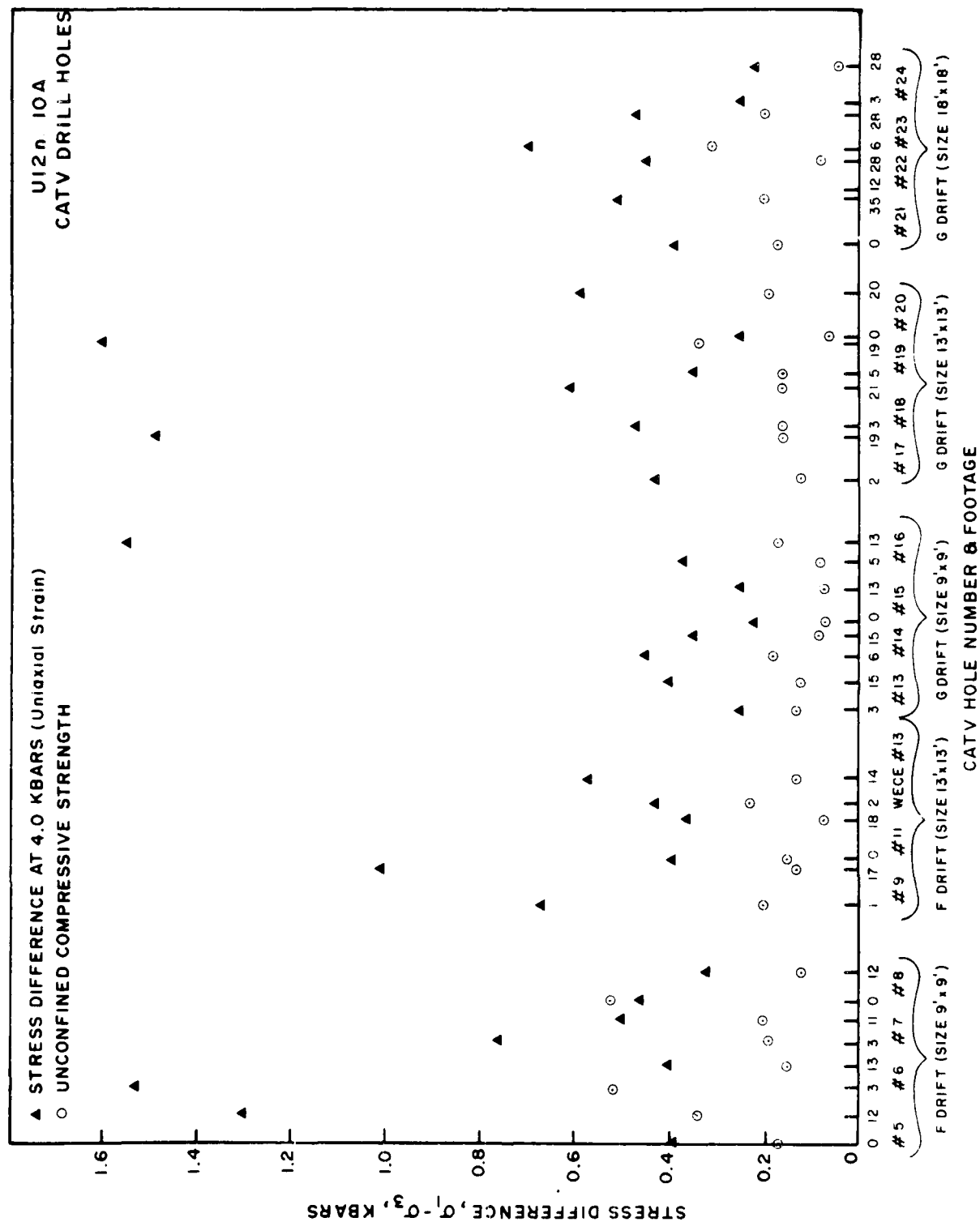
Figure 1. Unconfined compressive strength and uniaxial strain tests -- stress difference at 4 kb confining pressure.
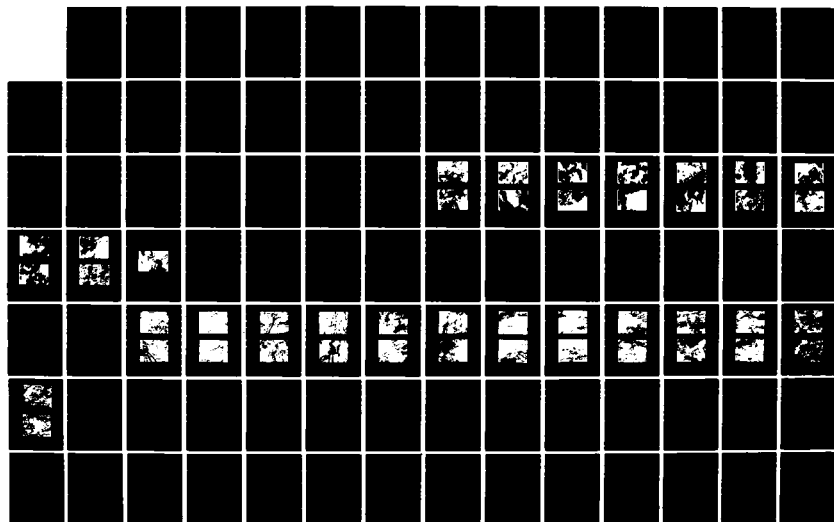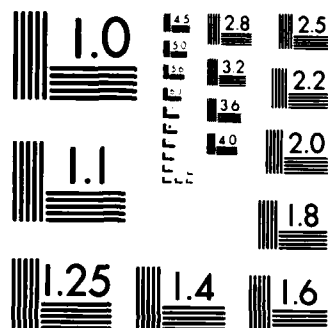
MICROCOPY RESOLUTION TEST CHART
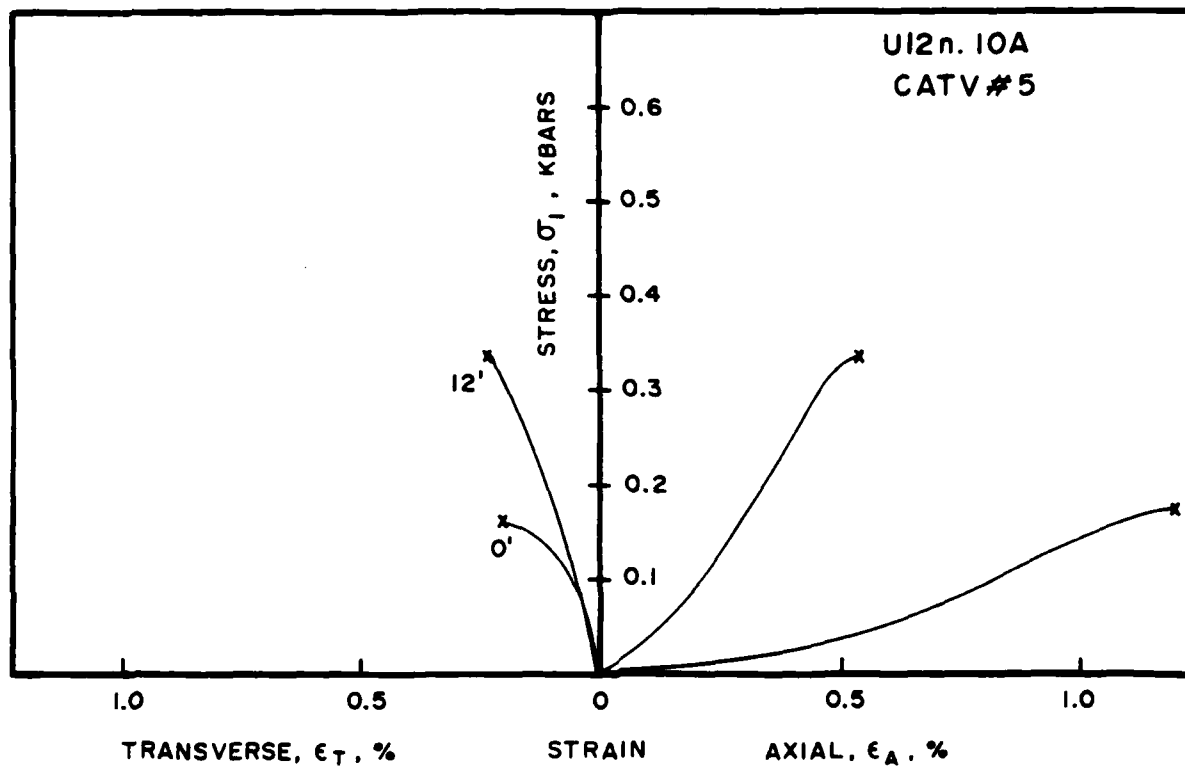NATIONAL BUREAU OF STANDARDS-1964-A

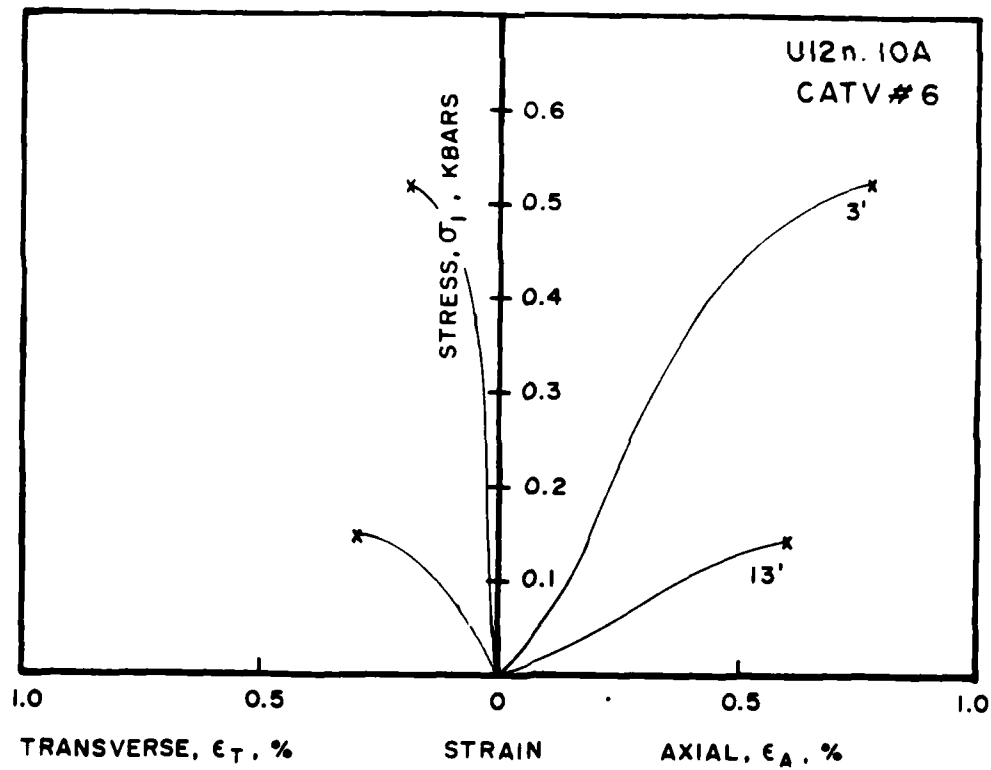Figure 2. Unconfined compression tests.

Figure 3. Unconfined compression tests.
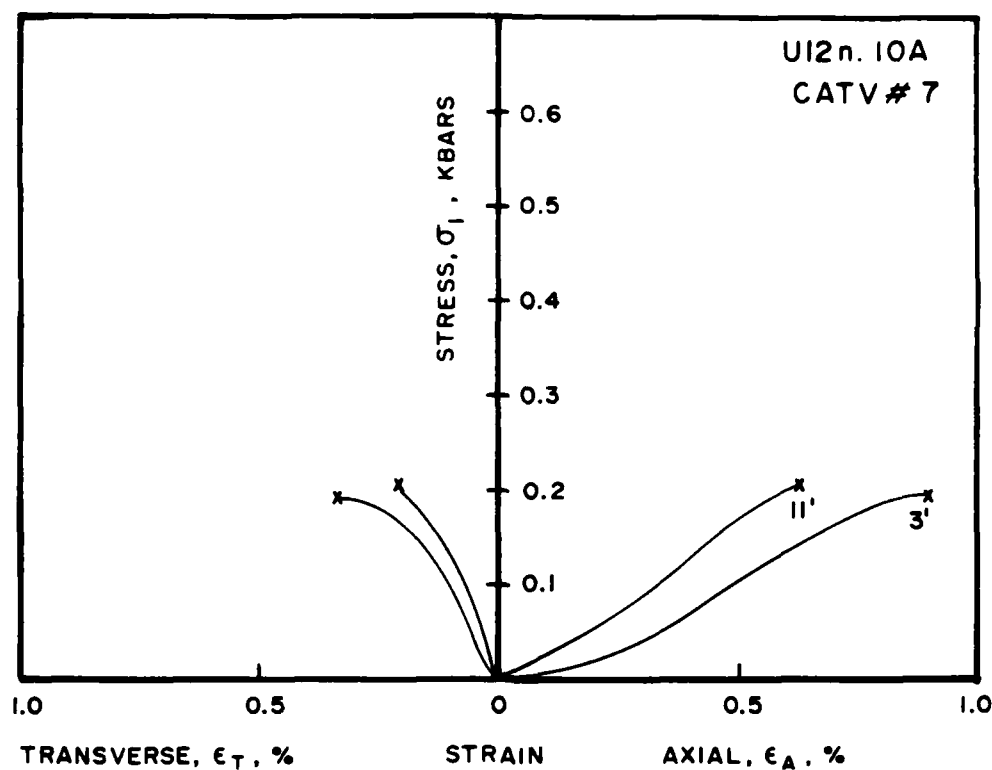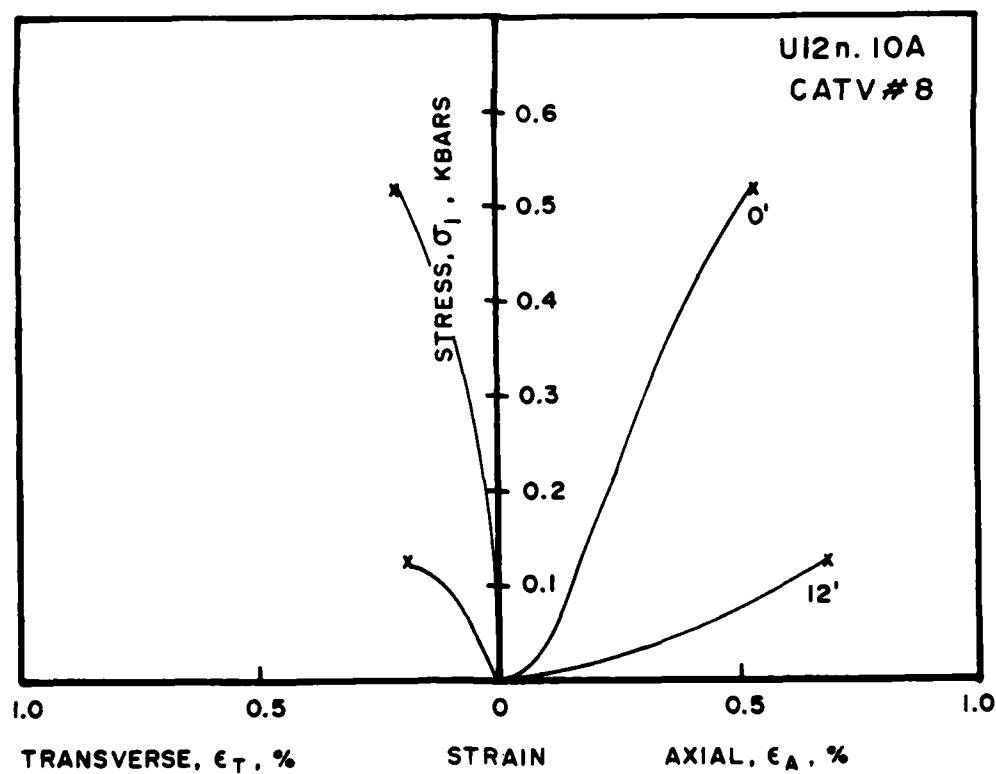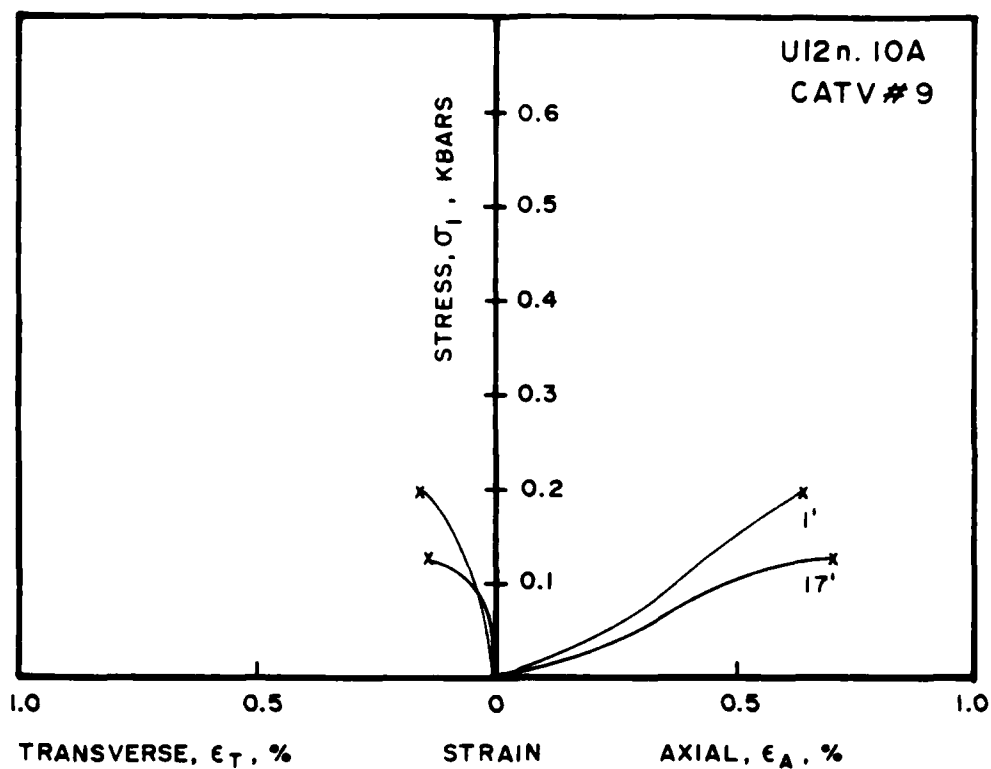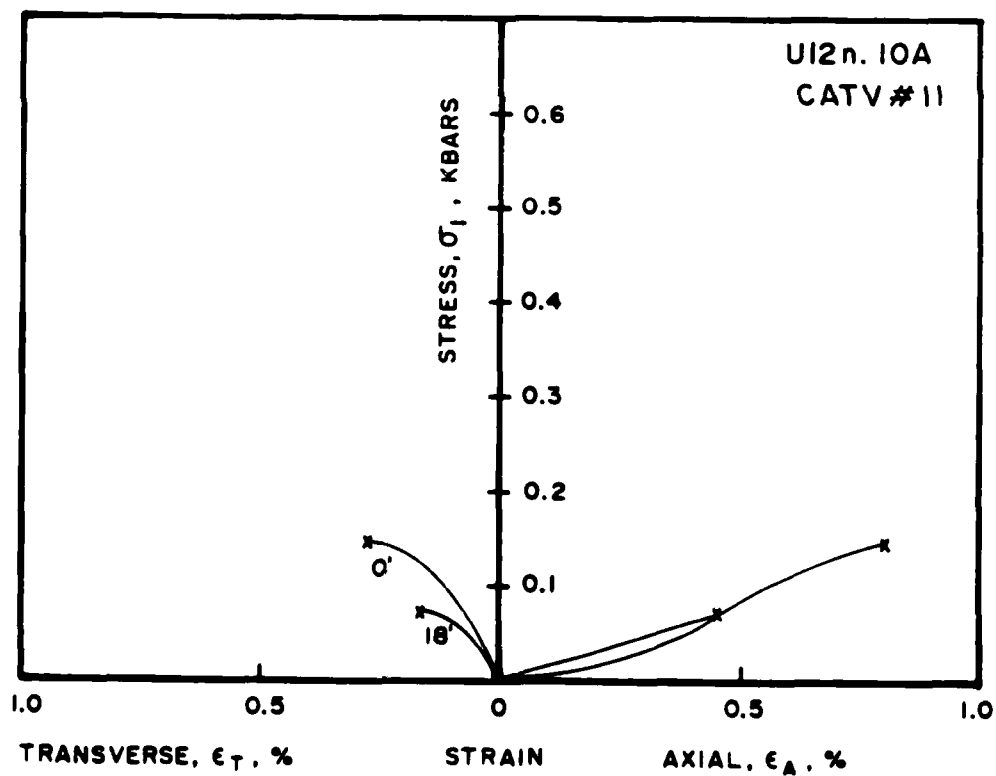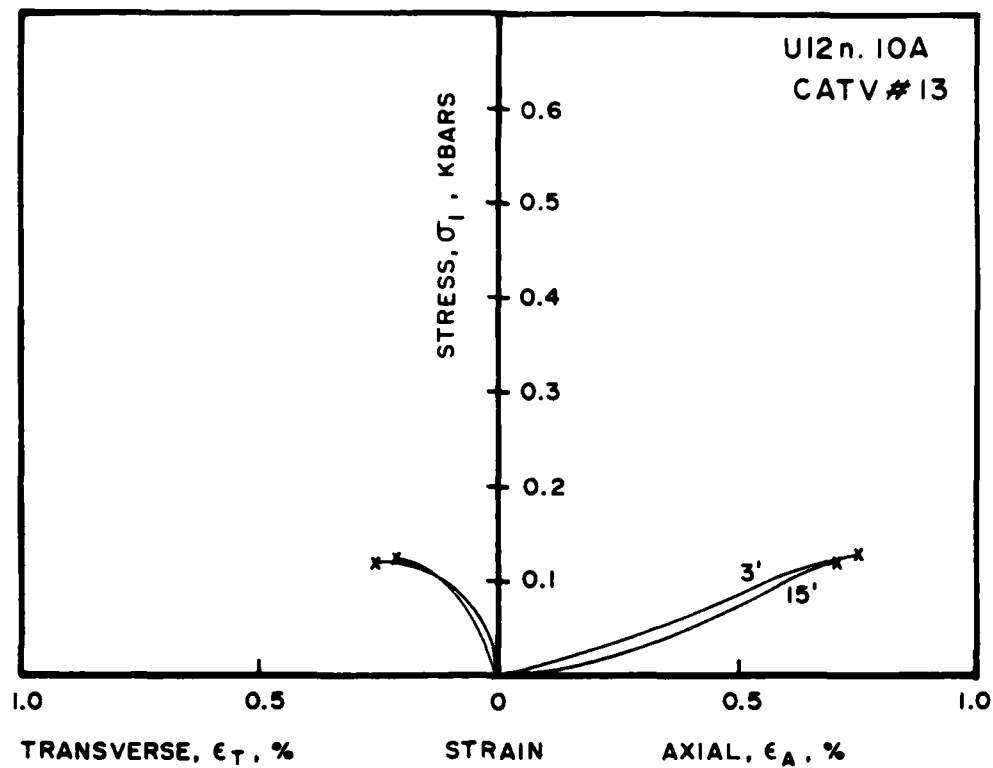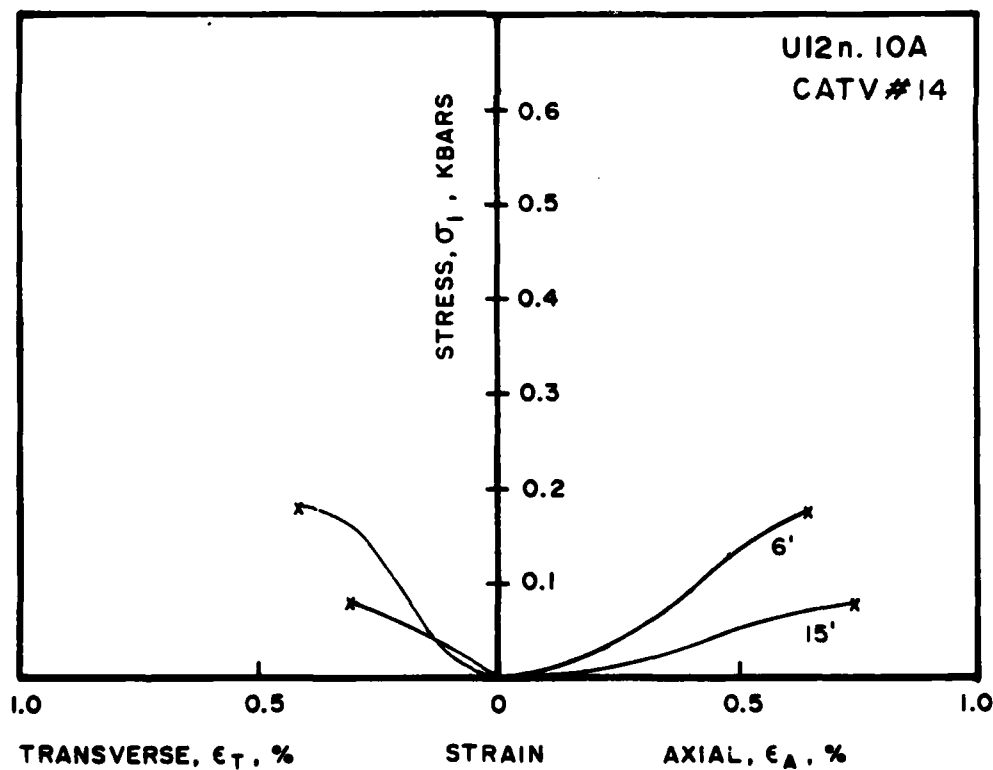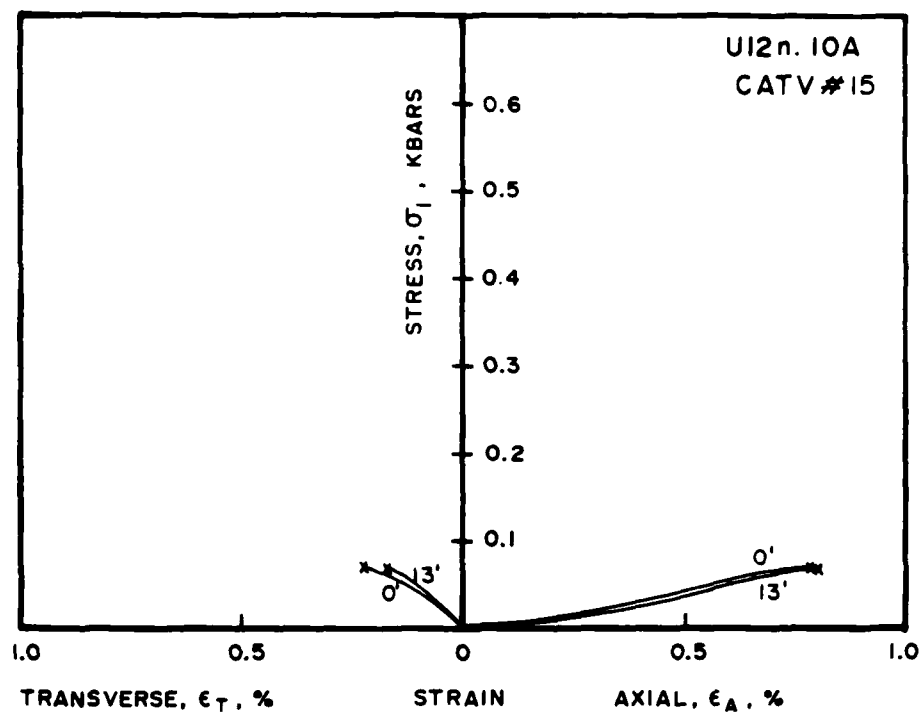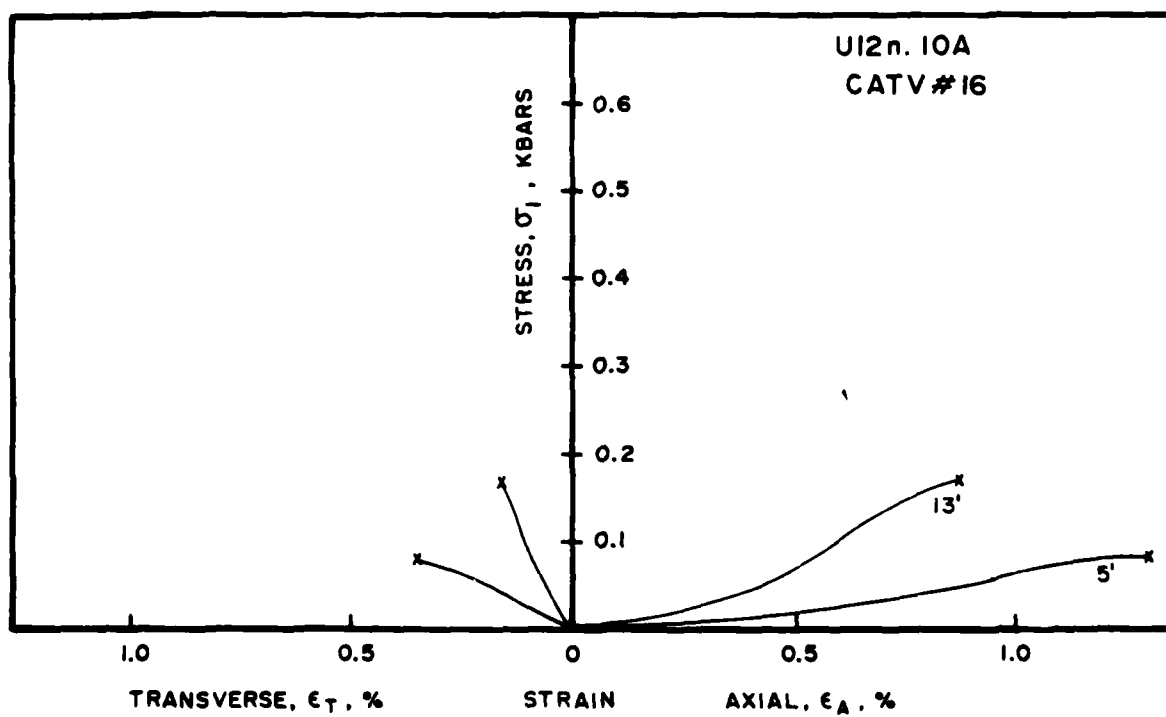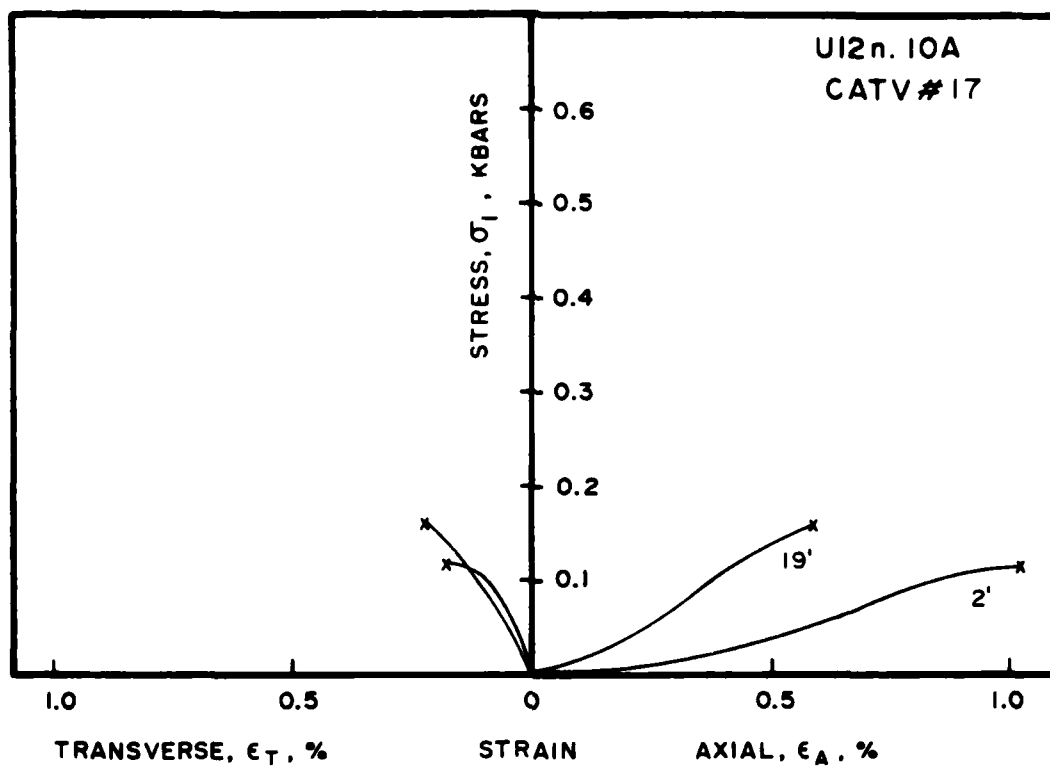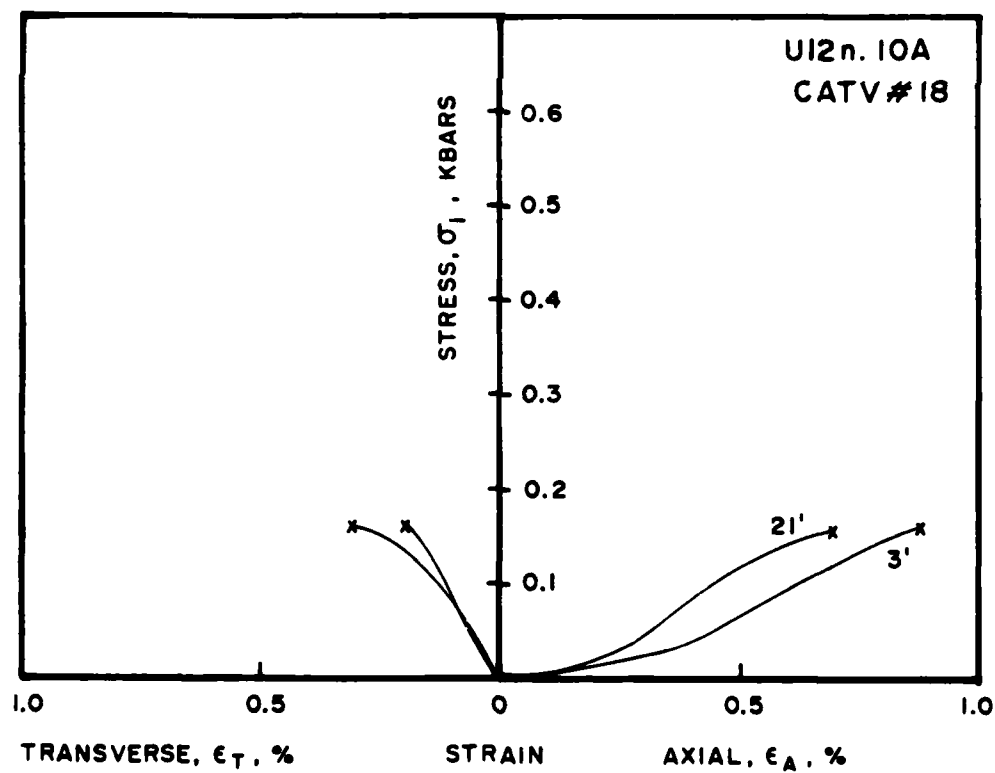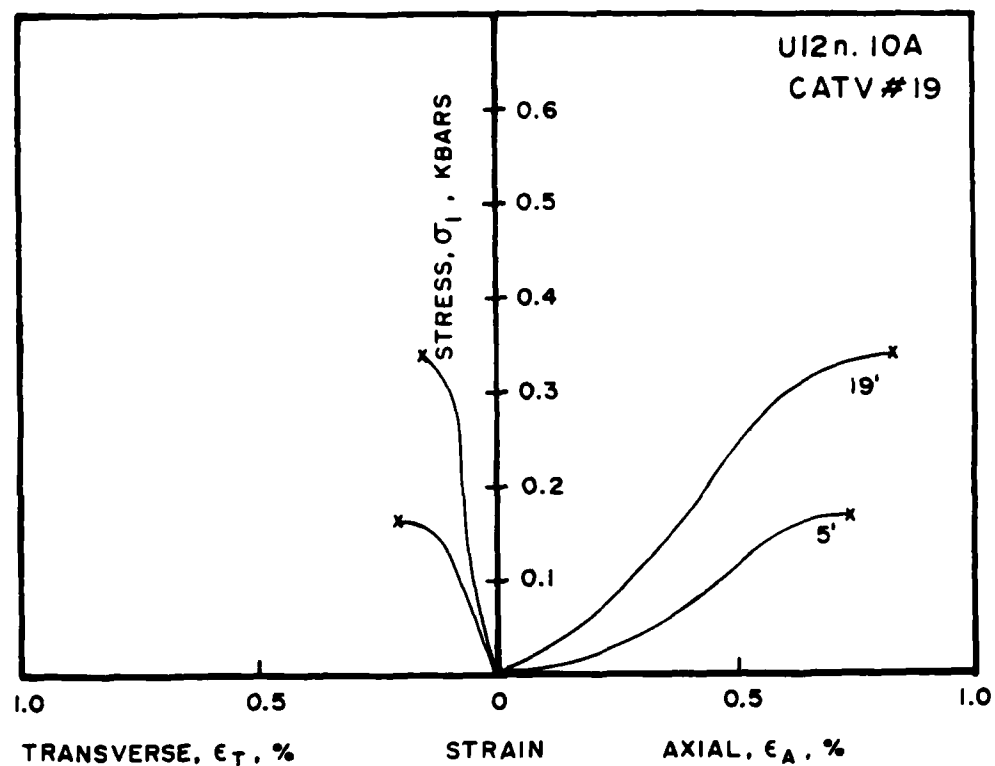
93

Figure 4.   Unconfined compression tests.
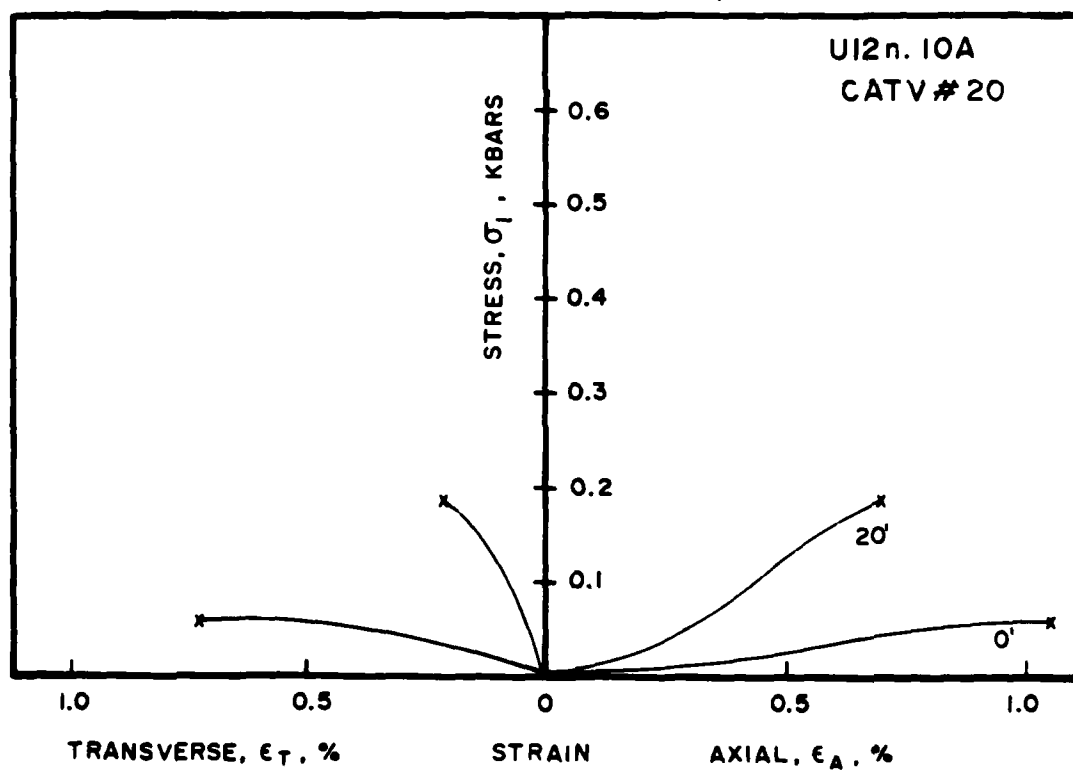

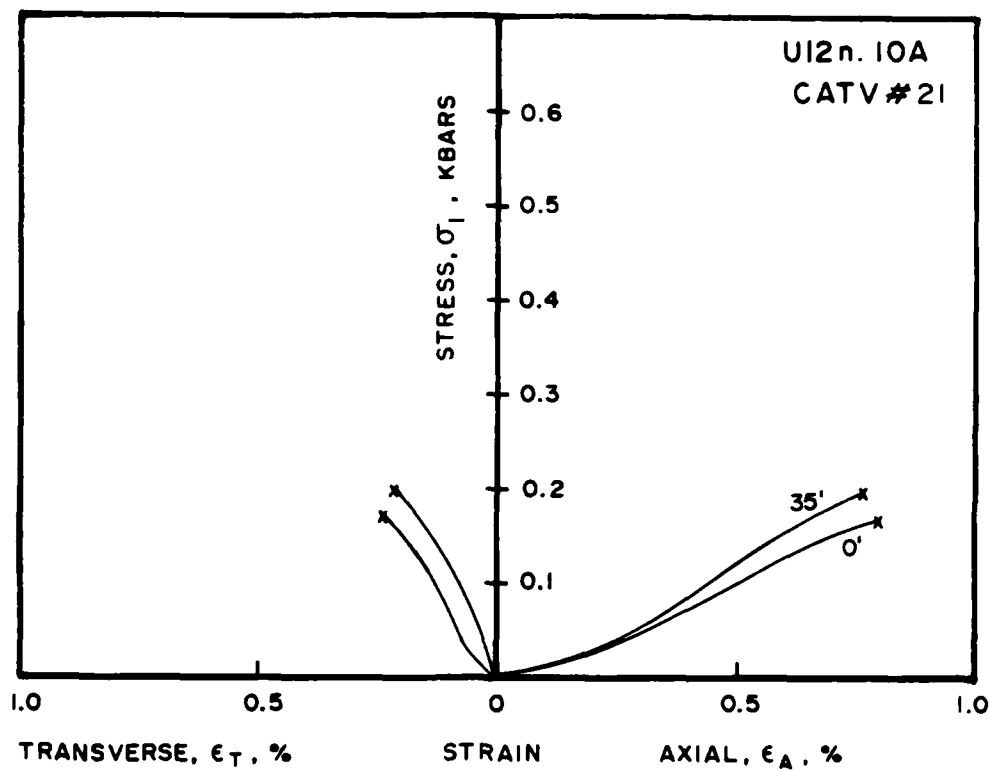Figure 5.   Unconfined compression tests.

94

Figure 6.   Unconfined compression tests.
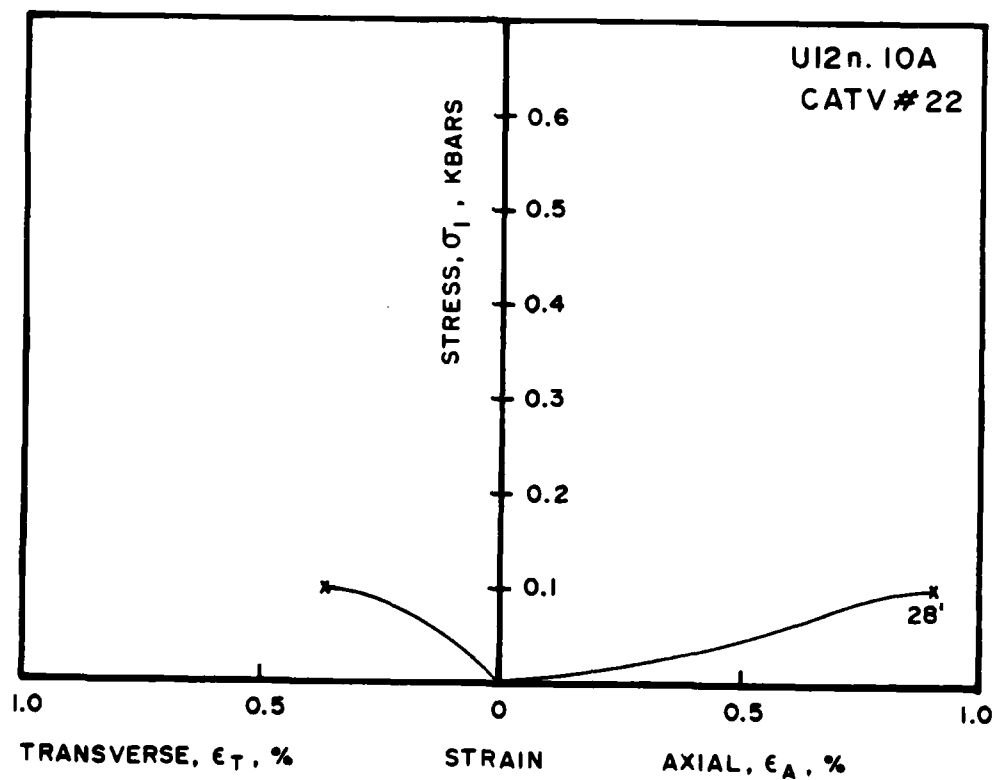

Figure 7.   Unconfined compression tests.

95

Figure 8.   Unconfined compression tests.

Figure 9.   Unconfined compression tests.

96

Figure 10. Unconfined compression tests.

Figure 11. Unconfined compression tests.

97

Figure 12. Unconfined compression tests.

Figure 13. Unconfined compression tests.

Figure 14.   Unconfined compression tests.

Figure 15.   Unconfined compression tests.

99

Figure 16.   Unconfined compression tests.

Figure 17.   Unconfined compression tests.

100

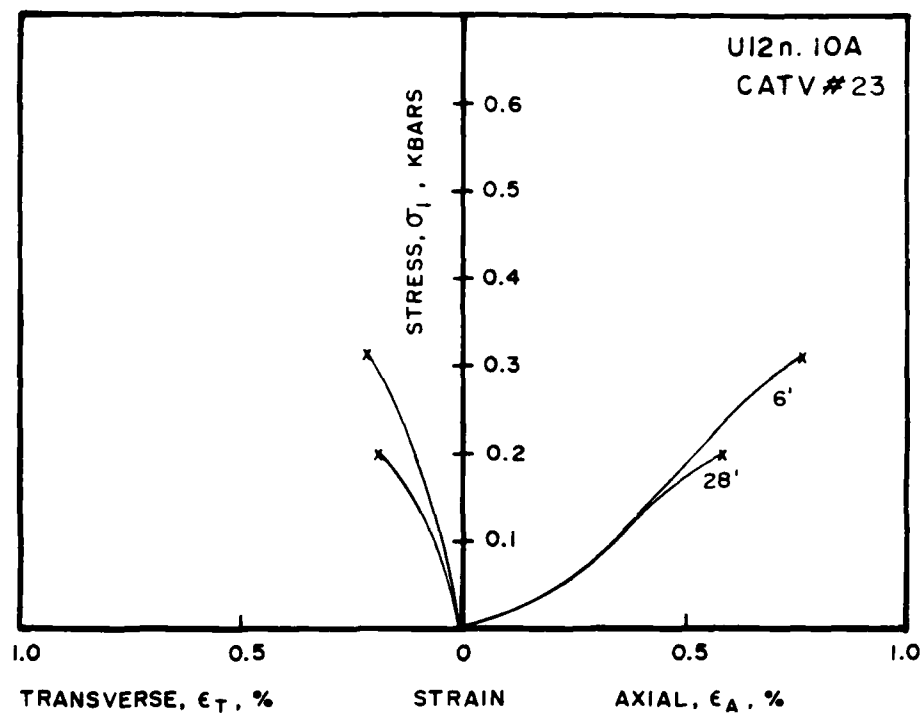Figure 18.   Unconfined compression tests.
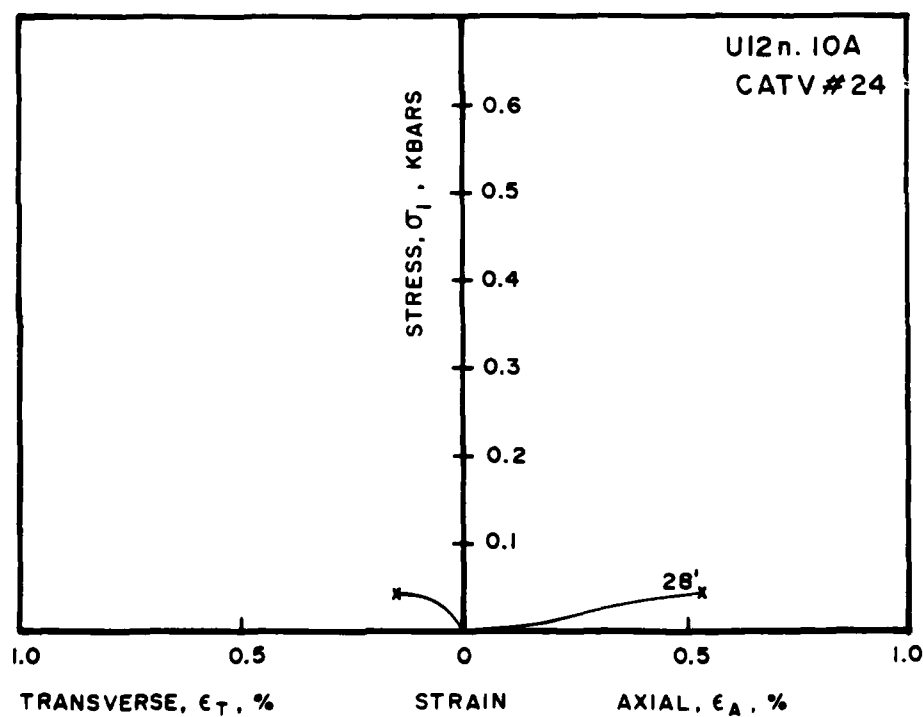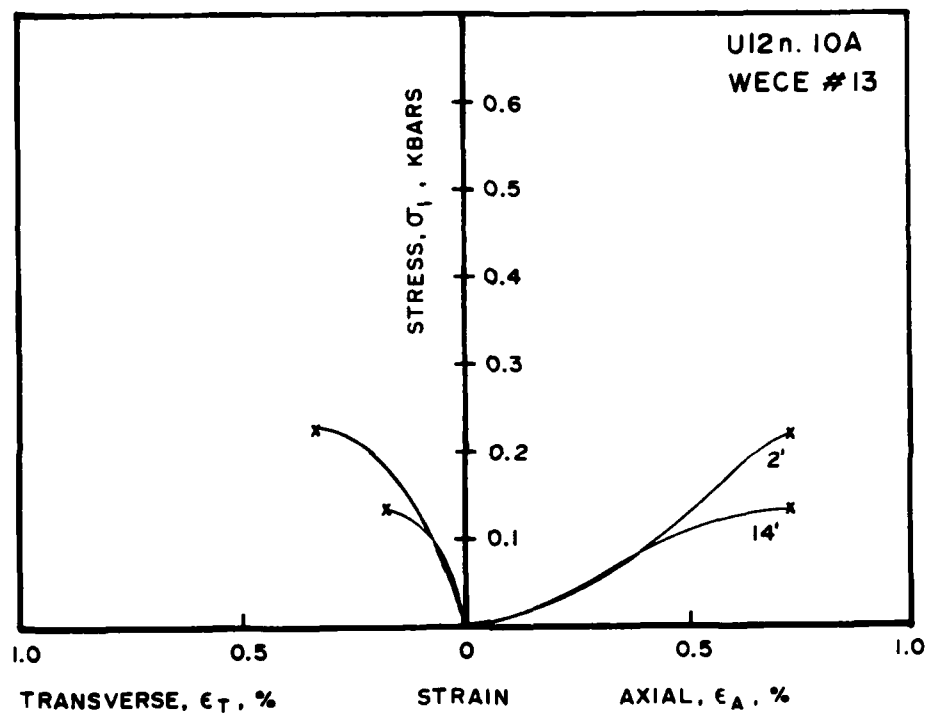

Figure 19.   Unconfined compression tests.

101

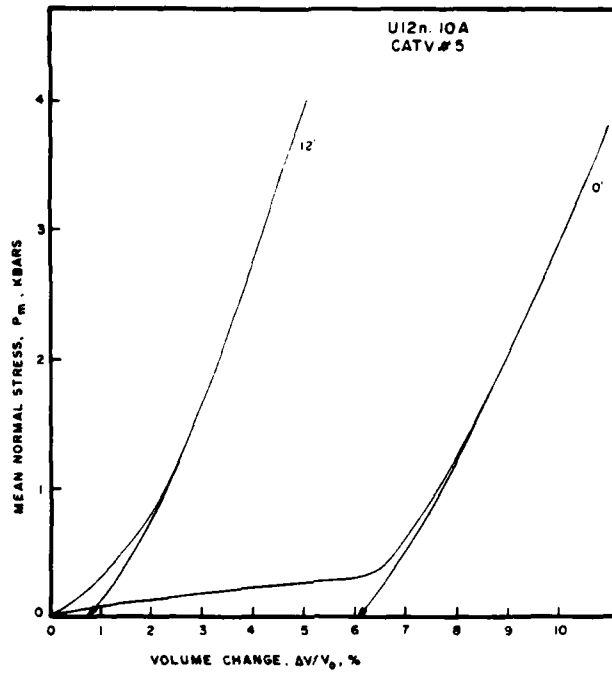Figure 20. Unconfined compression tests.

Figure 21.   Uniaxial strain tests, stress-strain response.

Figure 22.   Uniaxial strain tests, stress-stress response.

103

Figure 23. Uniaxial strain tests, stress-strain response.

Figure 24. Uniaxial strain tests, stress-stress response.

104

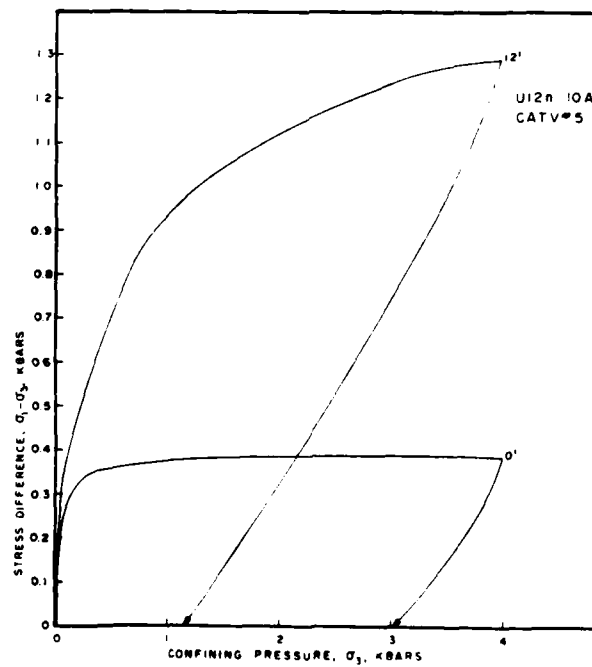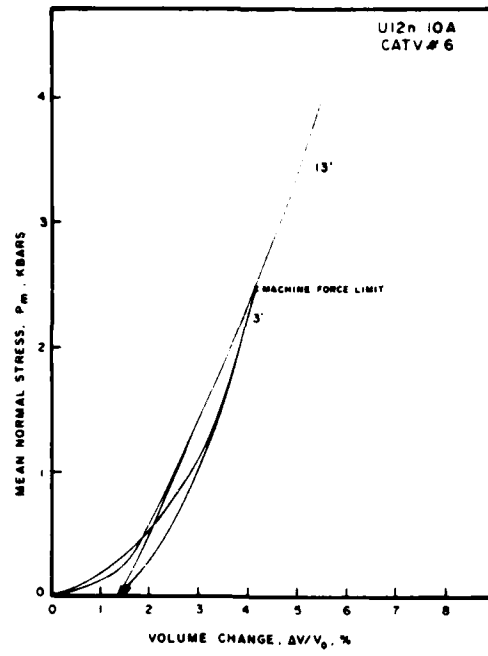Figure 25. Uniaxial strain tests, stress-strain response.

Figure 26. Uniaxial strain tests, stress-stress response.

105

Figure 27. Uniaxial strain tests, stress-strain response.

Figure 28. Uniaxial strain tests, stress-stress response.

106

Figure 29. Uniaxial strain tests, stress-strain response.

Figure 30. Uniaxial strain tests, stress-stress response.

Figure 31. Uniaxial strain tests, stress-strain response.

Figure 32. Uniaxial strain tests, stress-stress response.

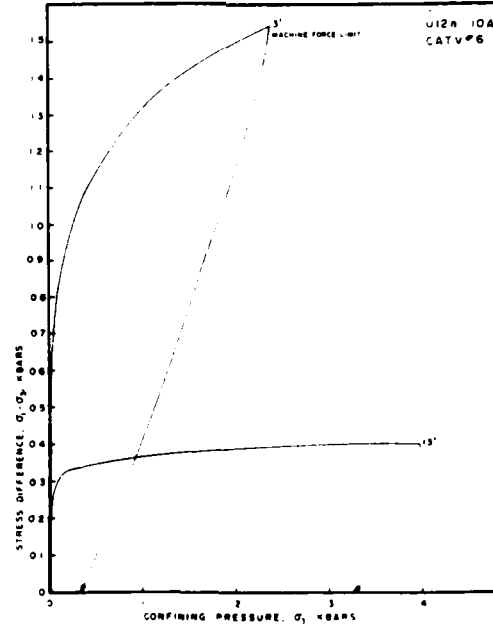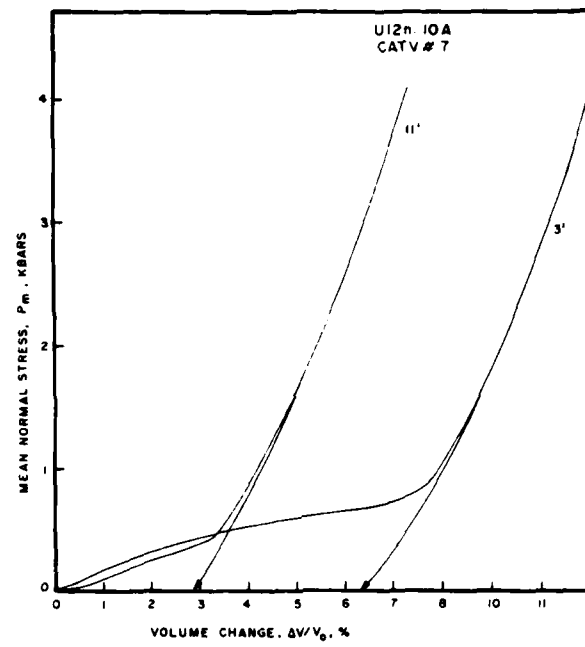Figure 33. Uniaxial strain tests, stress-strain response.

Figure 34. Uniaxial strain tests, stress-stress response.

109

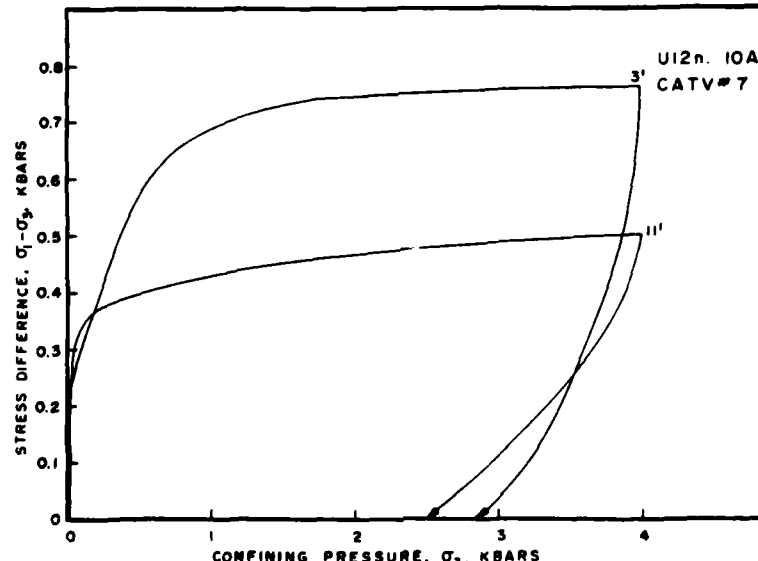Figure 35.   Uniaxial strain tests, stress-strain response.

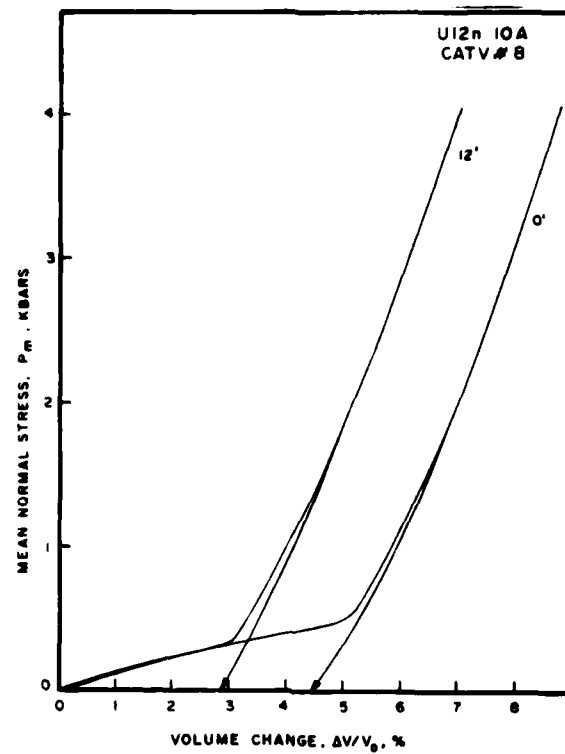Figure 36.   Uniaxial strain tests, stress-stress response.

110

Figure 37. Uniaxial strain tests, stress-strain response.

Figure 38. Uniaxial strain tests, stress-stress response.

111
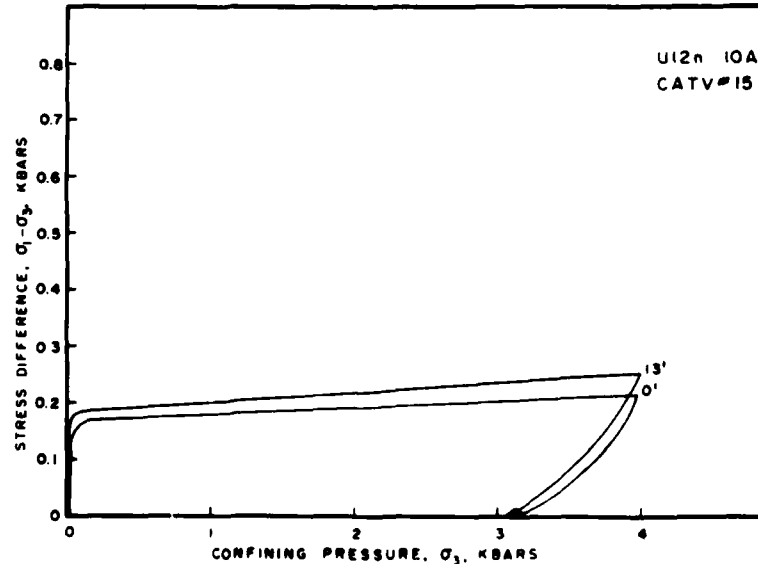
Figure 39. Uniaxial strain tests, stress-strain response.

Figure 40. Uniaxial strain tests, stress-stress response.

112

Figure 41. Uniaxial strain tests, stress-strain response.

Figure 42. Uniaxial strain tests, stress-stress response.

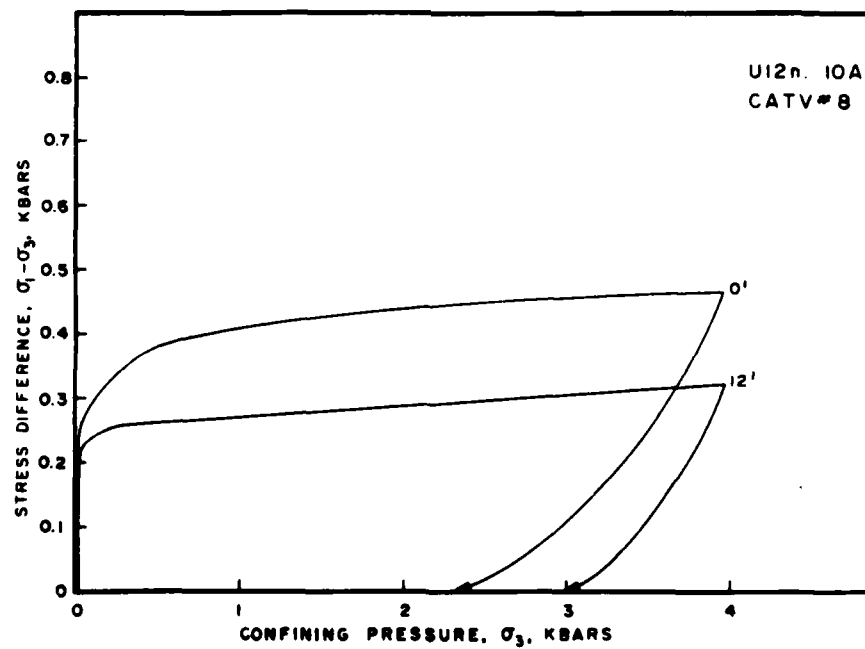Figure 43.   Uniaxial strain tests, stress-strain response.

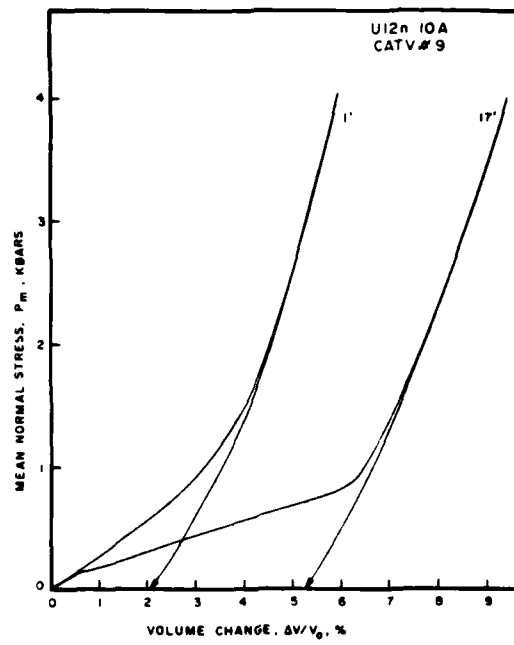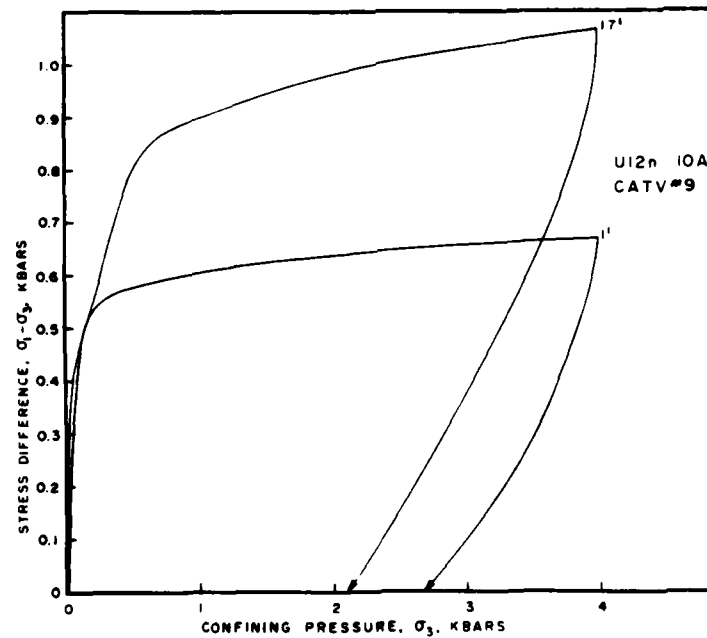Figure 44.   Uniaxial strain tests, stress-stress response.

114

Figure 45. Uniaxial strain tests, stress-strain response.

Figure 46. Uniaxial strain tests, stress-stress response.

115

Figure 47.   Uniaxial strain tests, stress-strain response.

Figure 48.   Uniaxial strain tests, stress-stress response.

116

Figure 49. Uniaxial strain tests, stress-strain response.

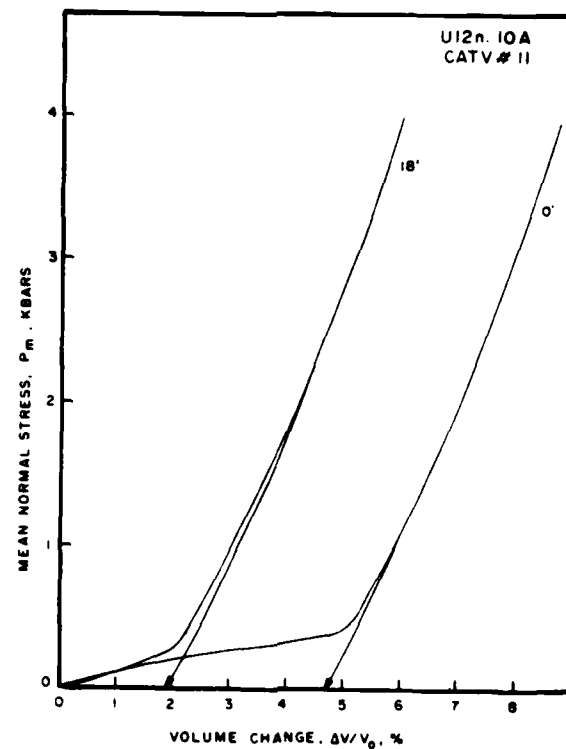Figure 50. Uniaxial strain tests, stress-stress response.

117

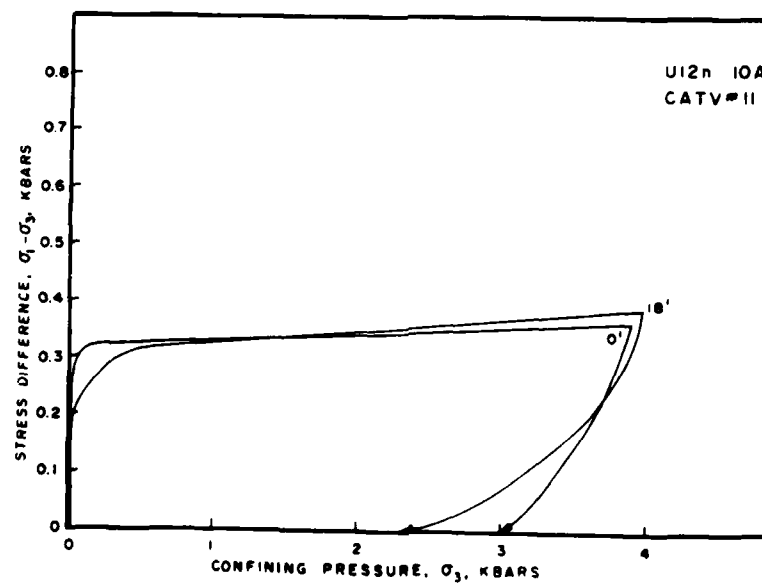Figure 51. Uniaxial strain tests, stress-strain response.

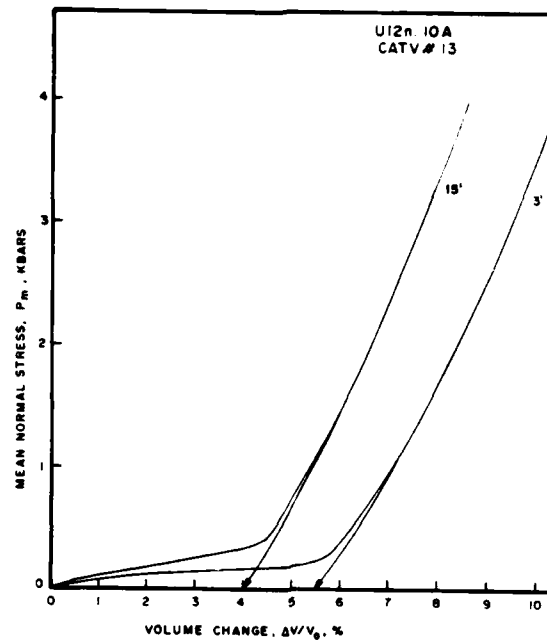Figure 52. Uniaxial strain tests, stress-stress response.

118

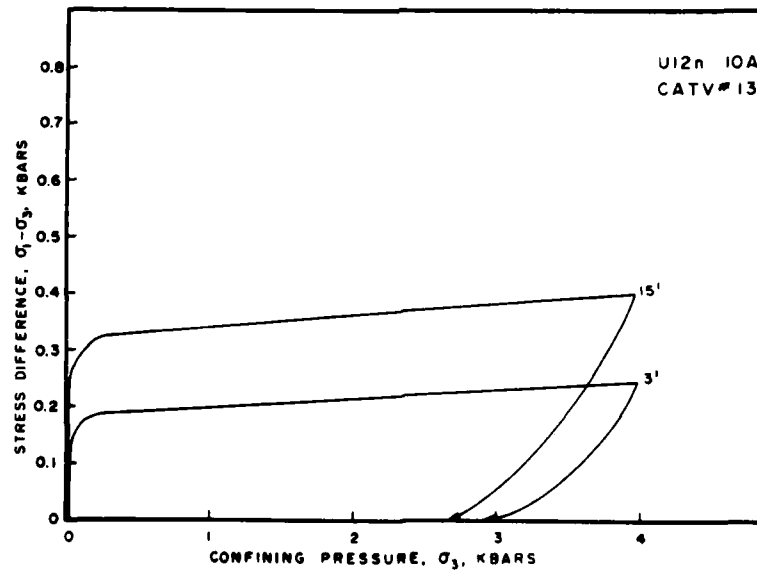Figure 53. Uniaxial strain tests, stress-strain response.

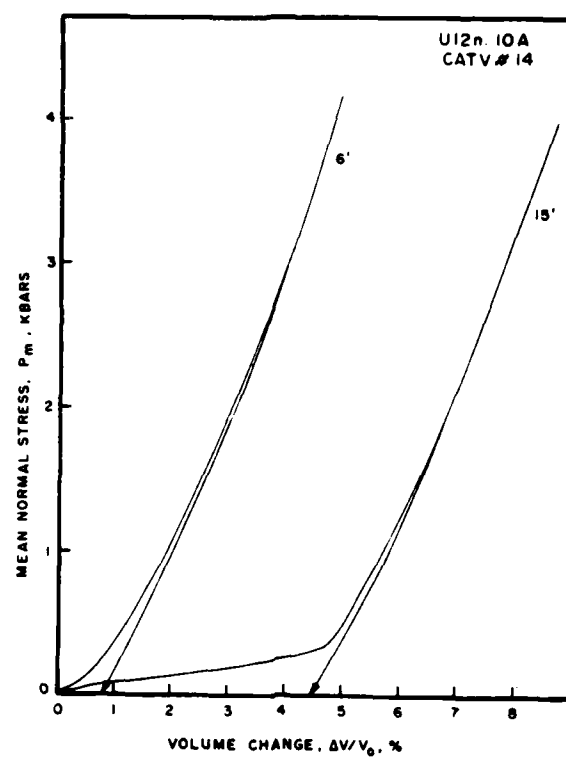Figure 54. Uniaxial strain tests, stress-stress response.

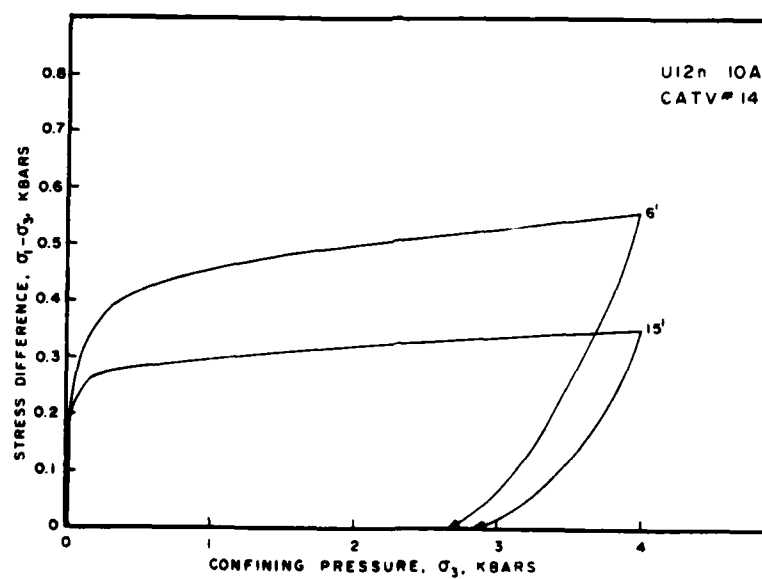119
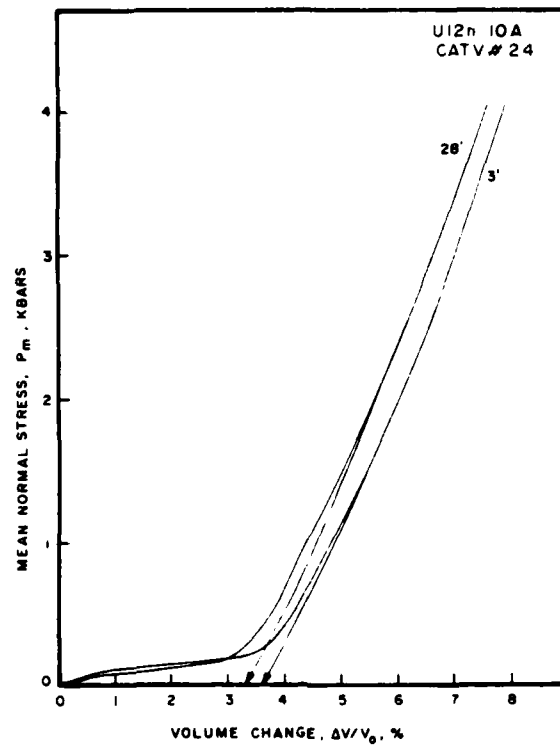
Figure 55. Uniaxial strain tests, stress-strain response.
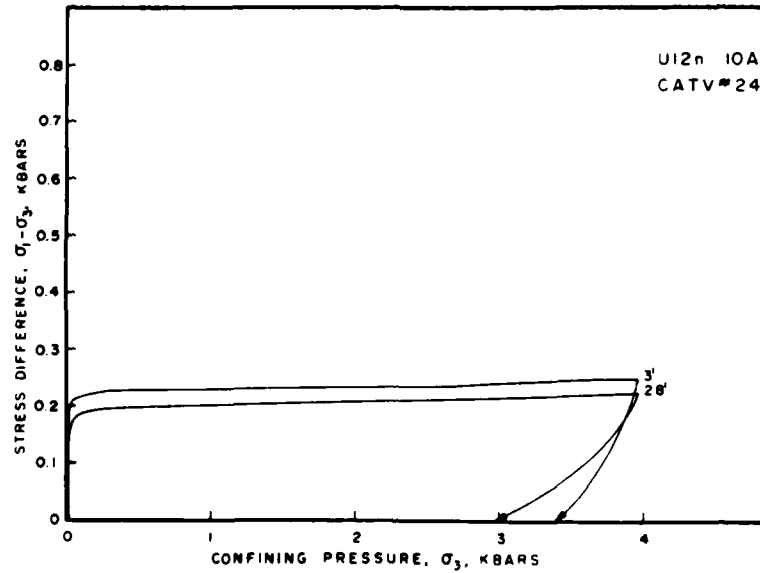
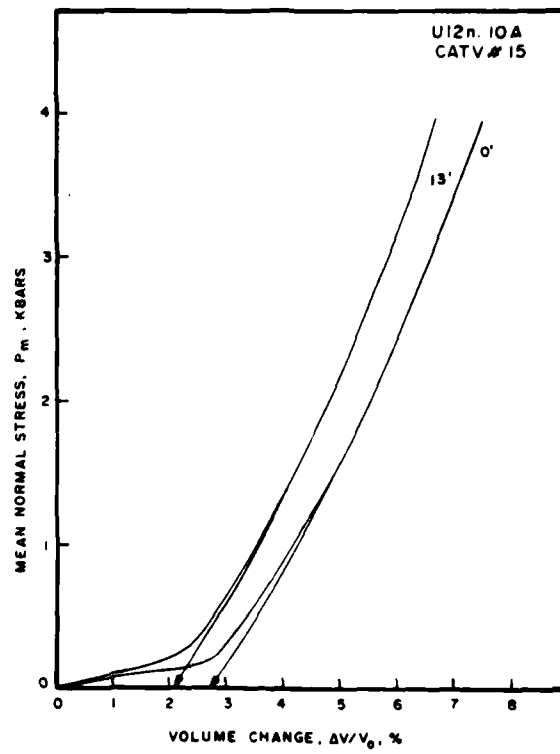Figure 56. Uniaxial strain tests, stress-stress response.

120
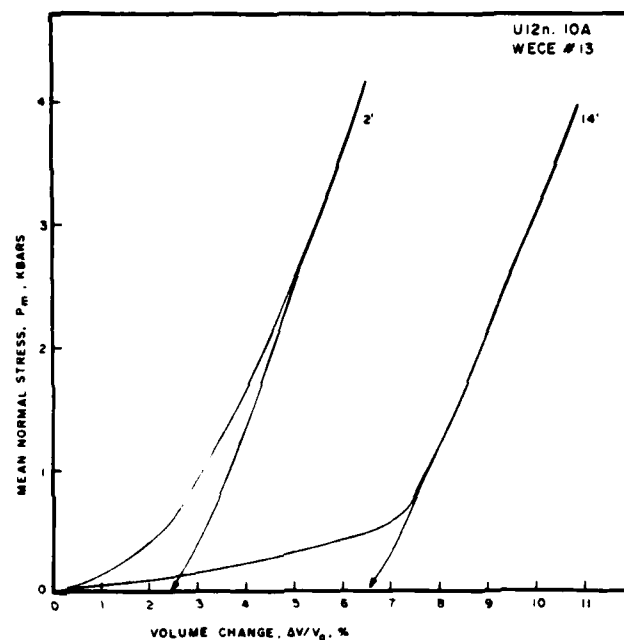
Figure 57. Uniaxial strain tests, stress-strain response.
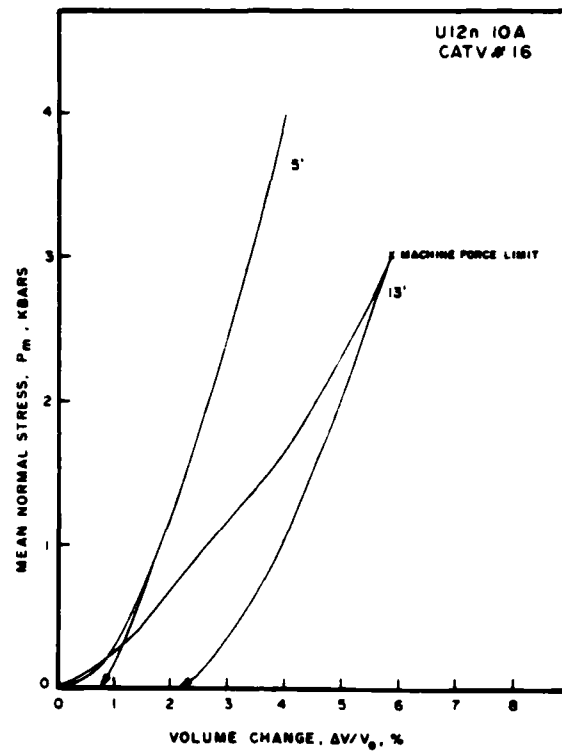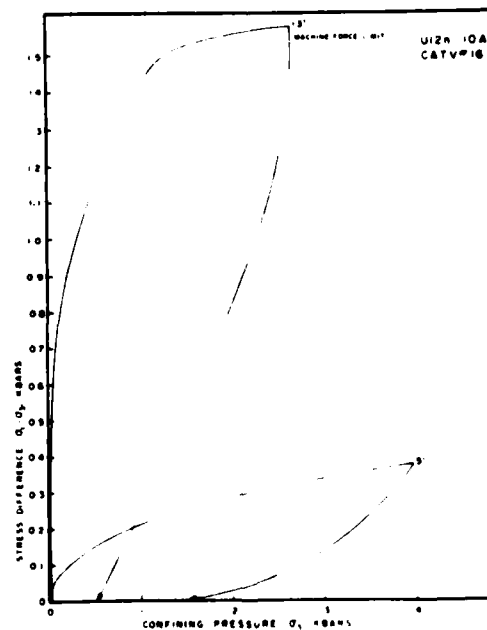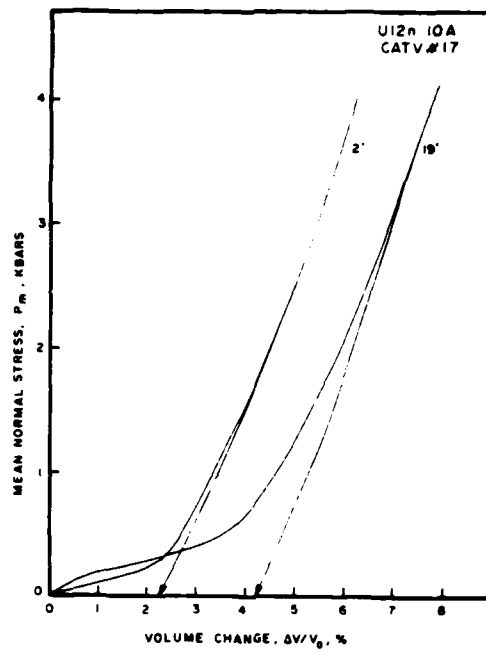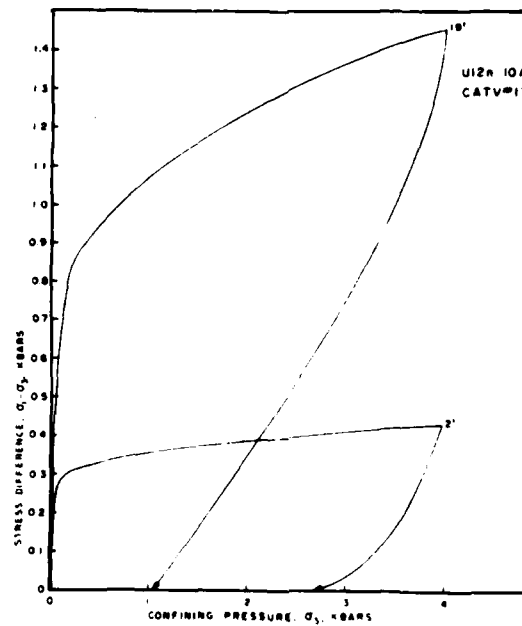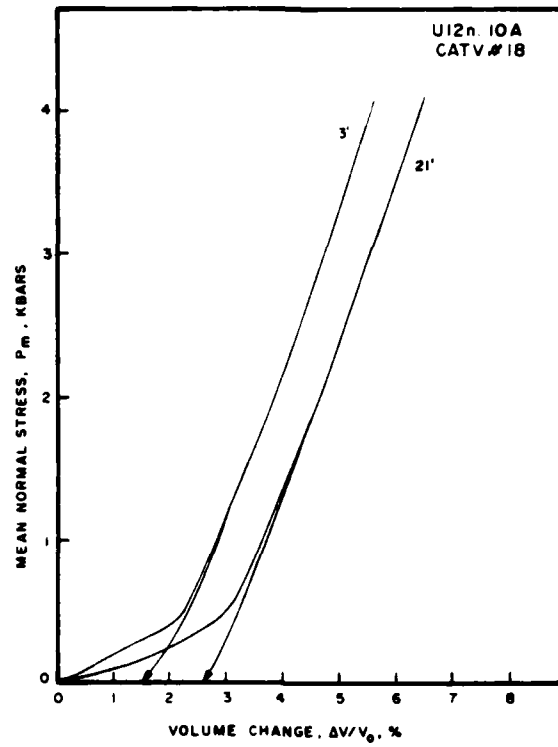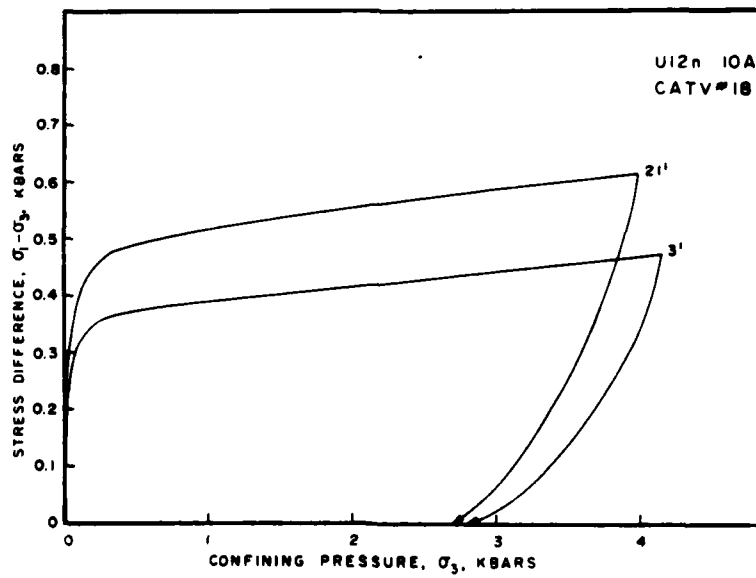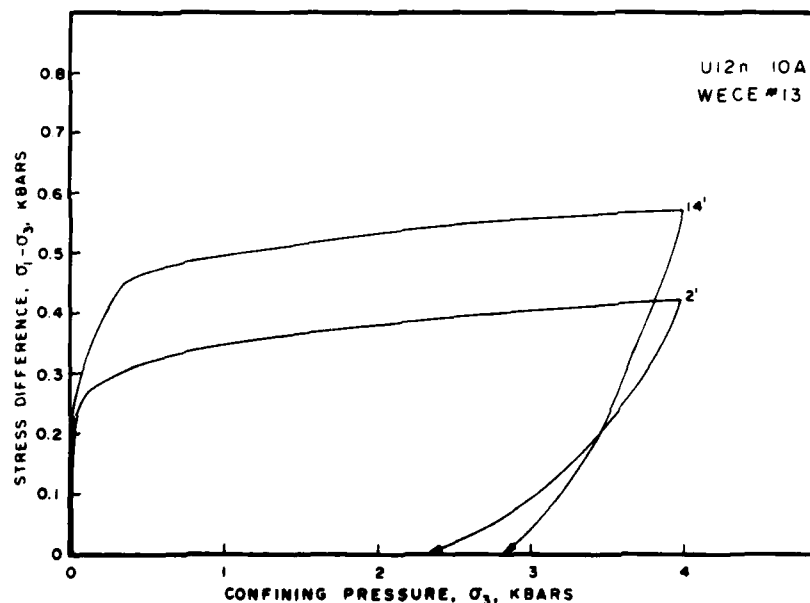

Figure 58. Uniaxial strain tests, stress-stress response.

121

MATERIAL PROPERTIES OF SELECT INTERFACE TUFFS

INTERFACE TUFF SUMMARY

Select "interface" tuffs from near the past Mighty Epic event were
tested to provide supplemental information on the interface region. The
samples were from holes UE12n#9, U12n.10 MH#1 and U12n.10 SSMG#3. Initial
characterization of this region is contained in an earlier Terra Tek
report*. Material testing included physical property and uniaxial strain
testing plus examination of individual specimens with a scanning electron
microscope. A list of physical properties is contained in Table 1.
Figures 1 through 4 show the individual uniaxial strain test curves.
Scanning electron microscope pictures are shown in Figures 5 through 23.

Test samples exhibited considerable material variation. Stress
difference at 4.0 kbars confining pressure during uniaxial strain ranged
from 0.1 to 0.9 kbars and the resulting permanent volume compaction ranged
from 0.9 to 4.8 percent. The U12n.10 MH#1 106' sample was friable and
prevented mechanical test sample preparation.

The scanning electron microscope examinations revealed very few
microfractures.

---

* Butters, S. W. and Green, S. J., "Progress Report One -- Material
    Properties for Mighty Epic Experiment," Terra Tek Report TR 75-
    36, June 1975.

TABLE 1

Physical Properties, Uniaxial Strain Permanent Volume Compaction and Ultrasonic Velocities

DRILL HOLE FOOTAGE	DENSITY (gm/cc)			WATER BY WET WEIGHT (%)	POROSITY (%)	SATURATION (%)	CALC. AIR VOIDS (%)	MEAS. PERMANENT COMP. (%)
	AS-RECEIVED	DRY	GRAIN					
UE12n#9								
1414'	1.84	1.47	2.41	20.0	38.8	94.7	2.1	4.8
U12n.10 MH#1								
*106'	1.79	1.36	2.45	23.8	44.5	95.6	1.9	---
107'	1.95	1.63	2.47	16.3	34.0	93.2	2.3	1.2
U12n.10 SSMG#3								
109'	1.88	1.52	2.45	19.1	37.9	94.5	2.1	0.9
*111'	1.86	1.48	2.40	20.6	38.4	99.7	0.1	3.2
113'	1.95	1.61	2.48	17.4	35.2	96.3	1.3	2.6

* Core samples were received dry and were resaturated prior to testing.
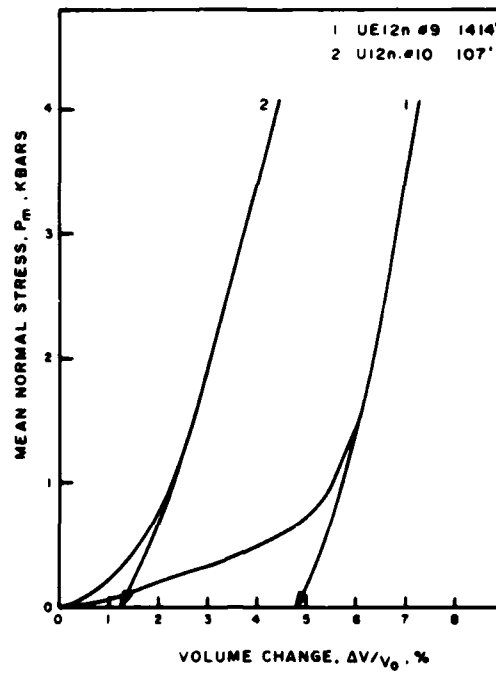
Figure 1.   Uniaxial strain tests, stress-strain response.
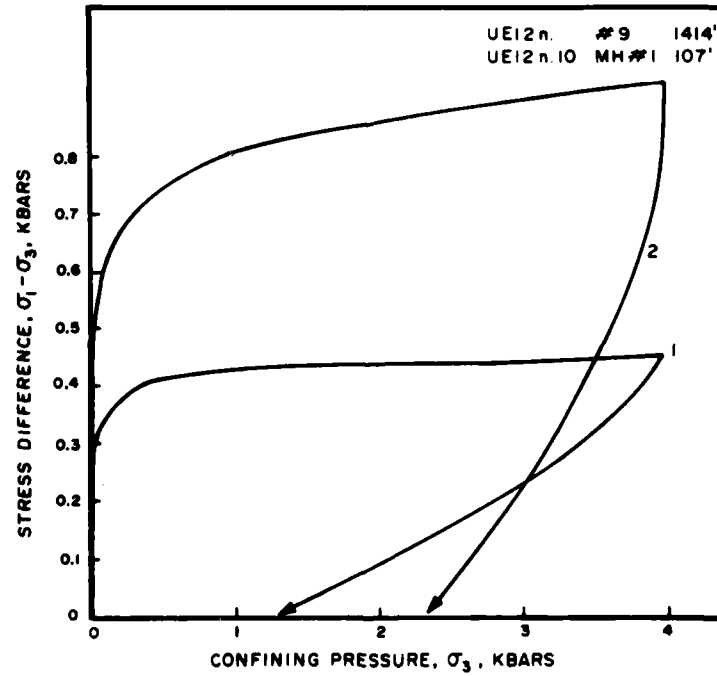
Figure 2.   Uniaxial strain tests, stress-stress response.

124

Figure 3. Uniaxial strain tests, stress-strain response.

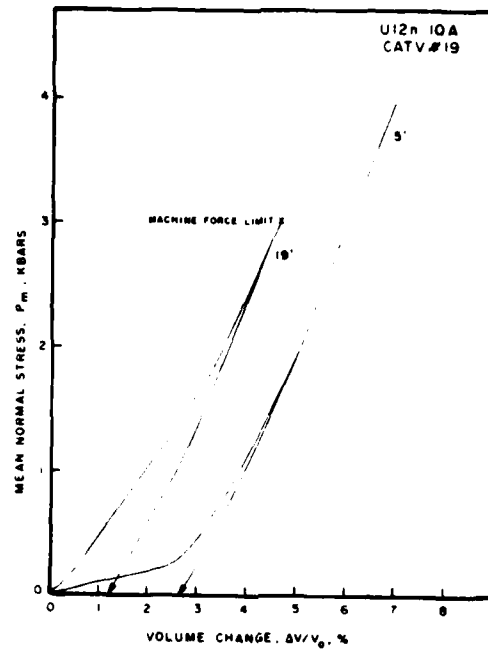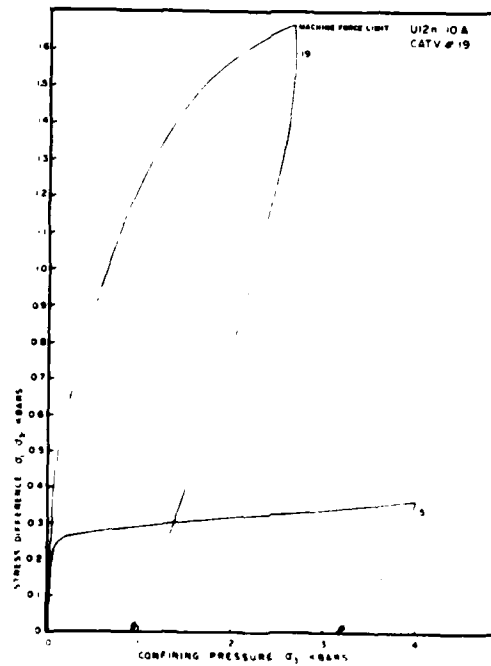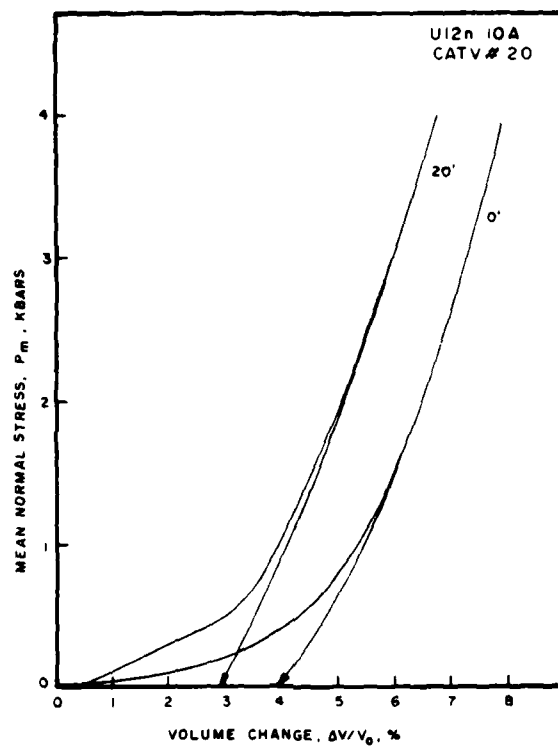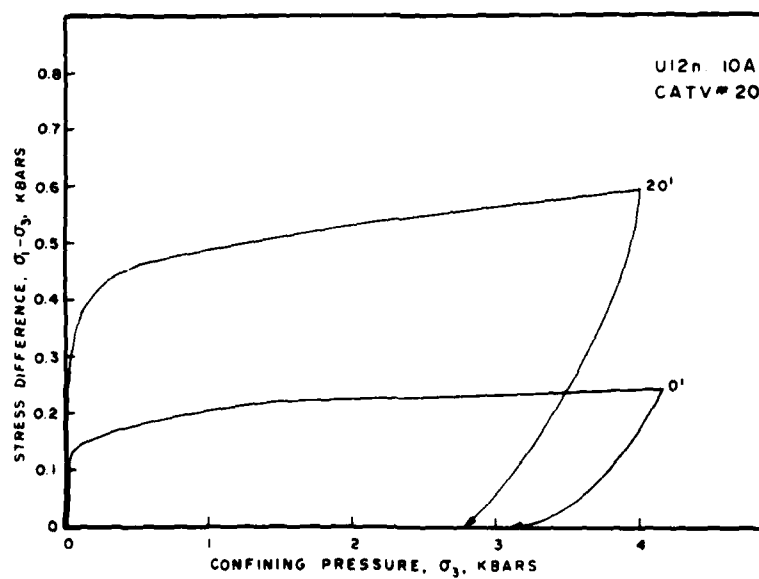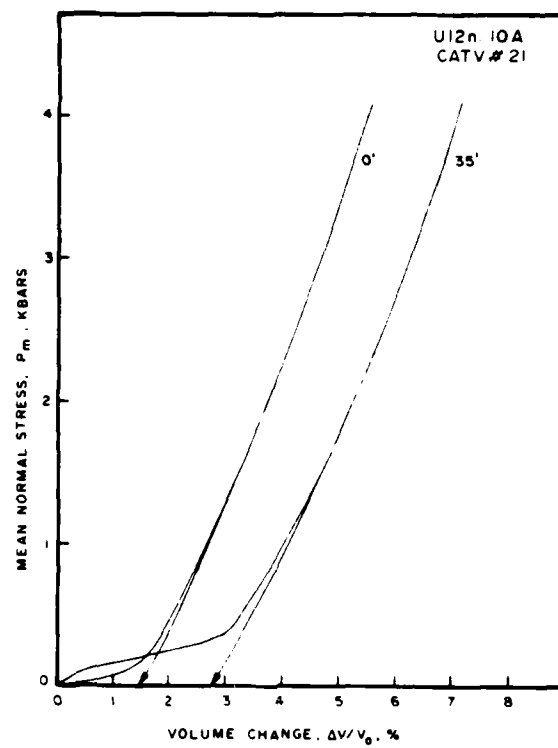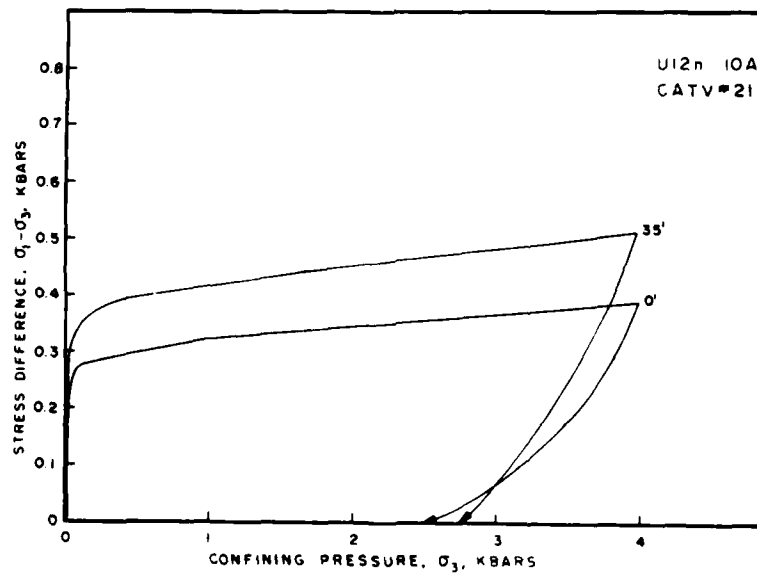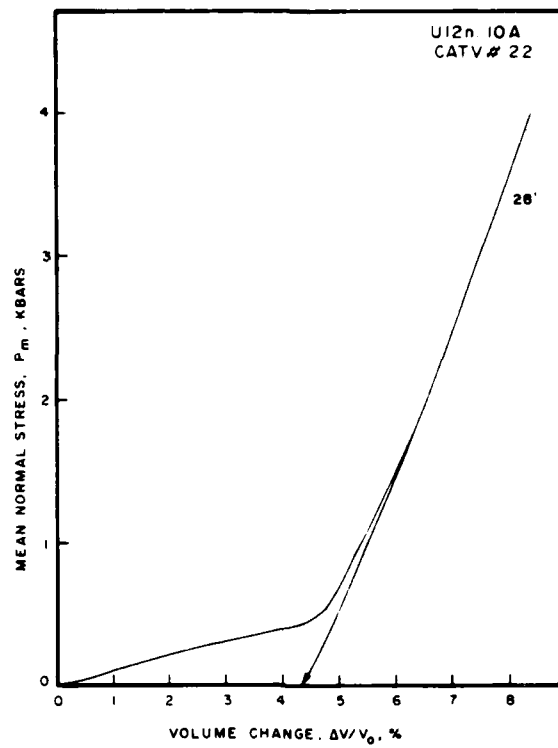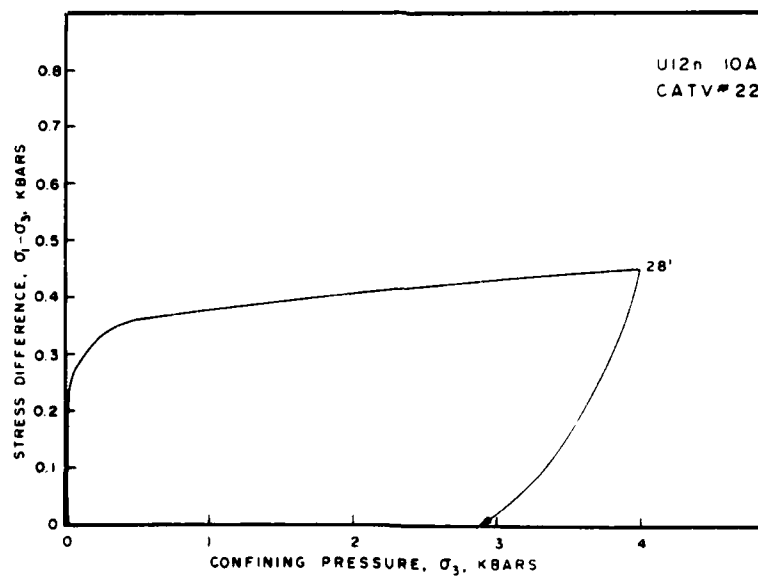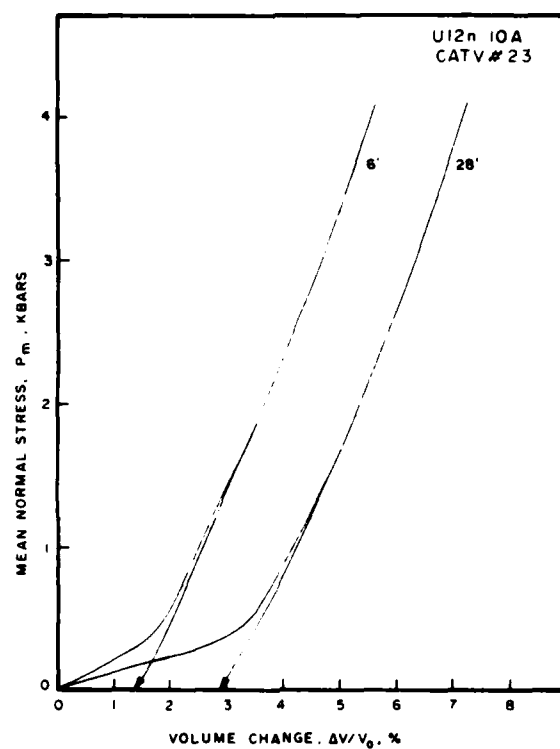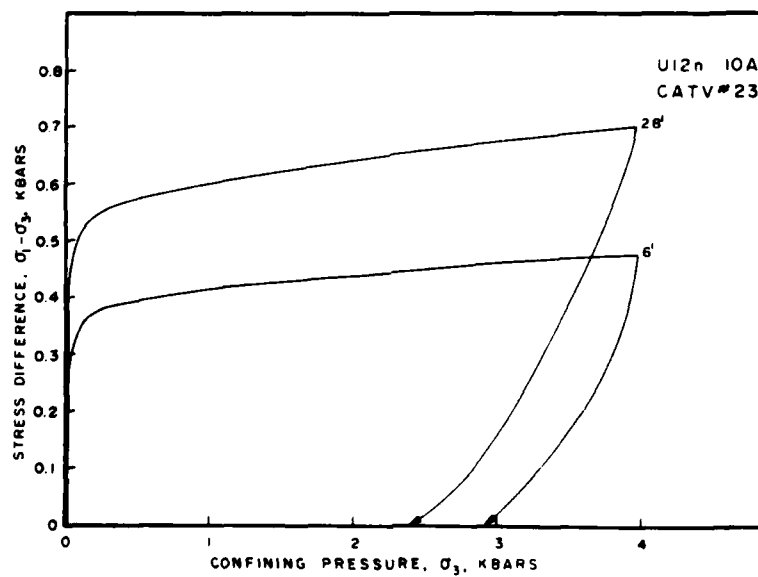Figure 4. Uniaxial strain tests, stress-stress response.

125
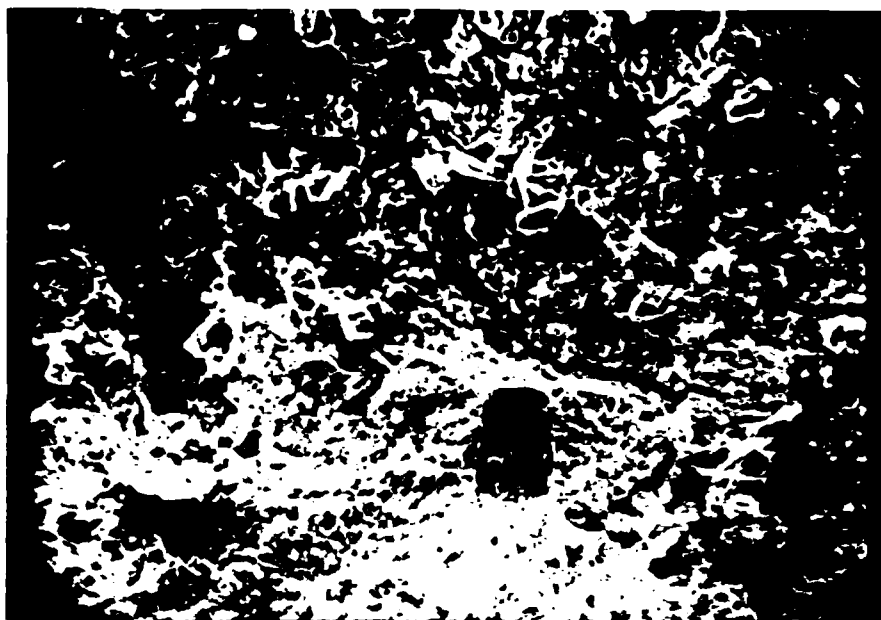
Figure 5. Scanning electron microscope photograph, 200X, on sample UE12n#9-1414'.
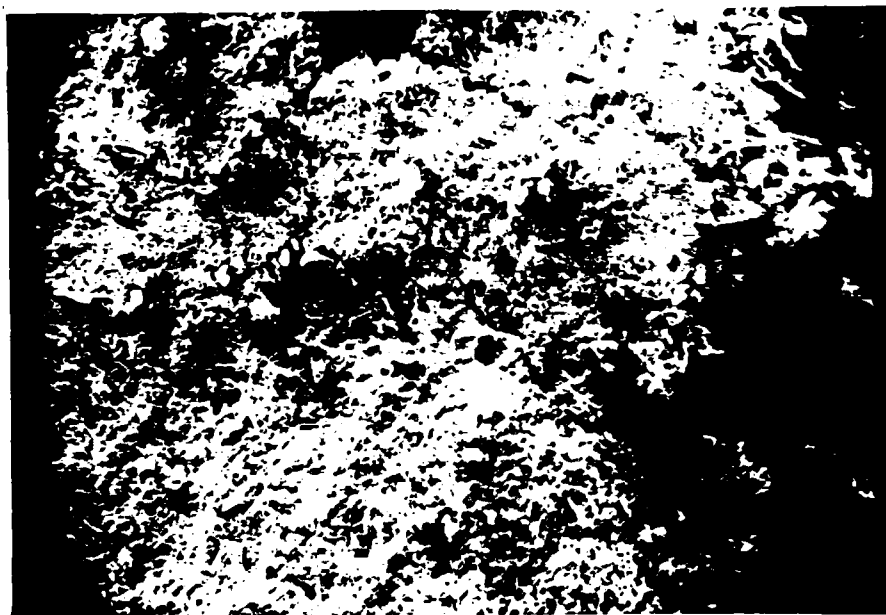
Figure 6. Scanning electron microscope photograph, 2000X, on sample UE12n#9-1414'.

126
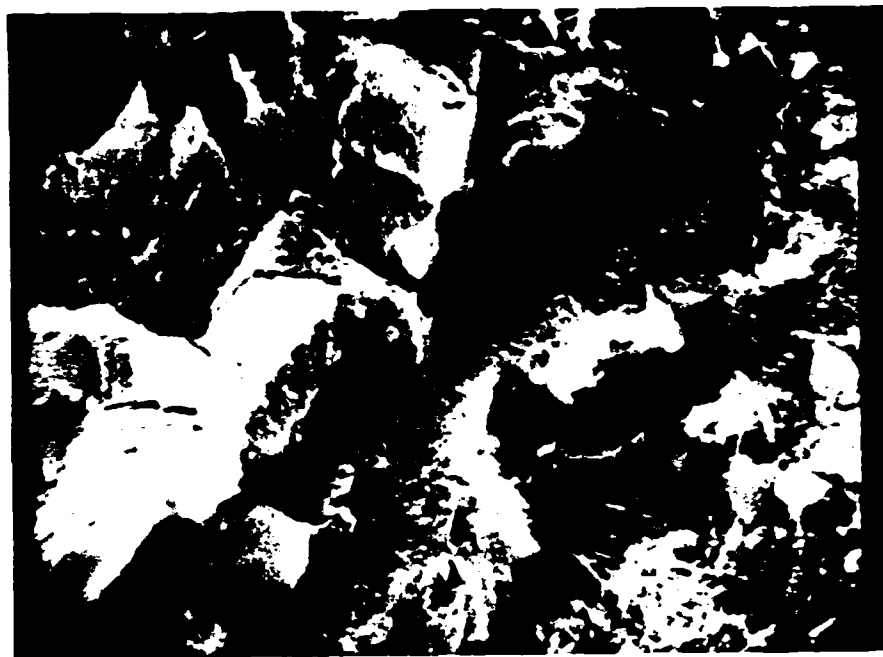
Figure 7. Scanning electron microscope photograph, 2000X, on sample UE12n#9-1414'.

Figure 8. Scanning electron microscope photograph, 2000X, on sample UE12n#9-1414'.

127
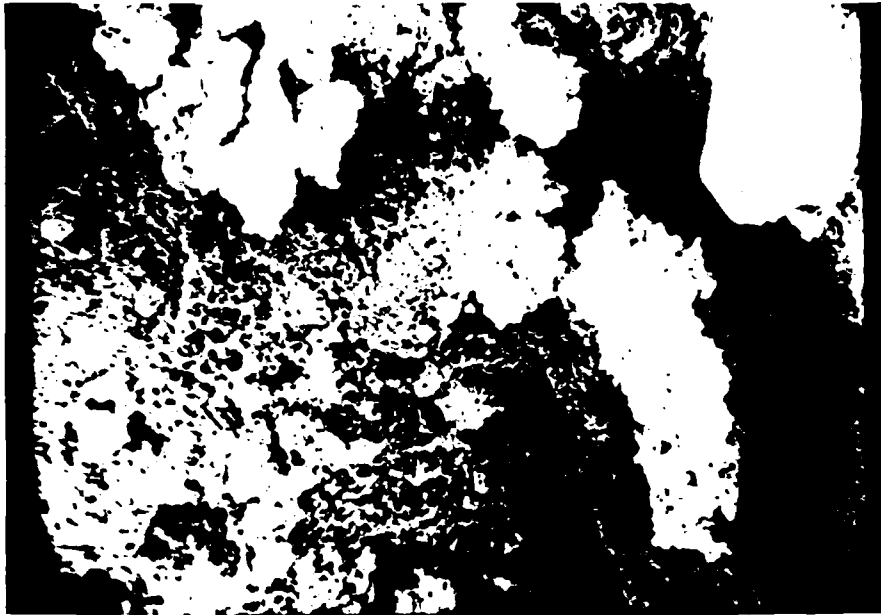
Figure 9.   Scanning electron microscope photograph,
50X, on sample U12n.10 MH#1-106'.
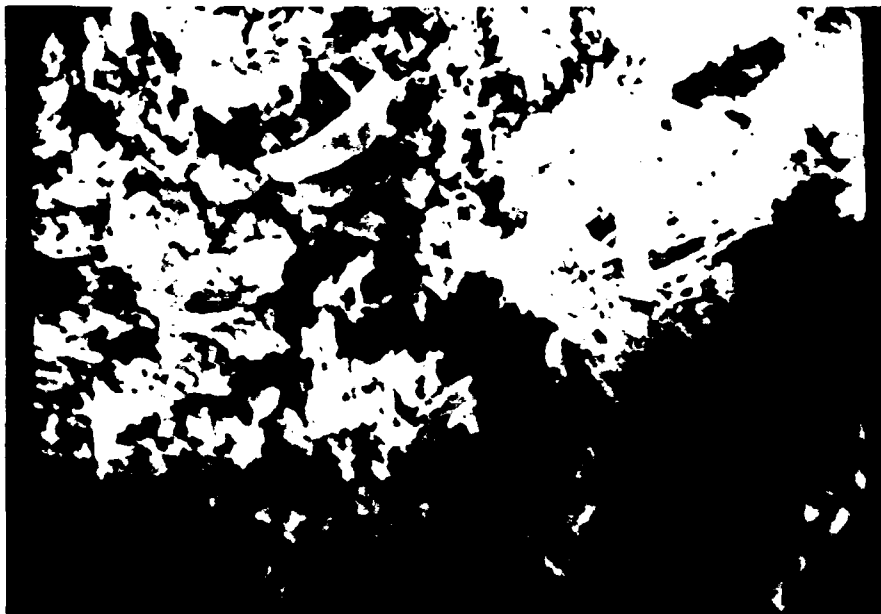
Figure 10.   Scanning electron microscope photograph,
50X, on sample U12n.10 MH#1-106'.

128
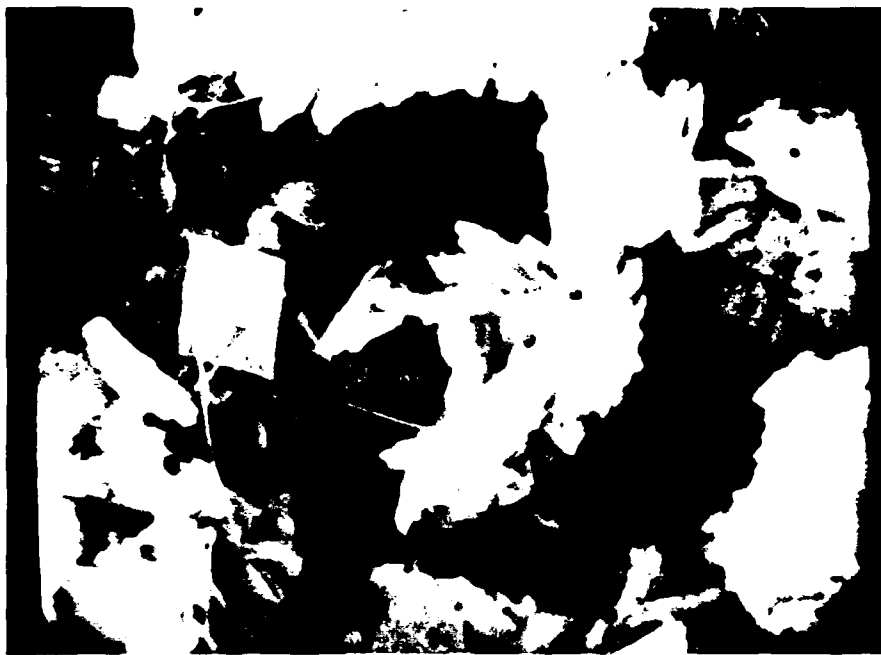
Figure 11. Scanning electron microscope photograph,
2000X, on sample U12n.10 MH#1-106'.
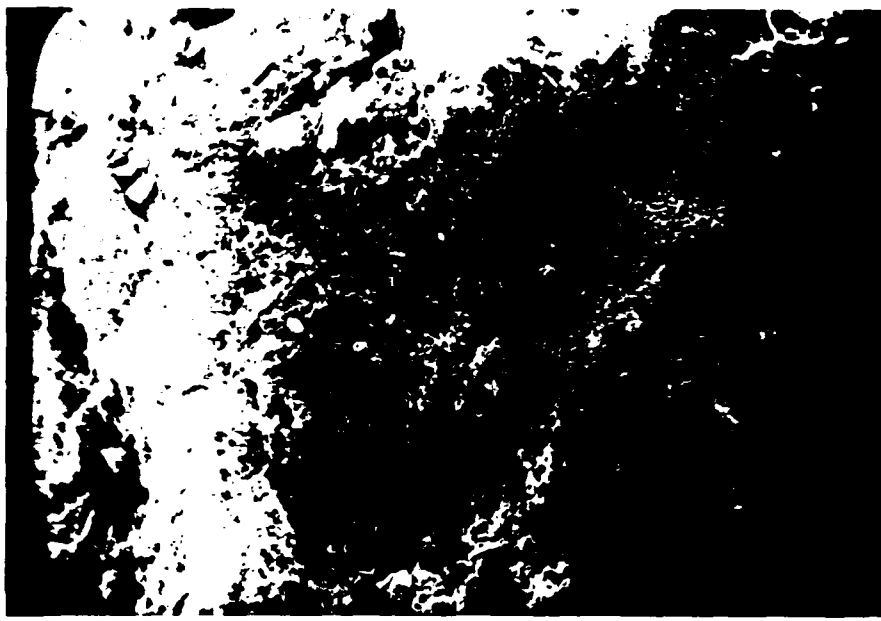
Figure 12. Scanning electron microscope photograph,
50X, on sample U12n.10 MH#1-107'.
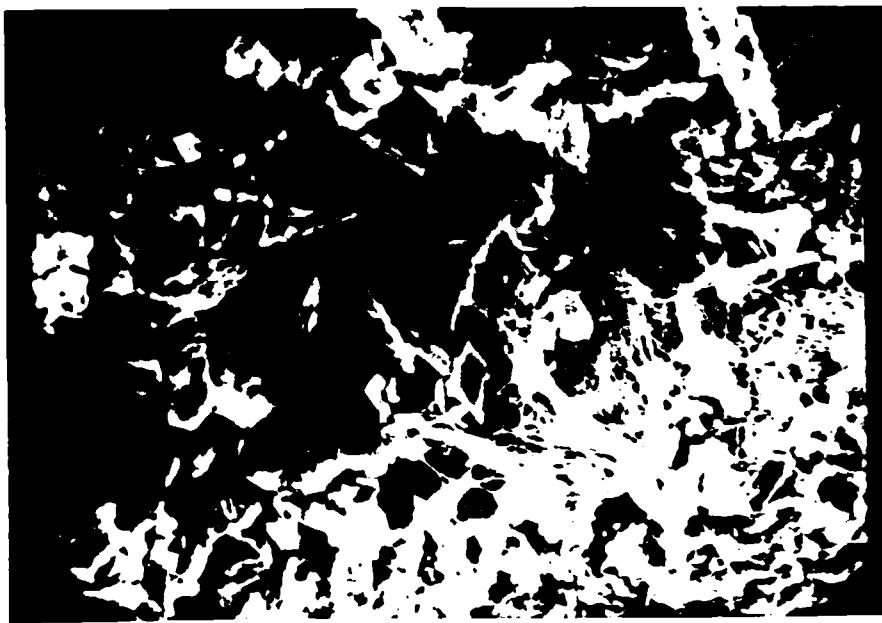
Figure 13. Scanning electron microscope photograph, 50X, on sample U12n.10 MH#1-107'.

Figure 14. Scanning electron microscope photograph, 2000X, on sample U12n.10 MH#1-107'.
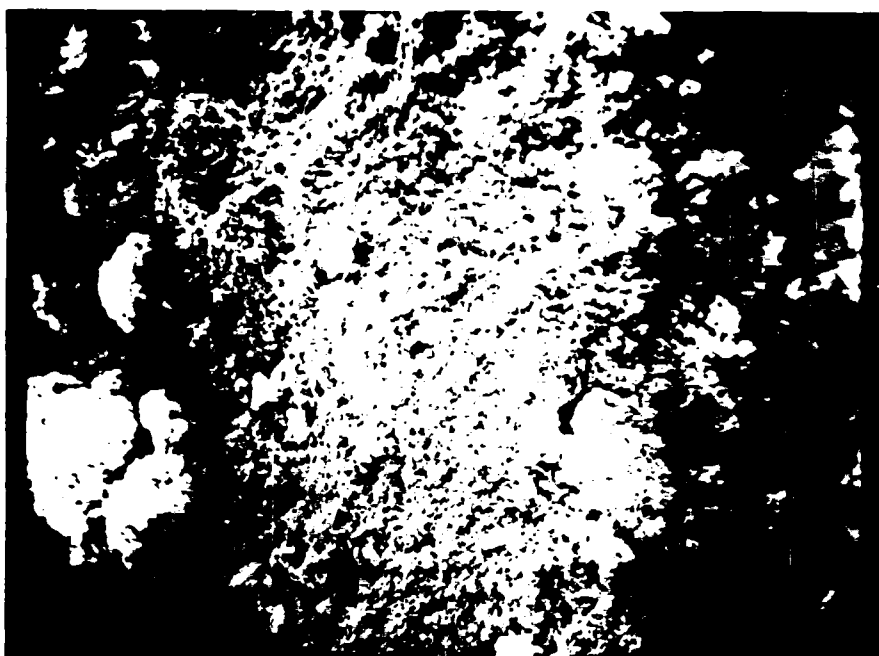
Figure 15.   Scanning electron microscope photograph,
              50X, on sample U12n.10A SSMG#3-109'.
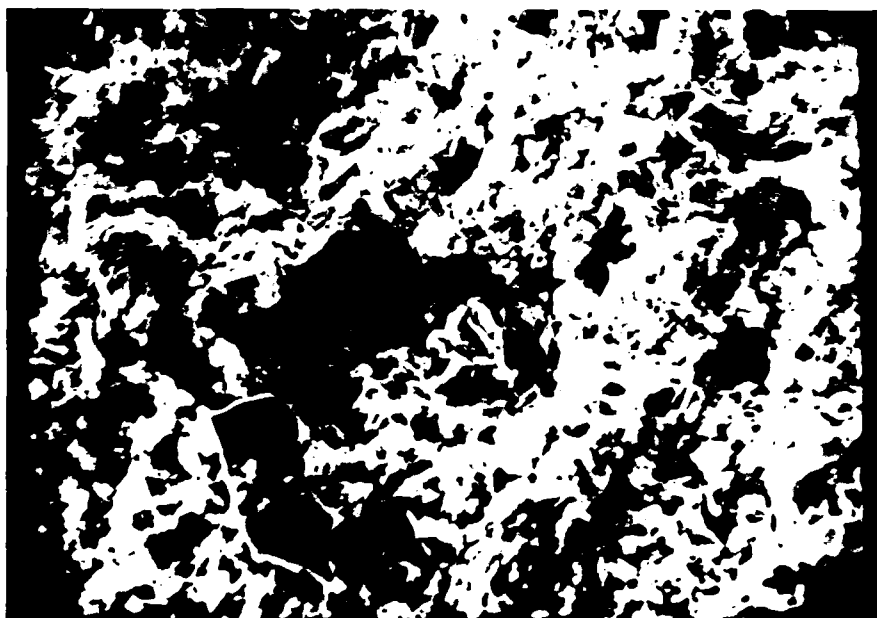
Figure 16.   Scanning electron microscope photograph,
              500X, on sample U12n.10A SSMG#3-109'.

131

Figure 17. Scanning electron microscope photograph, 2700X, on sample U12n.10A SSMG#3-109'.
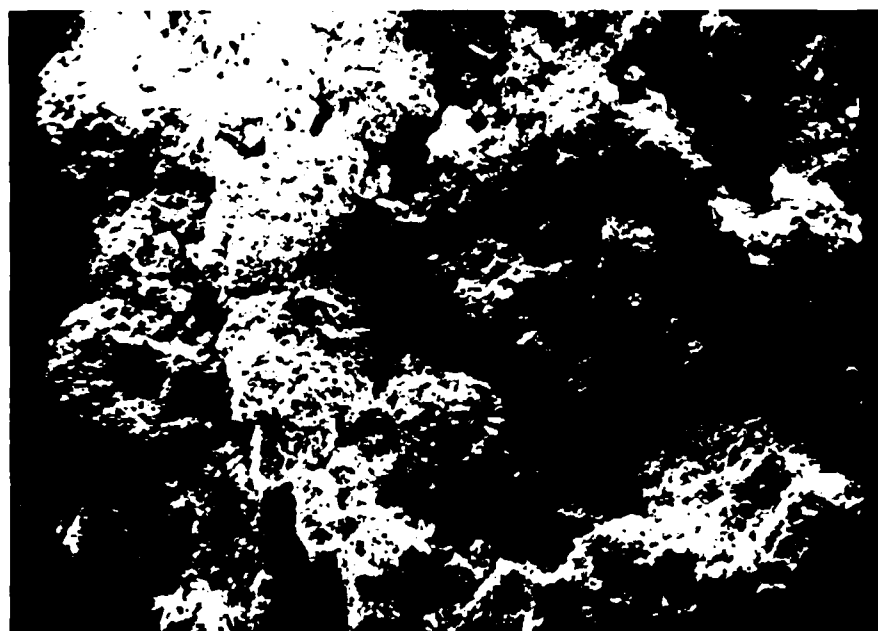
Figure 18. Scanning electron microscope photograph, 50X, on sample U12n.10A SSMG#3-111'.
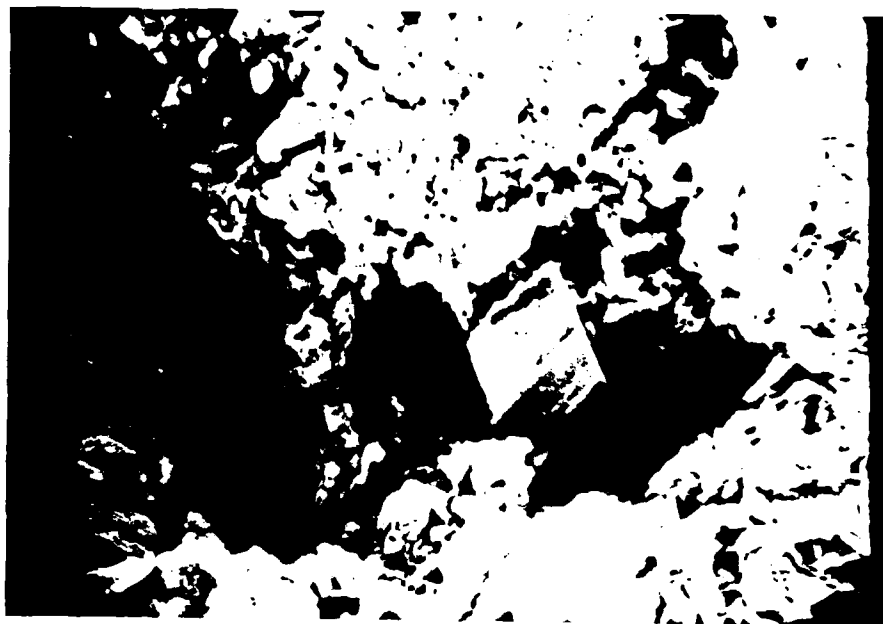
Figure 19. Scanning electron microscope photograph,
500X, on sample U12n.10A SSMG#3-111'.
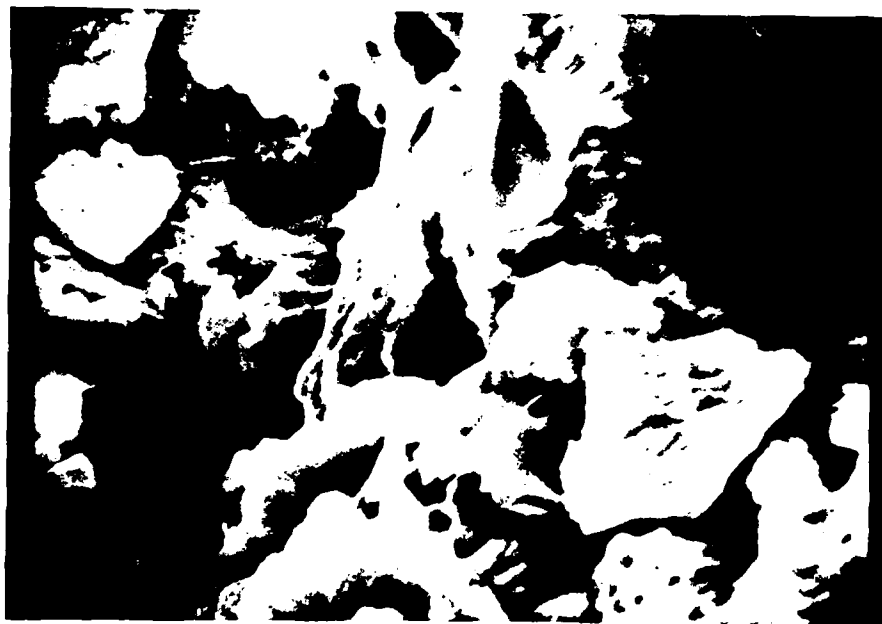
Figure 20. Scanning electron microscope photograph,
2000X, on sample U12n.10A SSMG#3-111'.
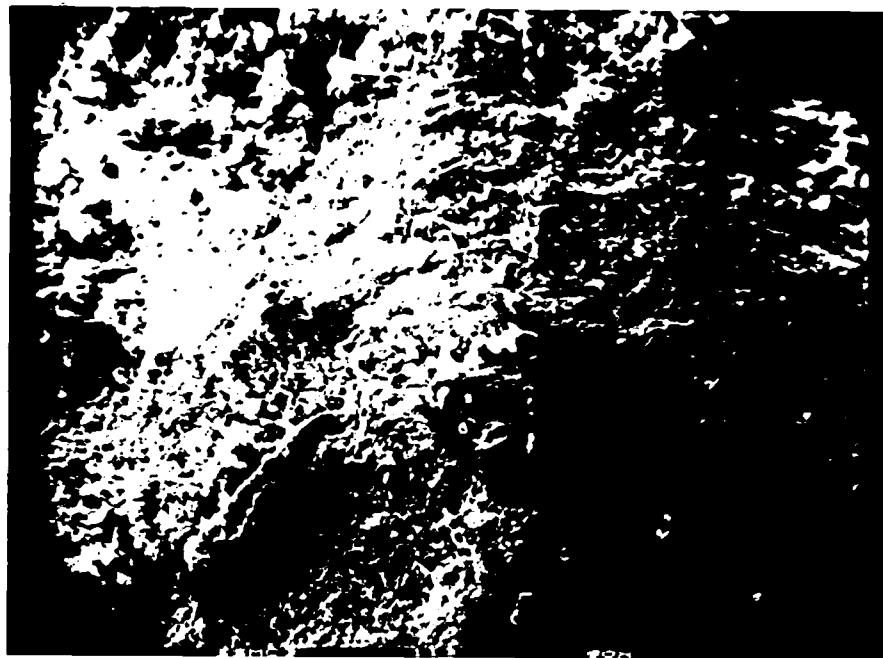
Figure 21. Scanning electron microscope photograph, 50X, on sample U12n.10A SSMG#3-113'.
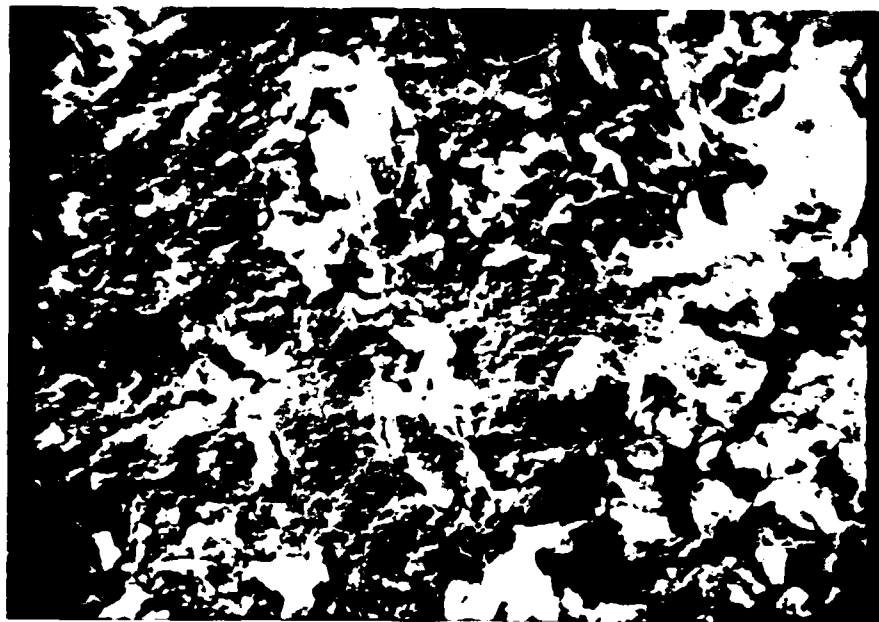
Figure 22. Scanning electron microscope photograph, 500X, on sample U12n.10A SSMG#3-113'.
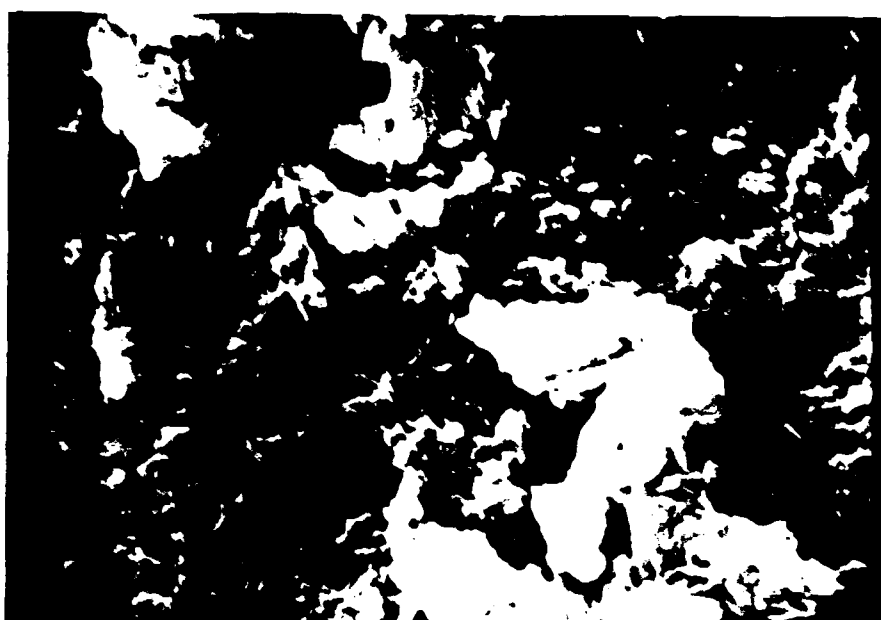
Figure 23. Scanning electron microscope photograph,
2000X, on sample U12n.10A SSMG#3-113'.

CONTAINMENT EVALUATION

INTRODUCTION

Evaluation of the media around past nuclear events is necessary to evaluate the material's response to subsequent nearby nuclear events. The effects, if any, the dynamic shock loading has on the media's containment potential are of primary concern*. Changes in both physical and mechanical properties are required for this evaluation. Re-entry drill hole tuffs from U12e and U12g tunnels were evaluated. The following drill holes were evaluated:

U12e.20 DNRE#4

U12g   R.S. #2, 3, and 4

U12g   DNEX #1, 2

The materials were evaluated via physical property, uniaxial strain and dry sample permeability (to gas) tests. Additionally, select samples were examined with the scanning electron microscope.

---

* Previous evaluation of the affects of the Dining Car event are contained in Terra Tek report, TR 77-96, November 1977.

TEST RESULTS

Drill Hole U12e.20 DNRE#4

Physical properties, uniaxial strain measured permanent compaction, ultrasonic velocities and permeabilities are listed in Table 1. Uni-axial strain test curves are shown in Figures 1 through 4. Appendix A contains scanning electron microscope (SEM) photographs of select samples. Physical property and uniaxial strain tests suggest air void contents from 2 to 4 percent. The SEM photographs showed microfractures (~10 microns wide) in the material. These probably account for a portion of the "foot" (and hence apparent air void content) seen on the stress-strain response of the uniaxial strain test (documented in previous liter-ature*).

Permeability varied considerably, ranging from 0.2 to 194.0 milli-darcies. As expected, gas-flow occurred primarily along fractures as verified by submersing the test samples under water and observing the exit pattern of the gas bubbles.

TABLE 1

Physical Properties, Uniaxial Strain Measured Permanent Compaction, Ultrasonic Velocities and Permeabilities for U12e.20 DNRE#4 Tuff Samples

DRILL HOLE FOOTAGE U12e.20	DENSITY (gm/cc)			WATER BY WET WEIGHT (%)	POROSITY (%)	SATURATION (%)	CALC. AIR VOIDS (%)	MEAS. PERMANENT COMP. (%)	VELOCITY (km/sec)		DRY SAMPLE PERMEABILITY (GAS) mdarcy
	AS-RECEIVED	DRY	GRAIN						LONG	SHEAR	
DNRE#4											
162	1.77	1.41	2.40	20.6	41.5	37.8	5.0	2.3	2.32	1.01	1.5
165	1.77	1.40	2.43	21.0	42.6	86.7	5.7	3.6	1.91	0.93	0.2
173	1.79	1.35	2.43	24.7	44.6	99.0	0.4	3.0	2.21	0.82	1.2*
180	1.72	1.31	2.42	23.8	45.8	89.4	4.9	3.9	1.77	0.78	0.6
185	1.79	1.41	2.39	21.1	41.0	91.9	3.3	3.1	2.37	1.03	1.4*
196	1.78	1.35	2.48	24.1	45.5	94.6	2.4	2.1	2.02	0.62	11.3*
207	1.75	1.31	2.46	25.5	47.0	95.1	2.3	---	1.68	0.71	194.0*

* Obvious fracture permeability.

---

* Gardiner, D. S. and S. W. Butters, "Some Material Properties for the Hybla Gold Event," Terra Tek Report TR 77-46, June 1977.
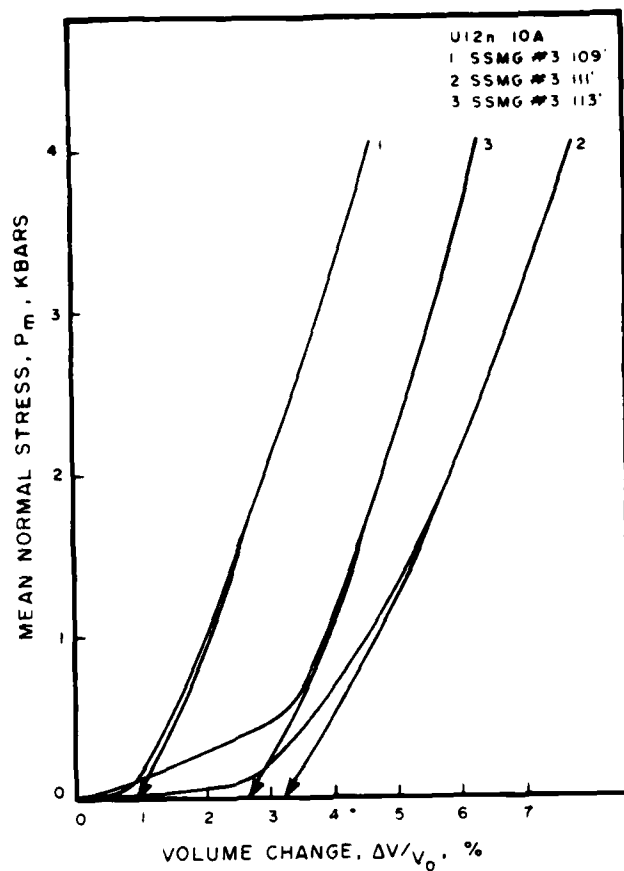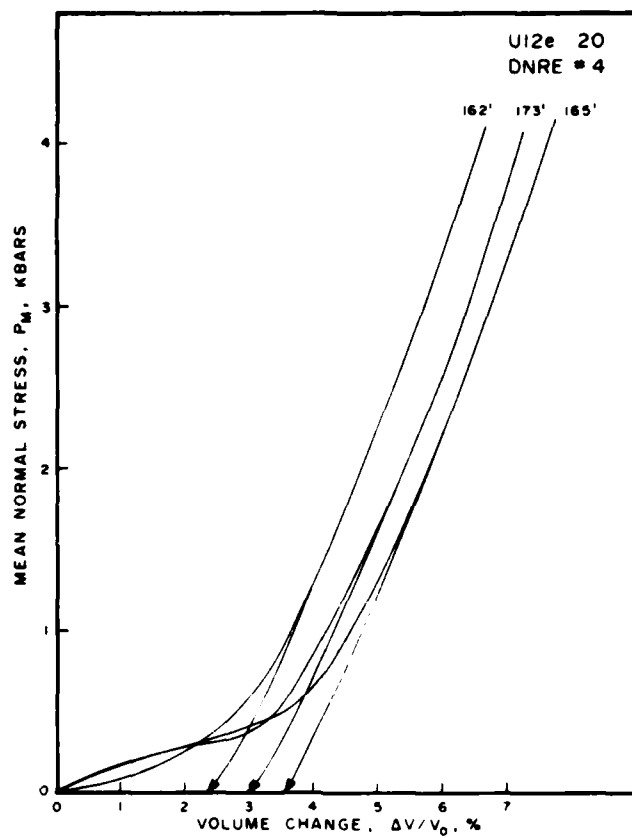
137

Figure 1.   Uniaxial strain tests, stress-strain response.

Figure 2.   Uniaxial strain tests, stress-stress response.

138

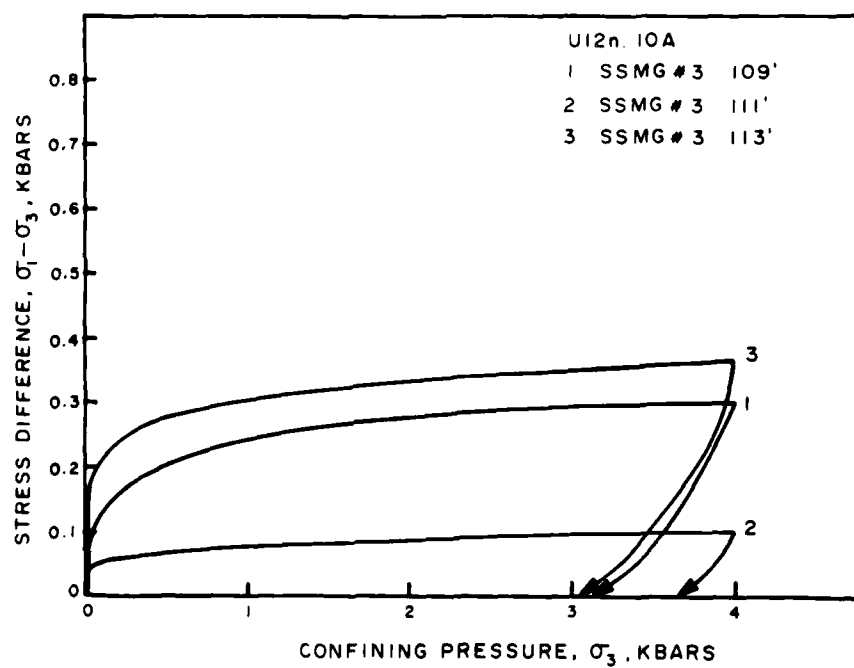Figure 3. Uniaxial strain tests, stress-strain response.

Figure 4. Uniaxial strain tests, stress-stress response.

139

Drill Holes U12g R.S.#2, 3, 4 and DNEX#1, 2

Physical properties, uniaxial strain measured permanent compaction, ultrasonic velocities and permeabilities are listed in Table 2. Individual uniaxial strain curves are shown in Figures 5 through 18. Test results indicate the R.S. holes to have very similar properties. Air void contents are consistent at about 2 percent and stress difference observed at 4.0 kbars confining pressure averaged 0.28 kbars.

The DNEX drill holes exhibited much more variation in air void content and strength. Air void contents ranged from ~0.5 to ~7.0 percent and stress difference at 4.0 kbars ranged from 0.16 to 0.81 kbars. The material variation was also apparent in the permeability which varied from 0.1 to 3.4 millidarcies. Microfractures were evident in some samples (see Appendix A for SEM photographs of DNEX drill hole samples).

TABLE 2

Physical Properties, Uniaxial Strain Permanent Volume Compaction
and Ultrasonic Wave Velocities of U12g Tunnel Tuffs

| DRILL HOLE FOOTAGE	DENSITY (gm/cc)			WATER BY WET WEIGHT (%)	POROSITY (%)	SATURATION (%)	CALC. AIR VOIDS (%)	MEAS. PERMANENT COMP. (%)	VELOCITY (km/sec)		GAS PERMEABILITY (DRY SAMPLE) mdarcy
	AS-RECEIVED	DRY	GRAIN						LONG	SHEAR	
R.S.#2											
24	1.92	1.56	2.50	18.6	37.5	95.3	1.8	1.8	2.58	2.15	
43	2.01	1.69	2.50	15.9	32.4	98.6	0.4	1.8	2.77	1.10	
R.S.#3											
73	1.90	1.53	2.48	19.7	38.5	97.3	1.1	1.5	2.81	1.27	
121	1.76	1.32	2.43	25.2	45.6	97.4	1.2	1.9	2.73	1.16	
R.S.#4											
37	1.87	1.51	2.45	19.1	38.2	93.3	2.6	2.4	2.83	1.31	
65	1.93	1.57	2.51	18.7	37.5	96.3	1.4	2.1	3.09	1.51	
DNEX#1											
303	1.89	1.54	2.38	18.6	35.4	99.3	0.2	1.8	2.67	1.14	0.1
312	1.77	1.43	2.34	19.1	38.8	87.0	5.0	4.3	2.00	1.13	3.2*
339	1.78	1.44	2.44	18.9	40.9	81.9	7.4	4.9	2.69	1.28	0.1
361	1.77	1.42	2.43	20.0	41.6	84.9	6.3	1.6	3.17	1.47	3.4*
380	1.78	1.45	2.36	18.7	38.4	86.8	5.1	5.9	3.75	2.13	2.2*
DNEX#2											
74	1.94	1.59	2.57	18.3	38.4	92.6	2.8	0.5	2.98	1.41	2.9*
92	1.88	1.50	2.46	20.3	39.0	97.6	0.8	1.4	3.03	1.31	0.1
108	1.84	1.45	2.51	20.9	41.8	92.2	3.3	1.1	2.50	1.26	0.9
116	1.92	1.57	2.48	18.1	36.4	95.3	1.7	0.9	3.02	1.42	0.1
120	2.03	1.78	2.49	12.2	28.5	87.0	1.7	2.1	3.03	1.52	0.2

* Obvious fracture permeability.
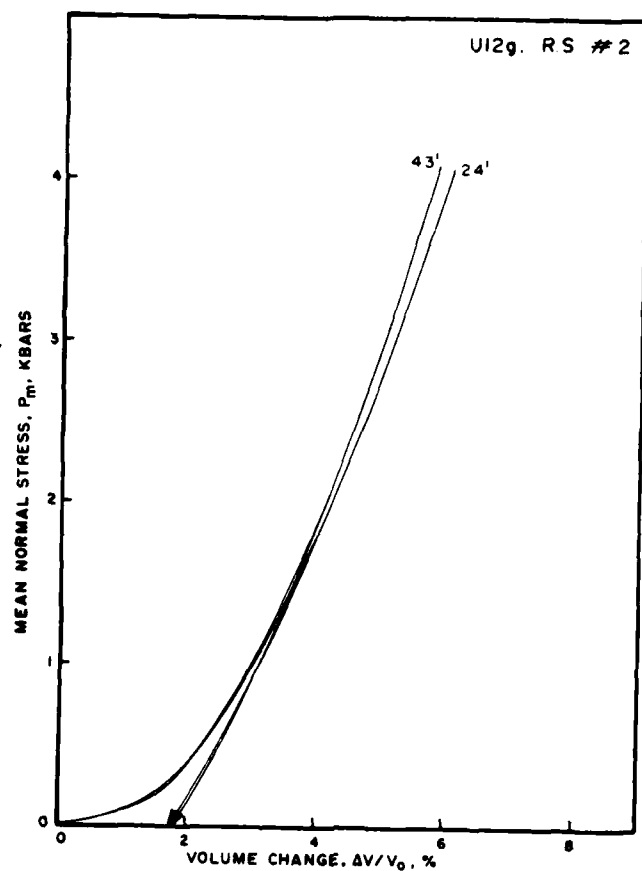
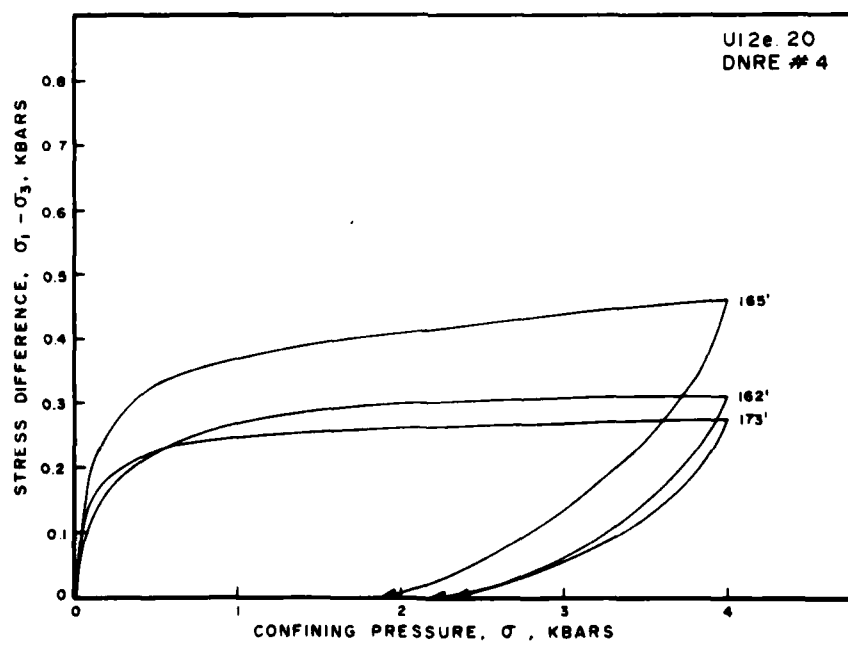Figure 5.   Uniaxial strain tests, stress-strain response.
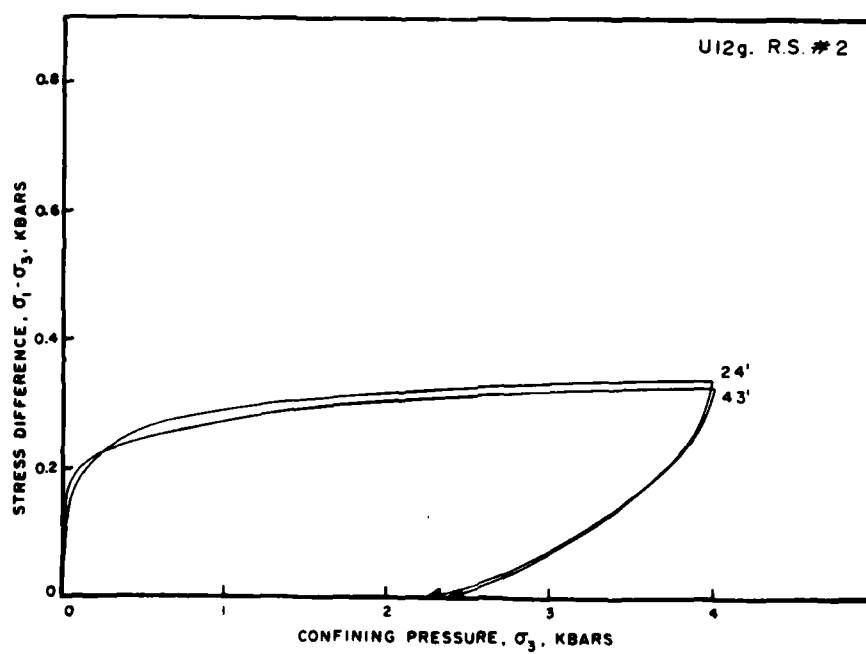
Figure 6.   Uniaxial strain tests, stress-stress response.

141
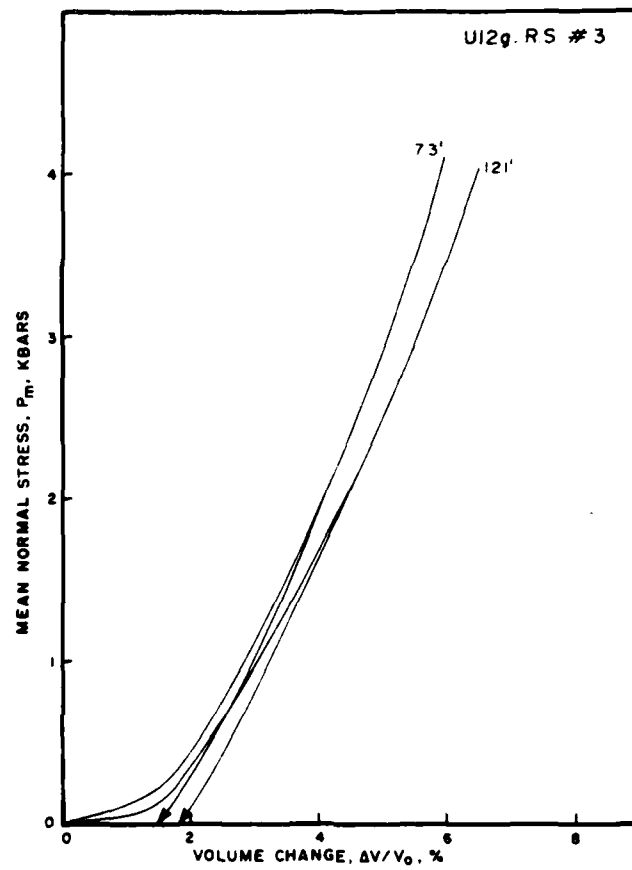
Figure 7. Uniaxial strain tests, stress-strain response.

Figure 8. Uniaxial strain tests, stress-stress response.
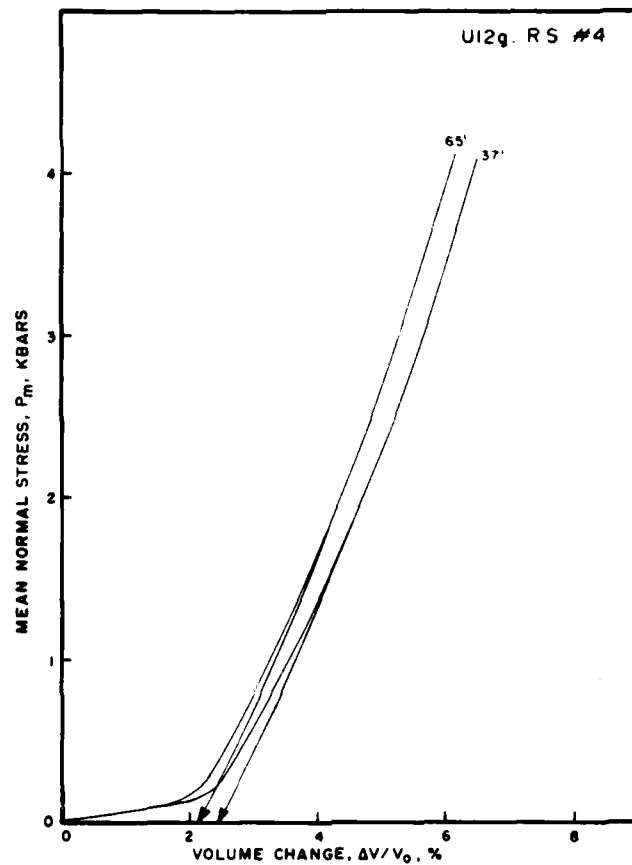
142

Figure 9. Uniaxial strain tests, stress-strain response.

Figure 10. Uniaxial strain tests, stress-stress response.

143
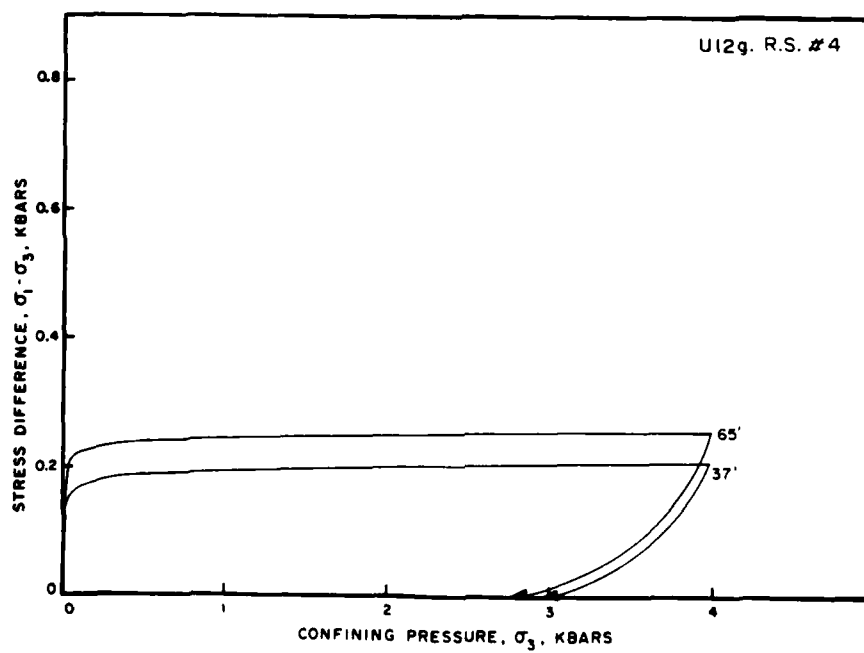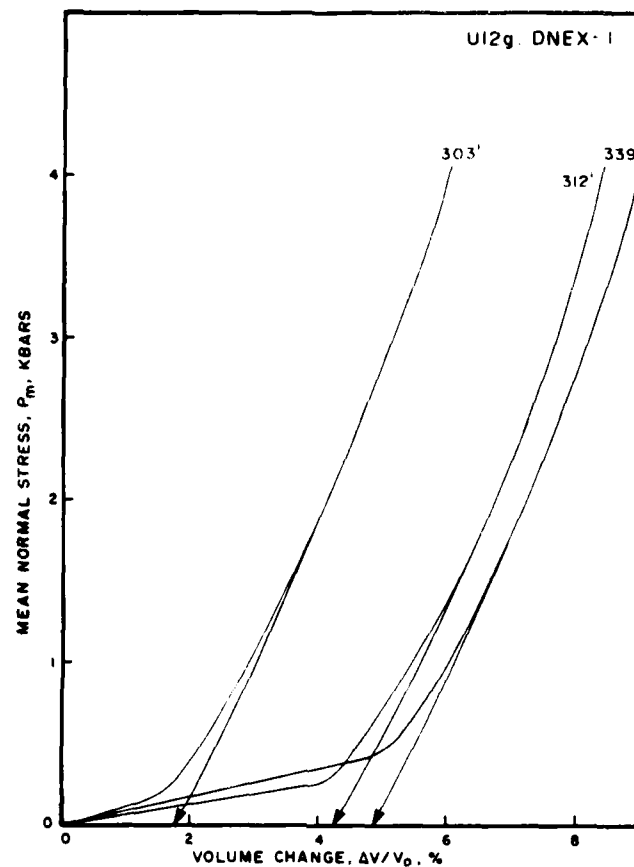
Figure 11.   Uniaxial strain tests, stress-strain response.
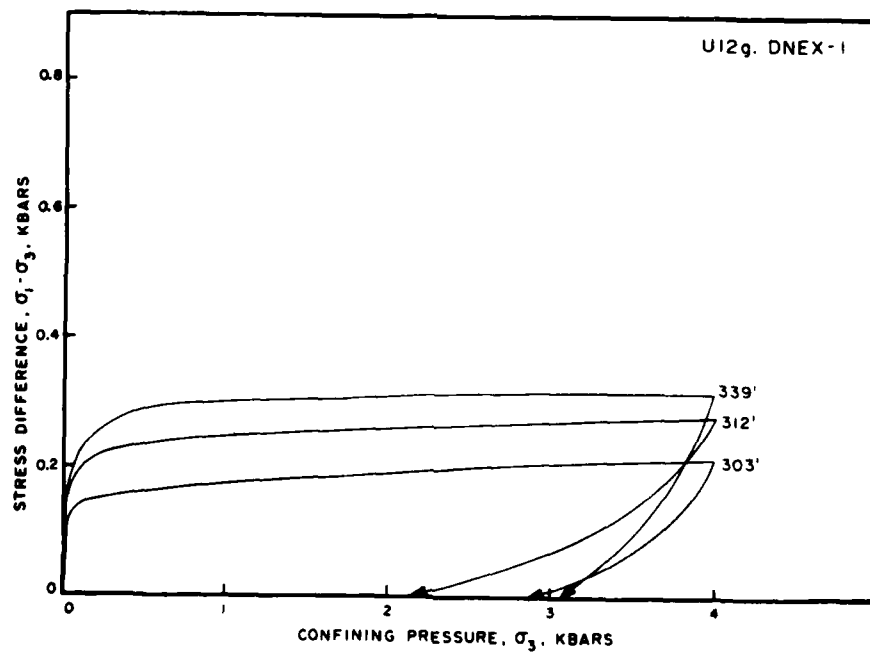
Figure 12.   Uniaxial strain tests, stress-stress response.

144

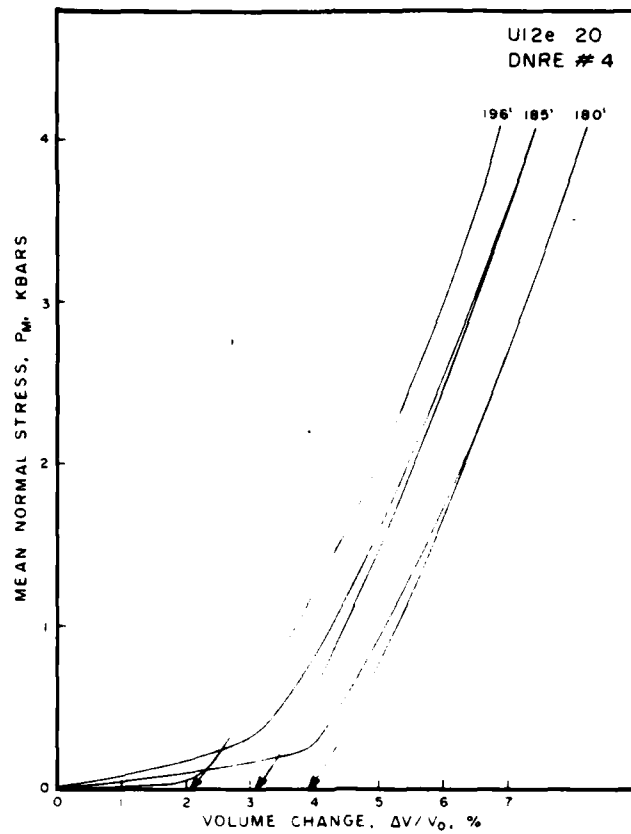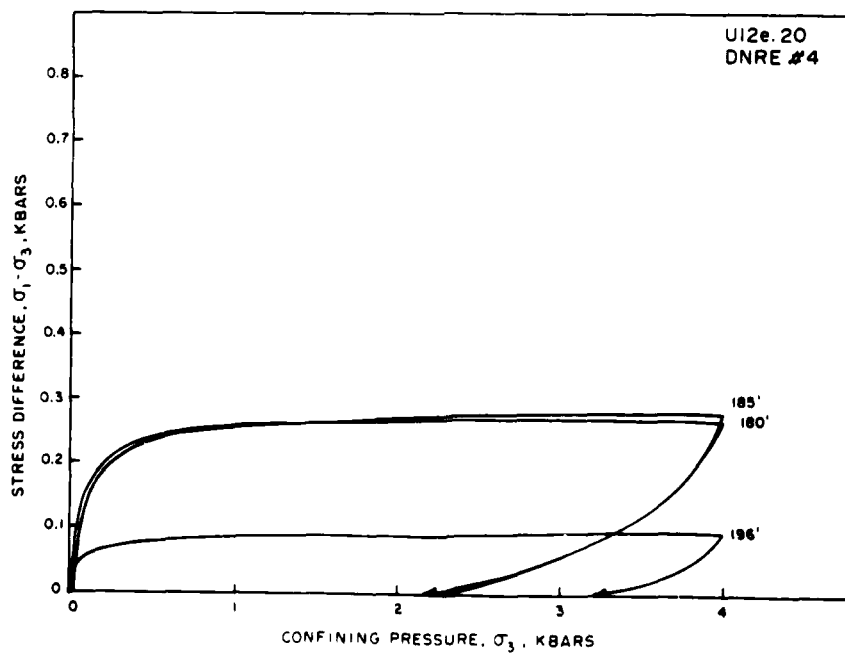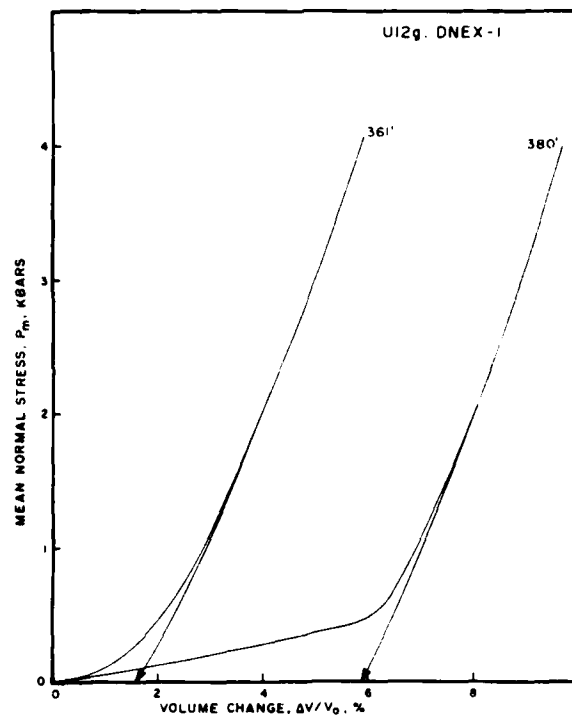Figure 13. Uniaxial strain tests, stress-strain response.
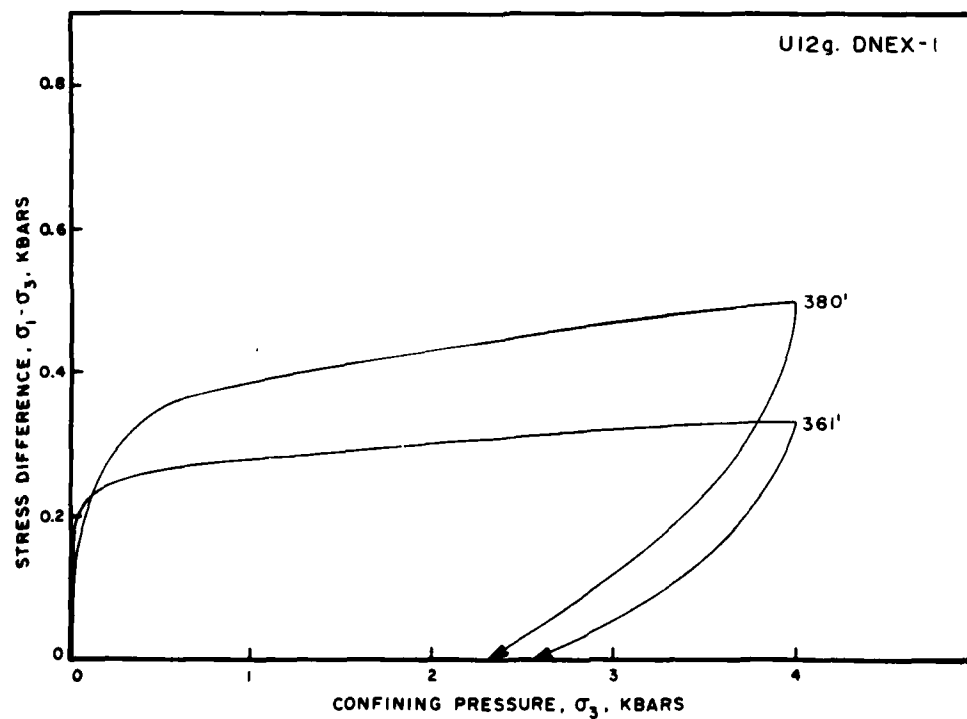
Figure 14. Uniaxial strain tests, stress-stress response.

145
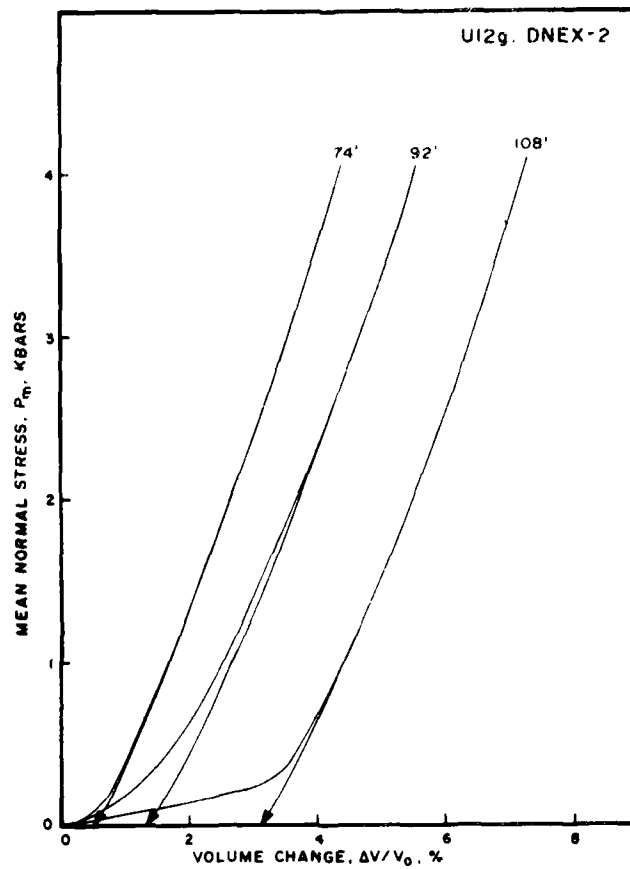
Figure 15.   Uniaxial strain tests, stress-strain response.
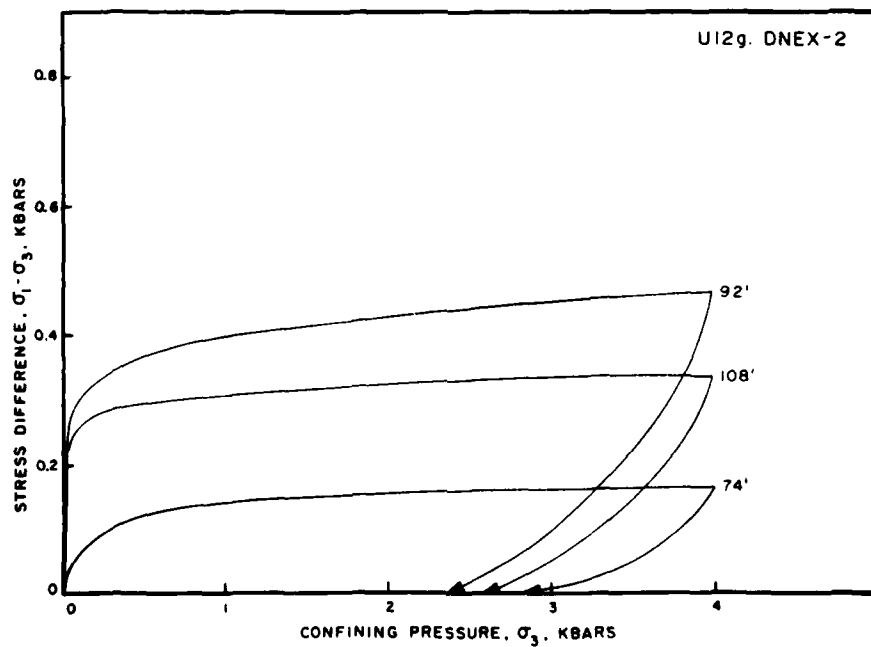
Figure 16.   Uniaxial strain tests, stress-stress response.

146
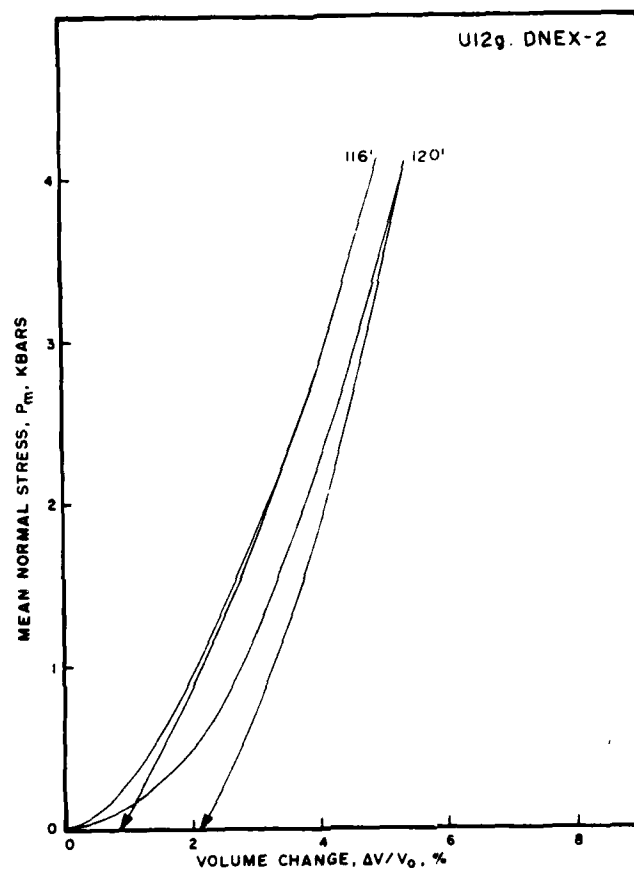
Figure 17. Uniaxial strain tests, stress-strain response.
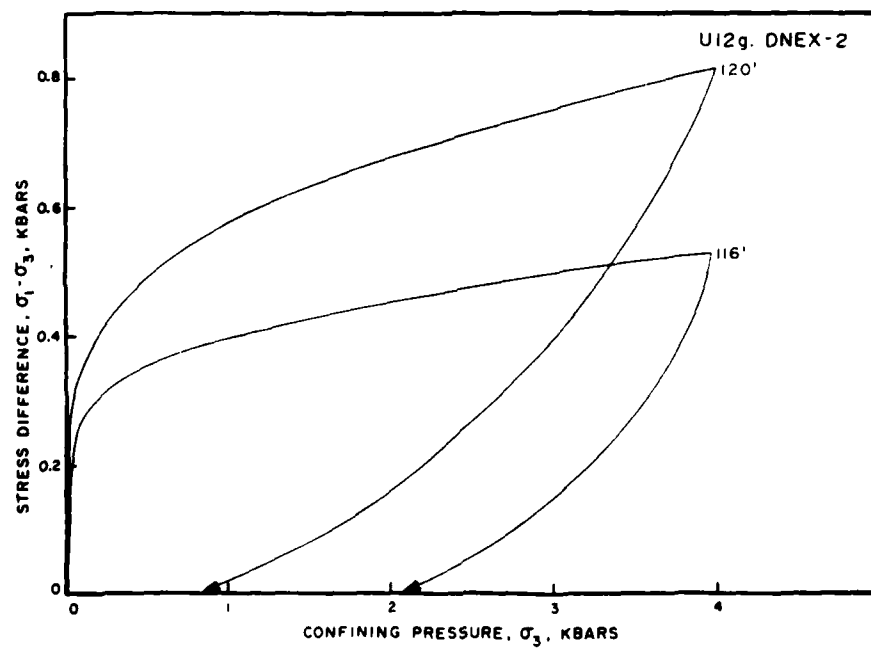
Figure 18. Uniaxial strain tests, stress-stress response.

147

148
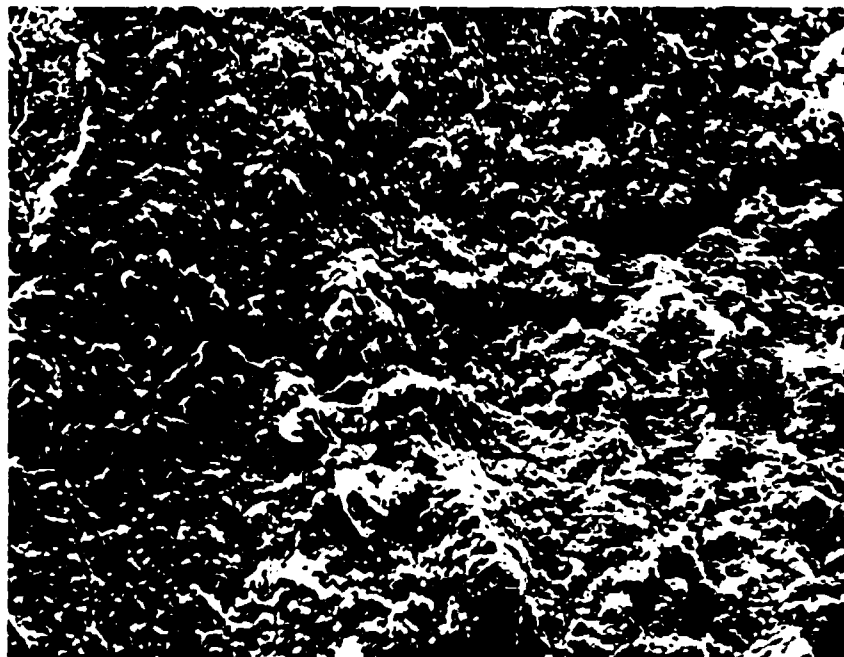
Figure A1. Scanning electron microscope photograph,
100X, on sample U12e.20 DNRE#4-162'.
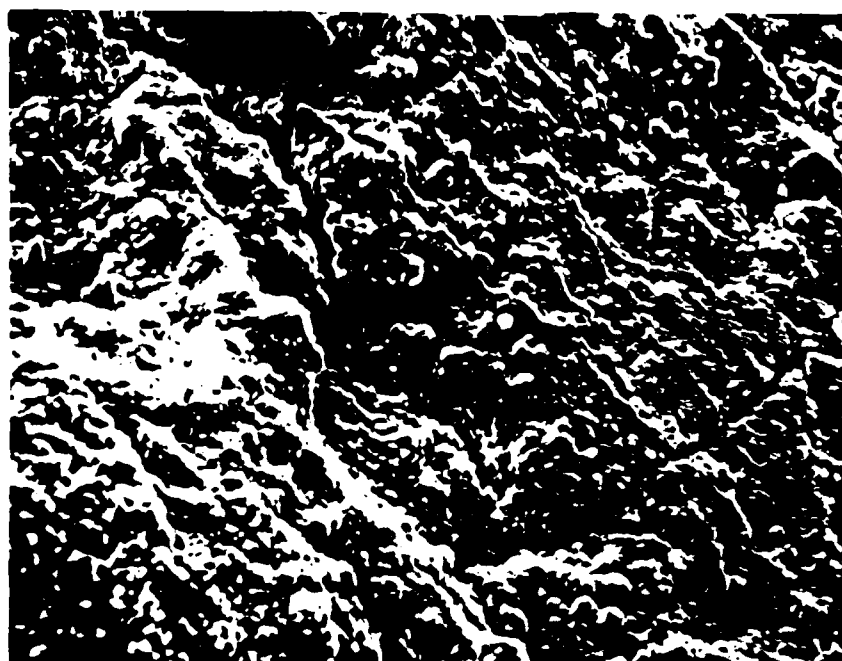
Figure A2. Scanning electron microscope photograph,
200X, on sample U12e.20 DNRE#4-162'.
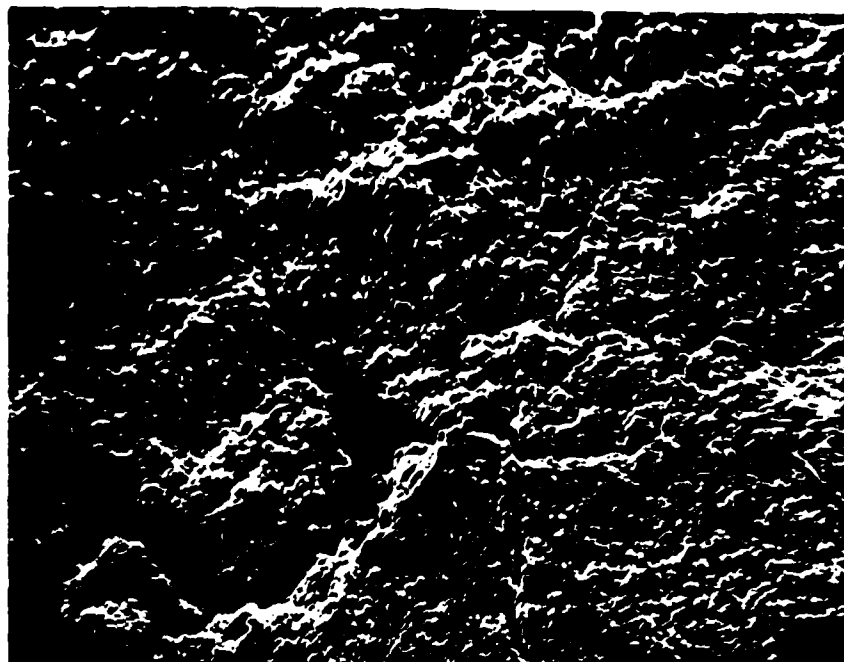
Figure A3.   Scanning electron microscope photograph,
             100X, on sample U12e.20 DNRE#4-180'.
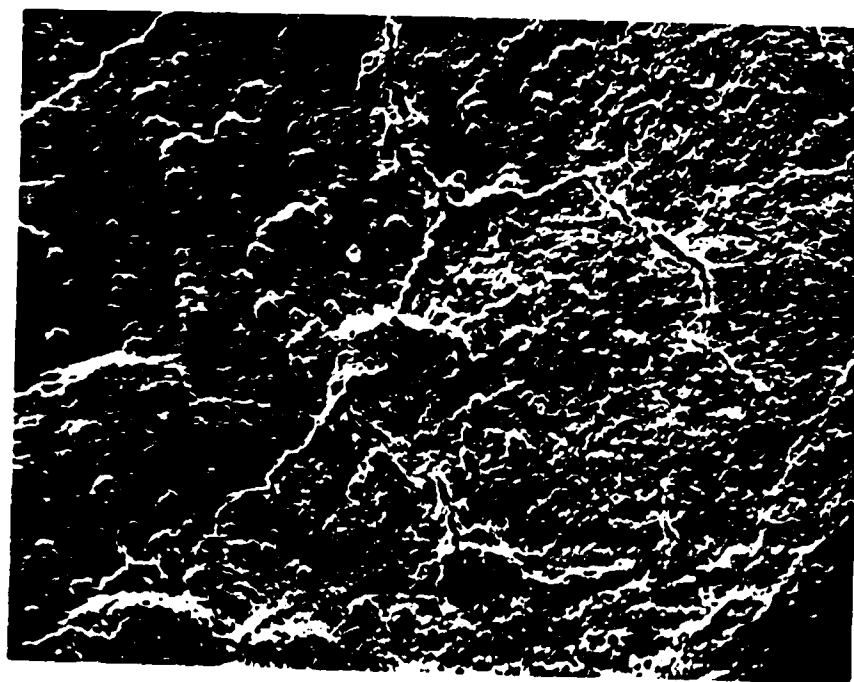
Figure A4.   Scanning electron microscope photograph,
             100X, on sample U12e.20 DNRE#4-180'.
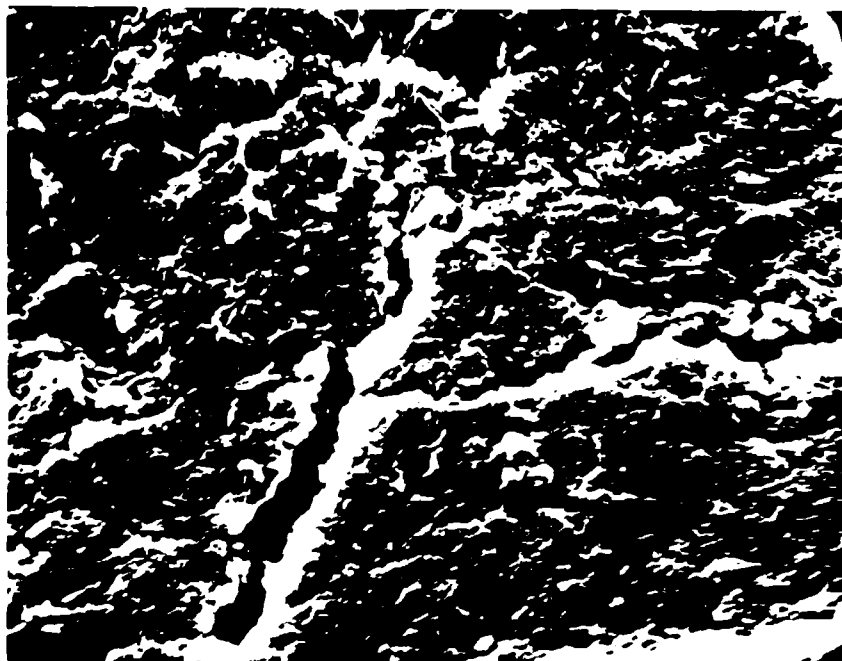
Figure A5. Scanning electron microscope photograph,
1000X, on sample U12e.20 DNRE#4-180'.
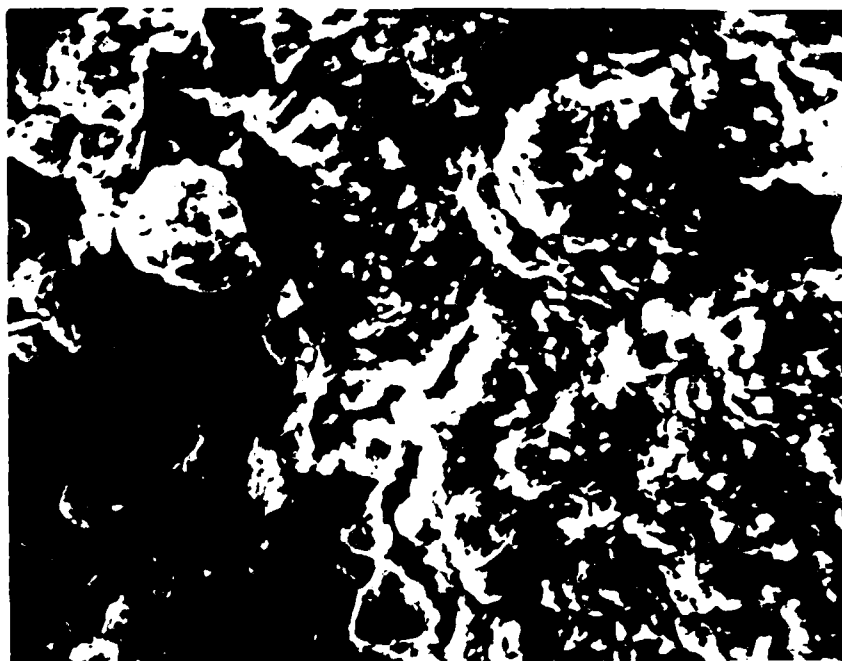
Figure A6. Scanning electron microscope photograph,
500X, on sample U12e.20 DNRE#4-185'.
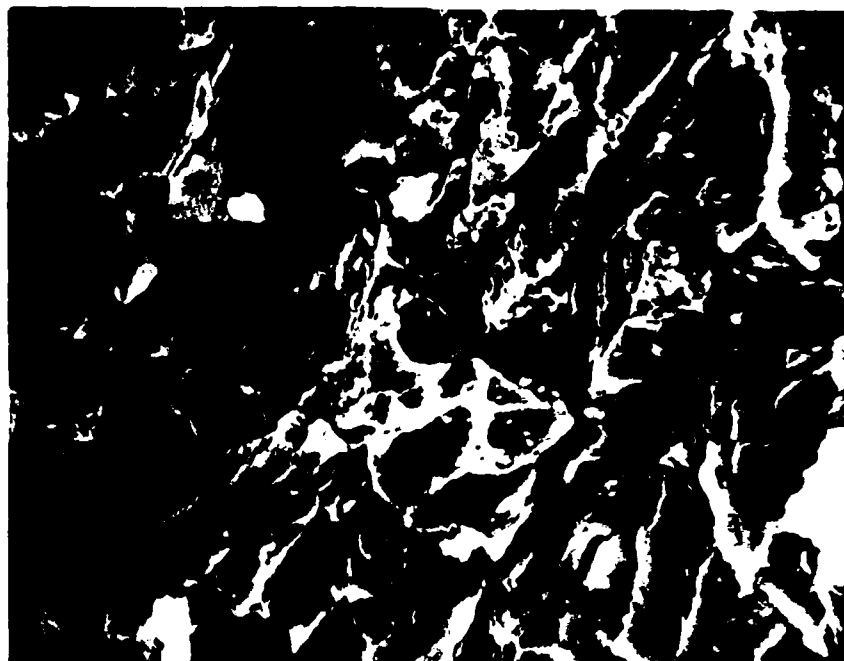
Figure A7. Scanning electron microscope photograph,
1000X, on sample U12e.20 DNRE#4-185'.
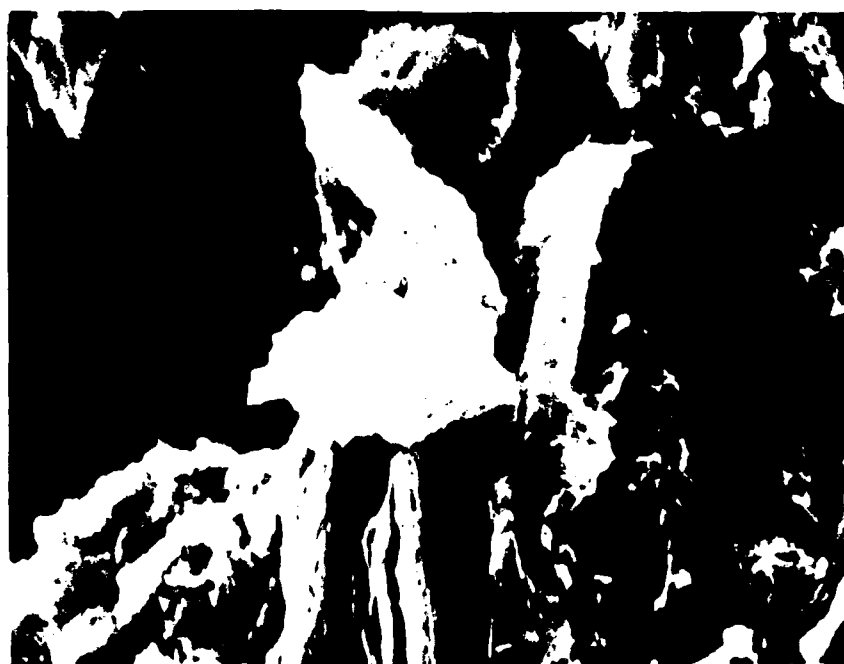
Figure A8. Scanning electron microscope photograph,
1000X, on sample U12e.20 DNRE#4-185'.
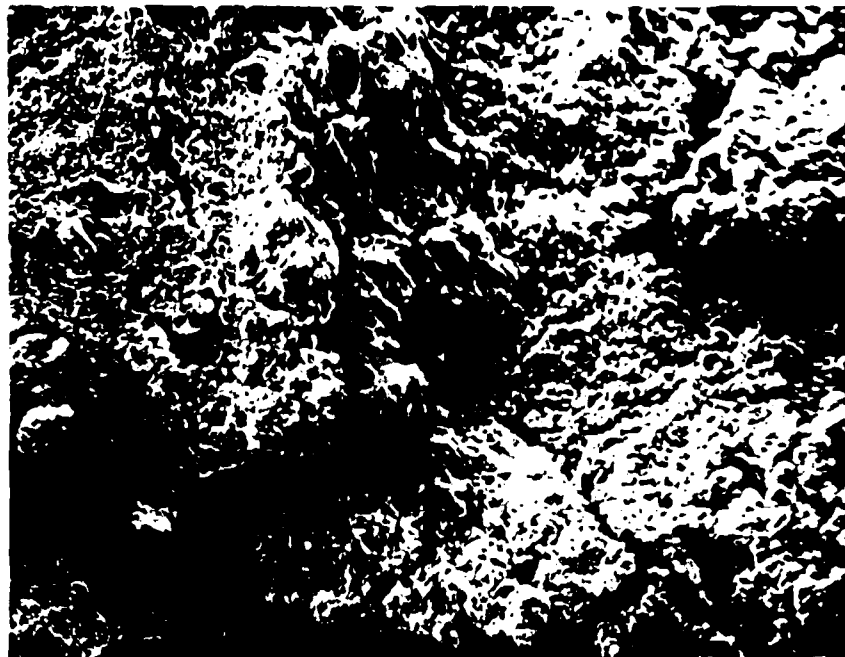
Figure A9. Scanning electron microscope photograph, 100X, on sample U12e.20 DNRE#4-207'.
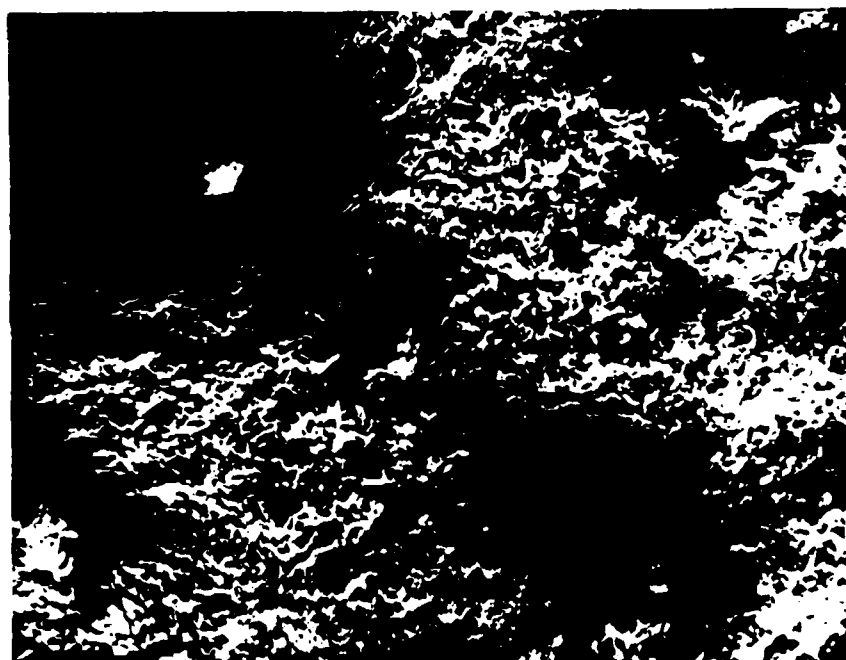
Figure A10. Scanning electron microscope photograph, 100X, on sample U12e.20 DNRE#4-207'.

Figure A11. Scanning electron microscope photograph,
200X, on sample U12e.20 DNRE#4-207'.
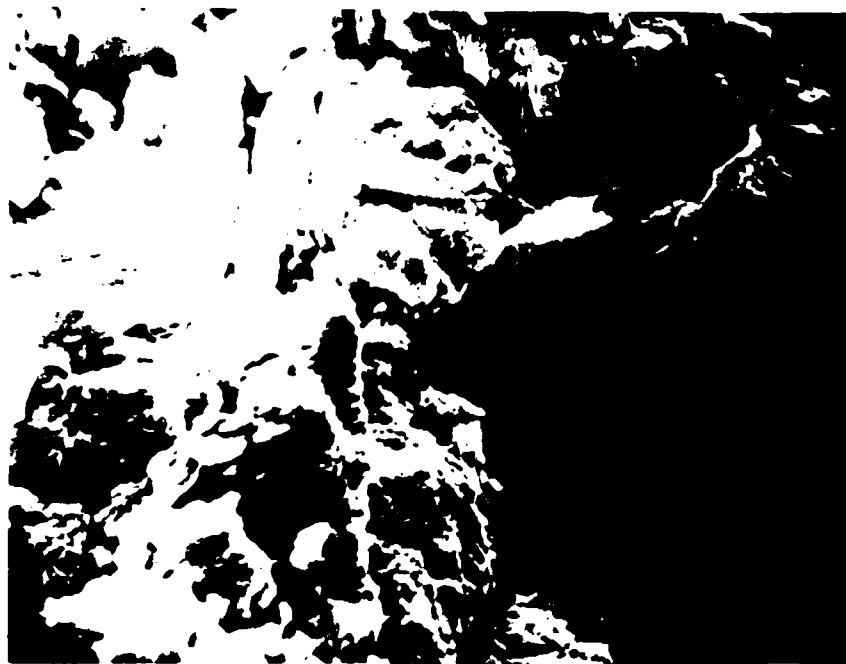
Figure A12. Scanning electron microscope photograph,
1000X, on sample U12e.20 DNRE#4-207'.
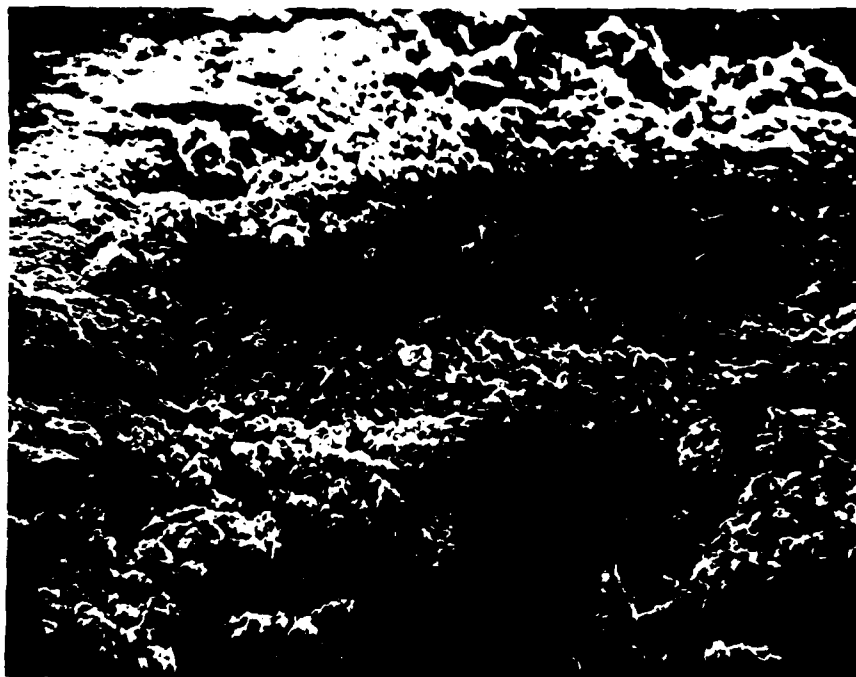
Figure A13. Scanning electron microscope photograph, 200X, on sample U12g DNEX#1-303'.
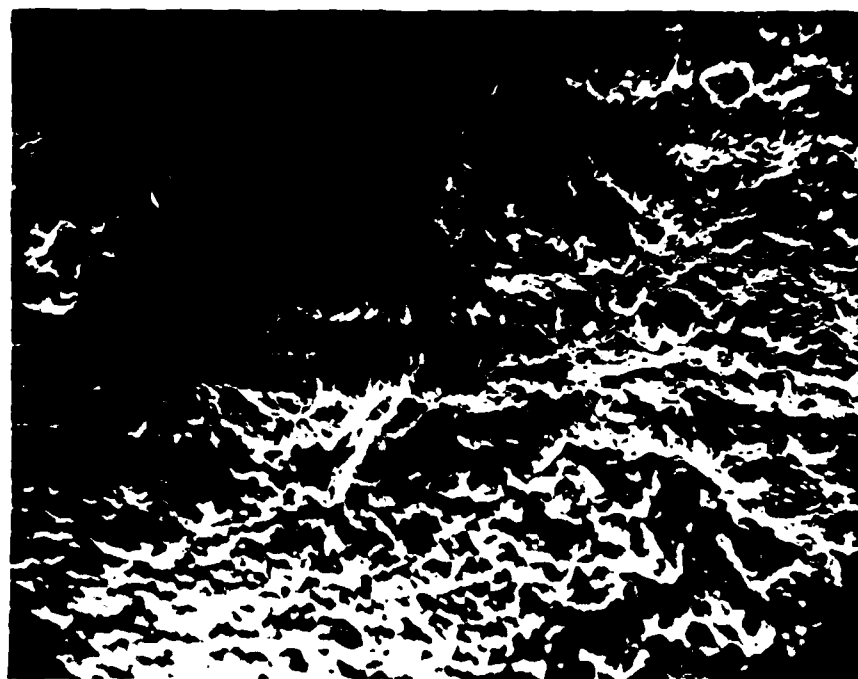
Figure A14. Scanning electron microscope photograph, 500X, on sample U12g DNEX#1-303'.

155
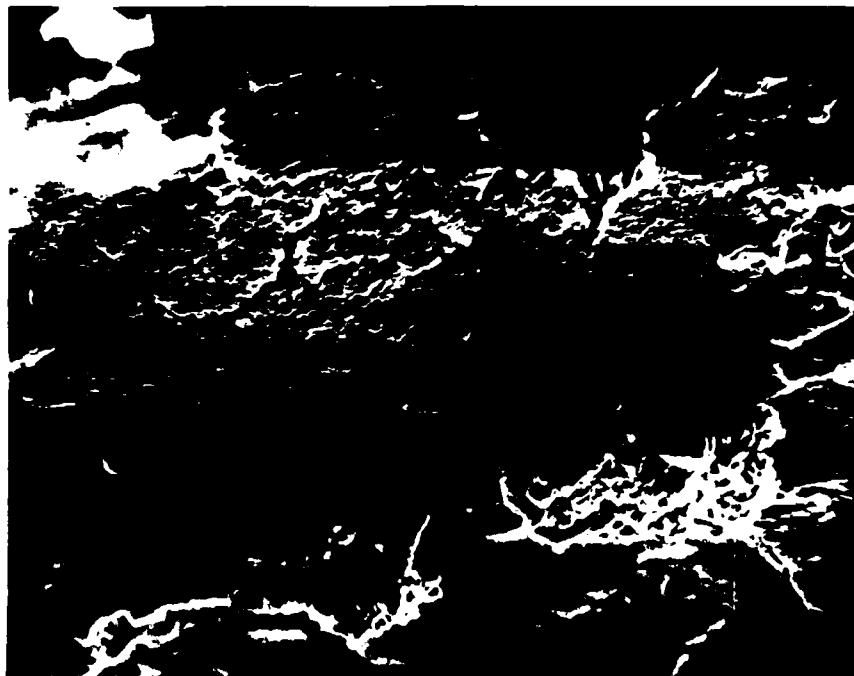
Figure A15. Scanning electron microscope photograph, 500X, on sample U12g DNEX#1-303'.
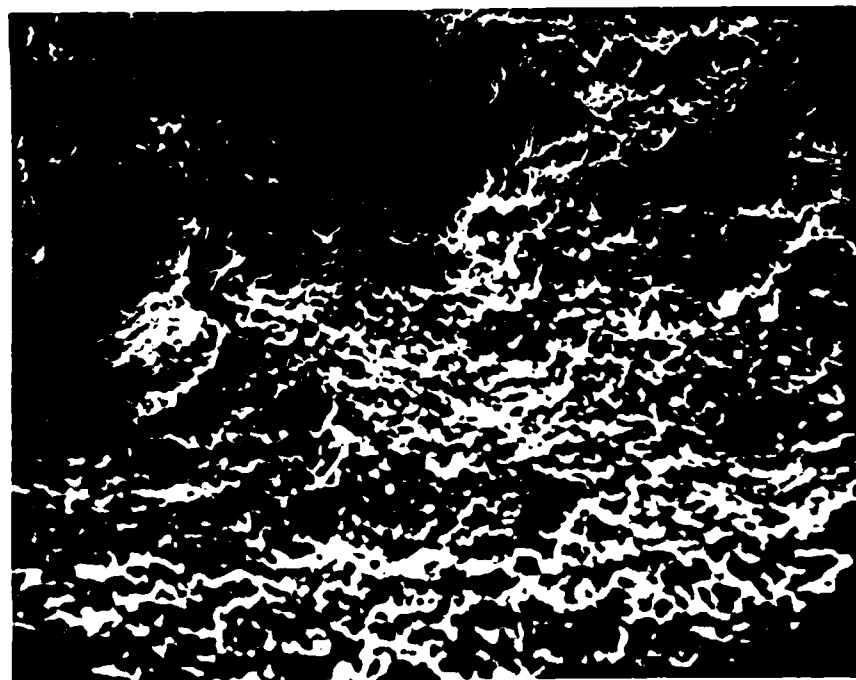
Figure A16. Scanning electron microscope photograph, 200X, on sample U12g DNEX#1-312'.

156
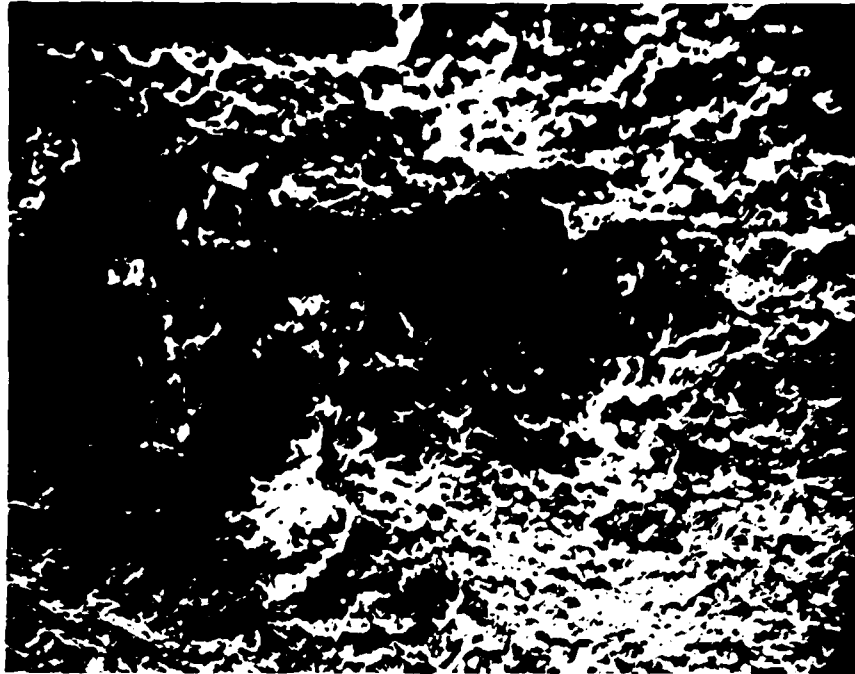
Figure A17. Scanning electron microscope photograph, 200X, on sample U12g DNEX#1-312'.
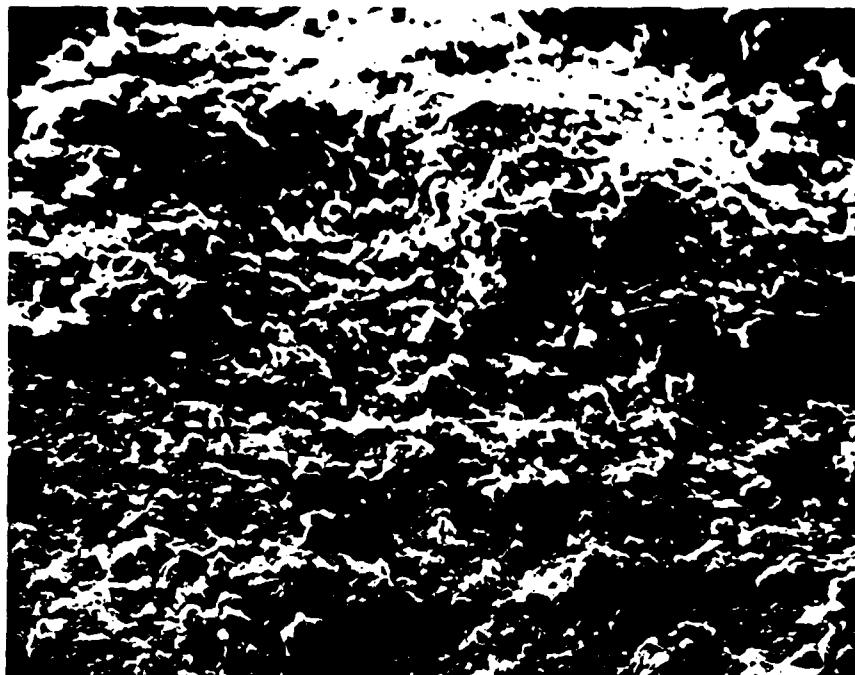
Figure A18. Scanning electron microscope photograph, 200X, on sample U12g DNEX#1-312'.

157
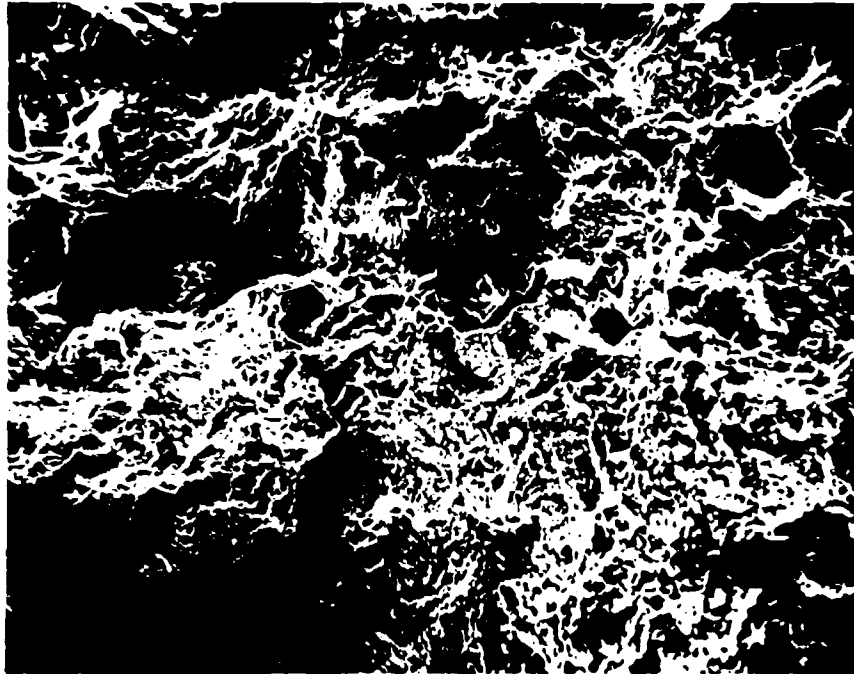
Figure A19. Scanning electron microscope photograph, 100X, on sample U12g DNEX#1-361'.
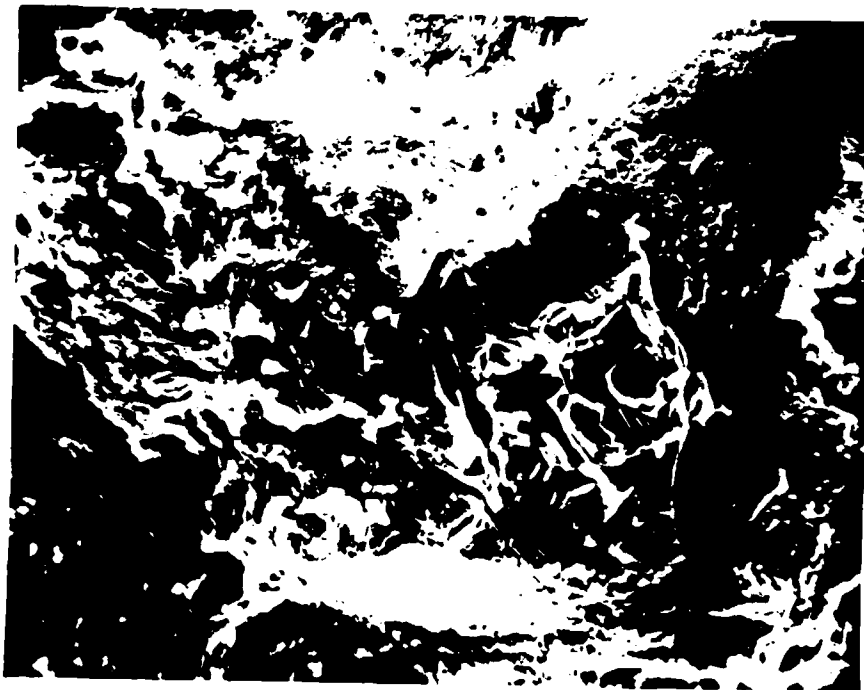
Figure A20. Scanning electron microscope photograph, 500X, on sample U12g DNEX#1-361'.
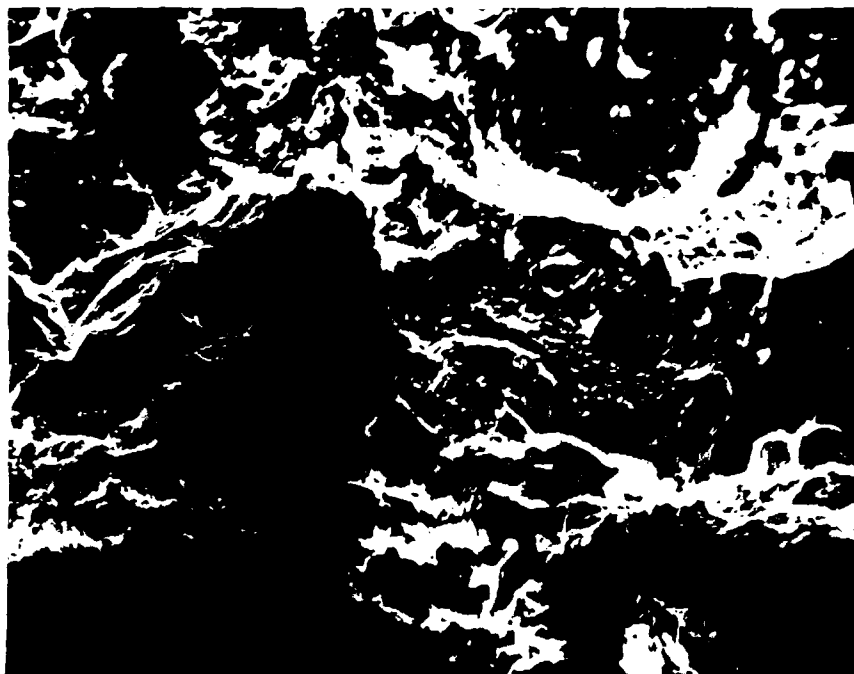
Figure A21. Scanning electron microscope photograph,
500X, on sample U12g DNEX#1-361'.
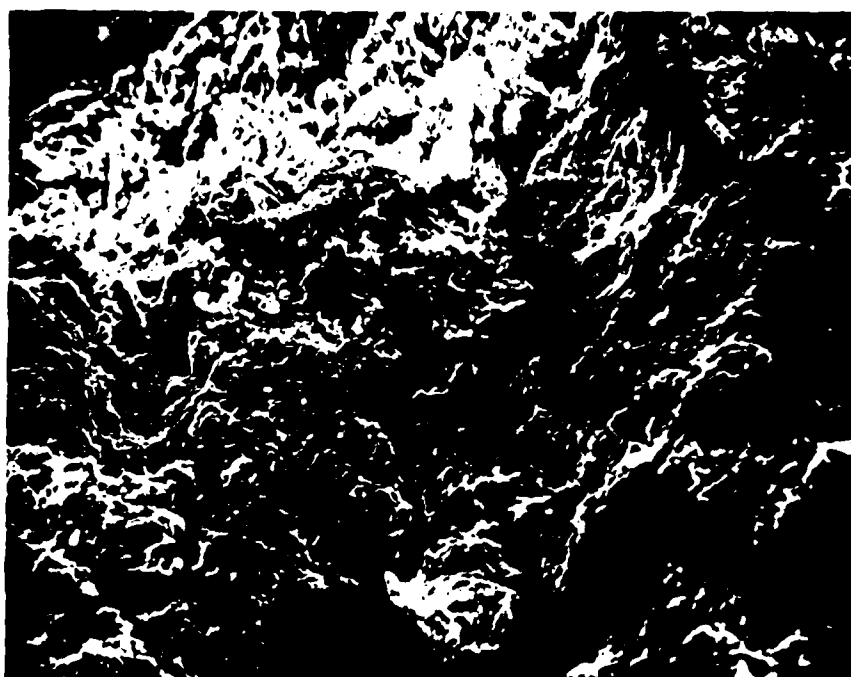
Figure A22. Scanning electron microscope photograph,
200X, on sample U12g DNEX#2-74'.

159
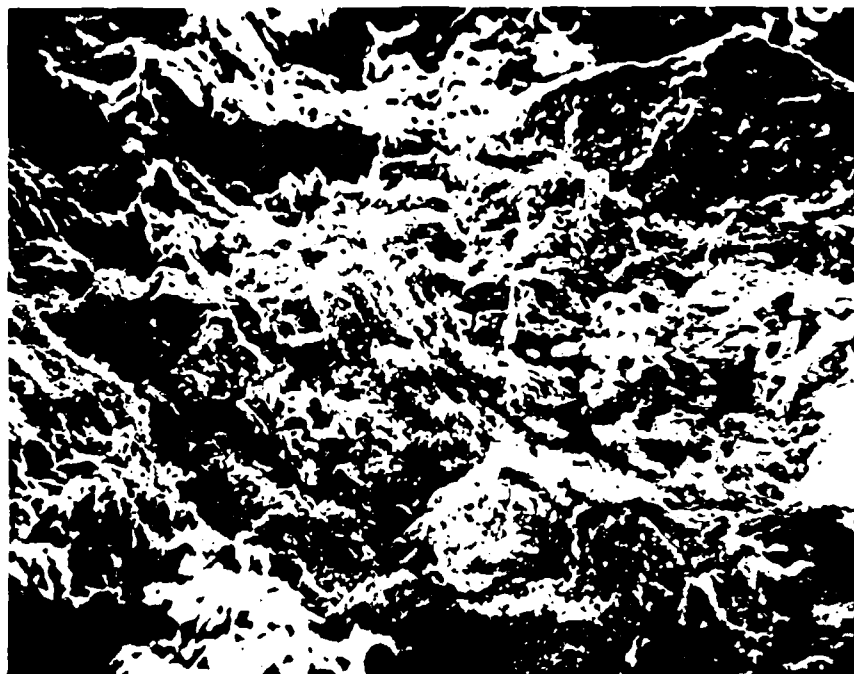
Figure A23. Scanning electron microscope photograph,
200X, on sample U12g DNEX#2-74'.
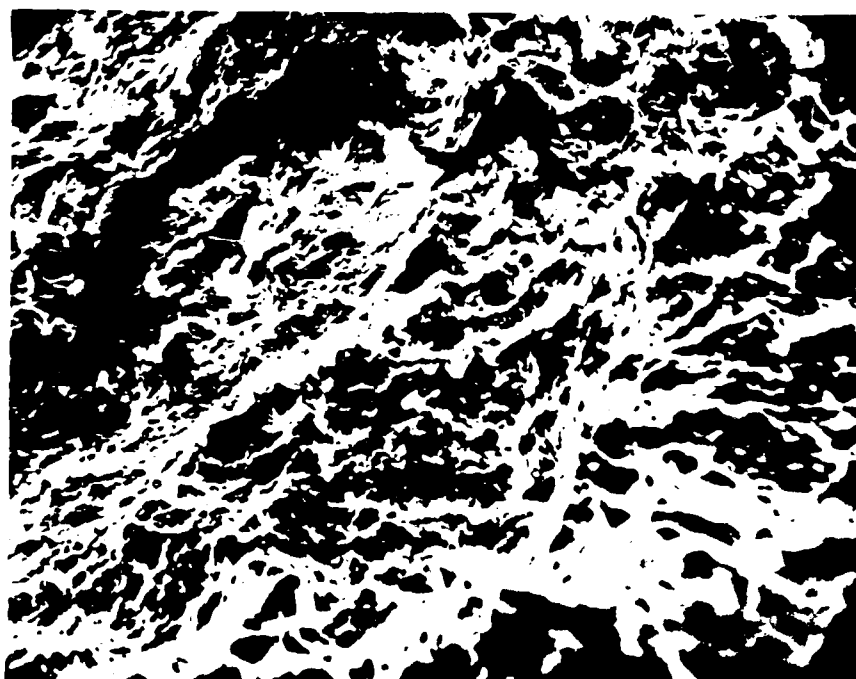
Figure A24. Scanning electron microscope photograph,
200X, on sample U12g DNEX-2-74'.

160
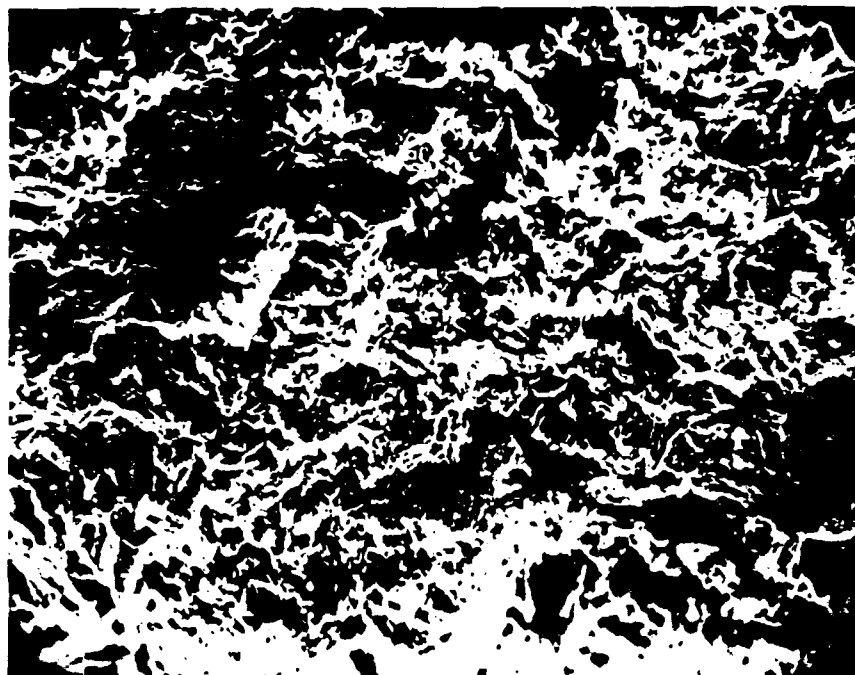
Figure A25.   Scanning electron microscope photograph,
200X, on sample U12g DNEX#2-108'.
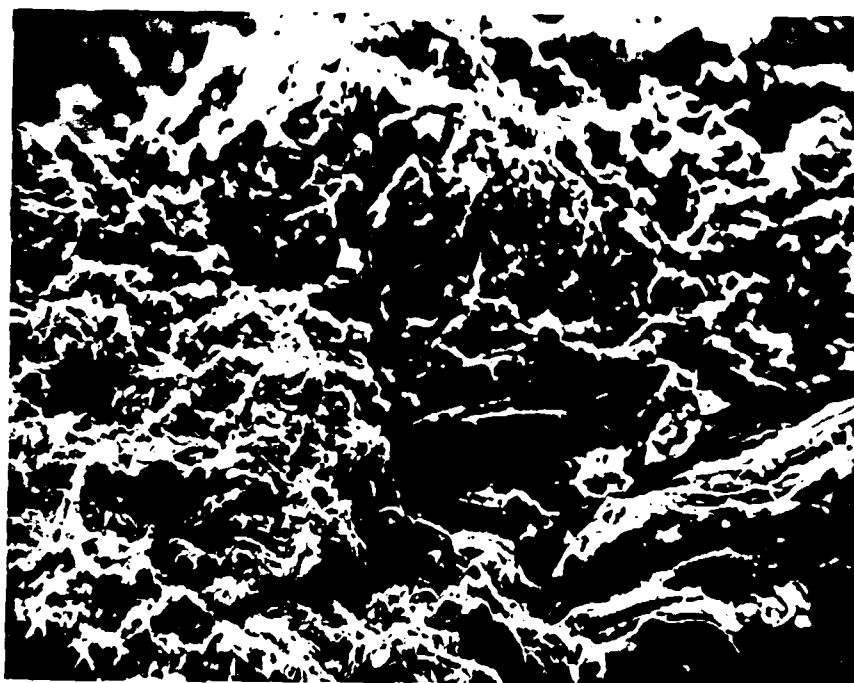
Figure A26.   Scanning electron microscope photograph,
200X, on sample U12g DNEX#2-108'.

EXPLORATORY DRILL HOLES IN
U12n.11 TUNNEL

INTRODUCTION

The U12n.11 tunnel is the prospective site of the future Miner's Iron event. Material property characterization has been conducted on both vertical and horizontal drill holes and tuff overcore samples to evaluate the site's potential as a test site. Physical and mechanical properties on cores from the following drill holes and overcores have been determined:

U12n.11 UG#2	horizontal drill hole
UE12n#11	vertical drill hole
U12n.11 O.C.#4	tuff overcore

The location of these drill holes relative to the tunnel layout is shown below in Figure 1.
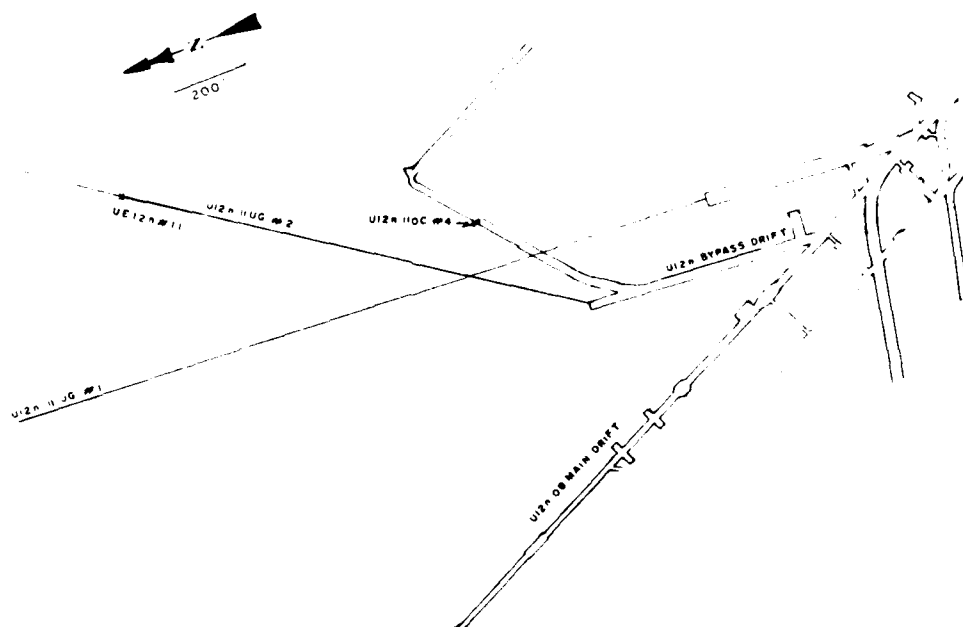
Figure 1. Plan view of U12n.11 tunnel complex.

TEST RESULTS

U12n.11 UG#2 Horizontal Drill Hole

Physical properties, uniaxial strain measured permanent compaction, and ultrasonic velocities are listed in Table 1. Figure 2 shows the stress difference observed at 4.0 kbars confining pressure during uni- axial strain as a function of drill hole footage. Individual uniaxial strain test stress-strain and stress-stress curves are shown in Appendix A.

Physical property tests indicate a region of low density and high porosity between footages 702 and 821 feet. The difference in physical properties is also reflected in both the ultrasonic velocity data and the uniaxial strain test results. Both velocity and strength are lower in this region. A comparison of select data is shown in Table 2 between this region and the remainder of the drill holes.

Physical properties and ultrasonic velocities correspond well with the mechanical test data throughout the entire drill hole and no regions of unusually high air void contents were observed.

UE12n#11 Vertical Drill Hole

Physical properties, uniaxial strain measured permanent compaction, and ultrasonic velocities are listed in Table 3. Figure 3 shows the stress difference observed at 4.0 kbars confining pressure during uniaxial strain as a function of drill hole footage. Individual uniaxial strain test curves are shown in Appendix B. Physical property tests indicate a

TABLE 1

Physical Properties, Uniaxial Strain Measured Permanent Compaction, and Ultrasonic Velocities for U12n.11 UG#2 Tuff Samples

DRILL HOLE FOOTAGE	DENSITY (gm/cc)			WATER BY WET WEIGHT (%)	POROSITY (%)	SATURATION (%)	CALC AIR VOIDS (%)	MEAS. PERMANENT COMP. (%)	VELOCITY (km/sec)	
	AS-RECEIVED	DRY	GRAIN						LONG	SHEAR
U12n.11 UG#2										
338	1.88	1.54	2.42	18.1	36.4	93.3	2.5	1.0	2.80	1.36
342	1.80	1.40	2.44	22.5	42.8	94.6	2.3	1.7	2.67	1.22
352	1.93	1.61	2.41	16.3	33.1	94.9	1.7	1.0	3.54	1.92
362	2.06	1.84	2.38	10.6	22.9	95.0	1.1	0.1	3.74	2.15
371	2.04	1.81	2.39	11.2	24.4	93.8	1.5	0.2	3.65	2.06
382	2.05	1.81	2.38	11.6	23.9	99.7	0.1	1.2	3.66	2.11
390	1.92	1.59	2.40	17.5	33.9	99.3	0.2	2.6	3.15	1.58
400	1.94	1.61	2.42	17.2	33.7	99.0	0.3	2.9	3.11	1.53
411	1.92	1.59	2.38	17.6	33.2	100.0	0.0	2.5	3.28	1.66
420	1.90	1.53	2.41	19.2	36.6	99.5	0.2	2.3	3.09	1.46
429	1.91	1.57	2.37	17.5	33.7	99.1	0.3	2.2	3.19	1.72
441	1.91	1.58	2.42	17.5	34.8	95.7	1.5	1.1	2.97	1.33
449	1.96	1.63	2.45	16.8	33.4	98.5	0.5	1.9	3.09	1.28
461	1.92	1.57	2.42	18.1	34.9	99.3	0.2	0.9	3.15	1.62
470	1.88	1.50	2.41	19.9	37.6	99.4	0.2	1.1	2.83	1.34
479	1.88	1.51	2.40	19.9	37.3	100.0	0.0	0.9	2.85	1.29
488	1.86	1.46	2.44	21.5	40.4	98.6	0.6	0.8	2.62	1.23
500	1.85	1.46	2.42	20.9	39.6	97.5	1.0	0.9	3.00	1.50
512	1.86	1.47	2.45	21.1	40.1	98.1	0.7	1.5	2.73	1.20
519	1.89	1.54	2.40	18.3	35.9	96.4	1.3	1.1	3.22	1.70
529	1.92	1.57	2.42	18.1	35.0	99.4	0.2	1.3	2.88	1.38
541	1.92	1.58	2.41	17.8	34.7	98.3	0.6	1.2	3.04	1.53
549	1.93	1.60	2.40	17.1	33.5	98.4	0.5	1.2	3.10	1.54
559	2.08	1.86	2.44	10.4	23.8	90.7	2.2	0.2	3.96	2.30
570	1.91	1.59	2.38	17.1	33.2	98.4	0.5	1.4	3.35	1.90
580	1.96	1.68	2.41	14.3	30.2	92.9	2.1	---	3.94	2.21
591	1.82	1.40	2.42	23.0	41.9	100.0	0.0	2.0	2.53	1.21
609	1.90	1.54	2.40	19.0	35.8	100.0	0.0	2.2	3.29	1.76
623	1.81	1.41	2.41	21.9	41.4	95.8	1.8	2.0	2.68	1.34
631	1.74	1.32	2.40	24.5	45.3	94.0	2.7	1.3	2.30	1.05
641	1.93	1.62	2.44	16.3	33.8	93.0	2.4	1.6	3.08	1.54
650	1.79	1.38	2.43	22.7	42.9	94.5	2.4	0.7	2.96	1.50
661	1.93	1.63	2.37	15.5	31.1	95.9	1.3	0.9	3.54	1.94
669	1.80	1.40	2.35	22.2	40.4	99.2	0.3	0.9	2.92	1.46
680	1.88	1.52	2.44	19.1	37.7	95.3	1.8	0.2	2.87	1.28
689	1.94	1.63	2.44	16.3	33.4	94.5	1.8	---	3.02	1.41
702	1.78	1.38	2.35	22.5	41.4	96.4	1.5	1.0	2.80	0.93
712	1.76	1.34	2.37	23.8	43.5	96.1	1.7	1.2	3.14	1.53
724	1.87	1.55	2.34	17.0	33.7	93.9	2.1	0.6	2.86	1.22
735	1.72	1.24	2.35	27.5	47.0	100.0	0.0	1.8	2.80	1.13
741	1.73	1.34	2.31	22.7	42.1	93.2	2.9	1.2	2.48	0.94
748	1.70	1.24	2.33	26.9	46.7	98.1	0.9	2.0	2.68	1.07
758	1.72	1.26	2.43	26.5	47.9	95.1	2.3	0.7	2.74	1.13
770	1.75	1.32	2.43	24.5	45.8	93.4	3.0	1.1	2.64	1.16
778	1.73	1.29	2.39	25.3	46.0	95.5	2.1	1.2	2.55	0.97
792	1.76	1.34	2.36	23.7	43.2	96.6	1.5	1.9	2.72	1.14
800	1.71	1.27	2.36	25.6	46.3	94.3	2.7	0.8	2.60	1.13
809	1.69	1.22	2.33	27.7	47.6	98.1	0.9	1.5	2.49	0.76
821	1.72	1.29	2.35	24.9	45.1	94.9	2.3	1.6	2.39	0.70
832	1.95	1.62	2.41	16.9	32.7	100.0	0.0	1.6	2.89	1.15
846	1.96	1.64	2.41	16.3	31.9	100.0	0.0	0.7	2.96	1.47
865	1.92	1.58	2.40	17.8	34.2	99.8	0.1	0.5	3.31	1.83
884	1.95	1.62	2.42	16.8	32.9	94.4	0.2	0.7	2.83	1.41
905	1.96	1.63	2.42	16.7	32.5	100.0	0.0	1.0	3.04	1.46
924	1.95	1.62	2.42	17.0	33.1	100.0	0.0	2.0	2.94	1.47
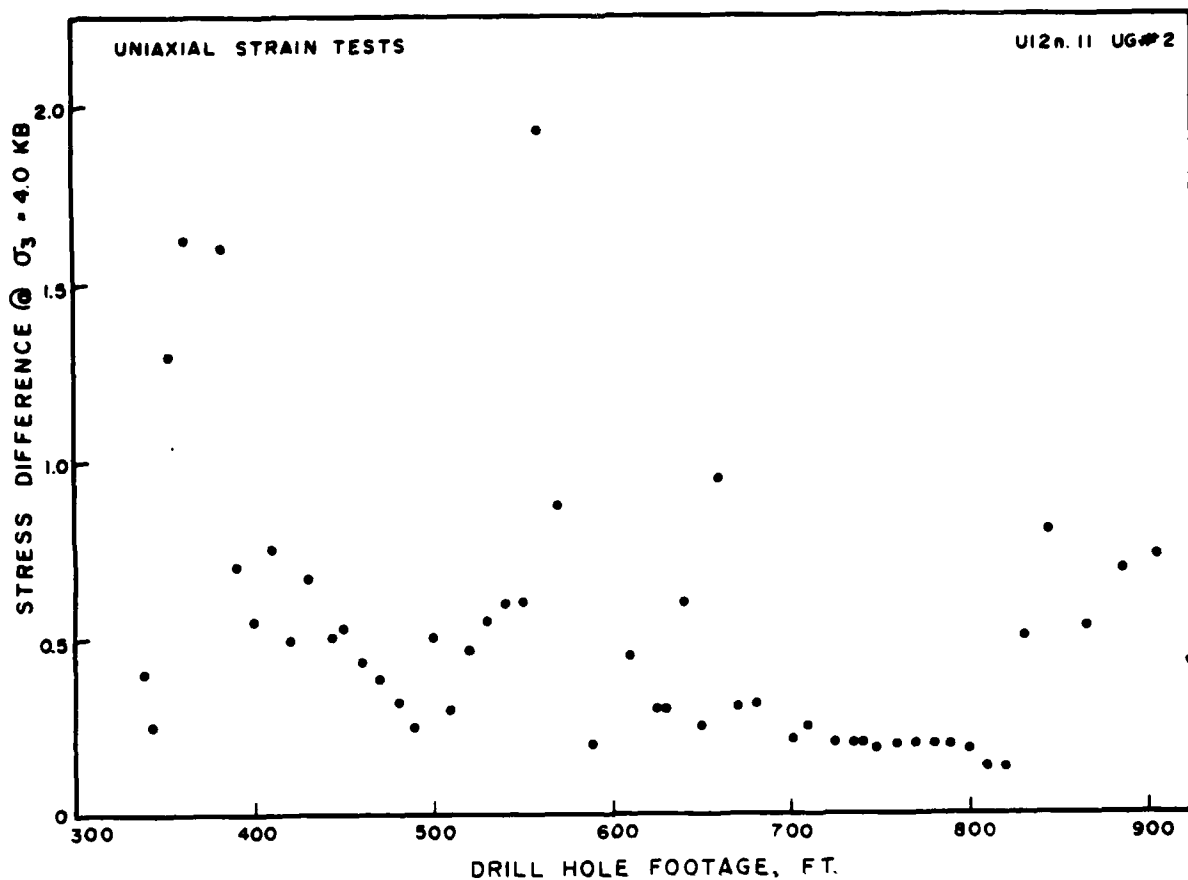
Figure 2. Stress difference observed at σ_3=4.0 kbars during uniaxial strain testing as a function of drill hole footage.

TABLE 2

U12n.11 UG#2 Average Material Properties

	338'-689', 832'-924'	702'-821'
Stress Difference @ σ_3 = 4.0 kb (kbars)	0.62	0.17
As-Received Denisty (gm/cc)	1.91	1.74
Total Porosity (%)	34.5	44.3
Saturation (%)	97.3	95.8
Longitudinal Velocity (km/sec)	3.09	2.68

165

TABLE 3

Physical Properties, Uniaxial Strain Measured Permanent Compaction,
and Ultrasonic Velocities for UE12n#11 Tuffs

| DRILL HOLE FOOTAGE	DENSITY (gm/cc)			WATER BY WET WEIGHT (%)	POROSITY (%)	SATURATION (%)	CALC. AIR VOIDS (%)	MEAS. PERMANENT COMP. (%)	VELOCITY (km/sec)	
	AS-RECEIVED	DRY	GRAIN						LONG	SHEAR
1081	1.94	1.59	2.47	18.1	35.7	98.3	0.6	1.8	3.10	1.51
1096	1.83	1.43	2.49	21.9	42.6	94.0	2.5	2.1	2.90	1.50
1109	1.78	1.33	2.49	25.4	46.7	96.9	1.5	2.2	2.53	1.33
1126	1.90	1.56	2.46	17.8	36.5	92.5	2.7	0.7	3.18	1.39
1139	1.94	1.61	2.47	16.8	34.7	93.6	2.2	0.1	3.18	1.42
1155	1.91	1.58	2.48	17.2	36.1	90.8	3.3	2.8	3.11	1.41
1169	1.84	1.49	2.40	19.2	38.1	92.8	2.7	2.2	3.16	1.56
1186	1.86	1.50	2.37	19.2	36.7	96.7	1.2	1.3	3.02	1.52
1201	1.93	1.59	2.48	17.4	35.9	93.6	2.3	1.6	2.83	1.27
1211	1.93	1.59	2.47	17.6	35.6	95.3	1.7	0.2	1.99	
1225	1.79	1.41	2.38	21.5	40.8	94.5	2.2	3.0	2.50	1.19
1237	1.85	1.51	2.39	18.6	36.9	93.1	2.5	0.6	1.83	
1250	1.86	1.52	2.42	18.3	37.0	91.8	3.0	2.1	2.87	1.43
1265	1.89	1.54	2.41	18.3	36.0	96.2	1.4	1.7	2.87	1.35
1276	1.95	1.63	2.51	16.4	35.0	91.3	3.0	2.0	2.94	1.33
1285	1.80	1.40	2.38	22.0	41.1	96.1	1.6	1.9	3.84	1.38
1295	1.93	1.59	2.44	17.8	34.9	98.4	0.6	1.1	2.72	1.33
1307	1.91	1.57	2.47	18.0	36.3	94.8	1.9	0.9	2.72	1.22
1317	1.92	1.57	2.46	18.0	36.1	95.5	1.6	1.3	3.38	1.69
1329	1.90	1.60	2.41	15.9	33.6	90.1	3.3	2.3	3.45	1.64
1342	2.05	1.78	2.50	13.2	28.9	93.2	2.0	0.6	3.02	1.33
1354	1.94	1.63	2.40	16.0	31.9	97.6	0.7	0.7	3.49	1.80
1367	1.91	1.57	2.46	18.0	36.4	94.3	2.1	1.3	2.93	1.35
1380	1.86	1.48	2.41	20.4	38.7	97.8	0.8	1.7	2.17	0.75
1390	2.04	1.75	2.48	14.4	29.6	98.9	0.3	0.3	3.00	1.47
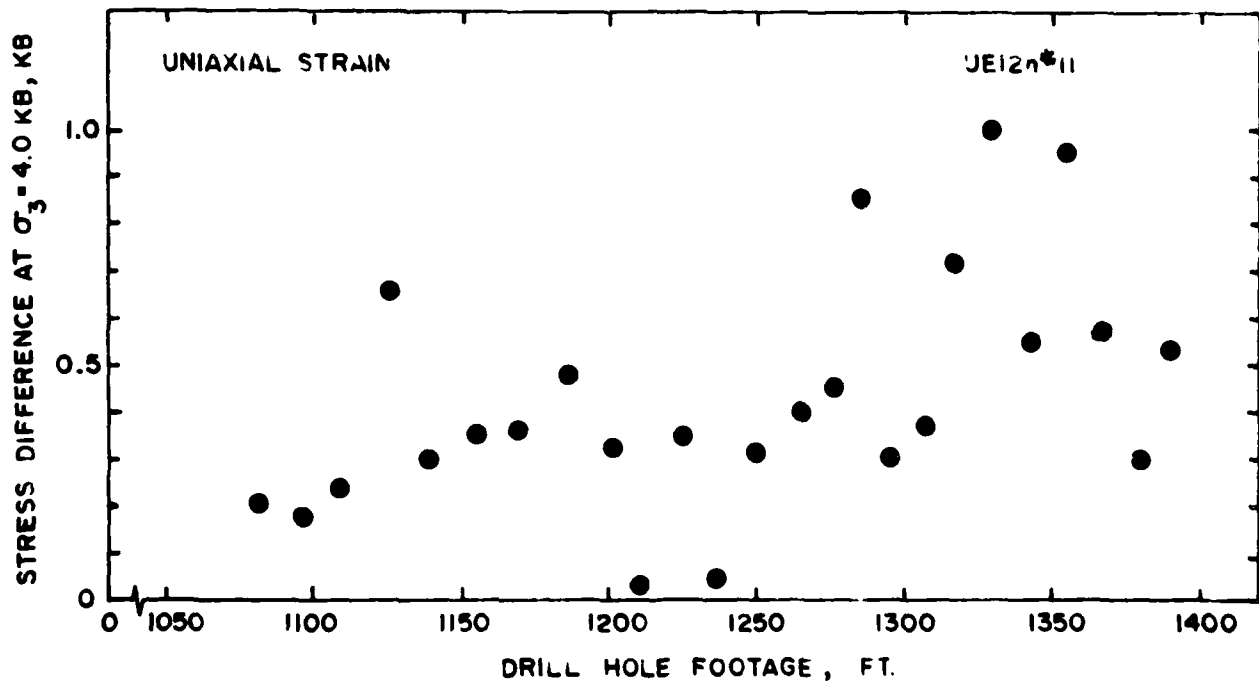
Figure 3.   Stress difference observed at σ_3=4.0 kbars during uniaxial strain testing as a function of drill hole footage.

166

fairly uniform tuff exhibiting only slight physical property changes with depth. The bulk density and ultrasonic velocities exhibited slight increases with increased depth while the porosity showed a small decrease. Calculated air void content showed no trends and was generally under 2 percent with a few samples at about 3.0 percent.

Uniaxial strain tests indicate the region below the 1250 foot depth to be stronger than the region above. Stress difference at 4.0 kbars confining pressure averaged ~0.3 kbars from 1081 to 1250 feet and ~0.6 kbars from 1250 to 1390 feet (see Figure 3). Measured permanent compaction resulting from the uniaxial strain loading compared well with the calculated air void content.

U12n#11 O.C.#4 Overcore

Results of the triaxial compression tests at 69 bars confining pressure on the U12n#11 O.C.#4 overcore are shown in Figure 4. The measured shear strength (τ) for footages 9.4 and 10.5 feet were 0.18 and 0.12 kbars, respectively. The shear moduli, computed from the Young's modulus and Poisson's ratio were 28 and 22 kbars, respectively.
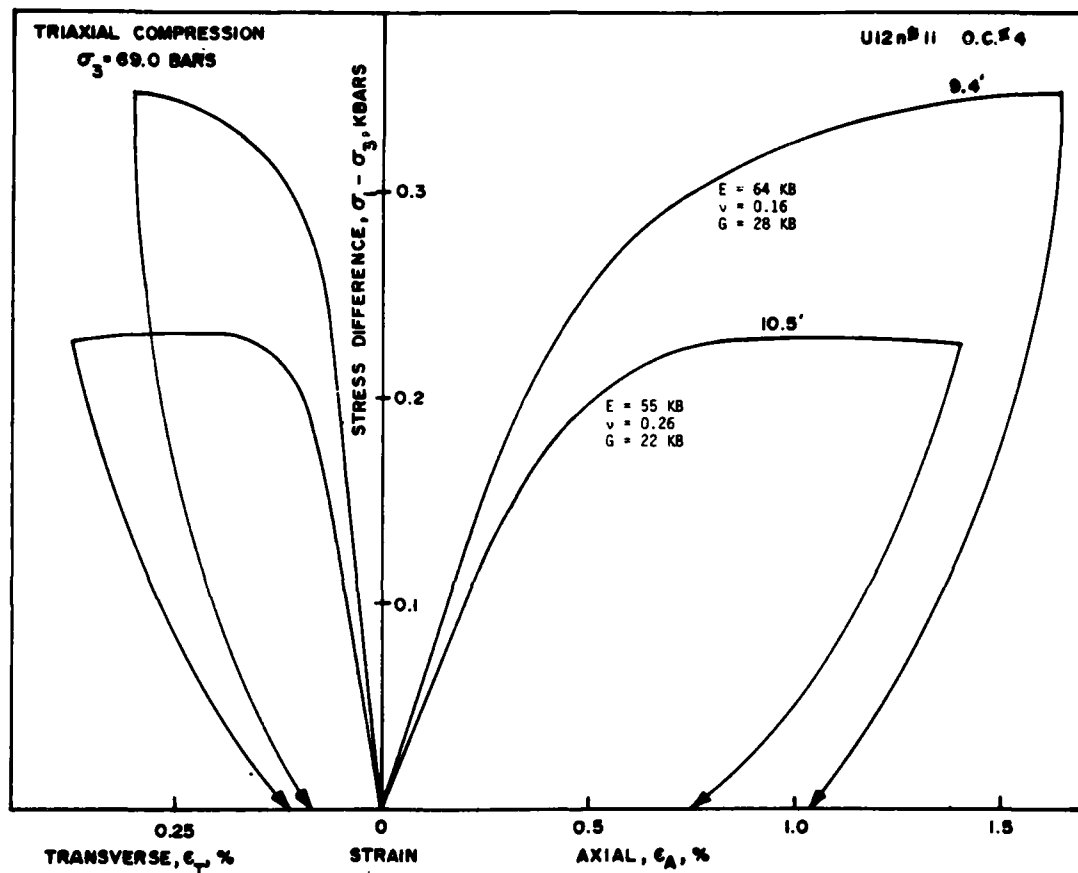
Figure 4. Triaxial compression tests.

Figure A1. Uniaxial strain tests, stress-strain response.

Figure A2. Uniaxial strain tests, stress-stress response.

Figure A3.   Uniaxial strain tests, stress-strain response.

Figure A4.   Uniaxial strain tests, stress-stress response.

170

Figure A5. Uniaxial strain tests, stress-strain response.

Figure A6. Uniaxial strain tests, stress-stress response.

171

Figure A7.   Uniaxial strain tests, stress-strain response.

Figure A8.   Uniaxial strain tests, stress-stress response.

172

Figure A9. Uniaxial strain tests, stress-strain response.

Figure A10. Uniaxial strain tests, stress-stress response.

173

Figure A11. Uniaxial strain tests, stress-strain response.

Figure A12. Uniaxial strain tests, stress-stress response.

174

Figure A13.   Uniaxial strain tests, stress-strain response.

Figure A14.   Uniaxial strain tests, stress-stress response.

175

Figure A15.   Uniaxial strain tests, stress-strain response.

Figure A16.   Uniaxial strain tests, stress-stress response.

176

Figure A17. Uniaxial strain tests, stress-strain response.

Figure A18. Uniaxial strain tests, stress-stress response.
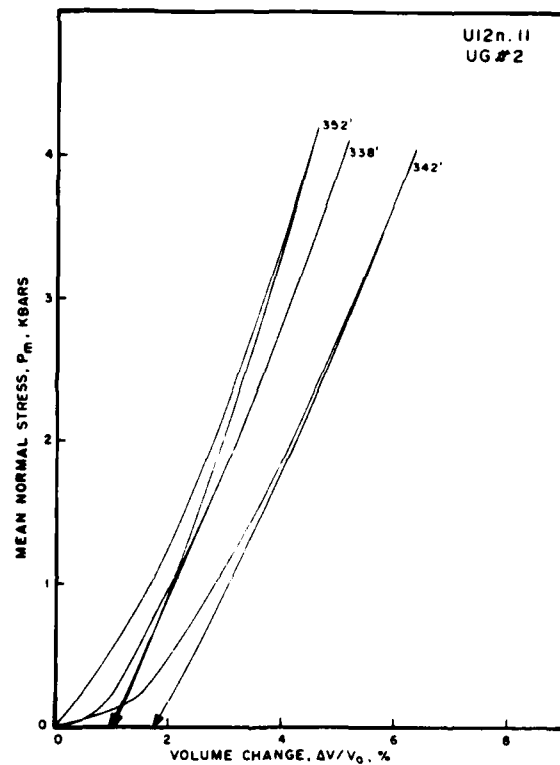
177

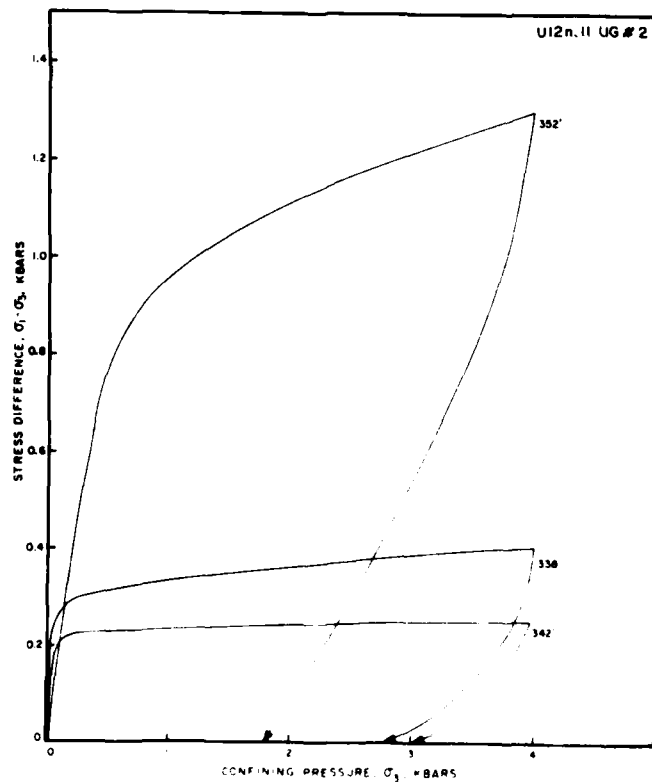Figure A19. Uniaxial strain tests, stress-strain response.

Figure A20. Uniaxial strain tests, stress-stress response.

Figure A21. Uniaxial strain tests, stress-strain response.

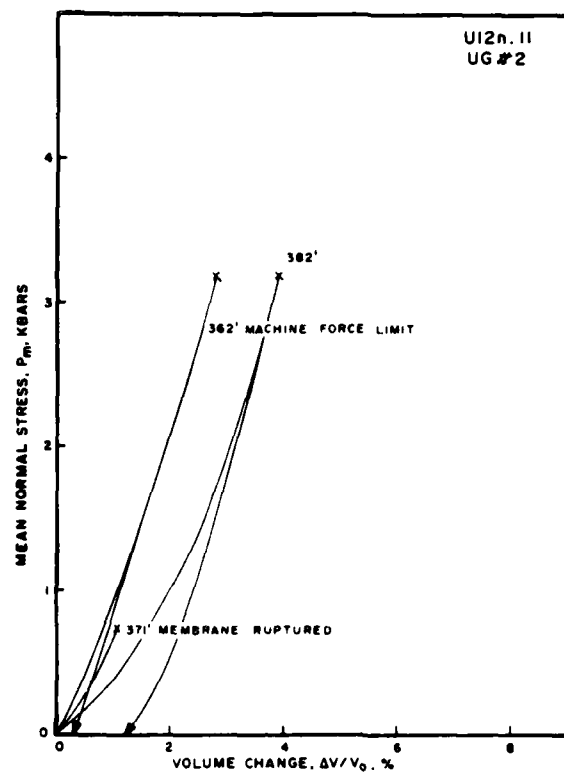Figure A22. Uniaxial strain tests, stress-stress response.

179
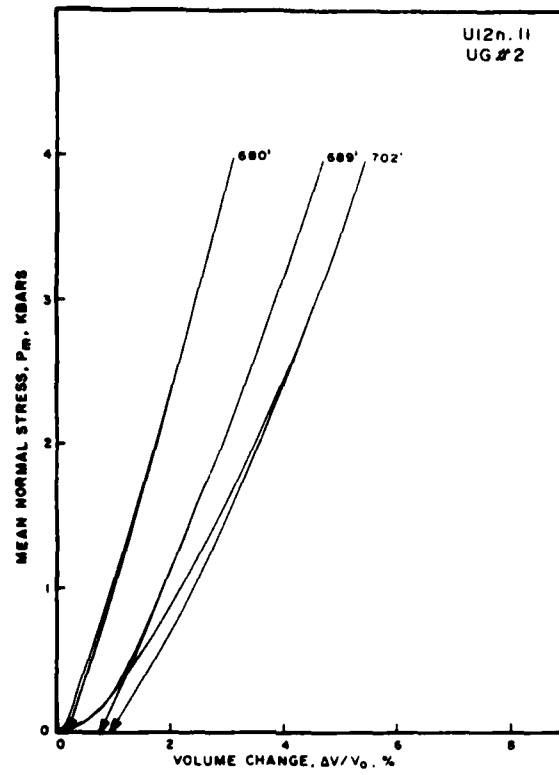
Figure A23. Uniaxial strain tests, stress-strain response.
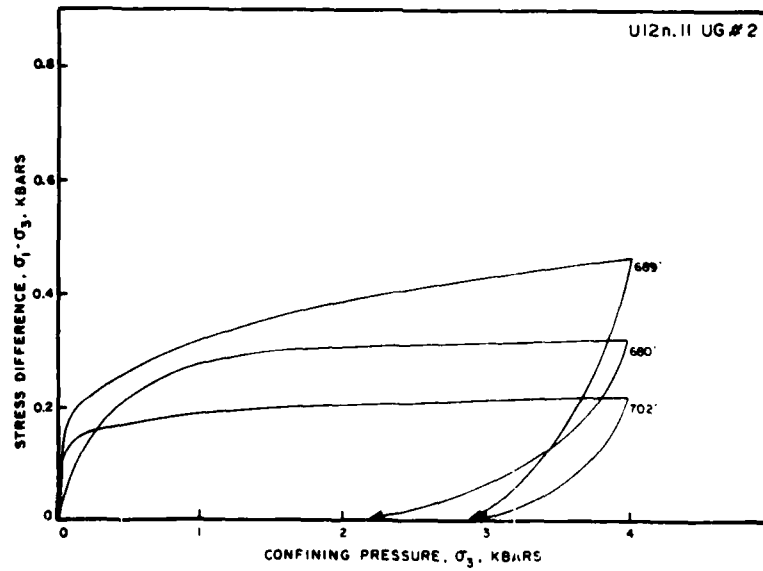
Figure A24. Uniaxial strain tests, stress-stress response.
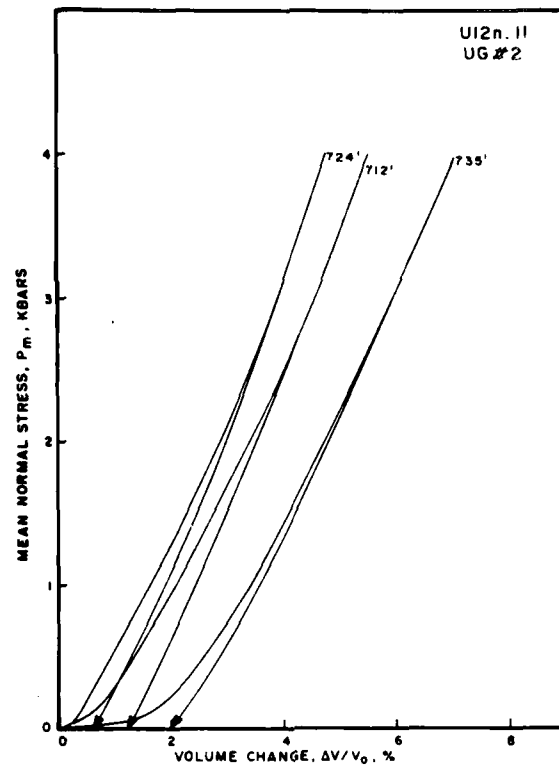
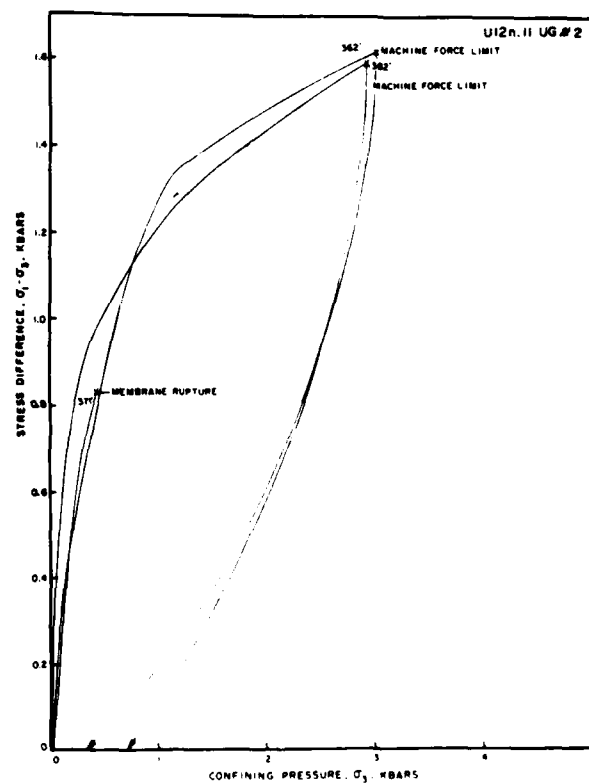Figure A25. Uniaxial strain tests, stress-strain response.
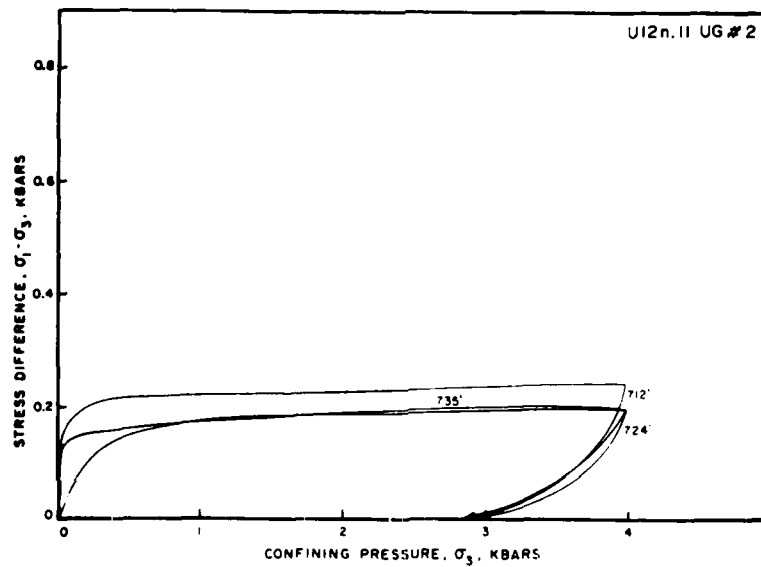
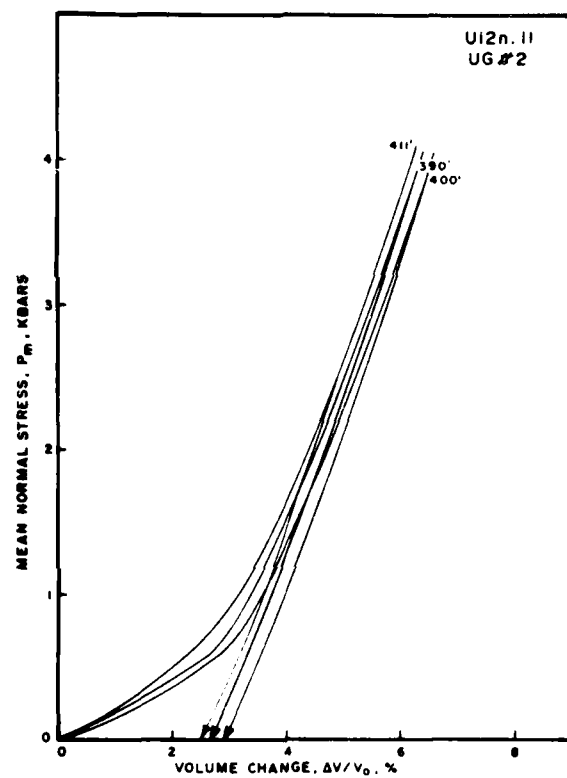Figure A26. Uniaxial strain tests, stress-stress response.

181
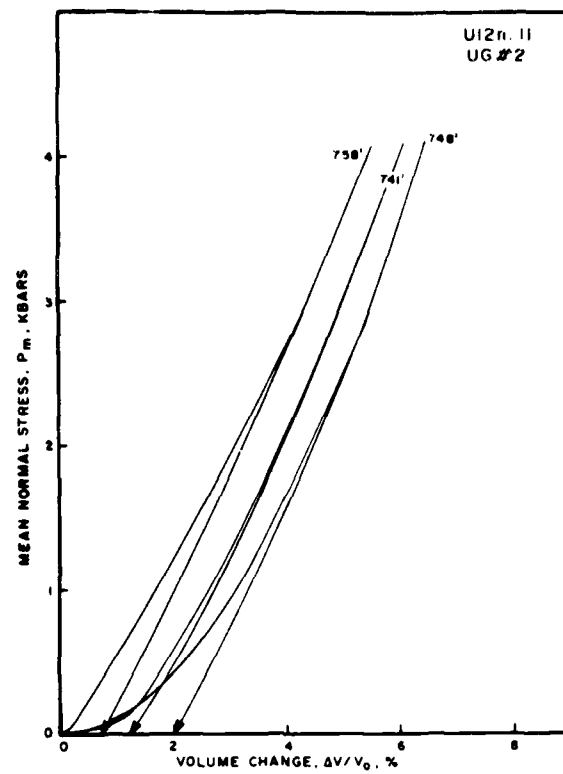
Figure A27. Uniaxial strain tests, stress-strain response.
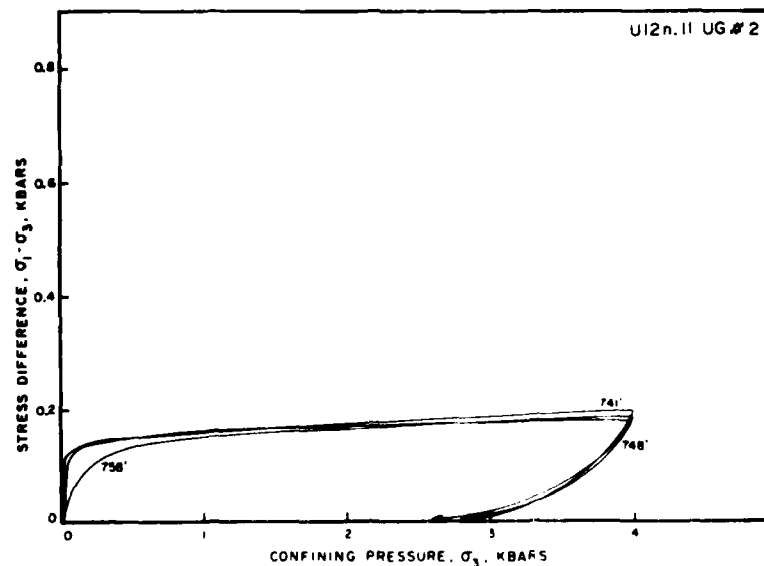
Figure A28. Uniaxial strain tests, stress-stress response.

182
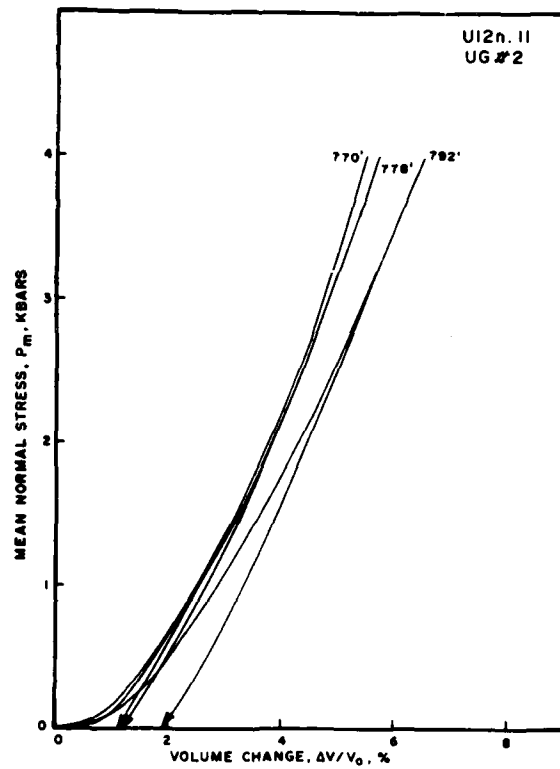
Figure A29. Uniaxial strain tests, stress-strain response.
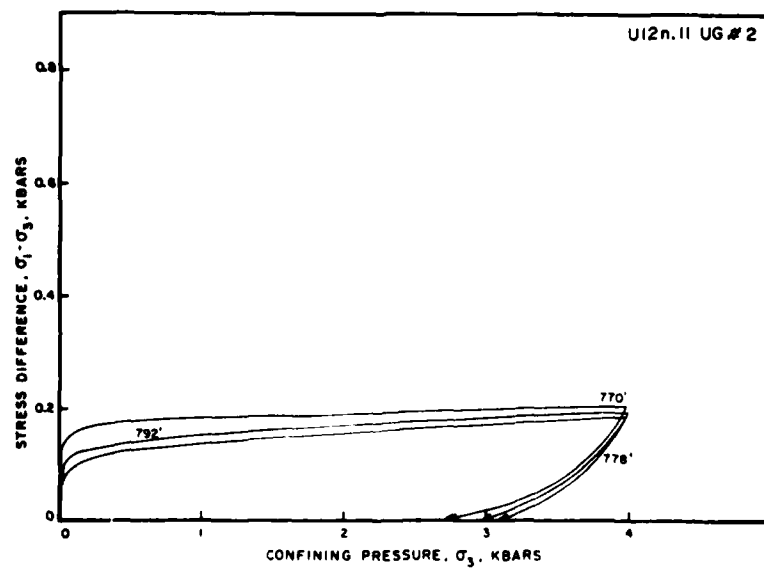
Figure A30. Uniaxial strain tests, stress-stress response.

183
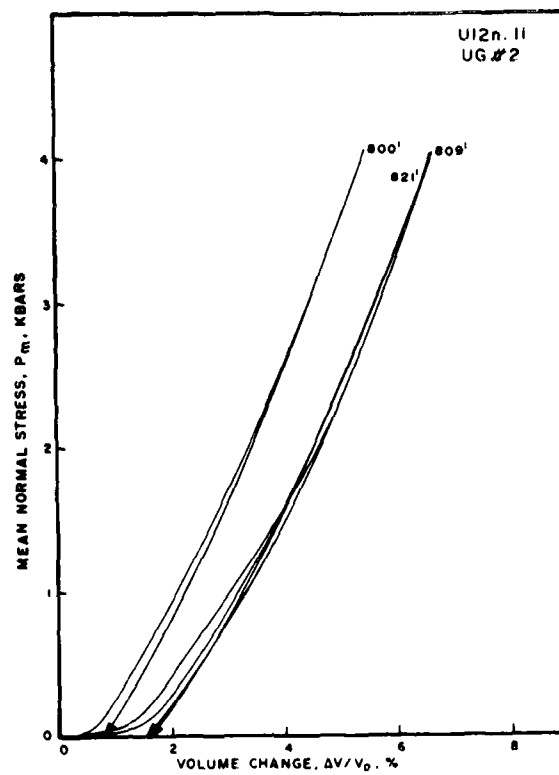
Figure A31. Uniaxial strain tests, stress-strain response.
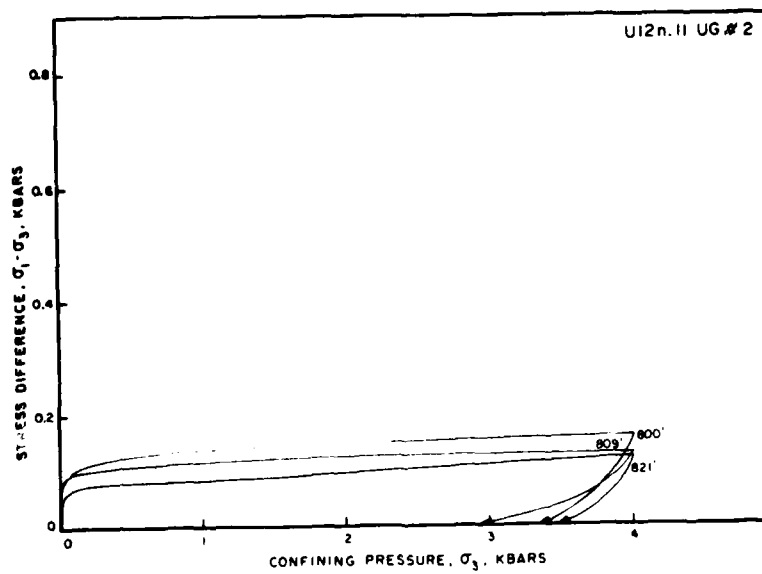
Figure A32. Uniaxial strain tests, stress-stress response.

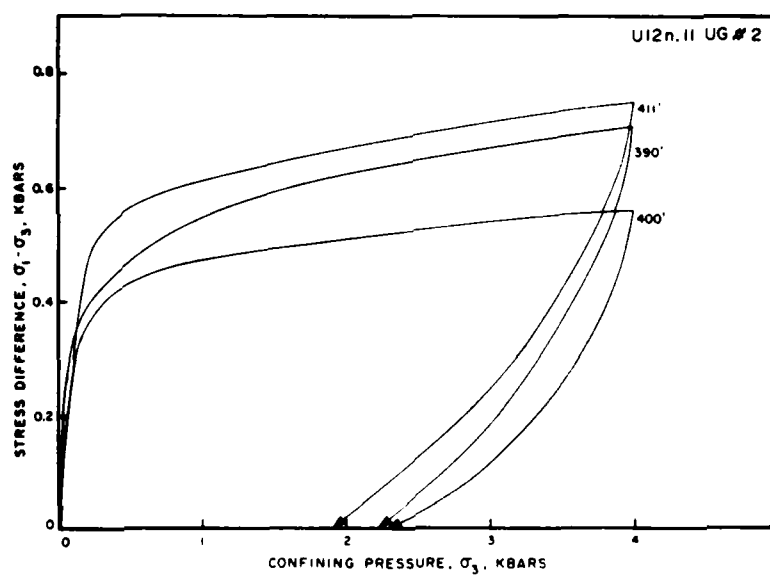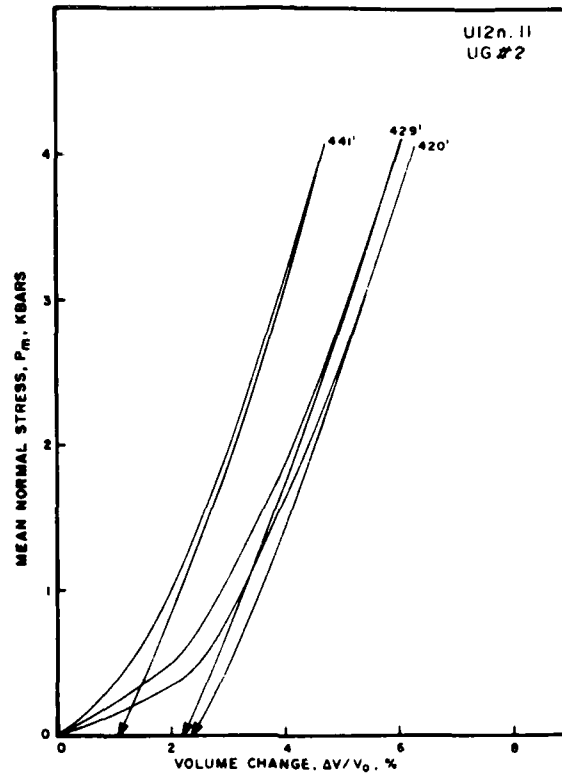184
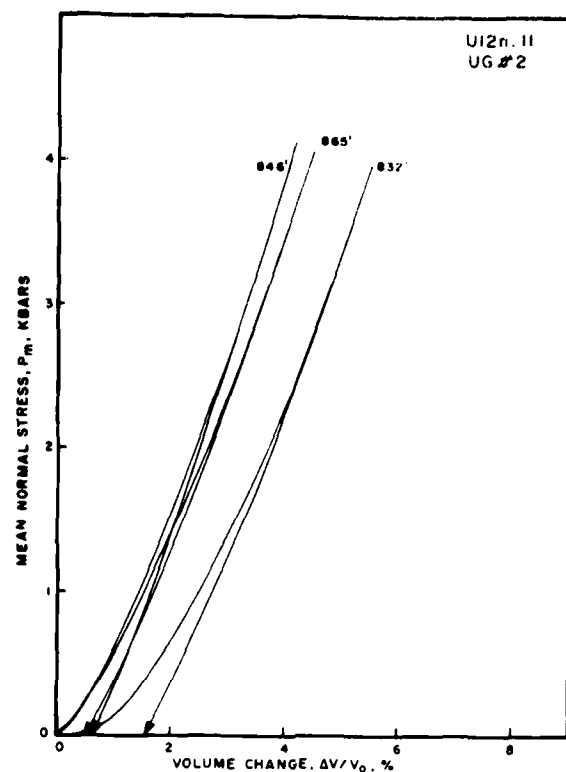
Figure A33.   Uniaxial strain tests, stress-strain response.
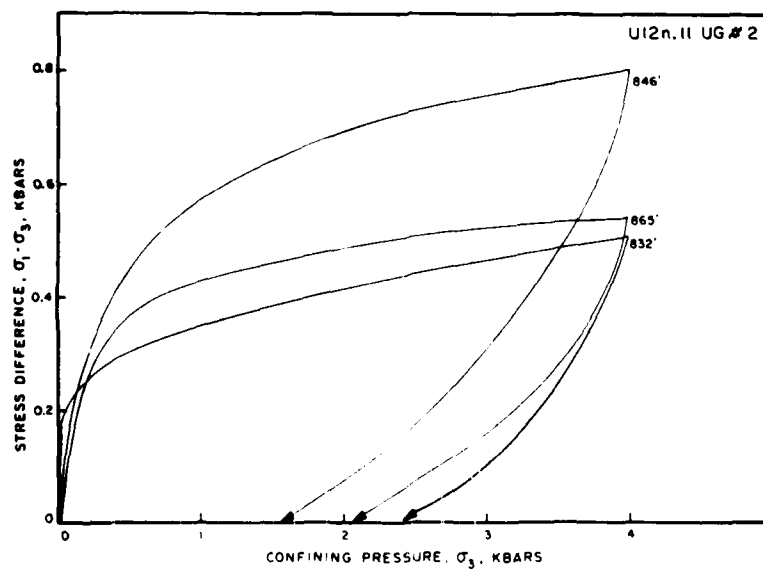
Figure A34.   Uniaxial strain tests, stress-stress response.

185
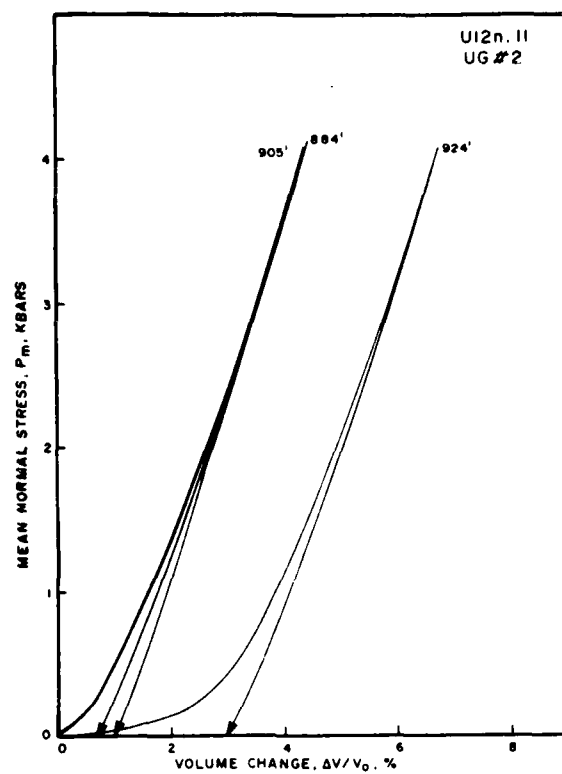
Figure A35. Uniaxial strain tests, stress-strain response.
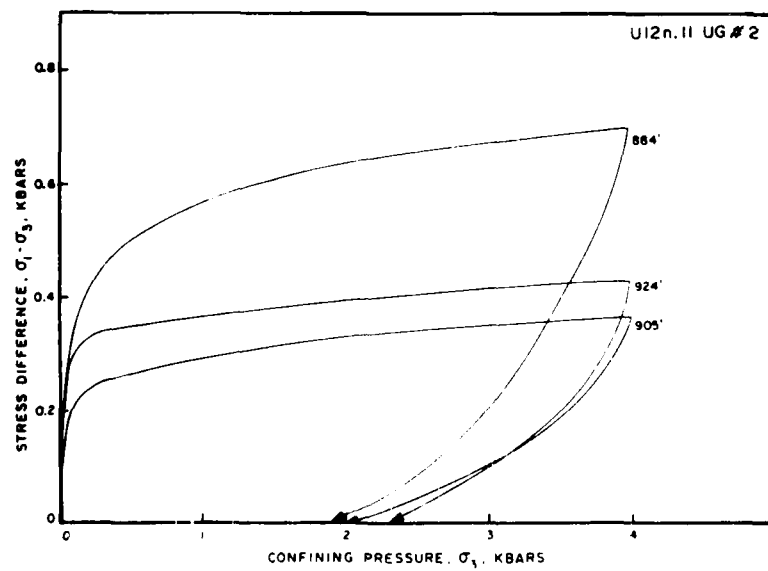
Figure A36. Uniaxial strain tests, stress-stress response.

186
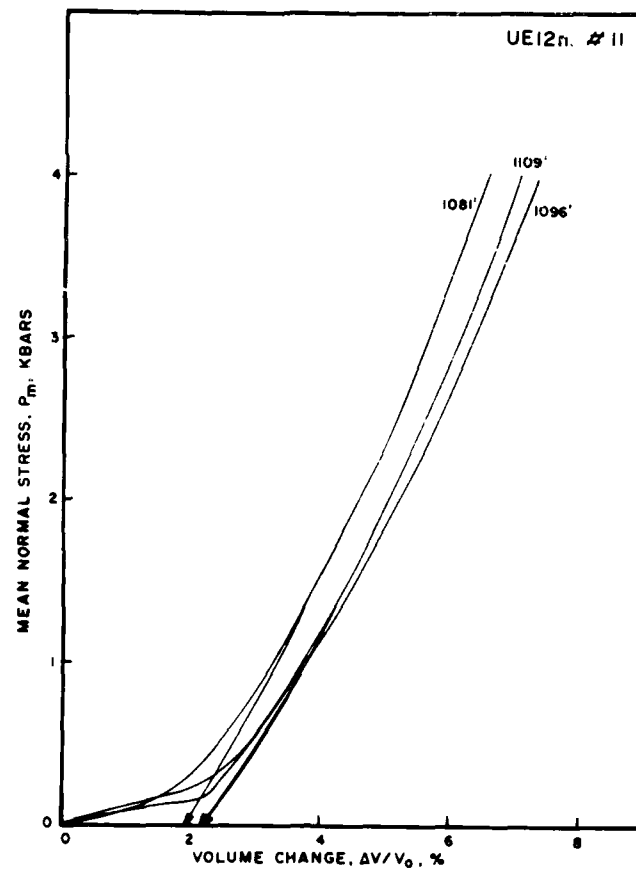
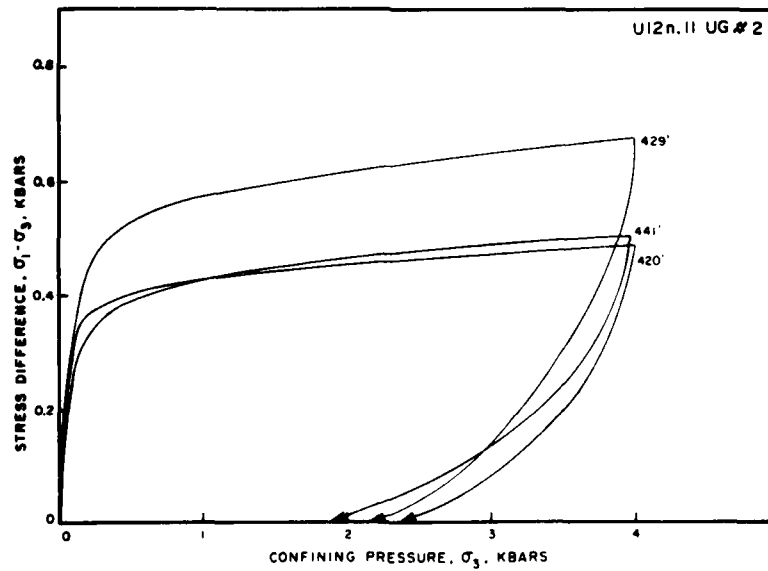Figure B1.   Uniaxial strain tests, stress-strain response.
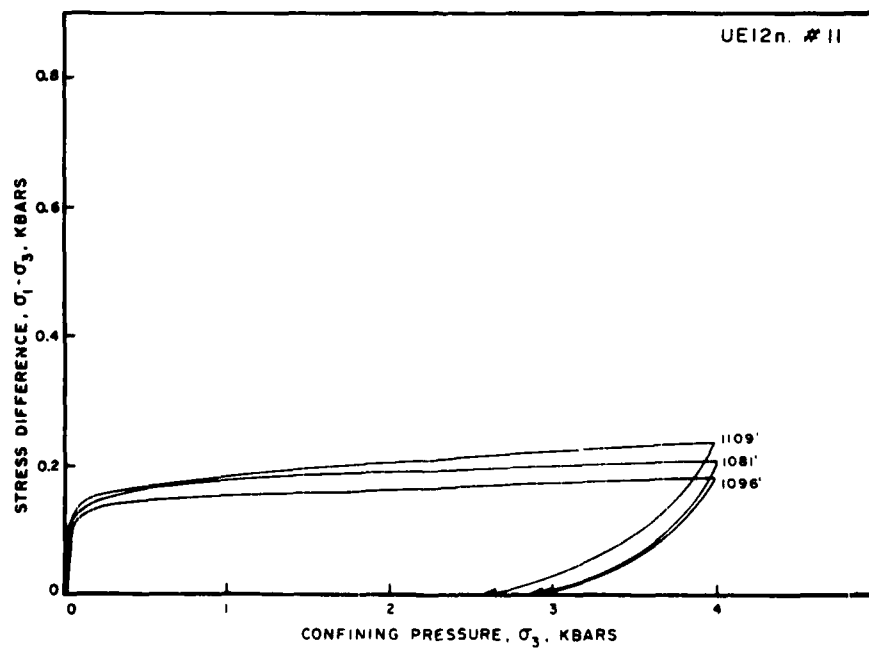
Figure B2.   Uniaxial strain tests, stress-stress response.

187
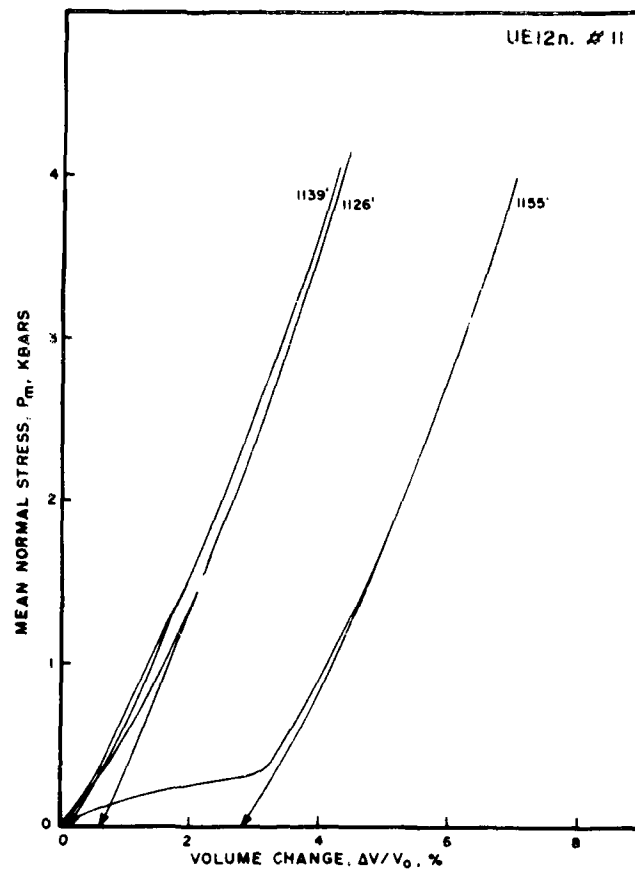
Figure B3. Uniaxial strain tests, stress-strain response.
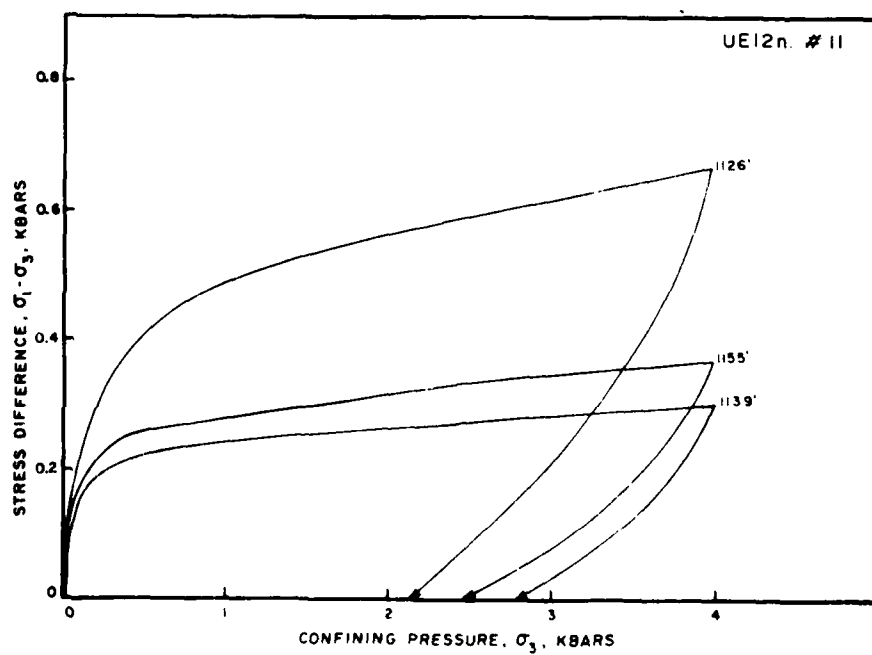
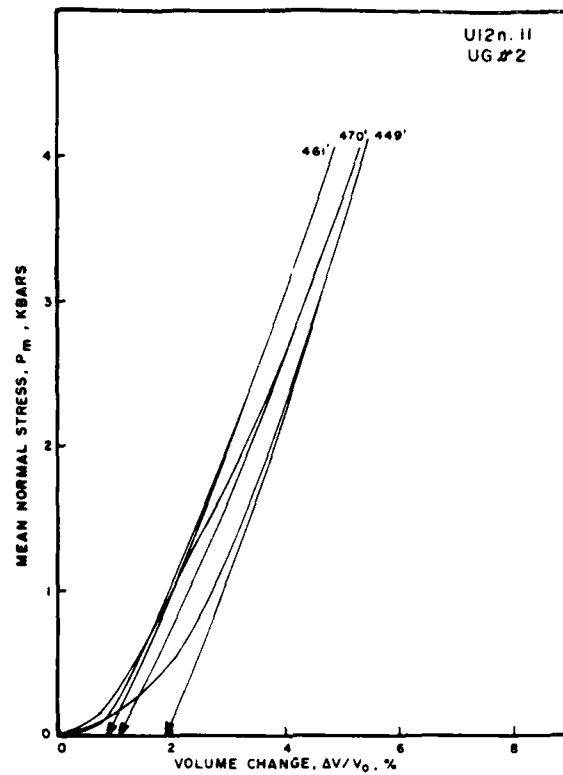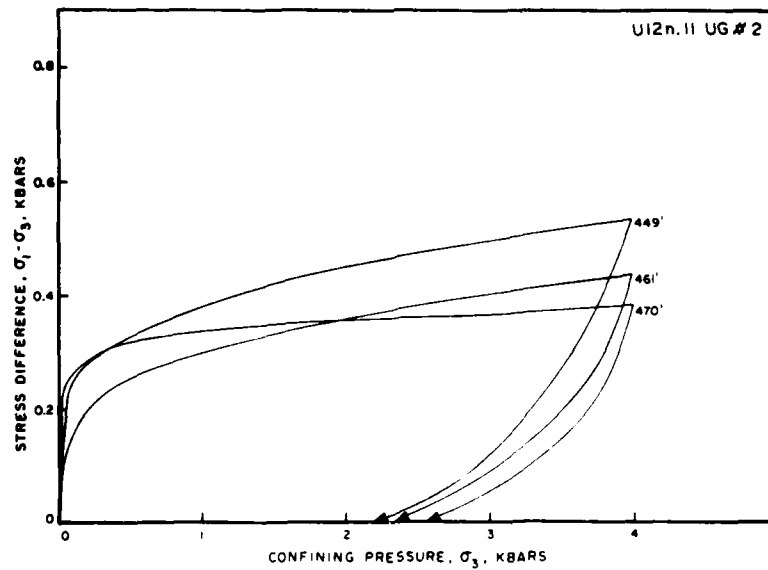Figure B4. Uniaxial strain tests, stress-stress response.

188

END

FILMED

DTIC
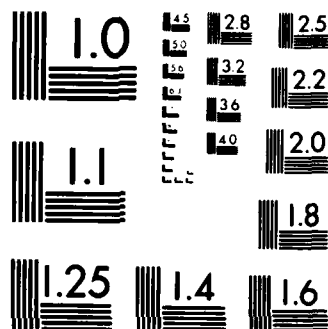
MICROCOPY RESOLUTION TEST CHART

NATIONAL BUREAU OF STANDARDS 1963-A

Figure B5. Uniaxial strain tests, stress-strain response.
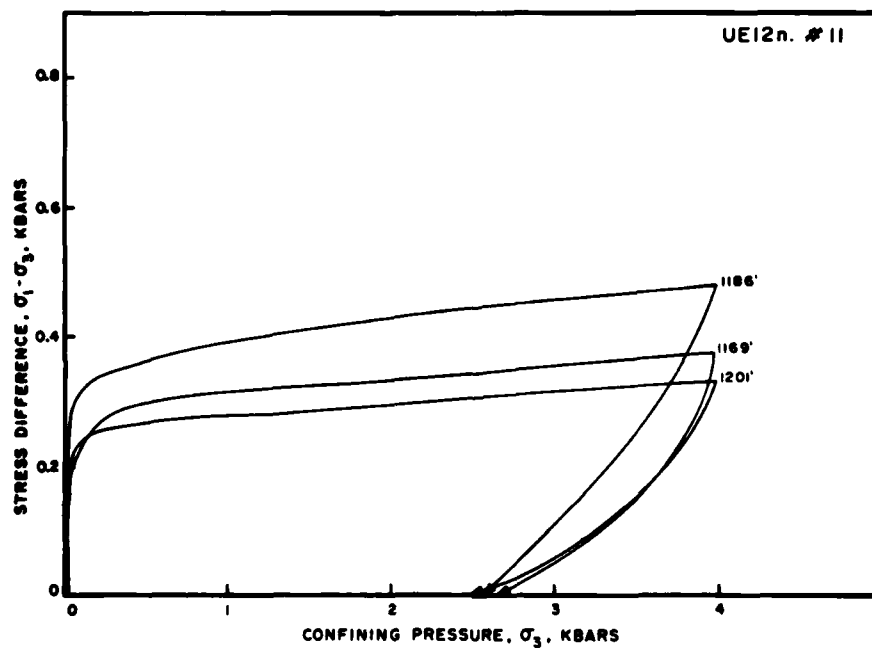
Figure B6. Uniaxial strain tests, stress-stress response.

189
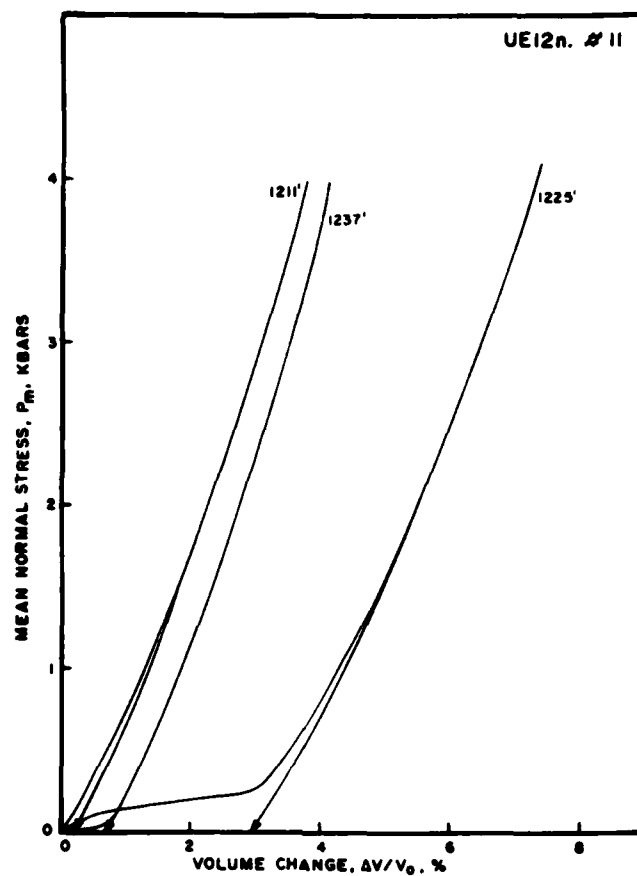
Figure B7.   Uniaxial strain tests, stress-strain response.
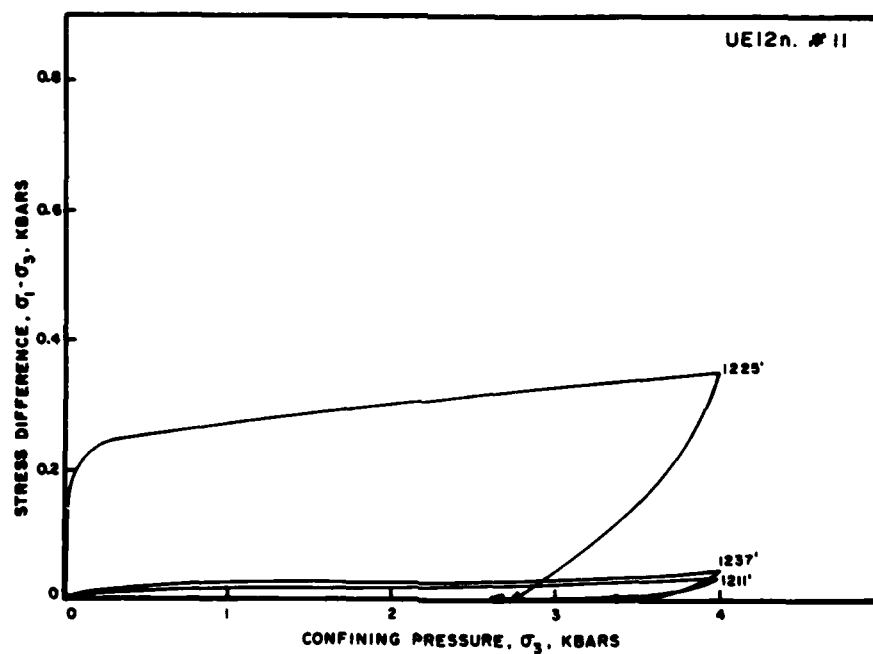
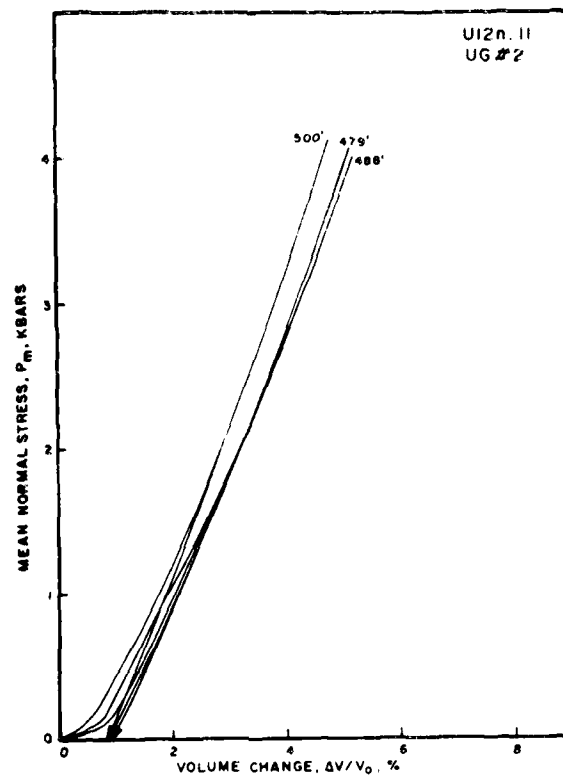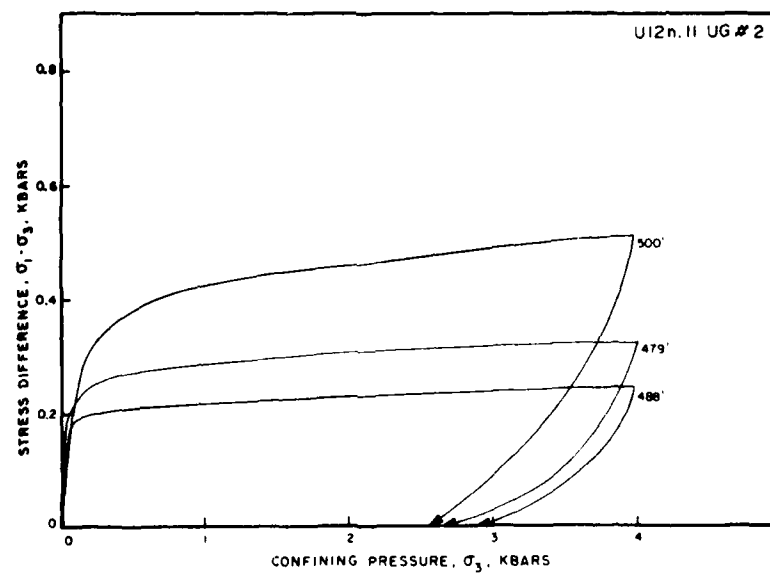Figure B8.   Uniaxial strain tests, stress-stress response.

190
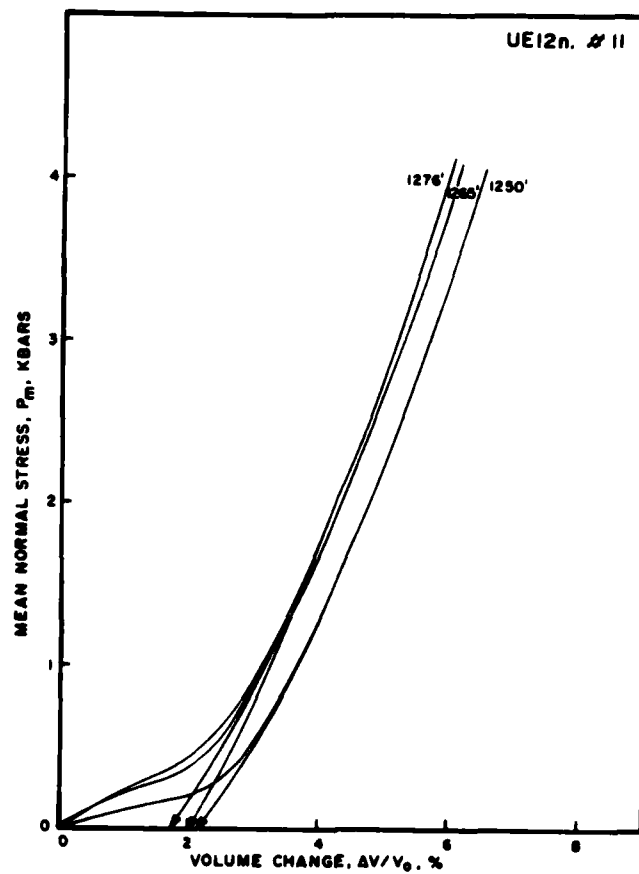
Figure B9. Uniaxial strain tests, stress-strain response.
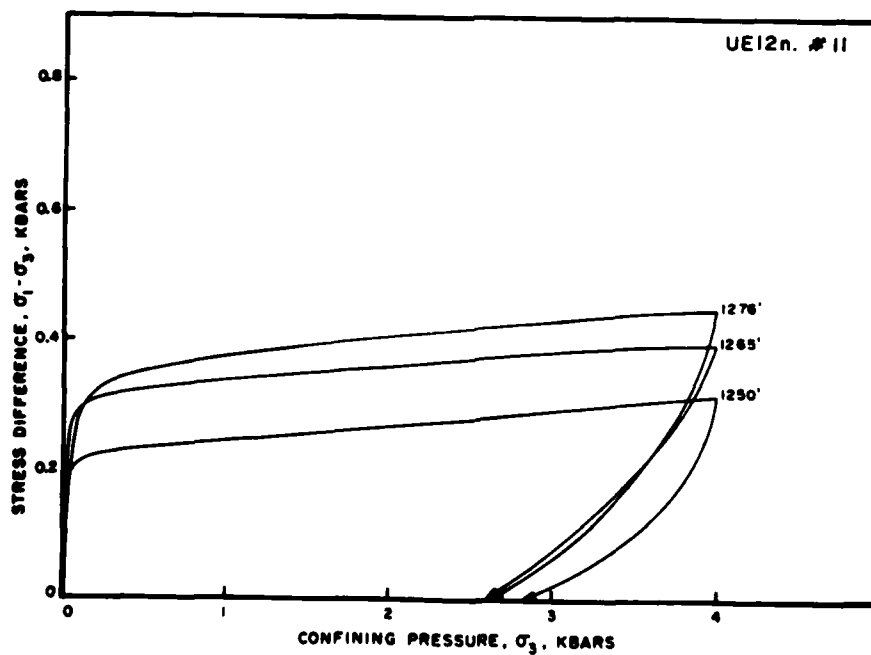
Figure B10. Uniaxial strain tests, stress-stress response.

191
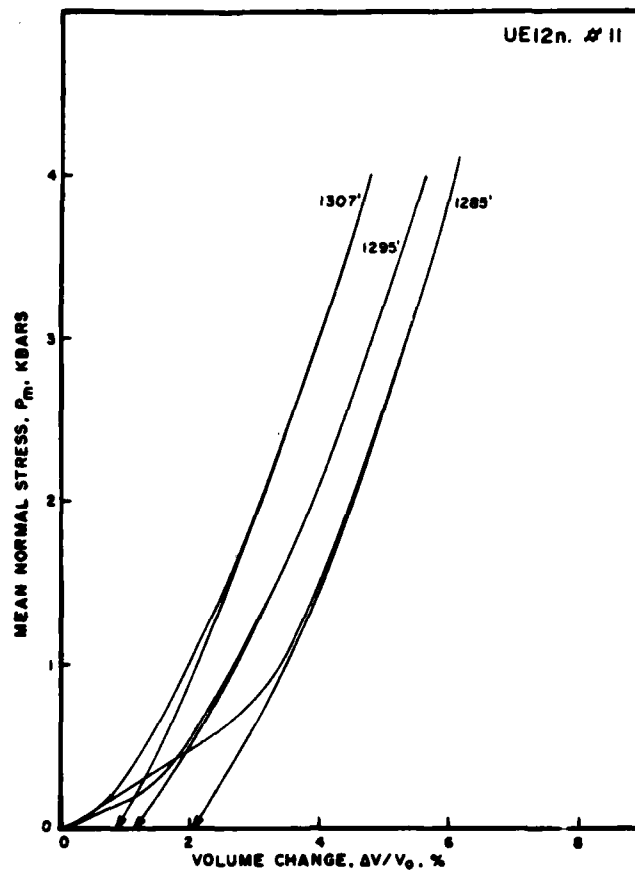
Figure B11. Uniaxial strain tests, stress-strain response.
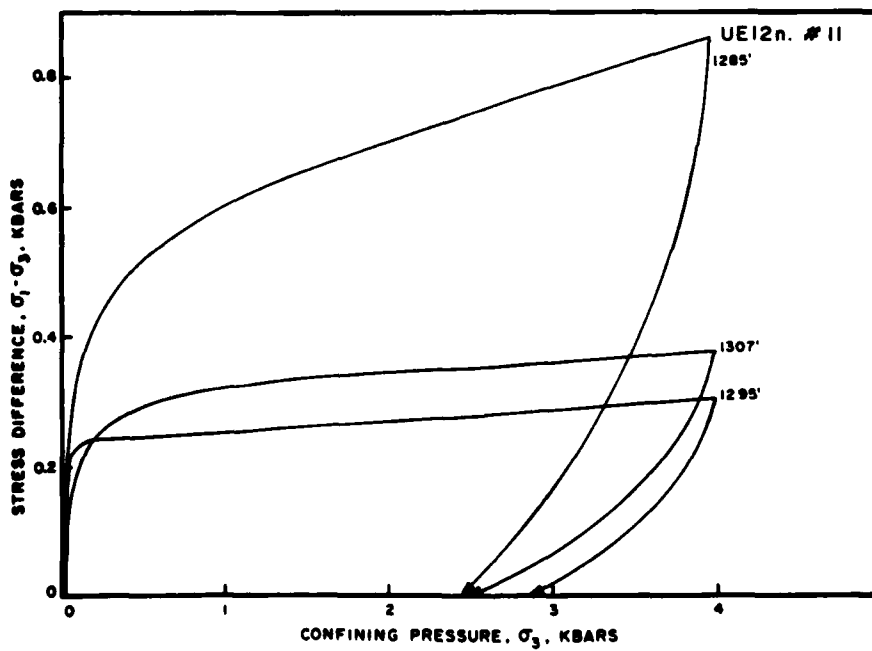
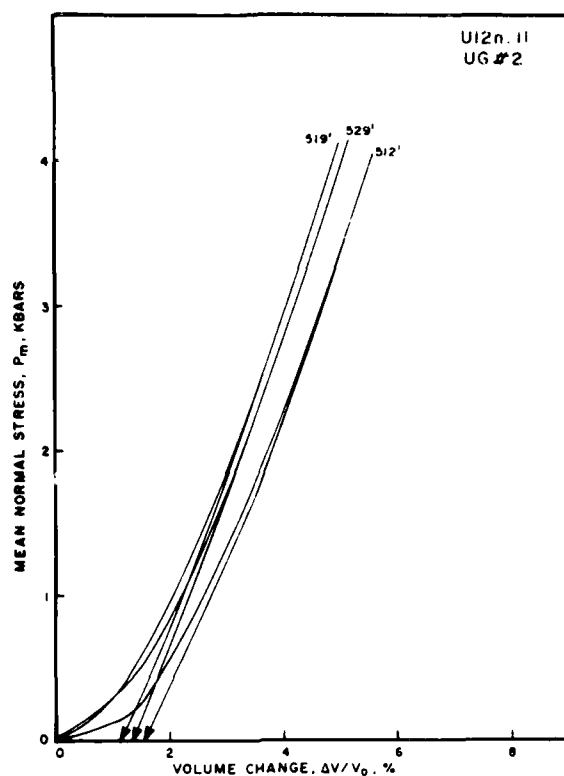Figure B12. Uniaxial strain tests, stress-stress response.

192
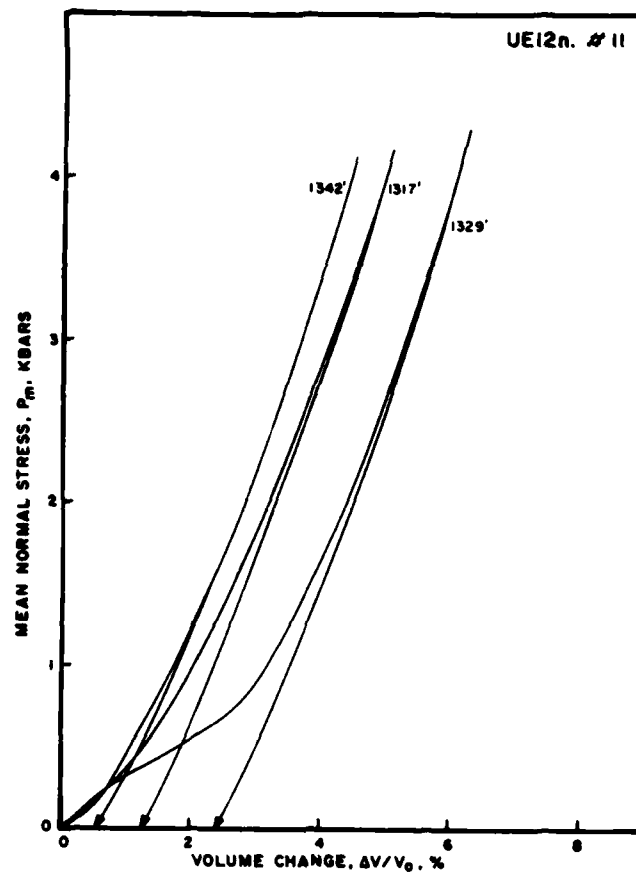
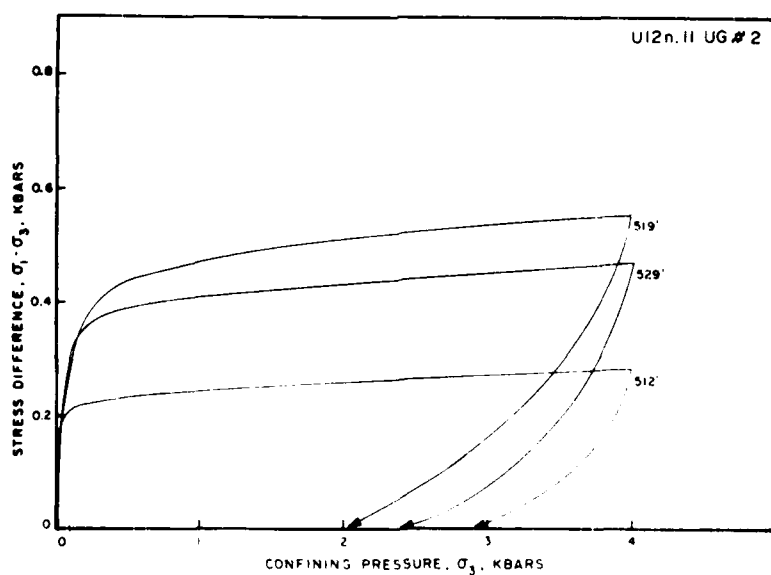Figure B13. Uniaxial strain tests, stress-strain response.
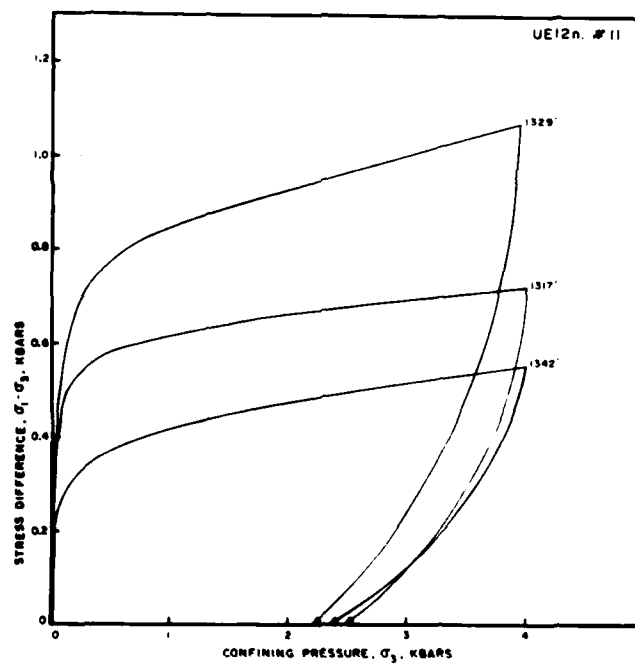
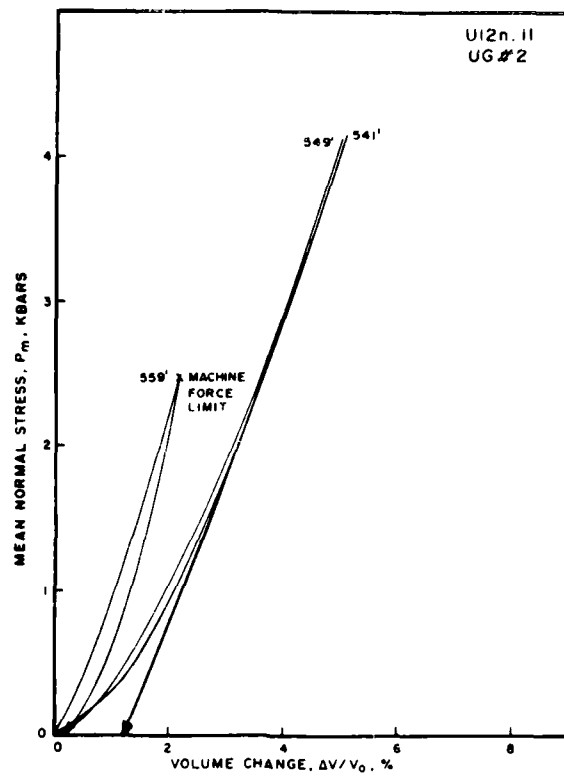Figure B14. Uniaxial strain tests, stress-stress response.

193
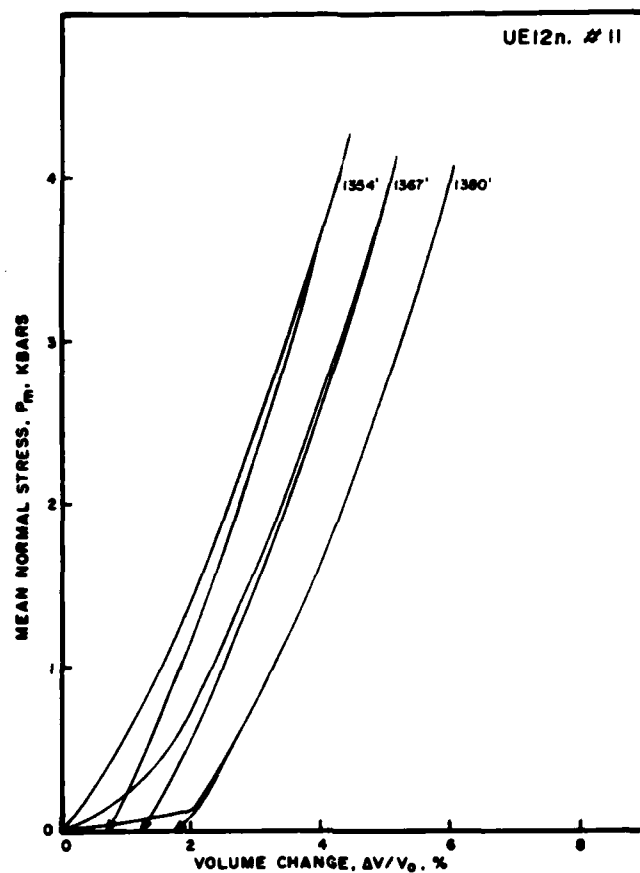
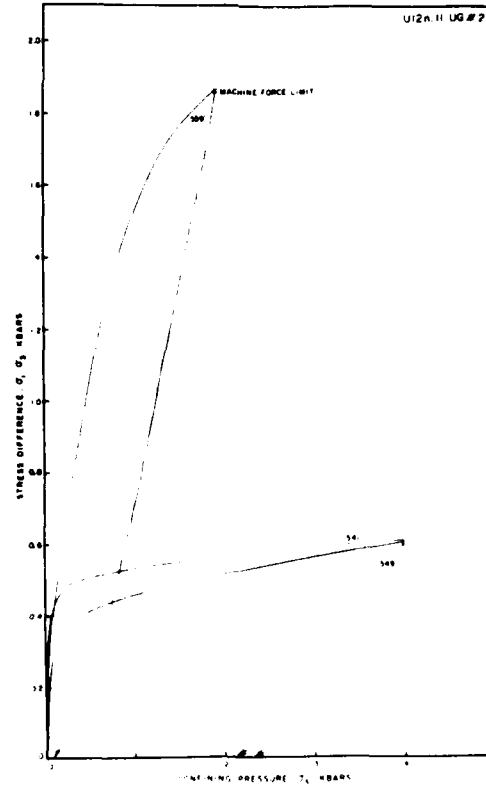Figure B15.   Uniaxial strain tests, stress-strain response.
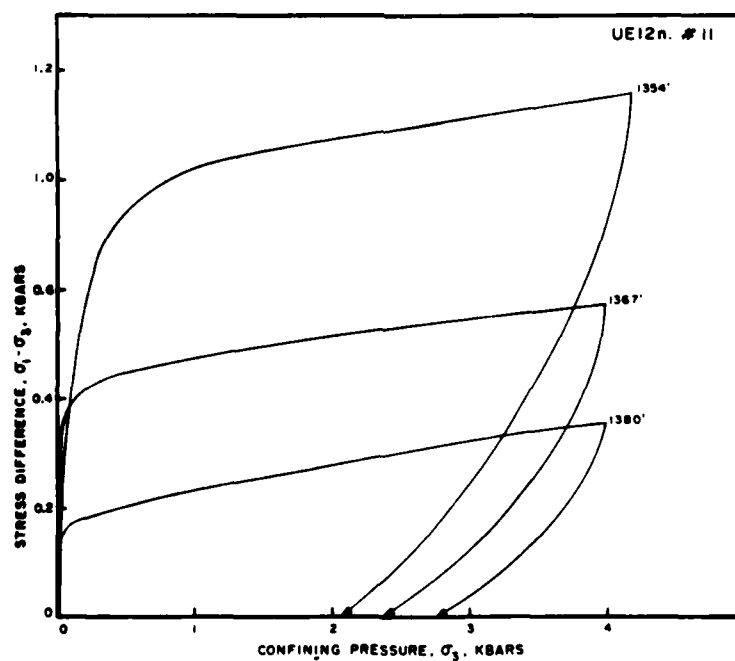
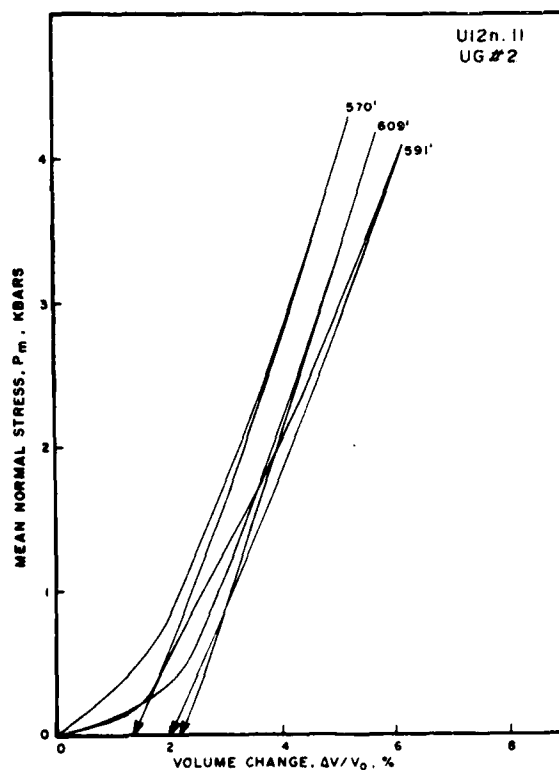

Figure B16.   Uniaxial strain tests, stress-stress response.

194
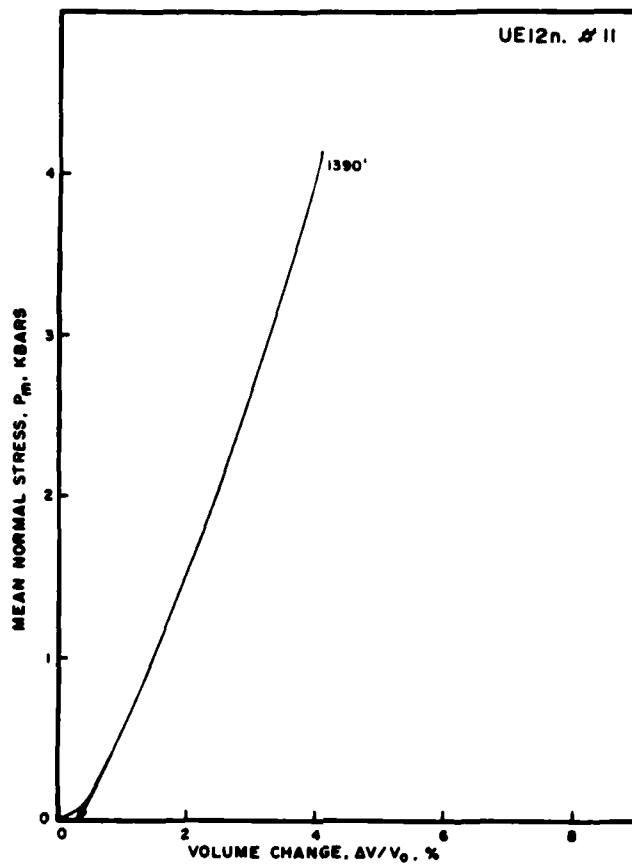
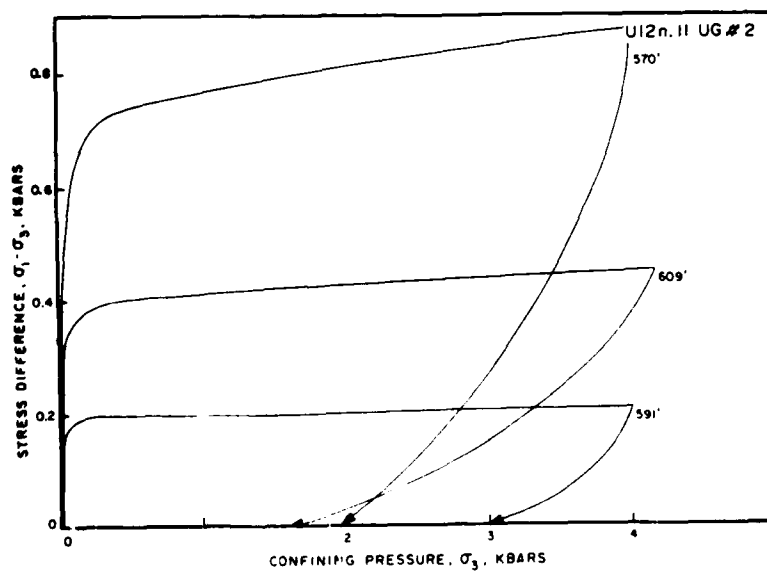Figure B17.   Uniaxial strain tests, stress-strain response.

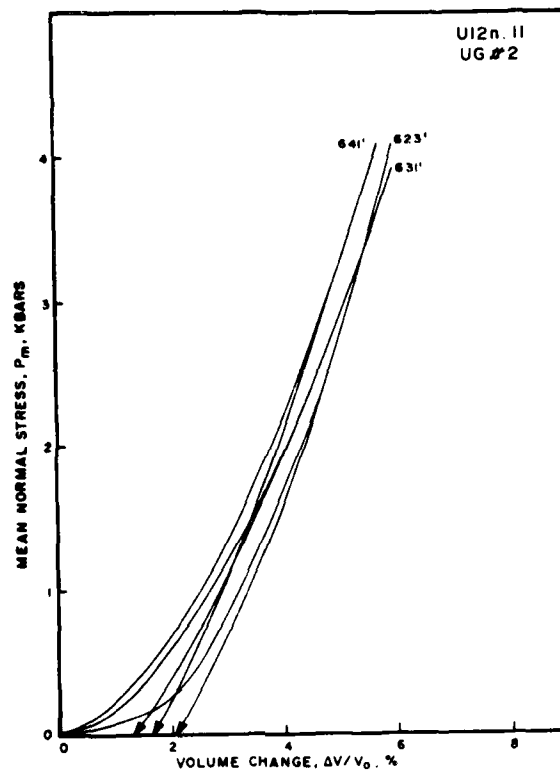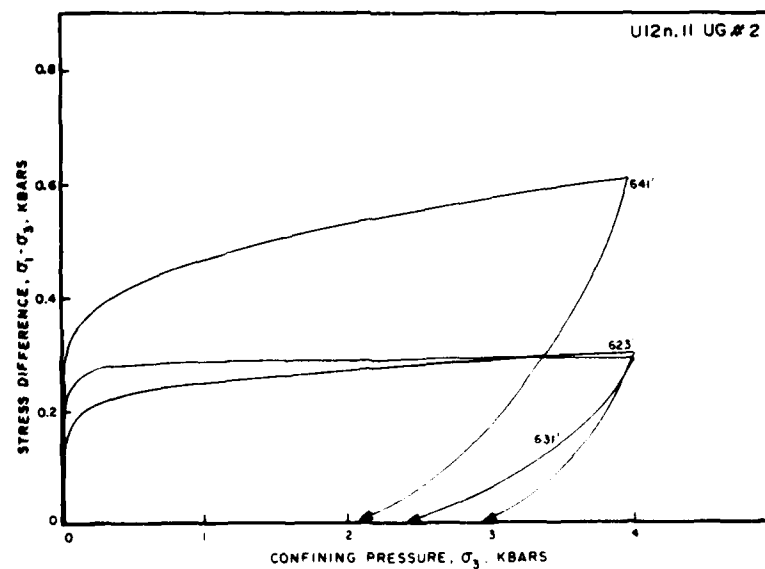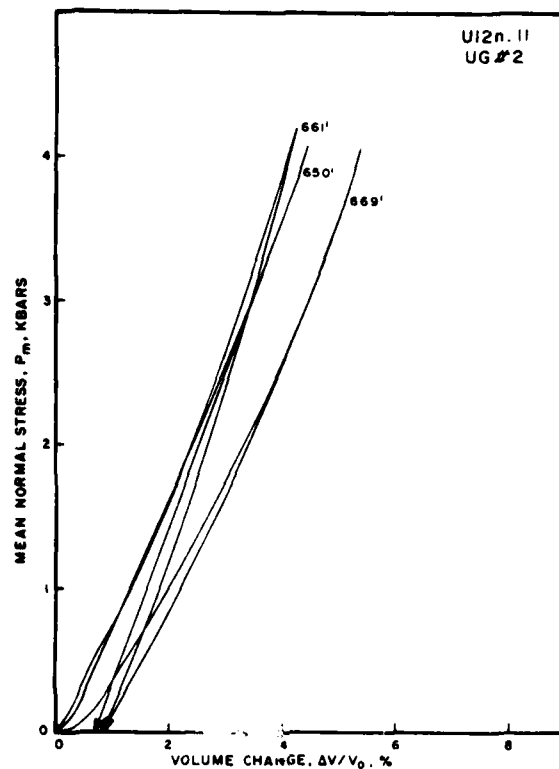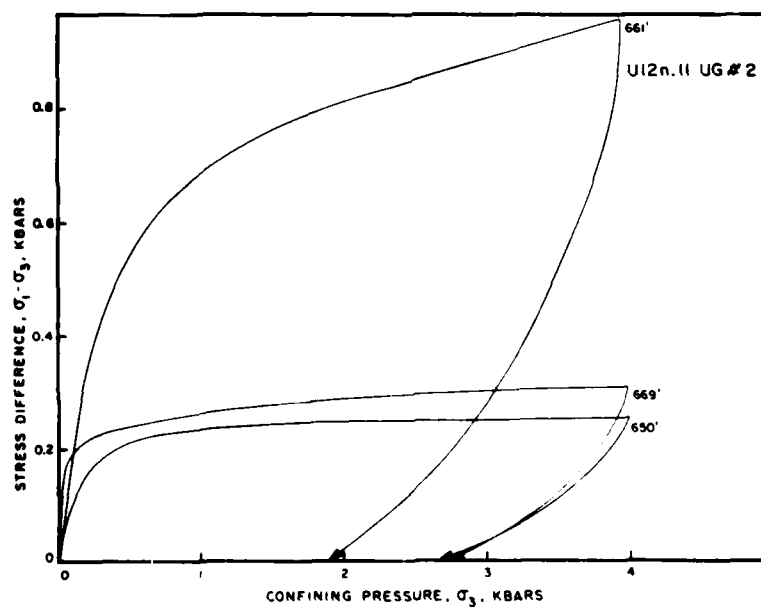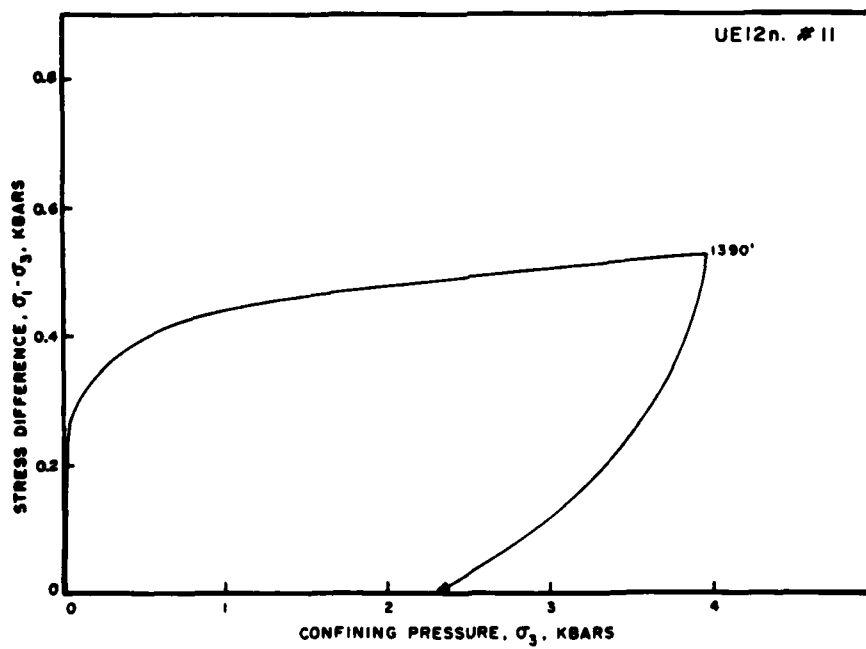

Figure B18.   Uniaxial strain tests, stress-stress response.

195

RESIDUAL STRESS IN THICK-WALLED CYLINDERS OF ASH-FALL TUFFS SUBJECTED TO INTERNAL PRESSURIZATION

ABSTRACT

Field stress measurements suggest that residual stress fields are formed during the creation of an underground nuclear cavity. Laboratory experiments, designed to investigate the possibility of creating residual stresses have been undertaken in an effort to verify this phenomenon. Internal pressurization tests (burst tests) on thick-walled tuff and grout cylinders have been used in initial efforts to produce residual stresses. During initial testing, residual stresses were successfully formed in grout samples but not in tuff samples. Continued testing on the tuff samples have since produced residual stresses in tuffs as well. This report summarizes the results obtained in the recent tuff tests.

PROGRESS SUMMARY

Since no residual stresses were observed in the initial tuff tests*, additional tests were conducted at increased stress levels. A second group of tuff samples from the U12n.10A TRCX#1 and #2 drill holes were chosen. After failing three samples unconfined, two samples from each drill hole were pressure cycled while confined at 70 bars (compared to the earlier 30 bars) and subsequently burst unconfined. Results of the test series are shown in Tables 1 and 2.

TABLE 1

Uncycled Tuff Burst Pressure Data

Sample Designation U12n.10A	Internal Pressure Cycle		Pressure at Failure		Diameter Ratio (Do/Di)	Comments
	External (bars)	Internal (bars)	External (bars)	Internal (bars)		
TRCX#1 -100'	--	--	0	47	6.25/1	Unconfined burst*
TRCX#2 - 35'	--	--	0	47	6.25/1	Unconfined burst
	--	--	0	36	6.25/1	Unconfined burst

* All internal bores were jacketed.

TABLE 2

Cycled Tuff Burst Pressure Data

Sample Designation U12n.10A	Internal Pressure Cycle		Pressure at Failure		Diameter Ratio (Do/Di)	Comments
	External (bars)	Internal (bars)	External (bars)	Internal (bars)		
TRCX#1 -100'	30	110	0	43	6.25/1	Internal pressure cycled while confined; burst unconfined*
	70	220	0	72	6.25/1	Internal pressure cycled while confined; burst unconfined
TRCX#1 -35'	70	240	0	47	6.25/1	Internal pressure cycled while confined; burst unconfined
	70	240	0	42	6.25/1	Internal pressure cycled while confined; burst unconfined

* All internal bores were jacketed unless noted otherwise.

---

* Enniss, D. O., and S. W. Butters, "Residual Stress in Thick-Walled Cylinders of Ash-Fall Tuffs and Tuff Matching Grouts Subjected to Internal Pressurization," Terra Tek Report TR 76-67, December 1976.

Only one sample indicated any increase in the unconfined burst pressure. Another set of tests were therefore conducted to include several more data points and at increased stress levels.

Nine samples from U12n.11 UG#2 drill hole were prepared and tested. Four samples were burst unconfined and five samples were pressure cycled while at 500 bars confining pressure and subsequently burst unconfined. Results are shown in Tables 3 and 4.

TABLE 3

Uncycled Tuff Burst Pressure Data

Sample Designation	Internal Pressure Cycle		Pressure at Failure		Diameter Ratio (Do/Di)	Comments
	External (bars)	Internal (bars)	External (bars)	Internal (bars)		
U12n.11 UG#2 -1000'	--	--	0	51	6.25/1	Unconfined burst*
	--	--	0	45	6.25/1	Unconfined burst
	--	--	0	50	6.25/1	Unconfined burst
	--	--	0	43	6.25/1	Unconfined burst

* All internal bores were jacketed.

TABLE 4

Cycled Tuff Burst Pressure Data

Sample Designation	Internal Pressure Cycle		Pressure at Failure		Diameter Ratio (Do/Di)	Comments
	External (bars)	Internal (bars)	External (bars)	Internal (bars)		
U12n.11 UG#2 -1000'	500	675	0	118	6.25/1	10 minutes*
	500	675	0	150	6.25/1	10 minutes
	500	675	0	44	6.25/1	20 minutes
	500	675	0	9	6.25/1	10 minutes
	500	675	0	390	6.25/1	2 minutes

* Time delay between internal pressure cycle and unconfined burst.

Results indicate an increase in burst pressure in three of the five cycled samples. One sample exhibited no increase in burst pressure and another showed a decrease (thought to be a result of partial failure caused by the pressure cycle). The test results also suggest a possible stress relaxation with time. Note that as the time period between the pressurization cycle and the unconfined burst increases, the burst pressure decreases. Planned future tests include repeating more cycled tests (σ_3 = 500 bars) on the sample UG#2 tuff with consistent time periods between the cycle and the burst. If these samples produce consistent burst pressure increases, a text matrix will be developed to address the time dependence.

PROPERTIES OF RECONSTITUTED TUFF

ABSTRACT

To attain maximum utilization of facilities, it is desirable to site nuclear tests closer together than previous practice. For this reason, it is important to characterize the "rubble zone" which exists in the "chimney" regions of previous events. The "rubble zone" is a highly broken region of material which is a result of cavity growth followed by cavity collapse and subsequent plunge downward of tuff above the cavity. Since representative materials from this region are impossible to obtain, test samples have been constructed from crushed tuff recompacted to typical "chimney" densities. This report summarizes the progress made in testing "reconstituted" Paintbrush tuff samples of varying sample sizes. The work is a follow-on to an initial effort previously reported by Terra Tek*.

---

* Gardiner, D. S., and S. W. Butters, "Physical and Mechanical Properties of Reconstituted Tuff," Terra Tek Report TR 77-94, October 1977.

PROGRESS SUMMARY

The reconstituted tuff test program requires several tests to evaluate parameters such as particle size, sample size, density and tuff type. This summary reports initial efforts in evaluating effects of sample size on material properties such as shear strength, elastic moduli and permeability.

Paintbrush tuff was chosen as the first tuff type because it is often times the material in which the "chimney" is contained. The target test density, thought to be representative of the chimney material, was ~1.65 gm/cc. Sample diameters of 2, 4 and 6 inches were chosen to examine the sample size effects on ½ inch minus particle size samples.

Sample Fabrication Techniques

The Paintbrush tuff used in the test program was received in an undersaturated condition. On receipt, all material was immersed in water and saturated to 97-100 percent. Physical property measurements conducted on twelve random samples indicated an average bulk density of 1.75 ± 0.05 gm/cc.

Molds and dies for the three sample sizes were designed and fabricated and the jaw crusher was modified to produce ½ inch minus particle size tuff. After crushing, the material was poured into an empty jacket, affixed to an endcap, supported laterally by the cylindrical mold, and compacted with ~2000 psi axial stress in layers to a predetermined density (1.6-1.7 gm/cc). After obtaining the desired length, the other endcap was sealed to the jacket of the specimen.

Physical property measurements were conducted on the fabricated samples to confirm the pre-test density. Post-test measurements indicate that the test samples were 80-85 percent saturated with 7-10 percent air voids. The reduction in water content (from 97 to 100 percent) undoubtedly resulted from the sample fabrication process. Particle size distribution analysis were also conducted to evaluate particle breakdown resulting from sample fabrication. Figure 1 shows typical particle size distribution curves after the material was crushed and placed in the sample configuration.

Mechanical Tests

4 inch diameter samples -- Three 4 inch diameter ½ inch minus particle size samples were tested. Volume strain curves during hydrostatic compression to 69.0 bars confining pressure are shown in Figure 2. Figure 3 shows the individual triaxial compression stress-strain curves and Figures 4, 5, and 6 show the post-test gradation analyses. Volume strain resulting from the hydrostatic compression was 3-5 percent. Subsequent triaxial compression tests indicate a shear strength of approximately 55 bars. The shear moduli, computed from the stress-strain curves, ranged from 3 to 6 kbars. Gradation analysis indicate further particle breakdown during triaxial compression.

6 inch diameter samples -- Three 6 inch diameter ½ inch minus particle size samples were also tested. Two of the three samples leaked during hydrostatic compression. Hydrostatic compression volume strain and triaxial compression stress-strain curves for the successful test sample are shown in Figures 7 and 8 respectively. Figure 9 shows
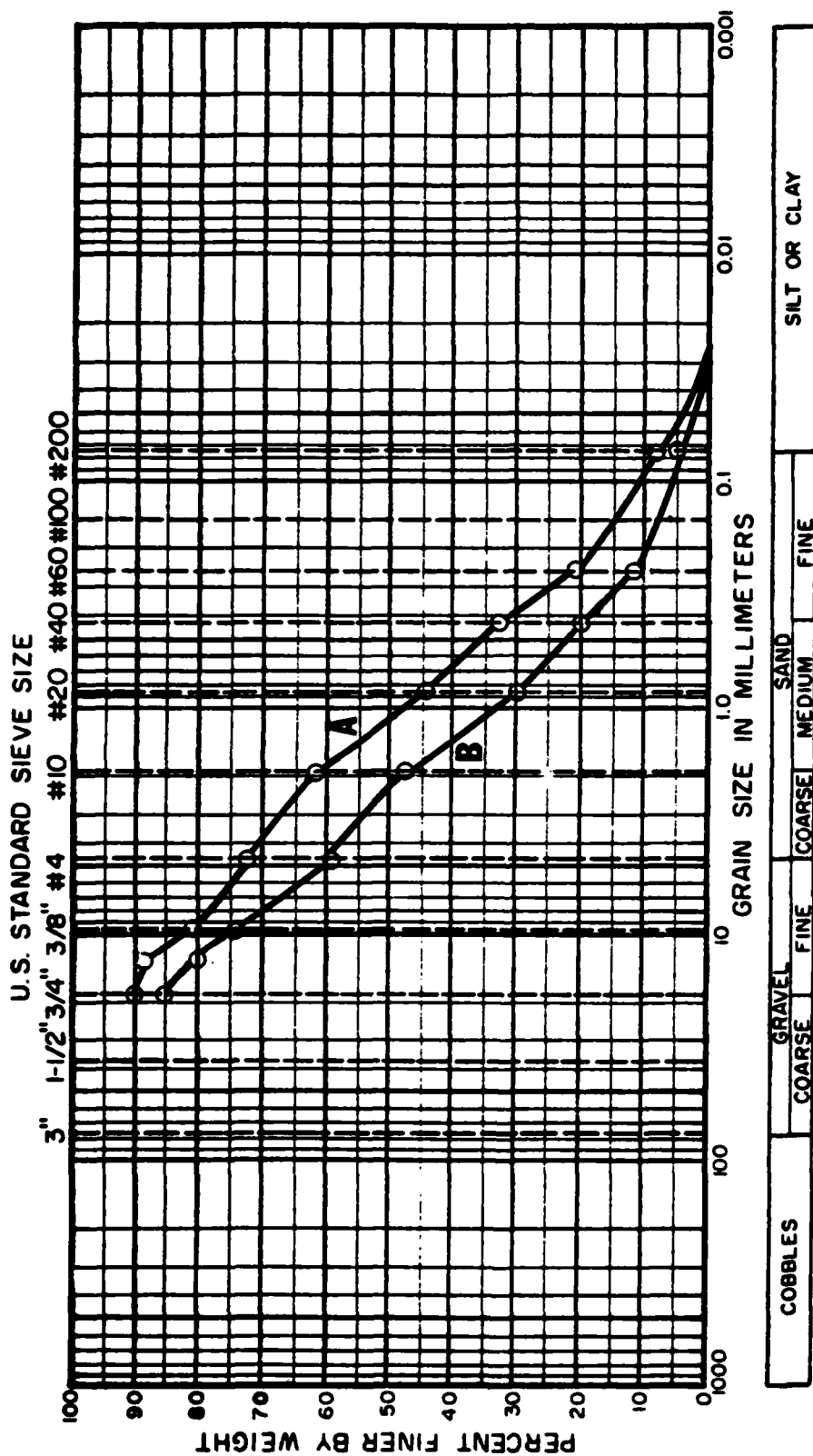
A -- Gradation after crushing (jaws set at 1/2" minimum opening).
B -- Gradation after pressing material into a sample (2000 psi).

Figure 1. Particle size distribution curves after crushing and after pressing material into a sample.
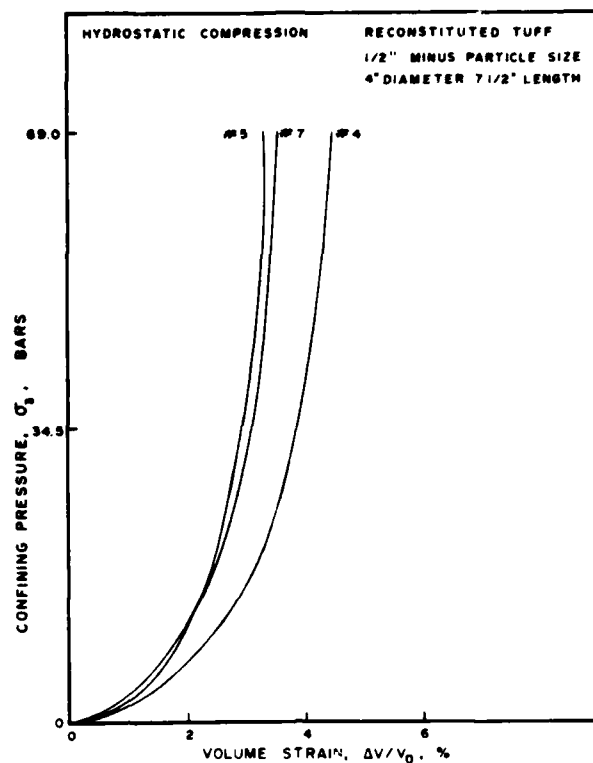
Figure 2. Volume strain curve for reconstituted (1/2 inch minus particle size) 4 inch diameter tuff sample.
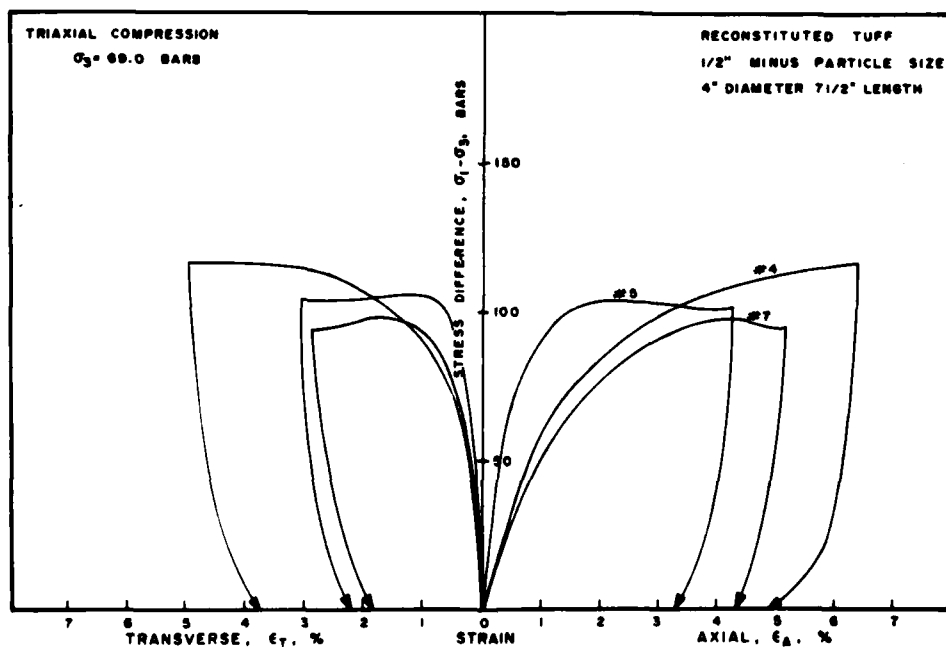
Figure 3. Triaxial compression results for reconstituted (1/2 inch minus particle size) 4 inch diameter tuff sample.
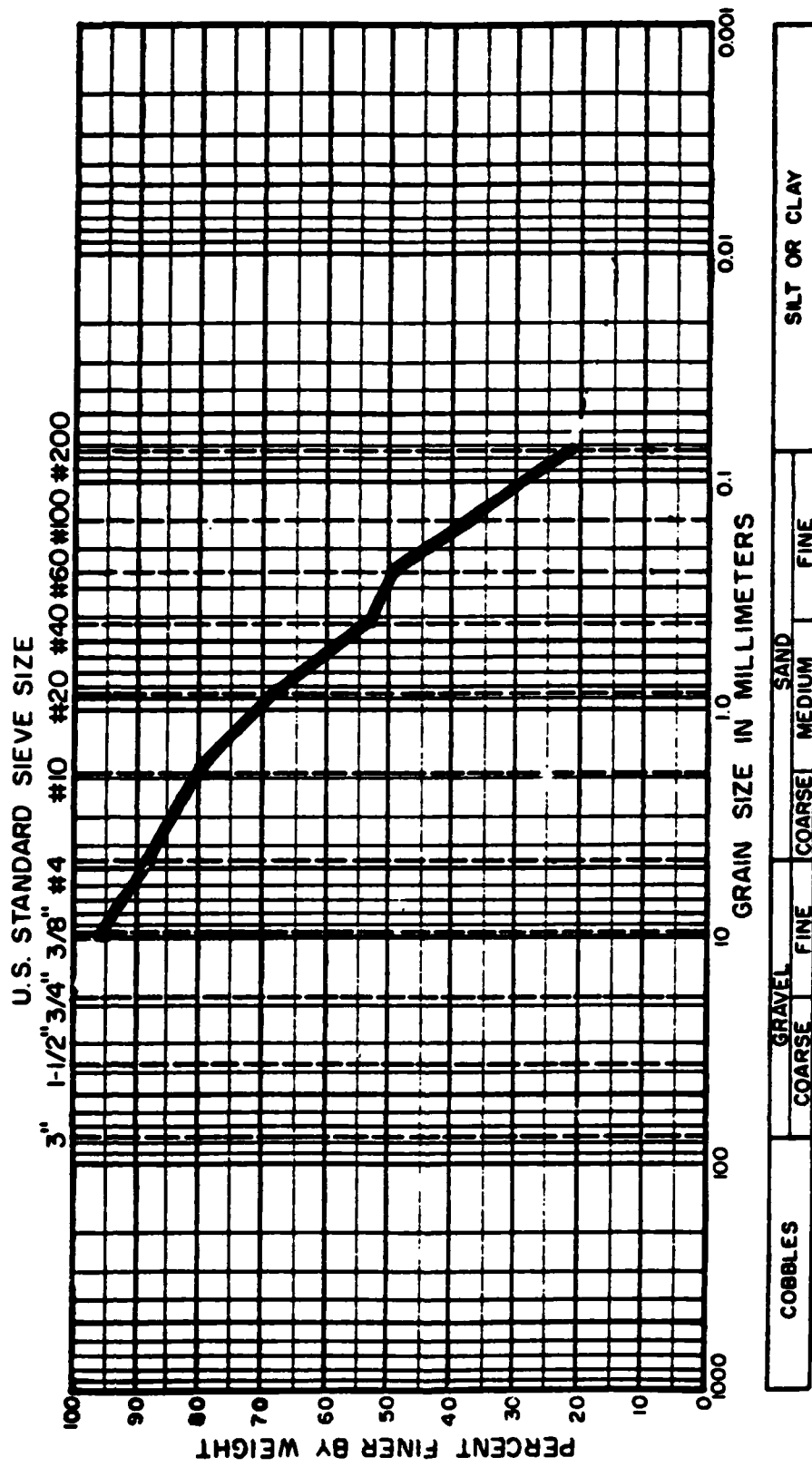
Figure 4. Size distribution on Sample #4 (4 inch diameter) after testing.

205
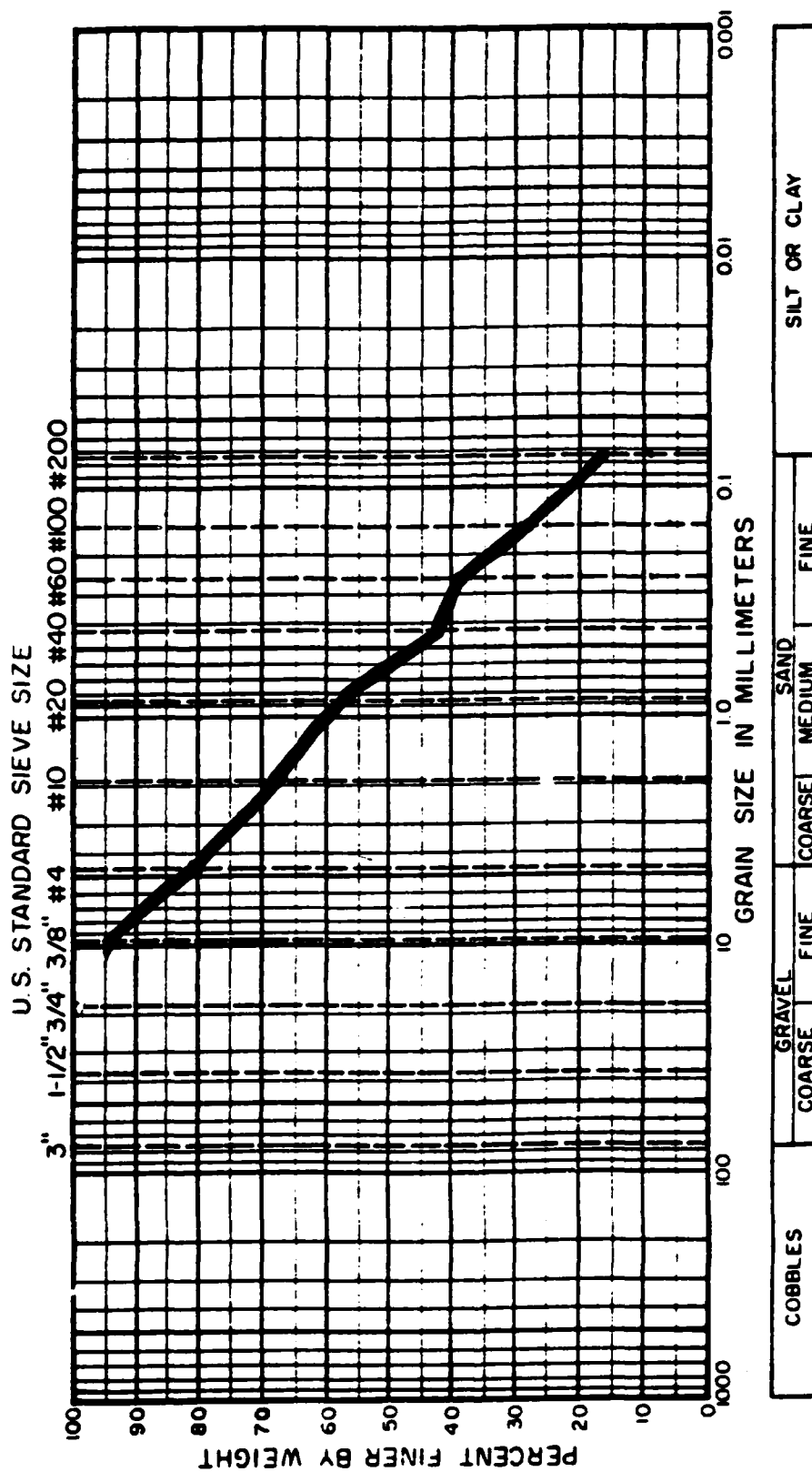
Figure 5. Size distribution on sample #5 (4 inch diameter) after testing.
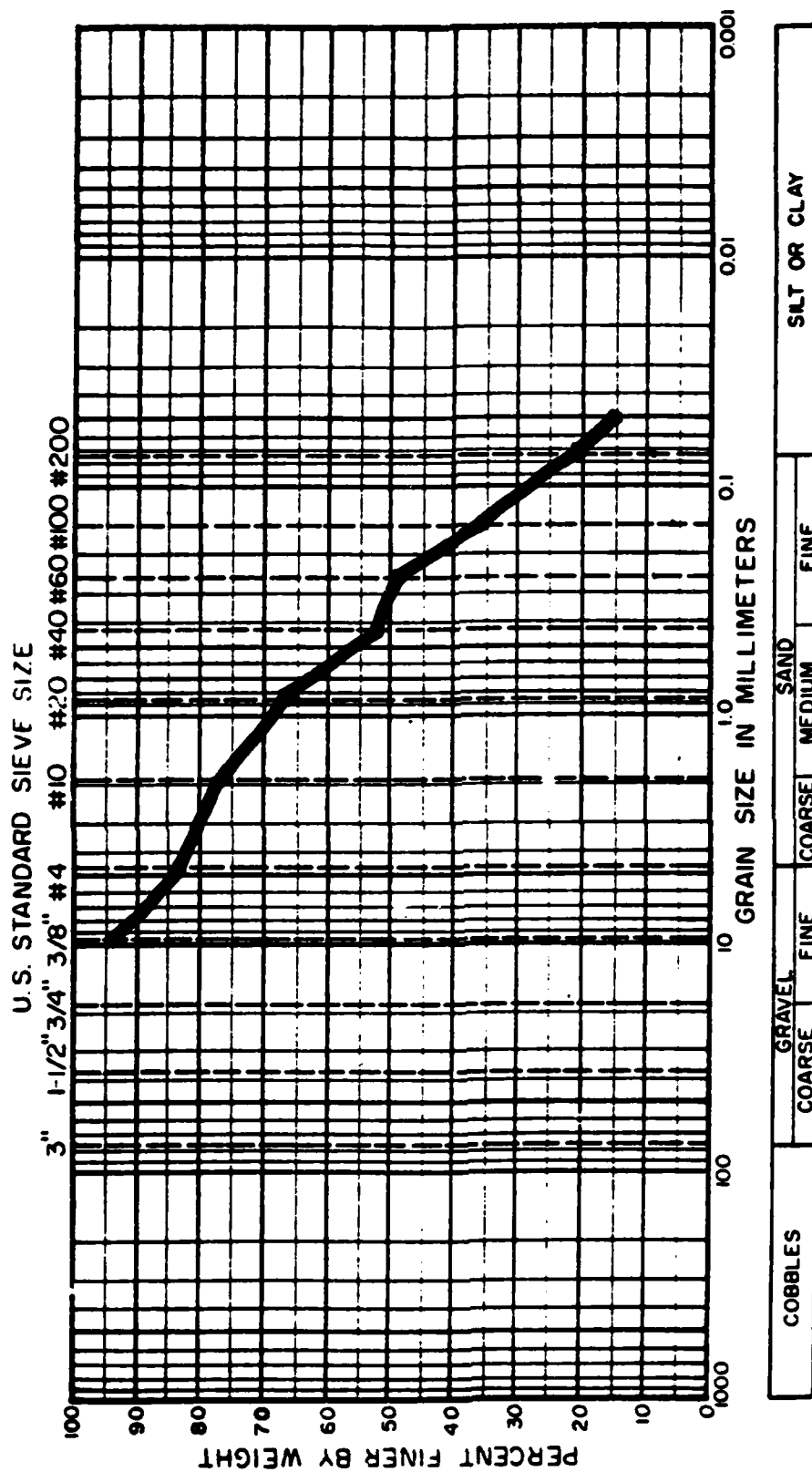
Figure 6. Size distribution on Sample #7 (4 inch diameter) after testing.

207
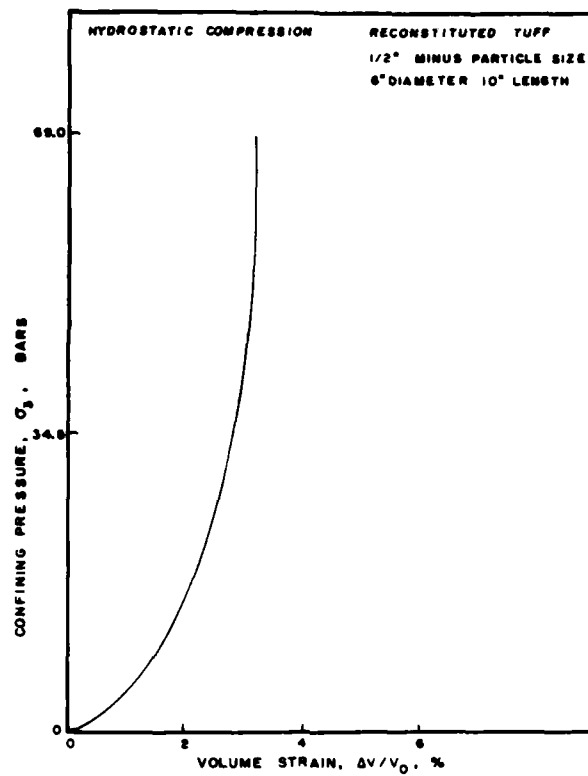
Figure 7. Volume strain curve for reconstituted (1/2 inch minus particle size) 6 inch diameter tuff sample.
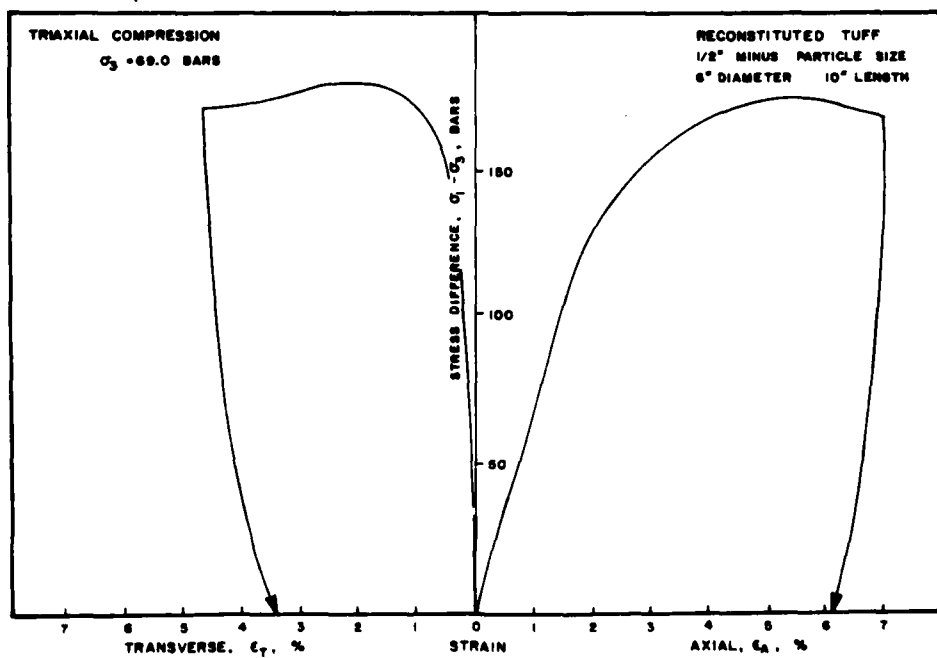
Figure 8. Triaxial compression results for reconstituted (1/2 inch minus particle size) 6 inch diameter tuff sample.

208

the post-test gradation analysis. Volume strain resulting from the hydrostatic compression was about 3 percent. Shear strength ($\frac{\sigma_1 - \sigma_3}{2}$) was somewhat higher (~85 bars) than the observed in the 4 inch diameter samples (~50 bars). Shear modulus was ~3 kbars. The gradation analysis indicates similar particle breakdown to that observed in the 4 inch diameter samples.

2 inch diameter samples -- To date no 2 inch diameter samples have been tested. Present plans are to repeat two more 6 inch diameter samples before proceeding to these tests.

Permeability Tests (Gas)

Work had only just begun on the permeability tests at the end of this contract year. Permeabilities on the order of 25 millidarcies were measured on ½ inch minus particle size 4 inch diameter samples. These measurements were obtained on wet reconstituted Paintbrush tuff samples (prepared via the same technique as the mechanical samples except to a 4 inch length). Further tests are planned on other sample sizes.
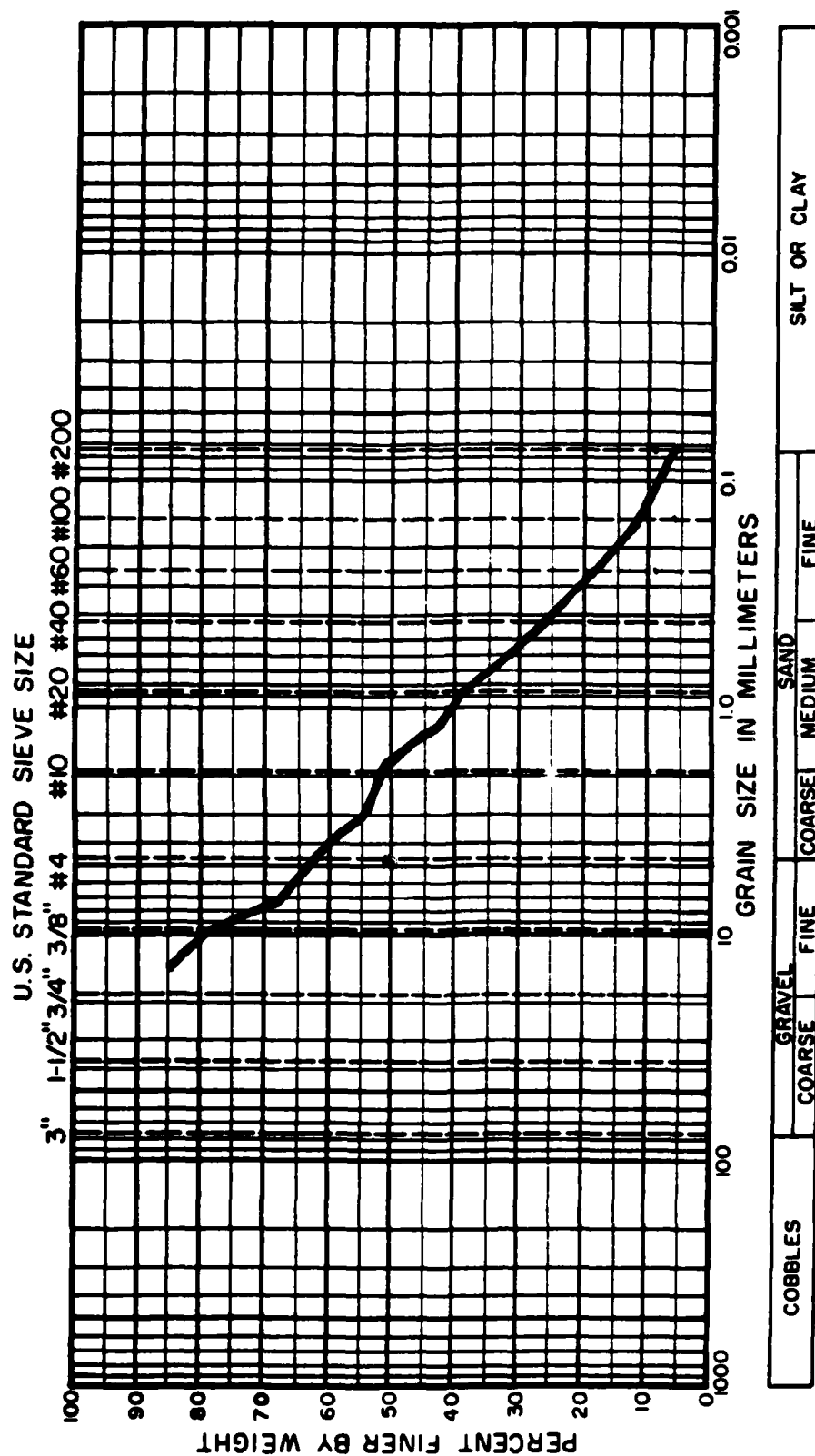
Figure 9. Size distribution on 6 inch diameter sample after testing.

210

ULTRASONIC VELOCITIES AS A FUNCTION OF FRACTURING

ULTRASONICS VELOCITIES AS A FUNCTION OF FRACTURING

A total of three (3) samples have been tested since the last report (February 1978). The samples were from hole U12n.05 UG#4; 1382, 1384 and 1390 ft.

The objective of these tests was to determine if the velocity reduction observed during dilatancy remained when the stress difference was removed from the damaged sample. The first sample (1382') failed abruptly during unloading, resulting in the loss of all signals through the rock.

The second test (1384') was much more successful. After applying a confining pressure, a shear stress was applied until about a 15 percent reduction in the p-wave velocity was observed (see Figure 1, Point 3). The shear stress was then reduced along with the confining pressure until the sample was at atmospheric conditions (Point 4). After the sample had remained undisturbed for more than twelve hours, the p-wave velocity had decreased further (Point 5). When the hydrostatic confining pressure was increased to 1000 psi the p-wave velocity did increase, but only to a value approximately 35 percent below the undamaged value (Point 6). Unfortunately, the s-wave signal amplitudes were reduced to the point where measurements could not be taken after the initial fracturing of the sample. However, the last reading showed a reduction of 21 percent in the horizontal polarized (perpendicular to the plane of the applied stress) s-wave velocity, while the vertical polarized (in the plane at the applied stress) only reduced by a little more than 6 percent (see Figure 2).
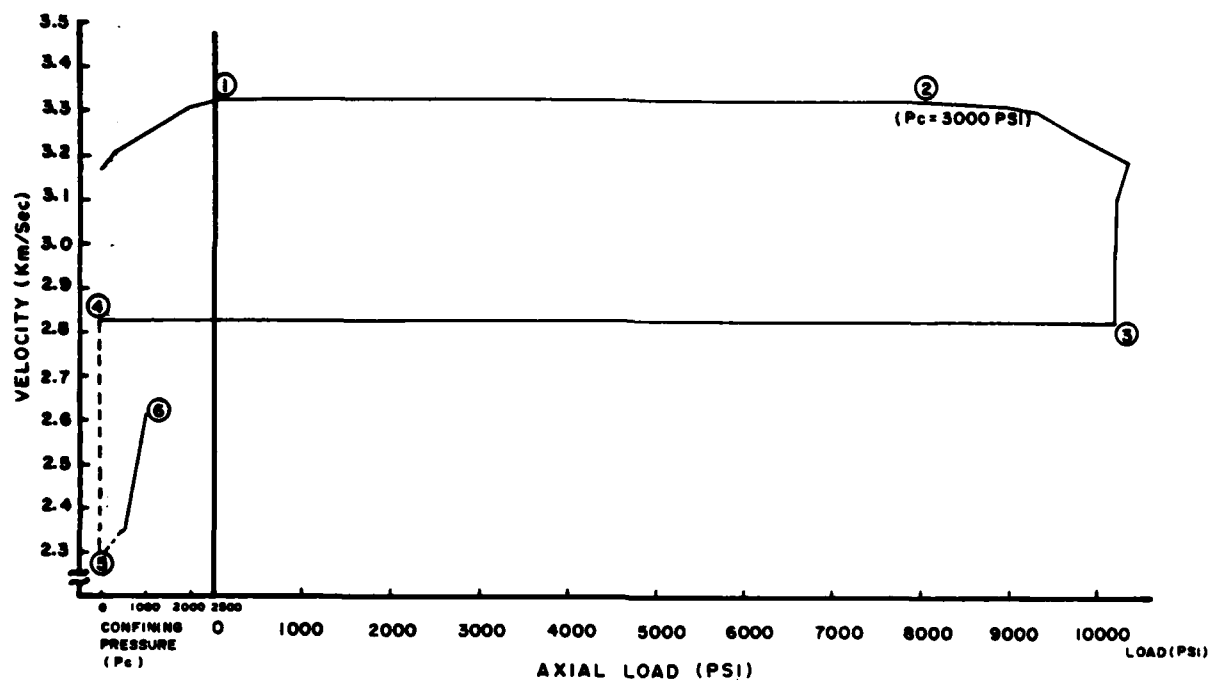
Figure 1.   Stress affects on p-wave velocity, sample 1384'.
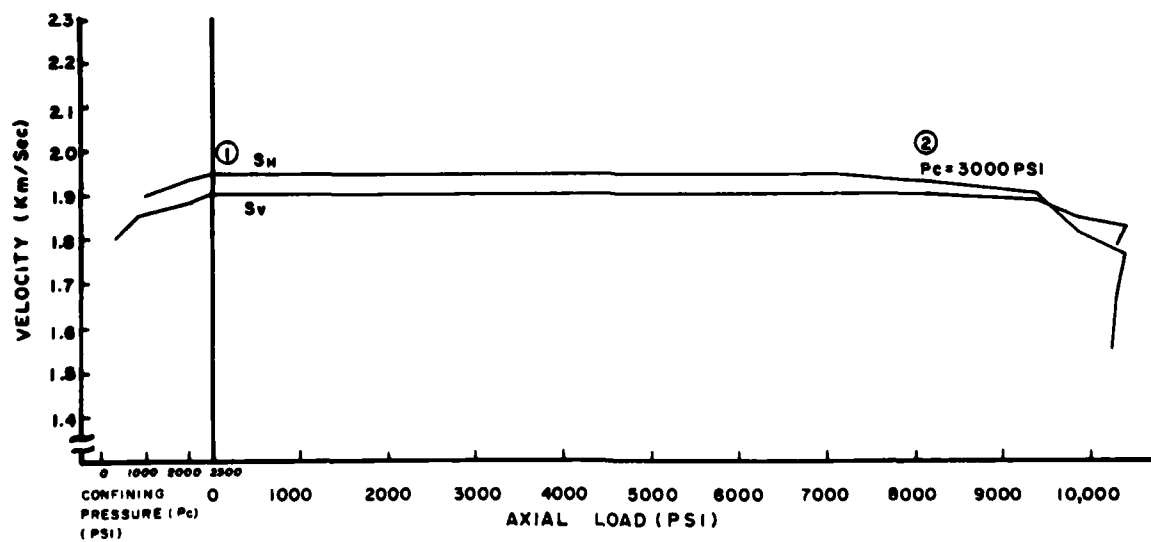
Figure 2.   Stress affects on s-wave velocity, sample 1384'.

212

The third test (1390') was to be similar to 1384' except the con-
fining pressure was to be maintained at 1000 psi after the load cycle
to determine the extent, if any, of healing (velocity increase). As
can be seen from Figure 3, the shear stress was applied until the p-wave
velocity dropped 16 percent (Point 3); however, during unloading, the
sample was damaged further starting at Point 4. By the time the sample
was back to atmospheric pressure (Point 5) the p-wave velocity had de-
creased a total of 25 percent. The confining pressure was increased to
1000 psi, resulting in an increase in velocity (Point 6). The intent
was to leave the sample at this confining pressure for two days but due
to a minute leak, the pressure dropped to zero during the two day period.
Point 6 indicates the measured p-wave velocity when the confining pres-
sure was again increased. The final value was approximately 24 percent
below that of the virgin material. An additional test is planned in which
the confining pressure will be held constant during the period after the
load cycle. As in the previous test, the s-wave signals became too weak
to measure.

These data suggest that once fracturing has occurred (as evidenced
by dilatancy), the samples does not regain its' original acoustic pro-
perties. These tests were, however, short term in a geologic sense, and
long term ("creep") tests would be required to further define this behavior.
Future tests are also planned to determine the effects on the amplitude
and velocity of the acoustic wave as a function of wave length as the
material is fractured.
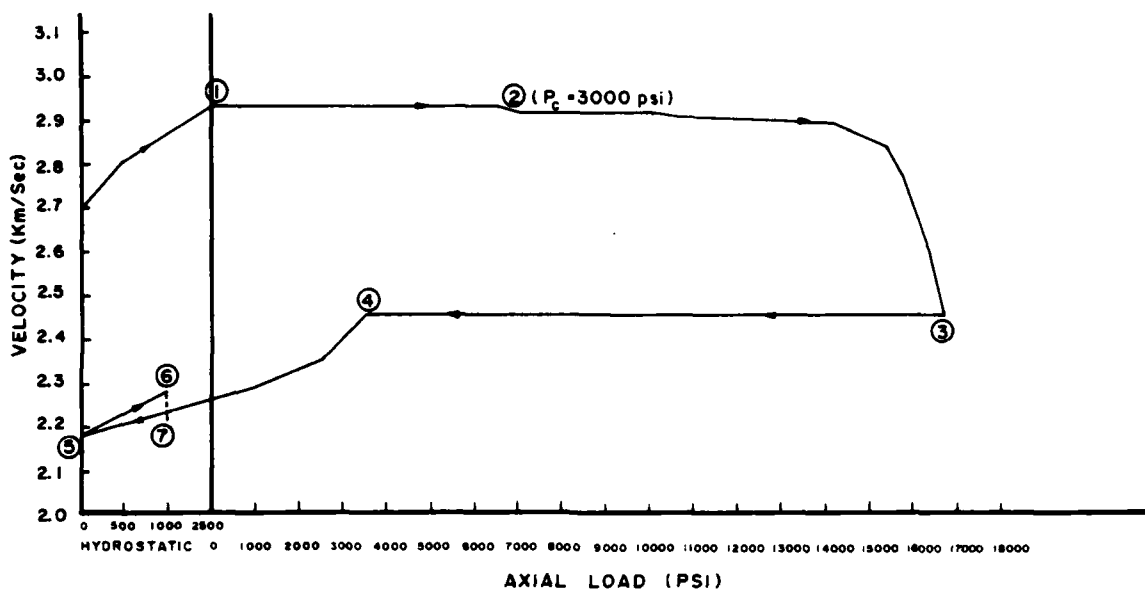
Figure 3.   Stress affects on p-wave velocity, sample 1390'.

SPECIFIC RETENTION TESTS ON TUFF

ABSTRACT

Because of the requirement to know the gas-filled void content of tuff material to a high degree of accuracy, tests were conducted to evaluate the possibility of fluid invasion during drilling. Apparent "wet" tuff samples were placed in a 100 percent humidity environment to determine if the samples would gain moisture.

Additionally, "dry" tuff samples were also placed in the high humidity environment to determine if they would return to their original "*in situ*" moisture content. Previous work has shown that dry samples placed in a near 100 percent relative humidity environment gain weight (moisture) to the suspected *in situ* condition.

PROGRESS SUMMARY

Twenty wet samples from drill hole UE12n#8 were oven dried at 105°C in order to determine their *in situ* moisture content. The average percent moisture loss (by dry weight) resulting from drying was 25 ± 10 percent. The samples were then placed in a room temperature 96 percent relative humidity environment for resaturation. After 17 days in the humidity chamber, the percent moisture gain (by dry weight) averaged 5.7 ± 1.5 percent with no appreciable moisture gains observed after the third day (see Figure 1).

Previously tested dry samples from drill hole UE12n#9* produced considerably different results. Percent moisture gains for these samples ranged from 20 to 50 percent for the same time period (suspected to be the *in situ* moisture content). A possible explanation for the difference in moisture gains is the difference in relative humidity. The relative humidity was 100 percent for the UE12n#9 tuffs while it was only 96 percent (maximum for our in-house chamber) for the UE12n#8 tuffs. Porosities were also somewhat different between the two drill holes. The porosities averaged 42 and 60 percent for UE12n#8 and UE12n#9 tuffs, respectively. The lower porosity in the UE12n#8 tuffs might have restricted water absorption into the samples. If this was the case, however, one might expect the samples to be drier in the center than near the surface. Subsequent tests comparing the percent moisture of the surface tuff and tuff from the sample centers indicated no difference in moisture content.

---

* Dropek, R. K., Butters, S. W., Jones, A. H., "Specific Moisture Retention of Nevada Test Site Tuffs," Terra Tek Report TR 76-35, July 1976.

The difference in results then appears to be the 4 percent difference in relative humidity.

Present plans are to repeat the test program in a 100 percent relative humidity environment to see if resaturation to *in situ* moisture states can in fact be accomplished via this method.
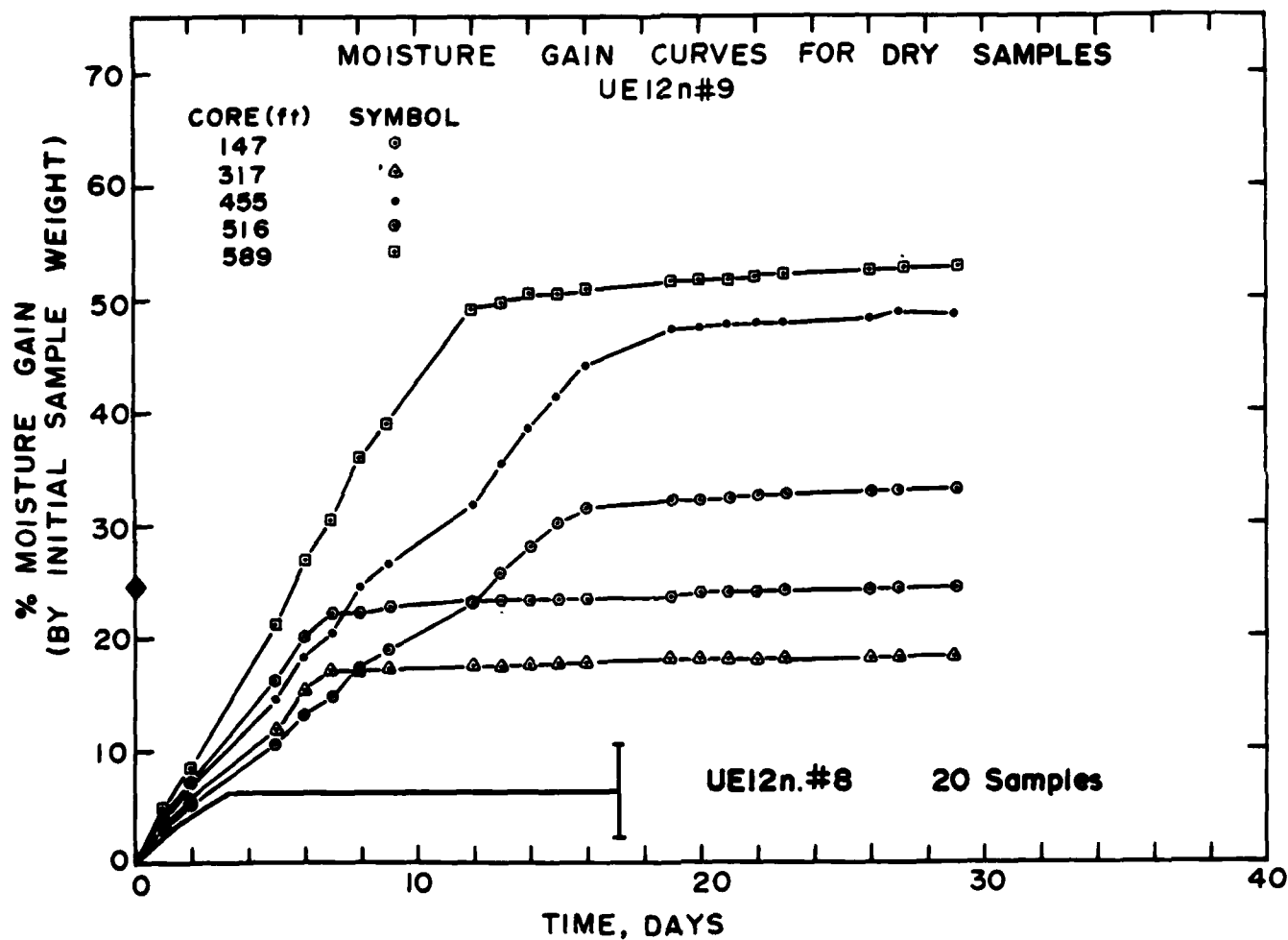
◆ - Average *in situ* moisture content of UE12n#8 samples.

Figure 1. Percent moisture gain versus time for the earlier tested UE12n#9 samples and the UE12n#8 samples.

217

STANFORD RESEARCH INSTITUTE GROUT

SUMMARY

Tests were conducted to determine select material properties on the superlean grout (SLG 9-15-77) by Stanford Research Institute. Mechanical tests included an unconfined compression, a 50 bar triaxial compression and a uniaxial strain test to 100 bars confining pressure. Tests were conducted on 5 and 6 October 1977. The unconfined and triaxial compression test results are shown in Figures 1 and 2 as stress-strain curves. Uniaxial strain test results are shown in Figures 3 and 4. Physical properties were also measured and are listed in Table 1.

Test results show that mechanical properties are similar to 28 day age superlean grout previously tested by Terra Tek*. Physical properties are also quite similar, however, densities are slightly lower and porosity is higher. The maximum stress and stress difference for the unconfined and 50 bar triaxial compression tests were 7 and ~14 bars respectively. Both tests exhibited a ductile type failure. The uniaxial strain test exhibited a maximum stress difference of 14 bars. Physical property measurements indicate the sample to be slightly undersaturated with ~2 percent aid voids.

---

* Butters, S. W., Nielsen, R. R., Jones, A. H., and Green, S. J., "Mechanical and Physical Properties of Nevada Test Site Tuffs and Grouts from Exploratory Drill Holes," TR 73-69, December 1973.
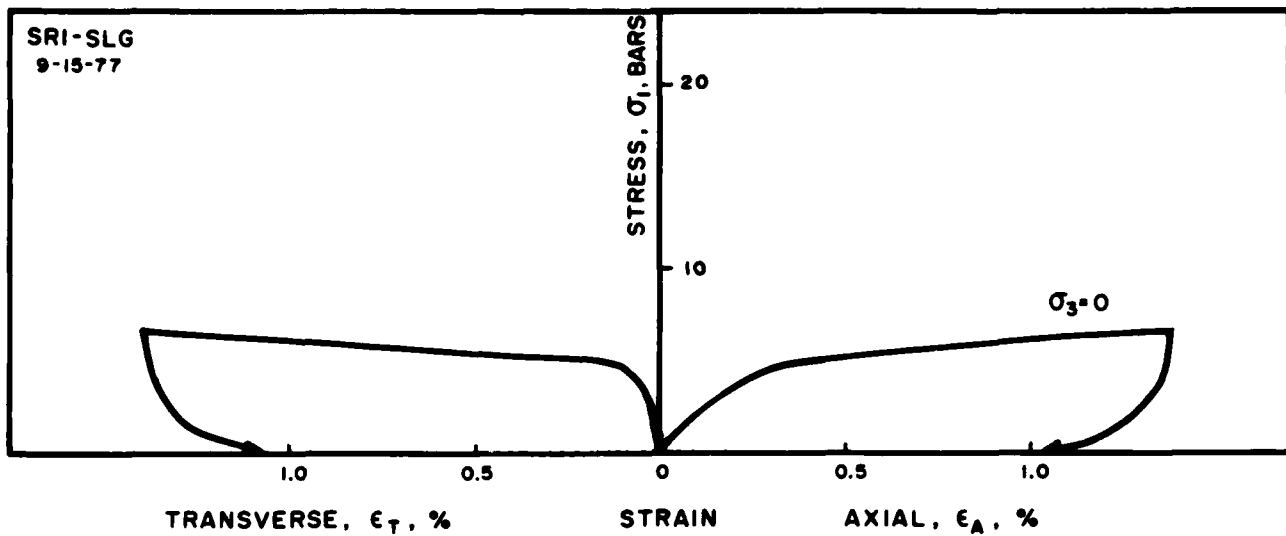
Figure 1. Unconfined compression test -- stress versus individual strains.
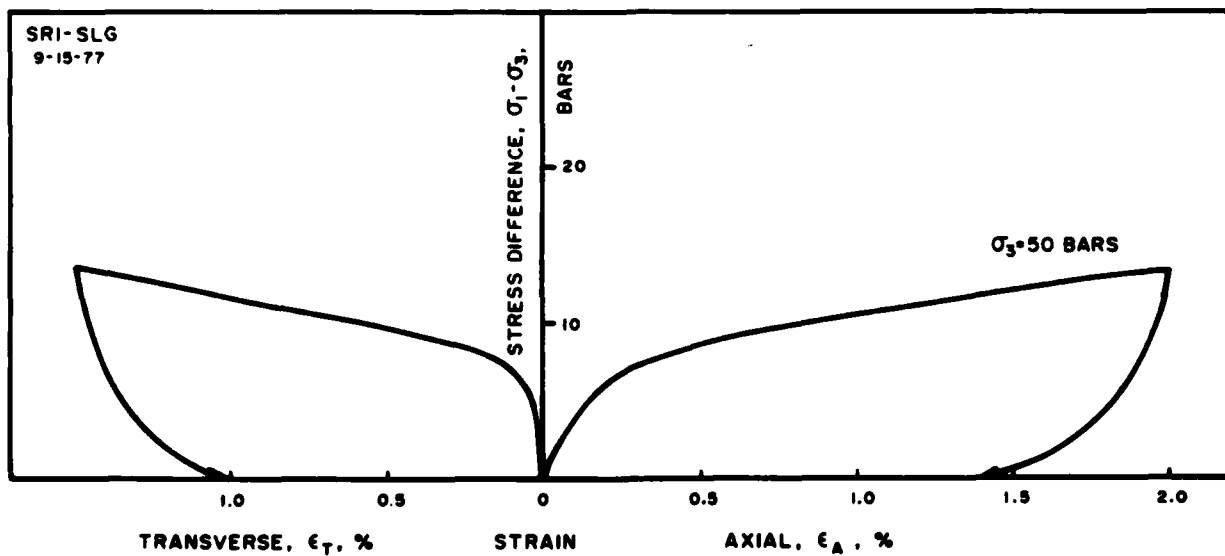
Figure 2. Triaxial compression test -- stress difference versus
individual strains.

219
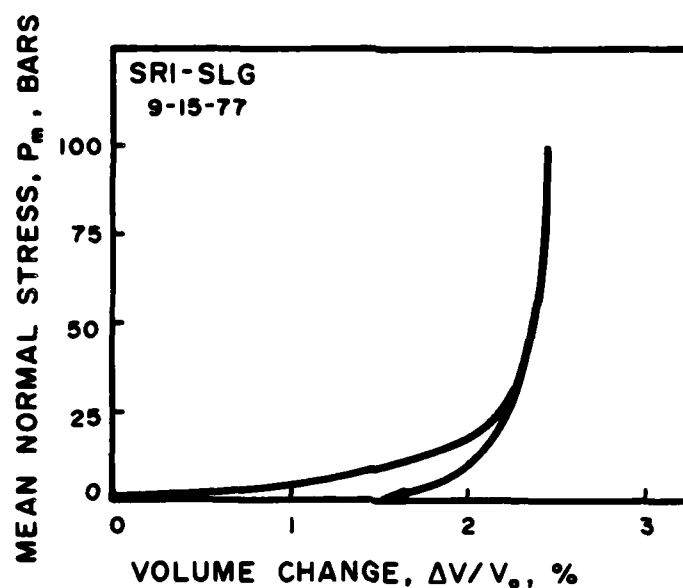
Figure 3. Uniaxial strain test -- mean normal stress versus volume change.
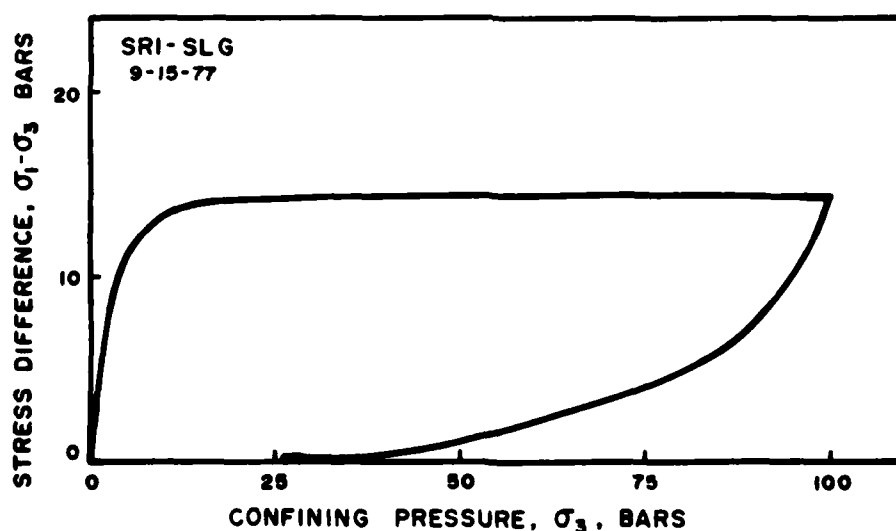
Figure 4. Uniaxial strain test -- stress difference versus confining pressure.

TABLE 1

Physical Properties of Stanford Research Institute
Superlean Grout

SAMPLE DESIGNTION	DENSITY (gm/cc)			WATER BY WET WEIGHT (%)	POROSITY (%)	SATURATION (%)	CALC. AIR VOIDS (%)	MEAS. PERMANENT COMP. (%)
	AS-RECEIVED	DRY	GRAIN					
SLG 9-15-77	1.57	0.97	2.57	38.4	62.3	97.1	1.8	(100 bars) 1.7

DISTRIBUTION LIST

DEPARTMENT OF DEFENSE

Defense Nuclear Agency
    ATTN: SPSS, G. Ullrich
    ATTN: SPSS, K. Goering
    ATTN: SPSS, K. Linger
    ATTN: SPTD, T. Kennedy
    ATTN: STSP
4 cys ATTN: STTI/CA

Defense Technical Info Center
12 cys ATTN: DD

Field Command
Defense Nuclear Agency
    ATTN: FCT, G. Ballantine
    ATTN: FCTOU
    ATTN: FCTE
    ATTN: FCTK, C. Keller
    ATTN: FCTK, Dr Rinehart

Field Command Test Directorate
10 cys ATTN: FCTC, J. LaComb

Field Command
DNA, Det 1
Lawrence Livermore Natl Lab
    ATTN: FC-1
    ATTN: Document Control

Weapons Systems Evaluation Group
    ATTN: Tech Library

DEPARTMENT OF THE ARMY

Explosive Excavation Rsch Lab
Lawrence Livermore National Lab
    ATTN: Document Control

Harry Diamond Laboratories
    ATTN: DRXDO-NP

US Army Engrg Waterways Exper Station
    ATTN: D. Day
    ATTN: J. Zelasko
    ATTN: W. Flathau
    ATTN: Research Ctr Library
    ATTN: L. Ingram
    ATTN: P. Hadala
    ATTN: J. Jackson
    ATTN: J. Ehrgotz
    ATTN: J. Boa

DEPARTMENT OF THE NAVY

Chief of Naval Research
    ATTN: Document Control

Naval Civil Engrg Laboratory
    ATTN: J. Allgood
    ATTN: Code L-31

Naval Research Laboratory
    ATTN: Code 1065
    ATTN: Cont Branch

DEPARTMENT OF THE AIR FORCE

Air Force Geophysics Lab
    ATTN: Dr Thompson

Air Force Weapons Laboratory
    ATTN: DE-I
    ATTN: DEV-G, J. Bratton
    ATTN: DEC, M. Plamondon
    ATTN: SES, R. Henning
    ATTN: SUL, Tech Library
    ATTN: DEX

DEPARTMENT OF ENERGY

Department of Energy
Nevada Operations Office
    ATTN: R. Nelson
    ATTN: Technical Library

Department of Energy
Nevada Test Site Office
    ATTN: J. Dryder

OTHER GOVERNMENT AGENCIES

Department of the Interior
Bureau of Mines
    ATTN: L. Obert

Bureau of Mines
    ATTN: T. Ricketts
    ATTN: T. Atchinson

Department of the Interior
US Geological Survey
    ATTN: T. Fernald
    ATTN: R. Carroll
    ATTN: P. Orklid

US Environmental Protection Agency
Environmental Monitoring & Support Lab
    ATTN: R. Stanley

DEPARTMENT OF ENERGY CONTRACTORS

University of California
Lawrence Livermore National Lab
    ATTN: J. Hearst
    ATTN: V. Wheeler
    ATTN: Dr McKague
    ATTN: H. Rodean
    ATTN: J. Carothers
    ATTN: F. Morrison
    ATTN: C. Olsen
    ATTN: G. Higgins
    ATTN: R. Terhune
    ATTN: J. Shearer
    ATTN: B. Hudson

Sandia National Laboratories
    ATTN: C. Gulick
    ATTN: C. Smith
    ATTN: C. Broyles
    ATTN: C. Mehl

DEPARTMENT OF ENERGY CONTRACTORS (Continued)

Los Alamos National Lab
        ATTN: T. Scolman
        ATTN: Reports Library
        ATTN: F. App
        ATTN: R. Brownlee
        ATTN: B. Killian
        ATTN: J. House
        ATTN: B. Hudson

Desert Research Institute
        ATTN: P. Fenske
        ATTN: C. Case

Holmes & Narver, Inc
        ATTN: J. Calovini (A-6)

Fenix & Scisson
        ATTN: F. Waltman
        ATTN: D. Townsend

Reynolds Electrical & Engrg Co, Inc
        ATTN: H. Edwards/FOD/DOD

DEPARTMENT OF DEFENSE CONTRACTORS

Agbabian Associates
        ATTN: Document Control
        ATTN: C. Bagge

Boeing Co
        ATTN: K. Fridell

Kaman Tempo
        ATTN: DASIAC

Kaman Tempo
        ATTN: DASIAC

H-Tech Labs, Inc
        ATTN: B. Hartenbaum

Ken O'Brien & Associates, Inc
        ATTN: D. Donnegan

University of Illinois
        ATTN: N. Newmark

DEPARTMENT OF DEFENSE CONTRACTORS (Continued)

S-CUBED
A Div of Maxwell Labs, Inc
        ATTN: R. Duff
        ATTN: E. Peterson
        ATTN: Document Control

Weidlinger Associates, Inc
        ATTN: M. Baron

Pacifica Technology
        ATTN: D. Patch
        ATTN: J. Kent

Merritt CASES, Inc
        ATTN: J. Merritt

Terra Tek, Inc
        ATTN: S. Green
        ATTN: J. Schatz
    2 cys ATTN: D. Gardiner
    2 cys ATTN: A. Jones
    2 cys ATTN: S. Butters

TRW Electronics & Defense Sector
        ATTN: M. Shrader

Structural Mechanics Assoc, Inc
        ATTN: P. Kennedy

Massachusetts Institute of Technology
        ATTN: W. Brace

R&D Associates
        ATTN: R. Shaefer
        ATTN: J. Lewis
        ATTN: P. Haas

California Research & Technology
        ATTN: K. Kreyenhagen

SRI International
        ATTN: A. Florence
        ATTN: H. Lindberg

224

END

FILMED

3-85

DTIC